



RHODES UNIVERSITY
Where leaders learn

EXPLORING THE STRUCTURAL INTEGRITY OF A PICORNAVIRUS CAPSID

A thesis submitted in fulfilment of the requirements for the degree of

DOCTOR OF PHILOSOPHY

Of

RHODES UNIVERSITY

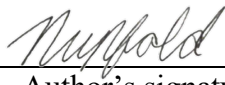
By

Nicole Sarah Upfold

July 2019

Declaration

I, Nicole Sarah Upfold (g11U0270) hereby declare that the thesis submitted is my own work. It is being submitted for the degree of Doctor of Philosophy at Rhodes University. It has not been previously submitted for assessment of any degree at any other university or other body, organisation outside of the university.



Author's signature

30 July 2019

Date

Abstract

Picornaviruses are a diverse family of small RNA viruses that cause a broad range of human and veterinary diseases. Despite decades of research into the molecular biology of these pathogens, no antivirals and few vaccines are commercially available for the treatment and prevention of picornavirus infections. The capsids of these non-enveloped viruses are involved in many important aspects of the picornavirus lifecycle, such as cell attachment and entry, uncoating, and protection of the viral RNA. Although the structures of many picornavirus capsids have been solved, a broader understanding of the molecular determinants that are required for structural integrity and stability is imperative for an improved understanding of the basic biology of these viruses, and for designing effective control strategies. Collectively, this thesis aims to elucidate the molecular determinants of structural stability and integrity in the Theiler's murine encephalomyelitis virus capsid (TMEV).

To study the TMEV GDVII capsid using biochemical techniques, neutralising polyclonal antibodies were generated against GDVII particles. The antibodies recognised linear epitopes in the C-terminus of the VP1 protein, but not those present in VP2 or VP3. The VP1 C-terminal residues were mapped to a loop above the putative receptor binding pit on the capsid surface, which prompted an investigation into the potential binding site of the TMEV co-receptor, heparan sulphate. Molecular docking revealed that heparan interacts with residues of the receptor binding pocket, as well as residues of the adjoining VP1 C-terminal loop. These findings suggest that the antibodies neutralise virus infection by preventing attachment of the virus to the co-receptor and possibly the unknown primary receptor.

Few studies have identified the specific residues and interactions at subunit interfaces that significantly contribute to picornavirus capsid stability, assembly, and function. A novel *in-silico* screen was developed for the prediction of hotspot residues at protein-protein interfaces of a virus capsid. This screen can be applied to elucidate the residues that contribute significantly to the intraprotomer, interprotomer and interpentamer interfaces of any picornavirus capsid, on condition that the structure of the virus is available. The screen was applied to TMEV GDVII resulting in the identification of hotspots, several of which correspond to residues that are known to be important for aspects of the virus lifecycle, such as those that contribute to pH stability or form part of receptor binding sites. This observation suggests that residues involved in specific capsid functions may also play a role in capsid

stability. Many of the residues identified as hotspots in TMEV corresponded to those required for assembly, uncoating, and virus growth in representative picornaviruses from various genera, suggesting that the residues that regulate capsid stability may be somewhat conserved across the family. Hotspots identified at the interpentamer interfaces of TMEV were individually substituted to alanine to further explore their importance to the TMEV lifecycle. All the amino acid substitutions prevented completion of the virus lifecycle as no CPE was observed following transfection of susceptible cells. Immunofluorescence experiments demonstrated that virus protein synthesis and RNA replication were not inhibited by substitution of the hotspot residues, but that infectivity was severely impeded. This confirmed that the residues were required for some aspect of the virus lifecycle, such as capsid assembly, or were critical for maintaining the conformational stability of the TMEV particles.

Virus capsids become unstable and are prone to dissociation under certain conditions such as extreme pH and non-physiological temperatures. The thermostability of TMEV was explored by selecting GDVII virions with improved thermal tolerance through serial passage and heat exposure. Thermostable virions that could tolerate temperatures above 57 °C had reduced infective titres compared to the wild type TMEV suggesting that the virus adapted to thermal stress at the expense of viral fitness. Sequencing the capsid encoding regions of the mutant virions revealed a pair of amino acid substitutions that were present in all mutants. Additional substitutions that were unique to viruses selected at different temperatures were also identified. Most of the substitutions were located within the intraprotomer interfaces of the virus, unlike previous studies on enteroviruses where mutations were mostly localised to the receptor binding pocket.

This thesis provides the first analysis of the structural determinants of TMEV capsid stability. The generation of tools to further explore the capsid structures of TMEV and other picornaviruses provides an opportunity for future studies which may contribute to the development of novel control strategies against this important family of viruses.

Acknowledgements

- Foremost, I would like to express my gratitude to my supervisor Prof Caroline Knox, for her advice and encouragement throughout the duration of this degree. Thank you for the many hours of discussion regarding the project and for providing support when problems were encountered.
- To Dr Garry Luke, thank you for your advice regarding some of the wet-lab experiments that were central to this study.
- To Dr Caroline Ross thank you for your assistance with the *in-silico* part of the project. Thank you for the many discussions we have shared regarding the structure and functioning of picornaviruses and for sharing interesting papers that were helpful to this study.
- To Prof Martin Hill, the Rhodes Department of Zoology and Entomology, and the technical team in the Department of Biochemistry and Microbiology, thank you for kindly providing me with (dust-free) lab space during the renovation of the Biological Sciences building. Thank you, Prof Heinrich Hoppe, for sharing your tissue culture facility with me.
- Thank you to Rhodes University and the National research foundation (NRF-DAAD) for the financial support during this project.
- To the members of lab 425, you've been great to work with! Thank you Tumi, Mel and Claire for making my time in the lab more memorable. Thank you to Mike and Marcel for holding down the fort during the renovations and for the advice and laughs during my time in the lab.
- To Melissa Lloyd and Steve Bentley, thank you for your friendship, support and constant encouragement.
- Finally, thank you to my wonderful family, Andrea Upfold, Chris Upfold, Jen Upfold (& Rob Rousseau), and Dylan Smith for your love, support, and encouragement throughout this degree. Thank you for keeping me sane and for being so understanding, I am forever grateful.

Table of Contents

Declaration.....	i
Abstract.....	ii
Acknowledgements.....	iv
Table of Contents.....	v
List of Figures.....	x
List of Tables.....	xiii
List of Abbreviations.....	xiv
List of Webservers and Applications.....	xvii
Research Outputs.....	xviii
Chapter 1.....	1
General Introduction.....	1
1.1. Introduction to the Picornaviridae: classification and importance.....	2
1.2. Picornavirus genome organisation and polyprotein processing.....	4
1.3. The picornavirus particle.....	7
1.3.1. Structure of the picornavirus capsid.....	7
1.3.2. Structure and antigenicity.....	11
1.3.3. Capsid assembly and RNA encapsidation.....	12
1.4. Receptor binding and uncoating.....	15
1.4.1. Receptor binding.....	15
1.4.2. Uncoating cues.....	18
1.4.3. Uncoating intermediates and end products.....	19
1.5. Capsid stability.....	22
1.5.1. The molecular determinants of picornavirus capsid stability.....	22
1.5.2. Mutational studies of hotspot prediction.....	23
1.5.3. Evolutionary selection of mutants with improved stability.....	25

1.5.4.	Computational assessment of stabilising residues	26
1.5.5.	Modulating capsid stability for improved vaccines	27
1.5.6.	Stabilising hotspots as potential drug targets	29
1.6.	Theiler's murine encephalomyelitis as an available replication system.....	30
1.7.	Problem statement	31
1.8.	Aims and objectives.....	32
1.9.	Overview of chapters.....	32
Chapter 2.....		35
The generation and characterisation of anti-TMEV capsid antibodies.....		35
2.1.	Introduction	36
2.2.	Materials and Methods	38
2.2.1.	Cells and virus.....	38
2.2.2.	Purification of TMEV GDVII particles for immunisation in rabbits.....	38
2.2.2.1.	Infection of monolayers	38
2.2.2.2.	Sucrose cushion purification.....	39
2.2.2.3.	Sucrose density gradient purification.....	39
2.2.3.	Transmission electron microscopy (TEM).....	40
2.2.4.	Preparation of TMEV infected cell lysate for Western analysis.....	40
2.2.5.	SDS-PAGE and Western analysis.....	41
2.2.6.	Construction of plasmids.....	42
2.2.7.	Expression of VP1 and truncated VP1 peptides.....	44
2.2.8.	Indirect immunofluorescence and confocal microscopy.....	44
2.2.9.	<i>In-silico</i> virus structure assembly and epitope mapping	45
2.2.10.	Molecular docking	45
2.2.11.	Antibody neutralisation assay.....	46
2.3.	Results	47
2.3.1.	Sucrose gradient purification of TMEV GDVII virus particles.....	47

2.3.2. Anti-TMEV capsid antibodies recognise linear epitopes in the VP1 capsid protein	48
2.3.3. Anti-capsid antibodies detect capsid proteins throughout TMEV infection by immunofluorescence	49
2.3.4. Anti-TMEV capsid antibodies recognise VP1 C-terminal epitopes	50
2.3.5. C-terminal residues 254–274 reside on a surface exposed loop over the putative receptor binding site	52
2.3.6. Heparan sulphate, the TMEV co-receptor, docks to the pit below the C-terminal loop	53
2.3.7. Polyclonal sera containing antibodies that recognise the C-terminus of VP1 neutralise virus infection <i>in vitro</i>	56
2.4. Discussion	58
Chapter 3	63
An <i>in-silico</i> screen for the prediction of hotspot residues that contribute to the structural stability of subunit interfaces of a picornavirus capsid	63
3.1. Introduction	64
3.2. Materials and Methods	67
3.2.1. Preparation of TMEV capsid interface subcomplexes	69
3.2.2. Interface hotspot prediction	71
3.2.2.1. Energy-based methods used for analysis	71
3.2.2.2. Feature-based methods used for analysis	72
3.2.3. Prediction of interacting residues	73
3.2.4. Identification of conserved hotspot residues	74
3.3. Results	74
3.3.1. Hotspot residues predicted within the intraprotomer interfaces of TMEV	74
3.3.2. Destabilising residues at interprotomer interfaces	78
3.3.3. Destabilising residues at pentamer-pentamer interfaces	83
3.4. Discussion	88
Chapter 4	100

The <i>in vitro</i> mutagenesis of hotspot residues within the interpentamer interfaces of the TMEV capsid	100
4.1. Introduction	101
4.2. Materials and Methods	103
4.2.1. Cells and plasmids.....	103
4.2.2. Generation of recombinant pGDVIIFL2 mutants	104
4.2.2.1. Preparation of vector pJetP1/P2/ <i>Hind</i> III-1 for site-directed mutagenesis.....	106
4.2.2.2. Site directed mutagenesis.....	107
4.2.3. Production and transfection of infectious wild type and mutant TMEV RNAs	109
4.2.3.1. <i>In vitro</i> synthesis of GDVII mutant RNA	109
4.2.3.2. Transfection of BHK-21 cells with wild type and mutant GDVII RNAs	110
4.2.4. Titration of replicating wild type and mutant TMEV by plaque assay	111
4.2.5. <i>Hind</i> III restriction analysis of RT-PCR products.....	111
4.2.6. SDS-PAGE and Western analysis.....	112
4.2.7. Immunofluorescence experiments.....	113
4.2.8. <i>In-silico</i> figure preparation, graph generation and statistical analysis	113
4.3. Results	114
4.3.1. Selection of hotspot residues for mutational analysis	114
4.3.2. Alteration of the <i>Hind</i> III restriction site in TMEV VP2 does not impact virus yield or protein synthesis	116
4.3.3. Monitoring cytopathic effect of mutant viruses	118
4.3.4. The absence of CPE is a result of the loss of individual hotspot residues and not defective viral RNA	120
4.3.5. TMEV replication and viral protein synthesis are not inhibited by substitution of the hotspot residues to alanine.....	122
4.4. Discussion.....	125
Chapter 5.....	133
The selection of TMEV GDVII virions with increased thermal tolerance	133

5.1.	Introduction	134
5.2.	Materials and Methods	136
5.2.1.	Cells and virus	136
5.2.2.	Short-term thermal inactivation assays	136
5.2.3.	Selection of virions with increased thermostability	138
5.2.4.	Plaque purification of heat selected virions	138
5.2.5.	RNA extraction and RT-PCR.....	139
5.2.6.	<i>In-silico</i> figure preparation, graph generation and statistical analysis	141
5.3.	Results	141
5.3.1.	Thermostability of the TMEV GDVII capsid	141
5.3.2.	Thermal tolerance of heat-selected virions	142
5.3.3.	Identification of underlying mutations following thermal selection.....	144
5.4.	Discussion.....	157
	Chapter 6.....	165
	General Discussion and future prospective.....	165
6.1.	Summary and future prospective	166
6.2.	Concluding remarks.....	175
	References.....	177
	Supplementary Data.....	209

List of Figures

Figure 1.1 Picornavirus genome organisation and translation.....	5
Figure 1.2 Structure of the picornavirus capsid and its subunits.....	8
Figure 1.3 Comparison of the different capsid topologies exhibited by picornavirus genera..	10
Figure 1.4 The stepwise assembly of picornavirus particles..	13
Figure 2.1 TMEV GDVII virus particles following sucrose purification.....	47
Figure 2.2 Detection of TMEV GDVII VP1 in purified TMEV particles and infected cell lysates.....	48
Figure 2.3 Subcellular distribution of capsid proteins during TMEV infection.....	50
Figure 2.4 Mapping of linear antigenic regions in VP1.....	51
Figure 2.5 Structure of the TMEV capsid showing antigenic regions.....	53
Figure 2.6 The predicted binding of heparan sulphate to the TMEV GDVII capsid.....	55
Figure 2.7 The <i>in vitro</i> neutralising abilities of polyclonal anti-TMEV capsid and anti-TMEV VP1 antibodies.....	57
Figure 3.1 Flow diagram of the methodology used to identify conserved and non-conserved hotspot residues and their interacting partners at capsid subunit interfaces.	68
Figure 3.2. TMEV capsid interface subcomplexes for hotspot and protein-protein interaction prediction..	70
Figure 3.3 Identification of hotspot residues and their interacting partners within intraprotomer interfaces of the TMEV capsid..	76

Figure 3.4 Network of hotspot residues and their interacting partners between two protomers of TMEV.....	80
Figure 3.5 Network of hotspot residues and their interacting partners at the pentamer-pentamer interface.....	86
Figure 4.1 Schematic overview of strategy used to engineer alanine substitutions into the TMEV cDNA.....	106
Figure 4.2 Schematic diagram of the site directed mutagenesis procedure used to engineer specific alanine substitutions into the P1 region of pJetP1/P2/ <i>HindIII</i> -1.....	107
Figure 4.3 Pentamer-pentamer interface hotspot residues selected for mutagenesis experiments.....	115
Figure 4.4 The <i>HindIII</i> -1 control mutant behaves like wild type TMEV.....	117
Figure 4.5 Comparison of the cytopathic effects induced by transfection of hotspot mutant, non-hotspot mutant and wild type TMEV RNAs.....	120
Figure 4.6 Controls to demonstrate that the lack of CPE was not due to defective mutant viral RNA.....	121
Figure 4.7 Immunofluorescence analysis of cells transfected with mutant and wild type TMEV RNAs.....	125
Figure 5.1 Flow diagram of the methodology to select TMEV GDVII isolates with improved thermal resistance and to assess the underlying mutations that contribute to this improved tolerance.....	138
Figure 5.2 Schematic diagram of the strategy used to RT-PCR amplify the TMEV P1 capsid encoding region of thermostable mutants.....	139
Figure 5.3 Thermal tolerance of TMEV GDVII.....	142

Figure 5.4 Thermal-tolerance assay of heat-selected TMEV isolates..	144
Figure 5.5 Positions of the individual mutations in the TMEV pentamer.....	145
Figure 5.6 Location of the mutation A201V within the VP1 protein at the VP1-VP2 intraprotomer interface and interactions between this residue and neighbouring residues within the protein and protomer.....	147
Figure 5.7 Location of the mutation D216N within the VP3 protein at the VP3-VP1 intraprotomer interface and interactions between this residue and neighbouring VP1 residues within the protomer.....	148
Figure 5.8 Location of the mutation E262K within the VP2 protein at the VP2-VP2 interpentamer two-fold interface and interactions formed between this mutant residue and neighbouring residues within the protein and across the interface	150
Figure 5.9 Location of the mutation V141I within the VP1 protein near the five-fold axis and interactions formed between this residue and neighbouring residues within the same protein..	151
Figure 5.10 The location of the A96T mutation within the VP3 protein at the base of the putative TMEV receptor binding site..	153
Figure 5.11 The location of the mutation M66T within the VP4 protein at the VP4-VP1 intraprotomer interface of the TMEV protomer..	155
Figure 5.12 The location of the V114I mutation within the VP3 protein at VP3-VP1 intraprotomer interface.....	157

List of Tables

Table 1.1. Overview of picornavirus genera containing pathogens of importance.	3
Table 2.1 Oligonucleotide primers used to generate plasmids expressing VP1 truncates.....	43
Table 3.1 Hotspot residues in the TMEV intraprotomer interfaces and their conservation within the picornavirus family.	77
Table 3.2 Hotspot residues in the TMEV interprotomer interfaces and their conservation within the picornavirus family.	82
Table 3.3 Hotspot residues in TMEV interpentamer interfaces and their conservation within the picornavirus family.	87
Table 4.1 Recombinant plasmids generated in this study	104
Table 5.1 Primers used for RT-PCR of the TMEV P1 capsid encoding region.	140
Table 5.2 Amino acid substitutions within the capsid coding regions of TME virions with increased thermal tolerance.....	145

List of Abbreviations

Abbreviations

%	Percentage
×g	Times gravitational force
°C	Degrees Celsius
~	Approximately
α	Alpha
β	Beta
Δ	Deletion
ΔΔ G	Change in binding free energy
μg/μl	Microgram/s per microliter
μg/ml	Microgram/s per millilitre
μl	Microliter
μM	Micromolar
Å	Angstrom/s
Amp	Ampicillin
APS	Ammonium persulphate
ATP	Adenosine triphosphate
AU	Absorbance units
BHK-21	Baby hamster kidney cells, clone 21
bp	Base pairs
BSA	Bovine serum albumin
C-	Carboxyl
CPE	cytopathic effect
ddH ₂ O	Deionised Water
DMEM	Dulbecco's minimum essential media
DNA	Deoxyribonucleic acid
dNTP	Deoxynucleoside triphosphate
E. coli	Escherichia coli
EDTA	Ethylenediaminetetraacetic acid
FCS	Foetal calf serum
h	Hour/s
His ₆	6x Histidine tag
Hsp	Heat shock protein
IPTG	Isopropyl-β-D-thiogalactopyranoside
IRES	Internal ribosome entry site
kb	Kilo base pairs
kDa	Kilo Daltons
LB	Luria-Broth culture medium

M	Molar
MD	Molecular Dynamics
mg	Milligram/s
min	Minute/s
ml	Millilitre
MOI	Multiplicity of infection
mRNA	Messenger RNA
MW	Molecular Weight
N-	Amino
NaCl ₂	Sodium chloride
OD	Optical Density
ORF	Open reading frame
PBS	Phosphate buffered saline
PCR	Polymerase chain reaction
PDB	Protein Databank
PFU/ml	Plaque forming units per millilitre
PIC	Protein Interaction Calculator
Poly-A	Poly-adenosine
RNA	Ribonucleic acid
S	Sedimentation coefficient
SDS	Sodium dodecyl sulphate
SDS- PAGE	Sodium dodecyl sulphate polyacrylamide gel electrophoresis
TBS	Tris-buffered saline
TBS-T	Tris-buffered saline with Tween
TEMED	N, N, N', N'-Tetramethyl ethylene diamine Thymidine
U	Units
UTR	Untranslated region
V	Volts
v/v	Volume
VPg	Viral protein genome-linked
w/v	Weight per volume

Viruses

AiV	Aichi virus
CV	Coxsackievirus
EMCV	Encephalomyocarditis
ERAV	Equine rhinitis virus
EV	Enterovirus
FMDV	Foot-and-mouth disease virus
HAV	Hepatitis A virus
HBV	Hepatitis B virus
HIV	Human immunodeficiency virus
HPeV	Human parechovirus
HRV	Human rhinovirus
MEV	Mengo virus
PV	Poliovirus
SAFV	Saffold virus
SVV	Seneca valley virus
TMEV	Theiler's murine encephalomyelitis virus

List of Webservers and Applications

BeAtMuSiC: (<http://babylone.ulb.ac.be/beatmusic/query.php>)

ENDscript 2: (<http://endscript.ibcp.fr>)

HotRegion: (<http://prism.cccb.ku.edu.tr/hotregion>)

jsPISA: (<http://www.ccp4.ac.uk/pisa>)

KFC2: (https://mitchell-lab.biochem.wisc.edu/KFC_Server/index.php)

PPCheck: (<http://caps.ncbs.res.in/ppcheck/>)

PredHS: (<http://predhs.denglab.org/>)

Protein Databank (PDB): (<http://www.rcsb.org/>)

Protein Interaction Calculator (PIC): (<http://pic.mbu.iisc.ernet.in/>)

PyMOL: (<https://pymol.org>)

ROBETTA: (<http://robeta.bakerlab.org/alaninescan>)

Research Outputs

Publications in peer-reviewed journals:

Onosi, O., **Upfold, N.S.**, Jukes, M.D., Luke, G.A., Knox, C., 2019. The First Molecular Detection of Aichi Virus 1 in Raw Sewage and Mussels Collected in South Africa. *Food Environ. Virol.* 11, 96–100. doi:10.1007/s12560-018-9362-4

Upfold, N., Ross, C., Bishop, Ö.T., Luke, G.A., Knox, C., 2018. The generation and characterisation of neutralising antibodies against the Theiler's murine encephalomyelitis virus (TMEV) GDVII capsid reveals the potential binding site of the host cell co-receptor, heparan sulfate. *Virus Res.* 244. doi:10.1016/j.virusres.2017.11.017

Ross, C*., **Upfold, N.S.*.**, Luke, G.A., Tastan, Ö., Knox, C., 2016. Subcellular localisation of Theiler's murine encephalomyelitis virus (TMEV) capsid subunit VP1 vis-à-vis host protein Hsp90. *Virus Res.* 222, 53–63. doi:10.1016/j.virusres.2016.06.003

* Equal authorship

Conferences:

Upfold, N. S., Ross, C., Bishop, Ö.T., Knox, C., Identifying amino acid residues that contribute to picornavirus capsid stability and assembly: A bioinformatics approach. Presented at the European Study Group on the Molecular Biology of Picornaviruses (EUROPIC), Egmond aan Zee, the Netherlands, June 2018.

Upfold, N. Theiler's Murine Encephalomyelitis Virus (TMEV) Capsid Subunit VP1 is Localised to the Perinuclear Region and Cytoplasm of Infected Cells and Colocalises with Host Protein Hsp90. Presented at the 25th South African Society of Biochemistry and Molecular Biology Congress, East London, South Africa, June 2016.

Chapter 1

General Introduction

1.1. Introduction to the Picornaviridae: classification and importance

The *Picornaviridae* comprises a heterogeneous family of small, icosahedral, positive-sense RNA viruses with global distribution (Zell, 2018). These viruses infect a broad range of vertebrates and are the causative agents of a wide variety of both mild and significant human and animal diseases (Cathcart et al., 2014). At present, the family consists of 110 species classified into 47 genera, but this number is ever increasing as new viruses are discovered (King et al., 2018; Zell, 2018). Notable genera containing pathogens of importance are the aphthoviruses, cardioviruses, enteroviruses, hepatoviruses, kobuviruses and parechoviruses (*Table 1.1*).

Picornaviruses primarily infect the tissues of the respiratory tract and gastrointestinal system, but viremia may disseminate these viruses to other tissues and organs including the central nervous system, liver and skin, where secondary infection results in diseases of clinical significance (Atmar et al., 2012; Baggen et al., 2018a; Muehlenbachs et al., 2015). The enteroviruses comprise the largest genus within the picornavirus family and are the causative agents of many disorders including the common cold, bronchitis, meningitis, pancreatitis, hand-foot-and-mouth disease, acute flaccid paralysis and poliomyelitis, that most often affect immunocompromised individuals and small children, (De Jesus, 2007; Hober and Sauter, 2010; Pons-Salort et al., 2015; Richardson and Morgan, 2018; Thibaut et al., 2016). The kobuvirus, Aichi virus 1 (AiV-1) causes gastroenteritis (Reuter et al., 2011), while infection with Hepatitis A virus (HAV), a member of the hepatovirus genus, results in hepatitis (Lemon et al., 2018). Foot-and-mouth-diseases virus (FMDV), the type species of the aphthovirus genus (King et al., 2018), infects cloven hooved animals including economically important livestock. Infection results in the blistering of oral and limb epithelia (Paton et al., 2018) as well as myocarditis in young animals which is often fatal (Gulbahar et al., 2007; Stenfeldt et al., 2016). Moreover, long term sequelae result in decreased milk and meat production leading to devastating

Table 1.1. Overview of picornavirus genera containing pathogens of importance.

Genus	Selected species	Notable strains/ serotypes	Host	Notable Diseases	Citation
<i>Aphthovirus</i>	Foot-and-Mouth Disease Virus*	Type A, C, O, SAT 1, SAT 2, SAT 3, Asia 1	Cloven hooved animals	Foot-and-Mouth Disease	(Paton et al., 2018)
	Bovine Rhinitis A Virus			Respiratory disease	(Hause et al., 2015)
	Bovine Rhinitis B Virus			Respiratory disease	(Bazanów et al., 2018)
	Equine Rhinitis A Virus			Respiratory disease	
<i>Cardiovirus</i>	Cardiovirus A*	Encephalomyocarditis virus	Mammals	Myocarditis, encephalomyelitis	(Carocci and Bakkalkassimi, 2012)
	Cardiovirus B	Saffold virus	Humans	Neurodegenerative diseases	(Gerhauser et al., 2019)
		Theiler's murine encephalomyelitis virus	Rodents		
	Cardiovirus C	Boone cardiovirus	Rodents		
<i>Enterovirus</i>	Enterovirus A	Coxsackievirus A6, A10, A16 Enterovirus A71	Humans	Hand-foot-and-mouth disease, acute flaccid paralysis, encephalitis and meningitis, neurogenic pulmonary oedema	(De Jesus, 2007; Muehlenbachs et al., 2015; Pons-Salort et al., 2015; Richardson and Morgan, 2018)
	Enterovirus B	Coxsackievirus A9, B3, B4 Echovirus 3, 6, 9		Myocarditis, pancreatitis, type I diabetes mellitus, pleurodynia, neonatal sepsis	
	Enterovirus C*	Poliovirus 1, 2, 3 Coxsackievirus A21, A24		Poliomyelitis	(Stobart et al., 2017)
	Enterovirus D Rhinovirus A, B, C	Enterovirus D68, D70		Acute haemorrhagic conjunctivitis (AHC) Respiratory diseases, AHC Common cold, exacerbations of COPD and asthma	
<i>Hepatovirus</i>	Hepatovirus A*	Hepatitis A virus*	Humans	Hepatitis /Fulminant hepatitis	(Lemon et al., 2018)
<i>Kobuvirus</i>	Aichivirus A*	Aichi virus 1	Humans	Gastroenteritis	(Reuter et al., 2011)
<i>Parechovirus</i>	Parechovirus A*	Human Parechovirus 1,3	Humans	Gastroenteritis, respiratory tract infections, encephalitis	(Olijve et al., 2018)
<i>Kobuvirus</i>	Parechovirus B	Ljungan virus	Rodents	Myocarditis (Zoonotic potential)	(Salisbury et al., 2014)
<i>Senecavirus</i>	Senecavirus A*	Seneca Valley virus 1	Porcine species	Porcine vesicular disease	(Zhang et al., 2018)

* Type species of the genus

economic losses in the agricultural industry (Tulloch et al., 2018).

The clinical and economic significance of picornaviruses has yielded decades of research into the molecular biology of these pathogenic viruses, for the purpose of developing vaccines and anti-viral therapeutics for their control. At present, effective vaccines have only been developed against Poliovirus (PV) (Bandyopadhyay et al., 2015), Enterovirus A71 (EV-71) (Yi et al., 2017) and HAV (Debing et al., 2014). Vaccines against FMDV have been developed but have exhibited varying successes in the control of different serotypes (Tulloch et al., 2018). One major hinderance to the development of potent vaccines is the instability of vaccine antigens, usually inactivated or live attenuated virus particles, that must remain intact for successful immunisation (Wang et al., 2013). Moreover, no antiviral therapies against picornaviruses are commercially available, although promising candidates targeting enterovirus capsids have been identified (Baggen et al., 2018a). These compounds work by stabilising or destabilising the virus particle thereby preventing infection (Dove and Racaniello, 2000; Lewis et al., 1998; Li et al., 2005). A comprehensive understanding of the molecular determinants involved in maintaining virus particle structure is important for designing vaccines with improved stability (Mateo et al., 2008, 2003; Mateu, 2011) and for designing antiviral compounds (De Colibus et al., 2014). The research in this thesis is primarily focused on investigating the residues that are critical to the structural integrity of picornavirus capsids.

1.2. Picornavirus genome organisation and polyprotein processing

Picornaviruses possess monopartite positive-sense single-stranded (ssRNA) genomes of approximately 7.2 to 8.5 kb, which serve as templates for translation and initial rounds of RNA replication following entry into the host cell (*Figure 1.1*) (Cathcart et al., 2014). The 5' end of the genome is covalently attached, through a phosphodiester bond, to a small peptide known as the viral linked protein (VPg) which is necessary for the initiation of viral RNA replication, while the 3' end contains a poly A tail which is thought to stabilise the viral RNA (Bedard and

Semler, 2004). Following the VPg is the 5' noncoding region or untranslated region (UTR) which comprises 8-12 % of the picornavirus genome (Stanway, 1990). The 5' UTR is highly ordered and contains a cloverleaf structure necessary for initiating the replication of viral positive sense RNA (Andino et al., 1990) and the internal ribosome entry site (IRES) required for CAP-independent translation initiation when host translation is shut off during infection (Bedard and Semler, 2004).

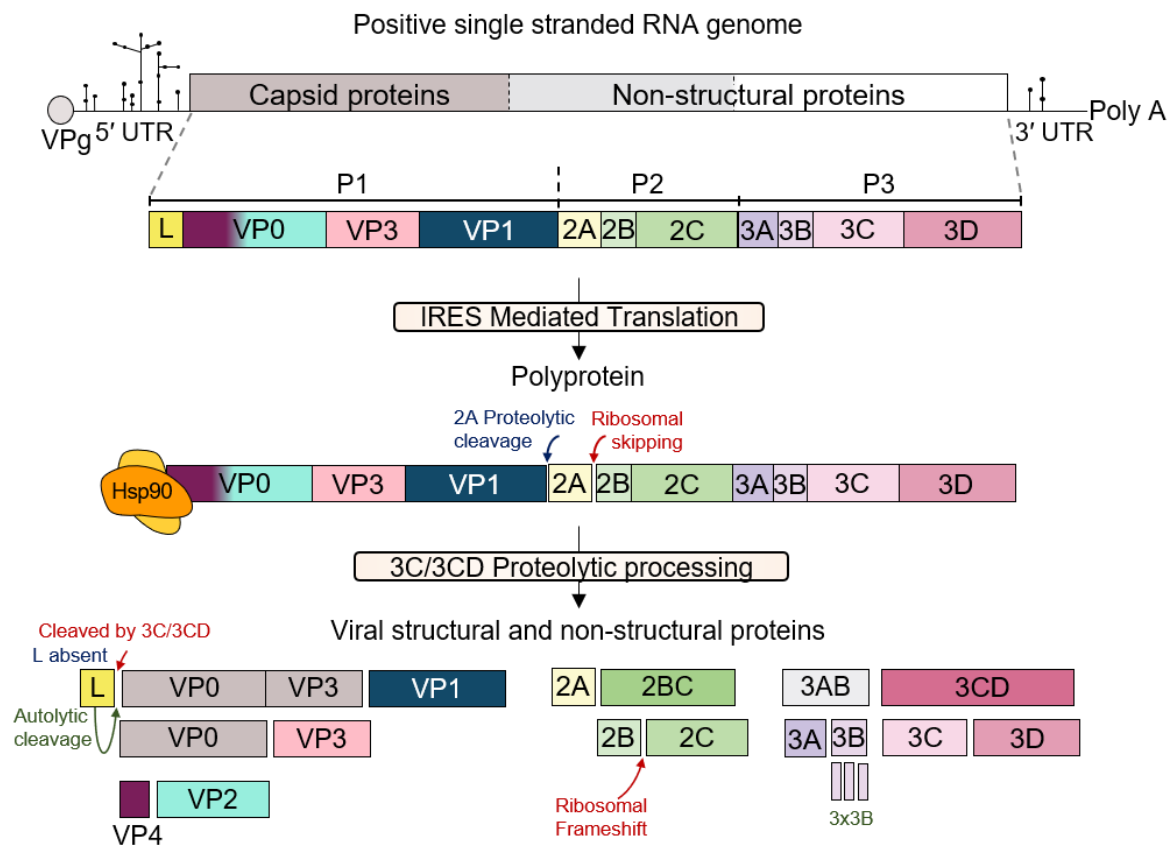


Figure 1.1 Picornavirus genome organisation and translation. The genome is translated into a single polyprotein that is separated by genus-specific events into the P1 and P2-P3 precursors. In enterovirus infection, 2A is auto-proteolytic and cleaves its own N-terminus from the rest of P1 (Sommergruber et al., 1989; Toyoda et al., 1986) (indicated in blue). In the aphtho- and cardioviruses the primary cleavage event is proteolysis-independent. Instead, a motif at the junction of 2A/B promotes ribosomal slippage, yielding P1-2A and 2B-P2-P3 (indicated in red) and 2A is subsequently removed from P1 by 3C the protease (Batson and Rundell, 1991; Brown and Ryan, 2010; Donnelly et al., 2001; Palmenberg et al., 1992). The P1 and P2-P3 precursors are then processed by the viral proteases 3CD and 3C, resulting in a set of structural and non-structural proteins (Cathcart et al., 2014). P1 cleavage depends on interactions

with the host cell chaperone Hsp90 (Geller et al., 2012). In the cardioviruses, a second short ORF overlapping the 2B-encoding sequence is translated as a result of a ribosomal frameshift. This event yields 2B*, a product comprising 11-15 N-terminal amino acids of 2B (Finch et al., 2015; Loughran et al., 2013). The L proteins encoded by the aphtho- and cardioviruses are cleaved by separate mechanisms. The aphthovirus L protein is a protease and cleaves itself from P1 (Piccone et al., 1995), whereas the L protein of cardioviruses is cleaved by the 3C protease (Borghese and Michiels, 2011). Genera specific features and events are colour-coded as green-aphthoviruses, red-cardioviruses and blue-enteroviruses. Adapted from Jiang et al. (2014); Sun et al. (2016); Zell et al. (2017).

Downstream of the 5' UTR is a single open reading frame encoding a large polyprotein divided into three domains: P1, P2 and P3. The P1 precursor encodes the virus structural proteins that assemble into the capsid, while P2 and P3 are precursors to the non-structural proteins involved in replication of the virus. Some picornaviruses such as the aphtho-, cardio-, erbo-, and kobuviruses encode an additional protein upstream of the polyprotein known as the Leader or L protein. In aphtho- and erboviruses the L protein exhibits proteolytic activity, in other genera such as cardioviruses the protein has been implicated in several mechanisms that regulate host cell antiviral responses (Borghese and Michiels, 2011; Freundt et al., 2018) and translation (Dvorak et al., 2001).

The separation of the P1 precursor from the rest of the polyprotein is the primary processing event and occurs via events that are genus-specific (Cathcart et al., 2014). The P1 and P2/P3 precursors are then further processed by 3C/3CD proteases. The requirement of host cell chaperones, particularly Hsp90, in the cleavage of P1 by 3C/3CD has been widely documented in PV, human rhinovirus (HRV), coxsackievirus (CV) and FMDV (Geller et al., 2012; Newman et al., 2017). It is thought that Hsp90 maintains the P1 precursor in a conformation that is required for successful cleavage by the protease. In PV Hsp90 has also been shown to protect newly synthesised P1 translation products from proteasomal degradation prior to capsid assembly (Geller et al., 2007).

A growing body of research is demonstrating that some of the non-structural proteins may function differently within members of the family. For example, the 2A protein of enteroviruses is a protease (Muto et al., 2006; Sommergruber et al., 1989), while the 2A protein of human parechovirus (HPeV)-1 lacks proteolytic activity and is involved in replication. HAV 2A forms part of the P1 precursor and is a signal for pentamer assembly (Probst et al., 1999, 1998), while the 2A of cardioviruses is required for localisation of the L protein to the nucleus and also inhibits host cell translation (reviewed by Yang et al. (2017)). Unlike some of the non-structural proteins, the function of the P1 structural proteins is highly conserved within the family. These proteins function to form the protective capsid in all picornaviruses.

1.3. The picornavirus particle

1.3.1. Structure of the picornavirus capsid

The general structures of picornavirus capsids are highly conserved, although there are some unique features between them. The picornavirus particle is a non-enveloped dodecahedron comprised of 60 repeating protomer subunits, arranged into a pseudo T=3 shell that encases the viral RNA genome (*Figure 1.2 A and B*). Each protomer consists of three main proteins, VP1, VP2, and VP3, that form the outer surface of the capsid and are arranged into pentameric intermediates such that five VP1 proteins meet at the five-fold axis and VP2 and VP3 proteins are placed at the two-fold and three-fold axes. The N-termini of these proteins are located on the inside of the capsid, while the C-termini are exposed at the surface. In most picornaviruses the protomer also contains a fourth smaller protein located on the inside of the capsid. This VP4 protein has little secondary structure and forms an internal network with the N-termini of VP1-VP3, which contributes to stability of the particle (Hogle, 2002).

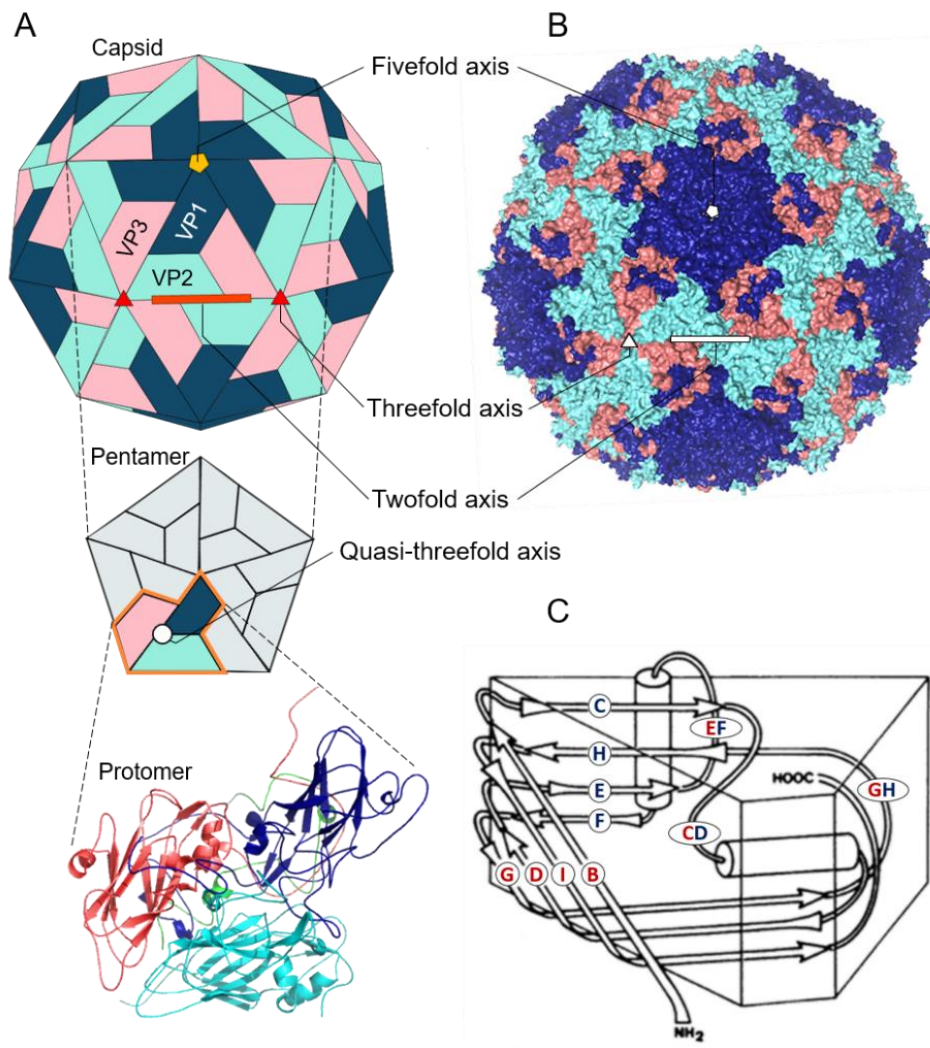


Figure 1.2 Structure of the picornavirus capsid and its subunits. A) Schematic representation of a picornavirus particle, showing the symmetry axes and the pentamer and protomer subunits - Adapted from Baggen et al. (2018a). The major capsid proteins are shown in navy blue (VP1), cyan (VP2) and salmon (VP3). The internal VP4 protein is coloured light green. B) Biological assembly of the cardiovirus Theiler's murine encephalomyelitis virus (TMEV) (PDB: 1TMF). C) Simplified diagram of the "wedge structure" conferred by the eight antiparallel β -strands, labelled alphabetically from B to H - Adapted from Hogle et al. (1985).

In most picornaviruses the N-termini of VP4 reside near the five-fold axis and each is covalently bound to a myristic acid group (Chow et al., 1987), which is thought to facilitate interaction with the host membrane for delivery of the viral RNA genome into the cytoplasm for replication (Panjwani et al., 2014; Smyth and Martin, 2002). The myristate molecules also

provide structural support and stability to the pentamer subunits (Moscufo et al., 1991); however, the specific residues involved in maintaining the interactions that provide structural support between the interfaces of pentamers, protomers and capsid proteins are less clear.

Capsid proteins VP1-3 are structurally similar, each has a wedge-shaped core that assumes an eight-stranded antiparallel β -barrel fold (*Figure 1.2 C*). The β -strands are named alphabetically starting from the N-terminus of the protein and are connected by loops whose names are derived from the β -strands they connect. These loops protrude from the capsid surface and are highly variable in length, composition and location, accounting for the differences in surface topology observed between picornavirus species and serotypes.

The loops in enterovirus capsids form two dominant structural features, a prominent star-shaped mesa, formed by the loops of converging VP1 proteins at the five-fold axis, and the three-fold propeller formed by loops belonging to VP2 and VP3 proteins at the three-fold axis. The absence of loops between these structures creates a surface depression known as the ‘canyon’ that encircles the five-fold axis (*Figure 1.3*) (Hogle et al., 1985; Muckelbauer et al., 1995; Rossmann et al., 1985). In most enteroviruses, including PV and HRV, the canyon floor opens into a hydrophobic pocket that is occupied by a lipid moiety known as the ‘pocket factor’, that maintains the stability and conformation of the particle. Dislodgement of this lipid upon receptor binding results in a cascade of conformational rearrangements required to destabilise the capsid for genome release (Plevka et al., 2013; Tuthill et al., 2007; Wang et al., 2012a). The Enterovirus D68 (EV-D68) VP3 protein contains a unique short C-terminal α -helix that forms part of the five-fold mesa resulting in a canyon that is much narrower and shallower than those of other enteroviruses (Liu et al., 2015a).

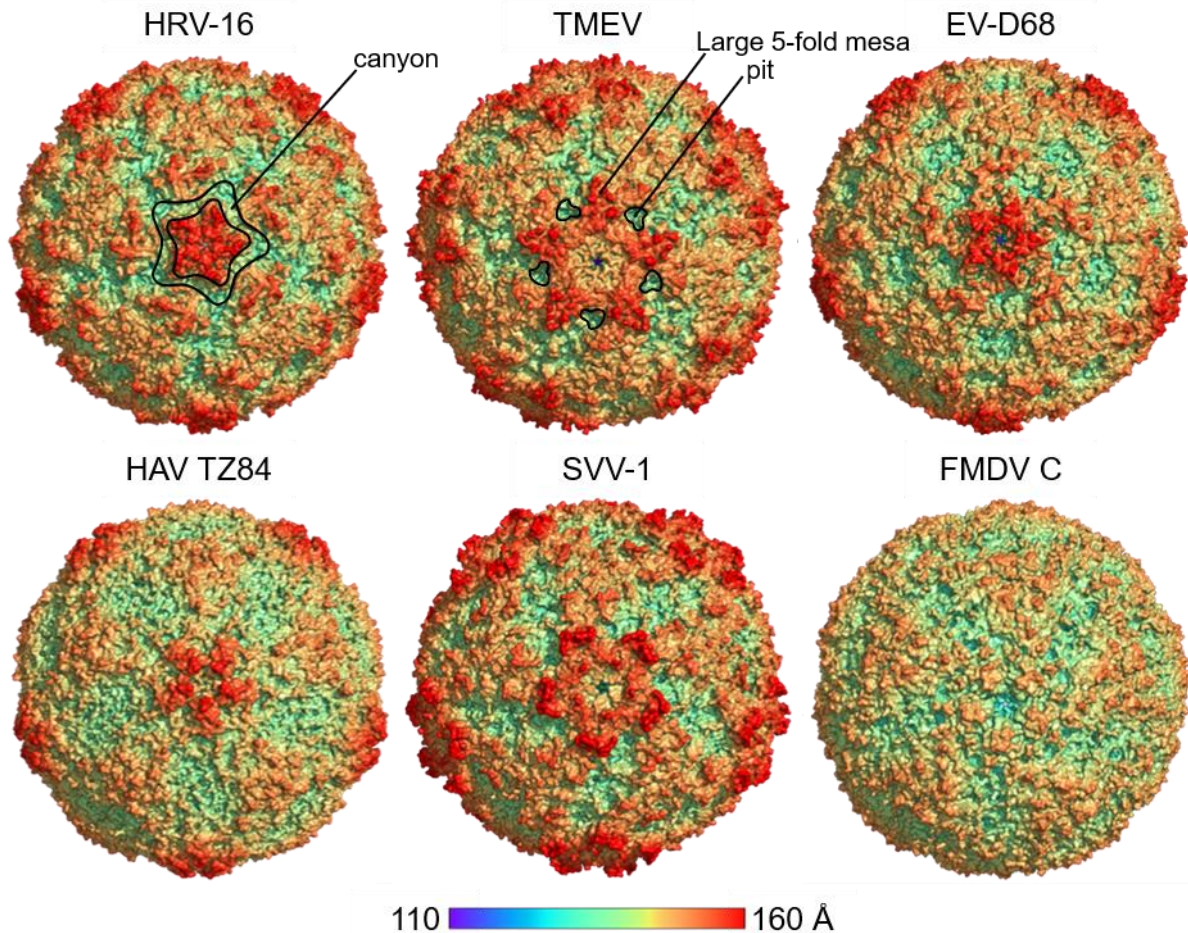


Figure 1.3 Comparison of the different capsid topologies exhibited by picornavirus genera. Enterovirus: Human Rhinovirus (HRV, PDB: 1AYN), Enterovirus D68 (EV-D68, PDB: 4WM8). Cardiovirus: Theiler's murine encephalomyelitis virus (TMEV, PDB: 1TMF). Hepatovirus: Hepatitis A virus (HAV, PDB: 5WTE). Senecavirus: Seneca valley virus 1 (SVV-1, PDB: 3CJI). Aphthovirus: FMDV Type C (FMDV-C, PDB: 1FMD). Surfaces are coloured according to their distance from the centre of the virion as shown in the colour bar.

Loops at the five-fold axis of cardiovirus capsids are much longer and partially fill in the canyon resulting in a series of small hydrophobic pits, that lack lipid factors (Grant et al., 1992; Luo et al., 1992, 1987). In Seneca Valley Virus 1 (SSV-1), the canyon is almost completely enclosed by VP1 residues and most loops belonging to proteins VP1-3 are longer than those of other viruses of the family, giving rise to elevated structures surrounding the five-fold axis (Venkataraman et al., 2008). Both HAV and FMDV capsids are devoid of canyon or pit

structures; the HAV capsid has shallow five- and three-fold surface structures creating an angular appearance, while the absence of protruding loops on the FMDV capsid results in a smooth spherical surface (Acharya et al., 1989; Wang et al., 2015). Besides imparting unique capsid topologies to different members of the picornavirus family, surface exposed loops are functionally important as they contain receptor binding sites as well as major neutralisation epitopes and thus directly influence virus host range, tropism and pathogenesis (Mateu, 1995; Rossmann et al., 2000; Tuthill et al., 2010).

1.3.2. Structure and antigenicity

Investigations into the antigenicity of picornavirus capsids have mapped immunodominant epitopes to the VP1 protein (Cameron et al., 2001; Collen et al., 1991; Edlmayr et al., 2011; Lim et al., 2012; Luo et al., 1992; Mateu, 1995; Nitayaphan et al., 1985; Oberste et al., 1999; Wu et al., 2002), although antigenic sites are found on the protruding loops of all surface exposed capsid proteins (Chong et al., 2012; Kiener et al., 2014; Meloen et al., 1983; Ren et al., 2015; Westerhuis et al., 2015). Neutralisation sites present on VP1 have been mapped to the N- and C-termini as well as the EF and GH loops of equine rhinitis virus (ERAV) VP1 (Horsington et al., 2012; Varrasso et al., 2001), the C-terminus, EF and GH loops of CV-A16 (Ren et al., 2015; Shi et al., 2013), DE loop of EV-D68 and the GH loops of EV-71 (Ku et al., 2015) and FMDV (Collen et al., 1991). In TMEV, neutralising epitopes have been mapped to the CD I and II loops and C-terminus of VP1 (Ohara et al., 1988; Zurbriggen and Fujinami, 1989), as well as puffs A and B of the EF loop in VP2 (Inoue et al., 1994; Sato et al., 1996).

PV exists as three serotypes, each expressing a unique set of major and minor neutralisation sites (Jiang et al., 2014). Conversely, HRV and FMDV constantly evolve new neutralisation sites and thus exist as a plethora of serotypes and subtypes, posing a difficult challenge for both vaccine design and efficacy (Papi and Contoli, 2011; Stobart et al., 2017; Tulloch et al., 2018). Furthermore, some picornavirus procapsids, empty virus particles, and disassembly products

generated through uncoating and dissociation are antigenically distinct from the mature particle, thus vaccines containing robust particles with some resistance to dissociation are required to preserve their efficacy (Hogle, 2002; Malik et al., 2017; Porta et al., 2013; Shingler et al., 2015; Zheng et al., 2019).

1.3.3. Capsid assembly and RNA encapsidation

The assembly of picornavirus capsids occurs through the stepwise oligomerisation of protein subunits (*Figure 1.4*). Following the co-translational separation of P1 from P2, Hsp90 associates with P1 (Geller et al., 2007) and maintains the capsid precursor in a conformation required for proteolysis by the viral encoded 3C/3CD protease to yield VP0, VP1 and VP3 (Palmenberg, 1990). These protein subunits remain associated as the 5S protomer, the smallest unit of the capsid (Bruneau et al., 1983). Five protomers then associate to yield the pentamer complex which has a sedimentation coefficient of 14S. This is followed by the assembly of 12 pentamers into the RNA containing, non-infectious 150S provirion (Guttman and Baltimore, 1977).

The exact mechanism of RNA encapsidation remains contentious. The currently accepted model proposes that the replicating viral RNA acts as a scaffold around which the pentameric units condense to form the provirion (Jiang et al., 2014). However, some picornaviruses including aphthoviruses (Grubman et al., 1985; Rowlands et al., 1975), enteroviruses (Cifuentes et al., 2013; Korant et al., 1975; Marongiu et al., 1981; Su and Taylor, 1976), hepatoviruses (Zhu and Zhang, 2015), but not cardiociruses (Jiang et al., 2014), have been shown to also form empty 75S procapsids (Koch and Koch, 1985). Thus, an alternative encapsidation model was proposed where the procapsid is an assembly intermediate into which the viral RNA is subsequently inserted through an unknown viral mechanism (Jacobson and Baltimore, 1968; Jiang et al., 2014; Li et al., 2012; Verlinden et al., 2000). Moreover, purified pentamers can

self-assemble into empty procapsids in a cell-free test tube environment, suggesting that the assembly of pentamers into procapsids is based on protein-protein interactions and has no

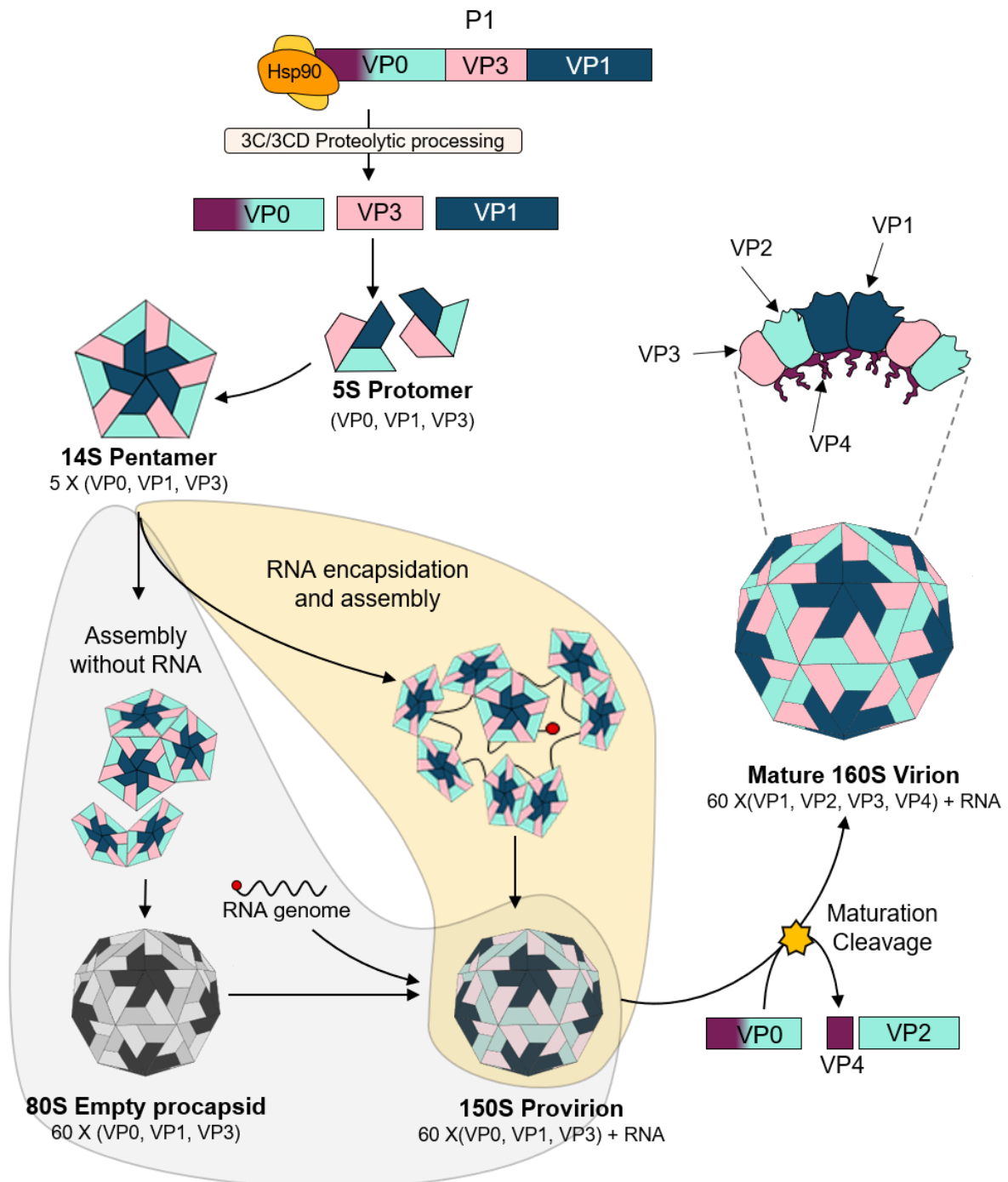


Figure 1.4 The stepwise assembly of picornavirus particles. Following separation from the rest of the polyprotein, Hsp90 maintains P1 in the correct conformation for cleavage by the 3CD and 3C proteases. The resulting VP0, VP1 and VP3 capsid proteins immediately form the protomer, of which five combine to yield the pentamer. The accepted encapsidation model suggests that 12 pentamers then

condense around the viral RNA to form the 150S procapsid (highlighted in yellow). Alternatively, twelve pentamers assemble without inclusion of the genome to yield empty 80S procapsids, into which the RNA genome is inserted (highlighted in grey). In a final maturation step, VP0 is cleaved yielding the outer facing VP2 capsid protein and the internally oriented VP4 protein. Adapted from Jiang et al. (2014) and Ross et al. (2016).

requirement for host cell factors (Li et al., 2012). However, the exact residues involved in forming these interactions between the assembling pentamers remain unknown.

Several alternative explanations for the purpose of empty procapsids have been proposed (Ansardi et al., 1996; Basavappa et al., 1994; Fernandez-Tomas and Baltimore, 1973; Li et al., 2012; Marongiu et al., 1981; Verlinden et al., 2000). One suggestion is that they are by-products of the assembly process (Koch and Koch, 1985; Li et al., 2012), or a mechanism for deterring viral recognition by neutralising antibodies, as they are antigenically distinct (Shingler et al., 2015). Most lines of evidence such as the RNA binding activity of pentamers but not procapsids (Nugent and Kirkegaard, 1995; Pfister et al., 1995; Verlinden et al., 2000) and the fact that empty procapsids, unlike pentamers, are not always observed during picornavirus infection (Putnak and Phillips, 1981), support the first model of simultaneous assembly and encapsidation. Furthermore, Shakeel et al. (2016) recently identified 60 identical contacts in HPeV-3 between packaging signal motifs in the ordered viral RNA and residues of the internal residues of VP1 and VP3, suggesting that binding of the folding RNA to these residues could mediate assembly of the capsid. Further experimentation revealed that disruption of the residues involved in these contacts negatively affected HPeV-3 capsid assembly (Shakeel et al., 2017). Signals essential for genome encapsidation have also been identified in the RNA genomes of AiV-1 (Sasaki and Taniguchi, 2003) and more recently FMDV (Logan et al., 2018). No such signal has been identified for PV, however, the non-structural 2C protein has been shown to mediate interactions between the genome and capsid that are required for encapsidation (Adeyemi et al., 2019; Liu et al., 2010; Wang et al., 2012b).

The role of RNA folding in encapsidation and assembly of other picornaviruses remains unknown. The viral RNA genome is not only required for virion infectivity; the N and C termini of VP1 and VP4 in RNA containing capsids are more ordered than in empty capsids. The ordered termini strengthen interactions within and between protomers, imparting increased stability to the capsid (Curry et al., 1997).

The final step in the assembly cascade is the cleavage of VP0 to VP2 and VP4 in a process known as maturation, which is requisite for infectivity (Ansardi and Morrow, 1995; Jiang et al., 2014). Evidence suggests that for most picornaviruses, excluding FMDV (Curry et al., 1997), maturation cleavage is autocatalytic and dependent on RNA encapsidation (Jiang et al., 2014). Provirions are highly unstable, but cleavage of VP0 triggers conformational rearrangement of the particle into a dynamically metastable virion with increased stability for survival in the harsh extracellular environment (Hindiyeh et al., 1999). Specifically, the separation of the VP2 and VP4 termini following cleavage allows for strong contacts to form between these ends, that reinforce the interactions between pentamer subunits (Curry et al., 1997). The stability of mature capsids can be diminished by conformational changes that occur at the protein structural level. Receptor binding or other chemical mechanisms induce these changes allowing for controlled destabilisation and genome release. Premature destabilisation of the capsid or prevention of the conformational changes that lead to uncoating directly jeopardise viral infectivity; however, the identities of the residues between neighbouring capsid subunits that are critical for modulating the conformational stability of these capsids remain unknown.

1.4. Receptor binding and uncoating

1.4.1. Receptor binding

Host cell receptor recognition is essential for virus binding and entry and is one significant determinant of viral tropism and pathogenesis (Baggen et al., 2018b; Tuthill et al., 2010). The

vast repertoire of receptors exploited by picornaviruses includes members of the immunoglobulin-like superfamily (Baggen et al., 2018b; Greve et al., 1989; Martino et al., 2000; Mendelsohn et al., 1989; Wei et al., 2016), integrin receptor family (Jackson et al., 2004, 2002, 2000; Merilahti et al., 2016; Monaghan et al., 2005; Triantafilou et al., 2000), low density lipoprotein receptor (LDLR) family (Hofer et al., 1994; Vlasak et al., 2005) and complement control proteins (Bergelson et al., 1994). The large variation in different receptors explains the differences in cell tropism, pathogenesis and the broad range of diseases caused by these viruses (Schneider-Schaulies, 2000). Studies have provided evidence that differences in pathogenesis and cell tropism between TMEV strains are associated with variation in receptor usage (Lipton et al., 2006). Neurovirulent strains such as GDVII make use of the proteoglycan heparan sulphate as a co-receptor, whereas persistent strains use α 2,3-linked N-acetylneuramic acid (sialic acid) (Lipton et al., 2006; Shah and Lipton, 2002).

Based on their functional role, receptors can be classified as “attachment” or “uncoating” receptors. Attachment receptors are solely involved in binding and attachment of the virus to the host cell and may be involved in virus entry. In addition to virus attachment and entry, uncoating receptors induce conformational changes upon binding that lead to destabilising rearrangements of the capsid proteins associated with uncoating and genome release. Several picornaviruses (Tuthill et al., 2007), exploit additional receptors (co-receptors) for the purpose of improved host cell attachment, but they play no role in uncoating (Baggen et al., 2018b; Shafren et al., 1997). For example, DAF binding merely facilitates the attachment of group B coxsackieviruses to host cells and triggers events that expose the CAR receptor, which is the primary receptor that induces capsid instability (Coyne and Bergelson, 2006).

The solving of the structures of several picornaviruses complexed with their receptors (Belnap et al., 2000; Fry et al., 1999; He et al., 2001; Kolatkar et al., 1999; Olson et al., 1993) has greatly improved the understanding of virus-receptor interactions. The receptor binding site in

many enteroviruses is the canyon and the lipid containing pocket at its base. The receptor and pocket factor cannot be simultaneously bound to the capsid as they share a common binding site (Rossmann, 1989; Smith et al., 1986). Thus, competitive binding of the receptor to the hydrophobic pocket dislodges the lipid moiety allowing interaction of the receptor and the capsid (Rossmann et al., 2002). For example, a recent study by Zhao et al. (2019) identified the uncoating receptor of major enterovirus B as human neonatal Fc receptor (FcRn), and found that binding of FcRn to the FCGRT subunit in the canyon, under acidic conditions, dislodges the pocket factor which induces the conformational rearrangements required for uncoating. The canyon binding site is conserved in most enteroviruses, the manner in which the various enterovirus receptors bind it is not. For example the PV CD155 receptor and SCARB2 receptor of EV-71 bind to different residues in the walls of the canyon (Belnap et al., 2000; Zhou et al., 2019). Moreover, several receptors of minor HRV serotypes, echoviruses and some coxsackie B viruses do not bind the canyon at all. Decay-accelerating factor (DAF) used by echoviruses and CV-B3, binds near to the two-fold axis at the pentameric interface (Pettigrew et al., 2006; Plevka et al., 2010), while very-low-density-lipoprotein (vLDLR) binds to VP1 residues at the five-fold axes of HRV2 (Hewat et al., 2000).

Little is known about cardiovirus receptor binding. Cardiovirus capsids have a series of smaller surface depressions analogous to the central region of the canyon in the enteroviruses (Luo et al., 1996, 1987). These pits are the putative receptor binding sites, although the identities of almost all cardiovirus receptors remain unknown (Mullapudi et al., 2016). Encephalomyocarditis Virus (EMCV)-D is the only cardiovirus for which a primary host cell receptor (Vascular cell adhesion molecule 1 (VCAM-1)) has been identified (Huber, 1994), although the co-receptors used by TMEV strains have been recognised (Lipton et al., 2006; Reddi et al., 2004; Shah and Lipton, 2002). The receptor binding pits are formed between the protomeric interfaces and the quasi-three-fold axes and involve residues from the VP1 and VP3

proteins belonging to separate protomers. The GH loop belonging to VP3 is located within the centre of the pit, and the C-terminus of VP1 forms a large loop that extends over the pit (Luo et al., 1992).

The receptors of other picornaviruses bind to various regions and features of the capsid. For example, the SVV-1 anthrax toxin receptor 1 (ANTXR1) was recently found to interact with various sites on the capsid surface including the surface-exposed BC loop of VP1, the puff of VP2 at the quazi three-fold axis, and the knob of VP3 located near the three-fold axis (Jayawardena et al., 2018). Surface exposed loops are also important binding sites in other viruses for example, the integrin receptors of field strains of FMDV (Monaghan et al., 2005) bind to the GH loops of VP1 via an arginine-glycine-aspartate (RGD) sequence (Acharya et al., 1989; Logan et al., 1993).

1.4.2. Uncoating cues

Virus capsids must be stable enough to protect the fragile RNA genome during cell-to-cell transmission but must also be capable of structural destabilisation to allow the release of the genome for the next round of infection (Mateo et al., 2003). To prevent the untimely release of the viral genome, viruses have evolved to rely on host cell signals to destabilise the capsid (Tuthill et al., 2010, 2007). In picornaviruses, receptor binding and/or endosomal acidification are the initiation cues for this uncoating process. For most enteroviruses, receptor binding to residues in the canyon displaces the pocket factor triggering the collapse of the hydrophobic pocket and the cascade of conformational changes that lead to capsid expansion and genome release (Dang et al., 2014; Hogle, 2002; Liu et al., 2015b; Ren et al., 2013). In some enteroviruses, receptor binding occurs away from the canyon leaving the lipid moiety intact (e.g. LDLR and DAF binding species) (Hewat et al., 2000; Plevka et al., 2010; Shakeel et al., 2013). Consequently, in many of these viruses uncoating rearrangements are triggered instead by exposure to low endosomal pH (Liu et al., 2018; Prchla et al., 1994). In the capsids of

aphtho- and cardioviruses, the canyon is absent (Acharya et al., 1989; Luo et al., 1992, 1987; Mullapudi et al., 2016; Tuthill et al., 2009) and uncoating is also dependent upon acidification within early or late endosomes (Berryman et al., 2005; Tuthill et al., 2009). Other picornaviruses require receptor binding in conjunction with low pH for successful capsid uncoating. For example, in EV-71 the conformational capsid rearrangements that lead to capsid expansion and RNA release depend on both SCARB2 binding and the acidic environment within endosomes (Dang et al., 2014; Yamayoshi et al., 2013).

1.4.3. Uncoating intermediates and end products

The pathways of picornavirus uncoating remain poorly understood and many details regarding the site of RNA release from the capsid remain unclear. The uncoating of picornavirus capsids appears to occur by one of two main mechanisms, either via a cascade of conformational changes that gradually destabilise the particle through a series of uncoating intermediates, such as in the enteroviruses, or through the rapid disassembly of virus particles into pentamers and naked genomic RNA, as in members of the aphthovirus genus (Tuthill et al., 2007).

PV capsids are dynamic molecular structures that undergo recurrent expansion and contraction coupled with the transient exposure and concealment of VP4 and the N-terminus of VP1, in a process known as “breathing” (Li et al., 1994). Binding of PV to its CD155 receptor induces internalisation of the particle by endocytosis (Brandenburg et al., 2007) and simultaneously triggers conformational changes within the capsid, that lead to the irreversible formation of the expanded early-RNA release intermediate, termed the “A” particle (Hogle, 2002). In these particles VP4 and the N-terminus of VP1 have been permanently externalised, but the viral RNA genome remains intact. The A particle has a different sedimentation coefficient to the native particle (135S compared to 160S of the native capsid), is more sensitive to protease degradation, and is antigenically distinct from the native capsid (Tuthill et al., 2007). Furthermore, the A particle is more hydrophobic due to the externalisation of myristic-VP4

and the N-terminus of VP1, which interact with the late endosomal membrane forming a pore for the release of the viral genome into the cytosol (Fricks and Hogle, 1990). The remaining 80S empty viral capsid is no-longer infectious and is the end product of the uncoating process (Hogle, 2002).

For efficient genome release the RNA must exit through a single site on the A particle surface. Originally, this site was proposed to be located at the five-fold axis of the particle (Hadfield et al., 1997; Hendry et al., 1999; Rossmann et al., 2000), but the recent accumulation of the cryo-EM structures of several enterovirus uncoating intermediates, including those for CV-A9 (Shakeel et al., 2013), CV-A16 (Ren et al., 2013), EV-71 (Lyu et al., 2014; Wang et al., 2012a), HRV-A2 (Pickl-Herk et al., 2013), HRV-B14 (Dong et al., 2017), PV (Butan et al., 2014) and EV-D68 (Liu et al., 2018) has revealed the formation of distinct pores at the two-fold axis and smaller holes at the quazi three-fold axis, suggesting that the site of RNA release may actually be between pentamer subunits. Bostina et al. (2011) produced asymmetric cryo-EM reconstructions of the various stages of RNA release from PV capsids, and were able to confirm that RNA is released near the two-fold axis and not channels at the five-fold. However, Lee et al. (2016) captured the asymmetrical uncoating of CV-B3 bound to membranes, using lipid bilayer nanodiscs and the virus receptor. This study identified an opening at the three-fold axis, between three pentamers, and not at the two-fold. This finding may be more biologically relevant as uncoating stimuli are likely to induce asymmetrical uncoating of the capsid during *in vivo* infection.

It has long been hypothesised that the uncoating of aphtho- and cardioviruses capsids occurs differently, where acidification within endosomes results in the rapid and direct dissociation of the native particle into pentameric subunits and naked genomic RNA without the formation of intermediate particles. The recent identification of transient uncoating intermediates following the acid exposure of ERAV (Bakker et al., 2014; Tuthill et al., 2009) and heat exposure of the

human coronavirus Saffold virus 3 (SAFV-3) (Mullapudi et al., 2016), suggests otherwise. Tuthill et al. (2009) identified intact empty particles with a sedimentation coefficient of 80S that preceded dissociation of the virion into pentamers. Unlike enterovirus A particles, the 80S intermediate did not contain two-, three- or five-fold pores, was not expanded, and had an overall structure that was very similar to the native particle. There were, however, rearrangements to the elements crucial for stabilisation of the pentamer interfaces (Tuthill et al., 2009). Mullapudi et al. (2016) induced the formation of SAFV-3 expanded particles by heating native capsids to 42 °C. These particles were very unstable and readily disassembled into pentamer subunits. Like the A particles of enteroviruses, the altered SAFV-3 particles had an increased radius of ~4 %, but pores were formed at the interfaces between protomers running from the five-fold to the three-fold axes, rather than at the two-fold axes. Formation of these pores involved rearrangements between a VP1 protein from one protomer and the VP1 and 3 proteins from the neighbouring subunit. Interestingly the pores overlap the five-fold pits that are thought to be putative receptor binding sites in coronaviruses (Luo et al., 1992). The identification of these structures in another two genera suggests that formation of uncoating intermediates may be a conserved feature during the uncoating of all picornaviruses.

The sizes of the pores formed in the A particles of enteroviruses and the expanded SAFV-3 capsids would not allow passage of the viral RNA from the virus without the assistance of mechanisms that relax the double-stranded segments, formed through secondary structure folding of the genome. Recently, Buchta et al. (2019) revealed that RNA release in echoviruses 18 and 30 involves the loss of at least one pentamer subunit from the particle, forming an opening that enables the release of the genome without the modification of double-stranded elements. Structures of these open particles were not dissimilar to the viruses' A particles, as both were expanded, had lost VP4, contained two-fold pores and had reduced inter-pentamer contacts (Buchta et al., 2019). Intermediate particles lacking pentamers but still containing

genomic RNA were also detected when HRV-2 was exposed to acidic conditions (Harutyunyan et al., 2013). Thus, a new scheme for enterovirus release was proposed. Firstly, receptor binding or exposure to low pH within endosomes triggers formation of the A particle, with reduced pentamer-pentamer contacts. Secondly, changes in the structure of the internal RNA, through exposure to acidic pH, put pressure on the remaining pentamer contacts. Together this triggers the expulsion of pentamers, resulting in the formation of open particles that allow rapid RNA release (Buchta et al., 2019). If confirmed, the loss of at least one, more (enteroviruses) or all (aphtho- and cardioviruses) pentamers would be a conserved feature during the uncoating of picornaviruses.

1.5. Capsid stability

1.5.1. The molecular determinants of picornavirus capsid stability

Virus capsids, such as those belonging to picornaviruses, are large multimeric assemblies, generated through the consecutive oligomerisation of protein subunits. The extensive network of non-covalent interactions between the viral structural subunits is imperative for the self-assembly, structural integrity and stability of the capsid (Li et al., 2012; Mateo et al., 2008, 2003; Mateu, 2013; Reguera et al., 2004). These inter-subunit interactions must impart enough strength to the capsid so that it may withstand denaturing conditions in the extracellular environment, yet not so much as to impair the conformational changes triggered by receptor binding and/or low pH that permit capsid dissociation and genome release (Bostina, 2019; Ellard et al., 1999; Mateo et al., 2003; Rincón et al., 2014; Veessler and Johnson, 2012). In response to these conflicting requirements, capsid subunit recognition has evolved as a fine-tuned balance, influenced by the forces imposed by a virus's lifecycle (Mateu, 2013; Rincón et al., 2014). As such, the inherent biophysical stability of viruses within one family, such as the picornaviruses, can be markedly different. For example, most enteroviruses are stable between pH 2.5 and 12 (Fry et al., 2003; Tuthill et al., 2010). These viruses rely on receptor binding to

induce conformational changes that lead to genome release (Baggen et al., 2018a). FMDV on the other hand, relies on acidification within early endosomes to induce capsid dissociation and RNA release (Yuan et al., 2017). As such these viruses, particularly O and SAT serotypes, are remarkably labile and readily dissociate in mildly acidic conditions close to neutrality (Scott et al., 2019; Yuan et al., 2017).

Importantly, residues involved in the interactions between proteins are not equally relevant for the conformational stability of the interface. Rather, a small fraction of moderately conserved residues termed “hotspots” contribute significantly to the binding energy, specificity and stability of the protein association (Bogan and Thorn, 1998; Clackson and Wells, 1995; Keskin et al., 2005; Moreira et al., 2007). Given the importance of hotspot residues in subunit interactions and their contribution to capsid assembly and stability (Bahadur and Janin, 2008; Boyd et al., 2015; Cheng and Brooks, 2015; Mateu, 2009), their identification would likely broaden the knowledge surrounding aspects of the virus lifecycle including morphogenesis, uncoating and genome release. Moreover, this knowledge could be applicable to the rational design of novel antivirals and the production of stable virus particles for use in biotechnology and medicine (Mateu, 2011; Wen et al., 2013).

1.5.2. Mutational studies of hotspot prediction

Several studies have attempted to identify these residues and their contribution to capsid assembly, stability, uncoating and virion infectivity in the picornaviruses (Airaksinen et al., 2001; Biswal et al., 2016; Caridi et al., 2015; Ellard et al., 1999; Maree et al., 2013; Rincón et al., 2015, 2014; Wang and Smith, 2005; Warwicker, 1992). In two separate studies, Rincón et al. (2003) and Mateu et al. (2015) systematically analysed the importance of 48 and 42 residues whose sidechains contribute to interprotomer and interpentamer interactions respectively, using charged-to-alanine scanning of infectious FMDV cDNA clones (Mateu et al., 2003; Rincón et al., 2015). The results revealed that while most of the amino acid residues involved

in interactions between protomers are not essential for FMDV infectivity, most of those involved in pentamer-pentamer interactions are. The authors suggested that given the large number of protein-protein interactions between protomers, the loss of one important interaction might not be sufficient to weaken the entire interface. Conversely, the removal of even one sidechain contributing to an interaction between pentamers may be more deleterious as there are far fewer interactions across these interfaces (Mateo et al., 2003; Rincón et al., 2015).

Recently, charged-to-alanine scanning was applied to identify residues important for capsid assembly and cell entry in EV-71 (Yuan et al., 2016). Following the mutational analysis of 27 positively charged residues belonging to VP1, Yuan et al. identified 16 substitutions that were non-viable, and seven amino acid substitutions that were replication defective. Upon serial passage, ten revertants or mutants with second site mutations in VP1 were isolated, supporting the importance of these residues within the virus lifecycle. One residue that proved essential for virus viability, K182, is conserved within EV A and D species. K182 was previously shown to form an elaborate network of hydrogen bonds with VP1 D185 from the neighbouring protomer which stabilises the five-fold axes during uncoating (Lyu et al., 2014). Another amino acid substitution, K215A, was replication defective, but drastically increased the thermostability of the capsid. This residue resides on the GH loop which is involved in major conformational changes following receptor binding, thus Yuan et al. (2016) speculated that the amino acid substitutions impaired movement of the loop and formation of uncoating intermediates.

The stability and dynamics of the HRV-B14 capsid were investigated by Wang and Smith (2005). Using hydrogen exchange and mass spectrometry, the authors found that the interfaces between two protomers, specifically interactions between VP1 and VP3, were very stable, but that VP4 and the N-terminus of VP1 as well as the interfaces surrounding the five-fold axes were not (Wang and Smith, 2005). The externalised VP1 N-terminus of EV is known to play a

functional role in the uncoating and entry of these viruses and contains an 11 residue motif that is highly conserved (Airaksinen et al., 2001). Residues within this motif form interprotomer contacts with residues of the surrounding VP2-4 capsid proteins, which are also highly conserved (Hendry et al., 1999; Hogle et al., 1985; Lentz et al., 1997; Muckelbauer et al., 1995). Airaksinen et al. (2001) dissected the effects of amino acid substitutions within this motif on the capsid stability of CV-A9 and found that two substitutions, A30S and V31I, partly increased particle lability, while substitutions A30G and V34A led to highly unstable capsids that readily formed 135S intermediate particles. This study suggests that the residues within the motif participate in maintaining the ideal balance of stability, preventing the premature or delayed externalisation of the VP1 N-terminus, and the uncoating rearrangements that follow (Airaksinen et al., 2001). In another study, Couderc et al. (1996) found that substitutions T22I in VP1 and S31T VP2 altered PV-1 capsid stability. T22I belongs to the N-terminus of VP1 that is expelled during entry, while T31 forms part of the pentameric interface that is important for capsid stability. These viruses could more readily undergo conformational changes required for uncoating, and capsid assembly was less efficient, but resultant virions were more thermolabile (Couderc et al., 1996)

1.5.3. Evolutionary selection of mutants with improved stability

Additional studies have selected virions with increased resistance to various destabilising factors using an evolutionary approach. Glutathione (GSH) is an essential stabilising cofactor during the assembly of EV protomers into pentameric subunits (Thibaut et al., 2014). Using the inhibitor TP219, Thibaut et al. (2014) serially passaged CV-B3 at reduced GSH levels and isolated GSH-resistant mutants that had a single amino acid substitution, T77M, in VP1. This residue belongs to the interprotomer interface and is surface exposed. Using another GSH inhibitor, BSO, Ma et al. (2014) assessed the capsid stabilities of PV-1 and CV-A20 under decreased GSH levels. Resistant PV mutants contained residue substitutions D219N, I239V

(VP1) and Q178L and T175A (VP3), while only one residue, Y97H (VP3), conferred resistance to CV-A20 mutants. These stabilising amino acid substitutions were also located at interfaces between protomers (Ma et al., 2014). Numerous studies have attempted to map the molecular determinants of the pH stability of FMDV by sequentially passaging FMDV at various pH values (reviewed by Yuan et al. (2017)). Collectively these studies identified residues at interprotomer and interpentamer (two- and three-fold axes) interfaces (Yuan et al., 2017).

1.5.4. Computational assessment of stabilising residues

Very few studies have computationally assessed the molecular determinants of capsid stability. Van Vlijmen et al. (1998) calculated the electrostatic energies as a function pH for FMDV O1BFS, A1061 and A22 Iraq. The study found that residues within 15 Å of the pentamer-pentamer interfaces are involved in the acid stability of these viruses. Furthermore, the study revealed that VP3 residues H142 and H145 are important for acid stability because of their many interactions with polar residues across the pentameric interface (van Vlijmen et al., 1998). Warwicker assessed the HRV-B14 capsid using the same approach and found that upon acidification, arginine, histidine and lysine residues surrounding the canyon and the pentamer interfaces had the strongest destabilising energies, and therefore contribute significantly to stability of the capsid (Warwicker, 1989). In a recent study, Ross et al. used normal mode analysis and perturbation response scanning to investigate the motions of EV-71 uncoating. One interesting finding is that during expansion to the A particle pentamers move in an anti-clockwise screw-like motion around the three-fold axis (Ross et al., 2018), which likely assists the separation of interacting VP2 residues across the two-fold axis so that pore formation can occur. Furthermore, the study identified highly flexible regions containing the residues VP1 131-155, 163-193, 233-257, VP3 1-31 and VP4 12-42. These residues are located near to the five-fold axes and expand towards the hydrophobic pocket, which is known to change its

conformation during uncoating. Additional residues showing various degrees of flexibility were noted at the five-fold interface between VP1 and VP3, which is known to be important for capsid assembly, and in the VP4 protein, which is proposed to interact with the viral RNA (Ross et al., 2018).

1.5.5. Modulating capsid stability for improved vaccines

The development of vaccines has been imperative for the control of several devastating viruses, including PV (Wang et al., 2013). A major hinderance to the development of vaccine antigens is the conformational instability of virus particles (Mateu, 2011). The preservation of antigenicity depends on the inherent stability of the viral capsid, as destabilised particles have different antigenic properties to infectious virions (Wang et al., 2013). To preserve antigenicity, vaccines require refrigeration during delivery and storage, which is not always possible and accounts for 80 % of the total cost of vaccination programs (Chen et al., 2011a; Tulloch et al., 2018). FMDV readily dissociates into pentamers above physiological temperatures and at mildly acidic conditions (Yuan et al., 2017), resulting in subunits that do not stimulate sufficient levels of protective neutralising antibodies (Doel and Baccarini, 1981). An understanding of the molecular determinants of the lability of virus particles, such as FMDV, is pertinent to the design of vaccine antigens with improved resistance to dissociation (Mateu, 2011). To this purpose, several investigations have probed the importance of specific residues to the stability, assembly and growth of FMDV. Identification of these indispensable residues in capsid subunit interfaces using *in vitro* alanine scanning (Mateo et al., 2003), provided a guide for the rational design of FMDV capsids with improved thermostability without negative implications for biological fitness (Mateo et al., 2008).

In a separate study, Rincón et al. (2014) found that electrostatic repulsions between the negatively charged residues at pentameric interfaces are responsible for the sensitivity of FMDV to thermal dissociation. With this in mind, the authors engineered a series of infectious,

genetically stable and antigenically identical virions with increased thermostability, by altering the residues involved in the electrostatic repulsions. Other studies have also rationally improved the stability of FMDV capsids by strengthening the interactions across pentamer-pentamer interfaces (Porta et al., 2013). Through molecular dynamics simulations, Kotecha et al. (2015) and Scott et al. (2017) identified amino acid substitutions that form stronger interactions across the two-fold interfaces thereby increasing the stability of pentamer-pentamer complexes in FMDV Type O and SAT2 capsids. Using these findings, the authors engineered a number of recombinant capsids with improved pH and heat stability that could elicit equivalent or higher virus neutralising antibody titres than the parental viruses, as potential vaccine candidates (Kotecha et al., 2015; Scott et al., 2017). The substitution S93Y in VP2 conferred the greatest increase in thermostability to the SAT2 capsid but had a reduced growth rate and slightly altered antibody footprint. Mutants containing the substitution S93H also showed increased stability against thermal dissociation, thus the authors selected these mutants as vaccine antigens for future investigation (Scott et al., 2017).

Virus-like particles (VLPs) offer an alternative approach to live-attenuated and inactivated vaccines for which biosafety concerns remain (Bhasin, 2008; Marsian et al., 2017). Enterovirus VLPs have moderately different antigenic properties and overall stabilities compared to the native particles, which are stabilised by both the genome and maturation events (Baggen et al., 2018a). Recently, Fox et al. (2017) engineered stable empty capsids for all three serotypes of PV, by introducing residue substitutions that were previously shown to stabilise the capsids of each PV serotype. The resultant particles were thermostable and induced efficient antibody responses. (Fox et al., 2017). In a similar approach Adeyemi et al. (2017) identified several mutations that conferred increased thermostability to PV-1 virions using thermal selection. These amino acid replacements also improved the antigenicity and thermostability of empty capsids (Adeyemi et al., 2017). Together these studies demonstrate that by probing the

molecular determinants of stability, particles can be successfully engineered as improved alternatives to existing vaccine antigens.

1.5.6. Stabilising hotspots as potential drug targets

No anti-picornaviral therapies are currently available, although promising antiviral compounds have been shown to disrupt aspects of the picornavirus lifecycle, such as cell entry, polyprotein processing and replication (Baggen et al., 2018a; Banerjee et al., 2019; Barnard, 2006; Tan et al., 2014). An array of capsid binding compounds has been identified for the enteroviruses and have been the focus of numerous studies. These compounds integrate into the hydrophobic pocket at the base of the canyon (Tan et al., 2014) inhibiting uncoating and RNA release, or viral attachment by stabilising the receptor binding site (Abzug et al., 2015; Benschop et al., 2015). Pleconaril has been shown to inhibit certain EV species (Liu et al., 2015a; Pevear et al., 1999), including CV-B3 (Martikainen et al., 2015) and HRV (Hayden et al., 2003) in this way, while WIN compounds are demonstrated to prevent the uncoating and breathing of CV-A9 (Hendry et al., 1999), EV-71 (Plevka et al., 2013), PV (Dove and Racaniello, 2000), and some HRV serotypes (Lewis et al., 1998; Mello et al., 2014). A comprehensive understanding of capsid structure is important for designing antiviral compounds with improved efficacy (Perilla et al., 2016). For example, De Colibus et al. (2014) were able to design pocket binding inhibitors against EV-71 with improved efficacy and solubility using a structural based analysis to rationally inform their design (De Colibus et al., 2014).

The protein-protein interfaces in viral capsids are complex and involve many interactions across large surface areas, unlike those of simpler generic protein complexes within a cell, making these unique interfaces attractive targets for antivirals (Cheng and Brooks, 2015). Recent studies have developed small molecule and peptide inhibitors targeting the subunit interfaces of human immunodeficiency virus (HIV) and hepatitis B virus (HBV) capsids (Blair et al., 2010; Bourne et al., 2008; Ternois et al., 2005). These molecules affect capsid assembly

by either altering capsid subunit interfaces upon binding (Tang et al., 2003; Ternois et al., 2005), or act as assembly agonists (Blair et al., 2010; Katen et al., 2010). Others can affect the inter-subunit geometry of the assembling particles (Bourne et al., 2008). Bocanegra et al. (2012, 2011) developed the first rational approach for the design of capsid interfacial inhibitors in HIV-1. More specifically, the authors engineered peptides that could act as competitive assembly inhibitors by mimicking capsid structural elements present in intersubunit interfaces (Bocanegra et al., 2012, 2011). Such inhibitors targeting the picornaviruses are yet to be developed, but knowledge regarding the capsid subunit interfaces and the residues involved in maintaining interface stability would be an important first step required for their design.

1.6. Theiler's murine encephalomyelitis as an available replication system

Theiler's murine encephalomyelitis virus (TMEV) causes enteric and neurological diseases in rodents and strains are classified into subgroups on the basis of their neurovirulence and antigenicity (Gerhauser et al., 2019; Lipton, 1975; Lipton and Friedmann, 1980). Theiler's original (TO) group includes the BeAn and DA strains which cause persistent inflammatory demyelination, while strains of the highly neurovirulent GDVII group induce an acute and often fatal encephalitis (Oleszak et al., 2004; Roos, 2010). Strains from both subgroups have been characterised (Lipton et al., 1991; Sato et al., 1996), and full-length cDNA clones have been generated for both DA and GDVII (Fu et al., 1990; Roos et al., 1989). Furthermore, the capsid structures of TMEV DA and BeAn have been determined using X-ray crystallography providing available templates on which other strains can be modelled (Grant et al., 1992; Luo et al., 1992).

TMEV permissively infects BHK-21 cell lines (Delhaye et al., 2004; Nedellec et al., 1998) and poses no risk to human health enabling its use in conventional tissue culture facilities. The cardiovirus genus to which TMEV belongs is related to the enteroviruses and clusters in the same supergroup as the aphthoviruses and senecaviruses, based on sequences encoding the

capsid and 3CD proteins (Zell, 2018). Despite minor differences in the capsid structure and replication of picornaviruses, TMEV provides a biosafe model for investigating aspects of picornavirus biology. Using this system, previous colleagues have investigated the non-structural proteins of TMEV and found that GDVII 2C localises to the Golgi apparatus and endoplasmic reticulum (ER) during infection (Jauka et al., 2010; Murray et al., 2009). Using site-directed mutagenesis of the GDVII cDNA clone, Murray et al. (2009) also identified conserved residues in the N-terminal domain of 2C that were essential for the function of the protein and those that were required for its localisation to the replication complex. Furthermore, Mutsunguma et al. (2011) found that Hsp90 colocalises with 2C and is required for TMEV replication. Recently, Ross et al. (2016) developed antibodies to the N-terminus of TMEV VP1 and revealed that this capsid protein localises to the perinuclear region of infected cells, in a similar pattern to FMDV VP1. Furthermore, the same study demonstrated that Hsp90 is likely involved in TMEV assembly, as the VP1 protein colocalised with this chaperone during infection. Considering the biosafety of TMEV and the robustness of the available replication system, this cardiovirus was used in the studies presented in this thesis to examine the molecular determinants of structural stability and integrity in a picornavirus capsid.

1.7. Problem statement

Picornavirus infections cause a broad range of important human and animal diseases with severe clinical and economic implications. Aside from PV, EV-71, HAV and FMDV, there are few vaccines for their prevention and control. Live vaccines elicit the strongest antibody response, but their efficacy is dependent on the structural integrity of virus particles, which must be maintained using cold-chain methods that are both costly and not always feasible, particularly in countries lacking the appropriate infrastructure. At present, no antivirals are commercially available for the treatment of picornavirus infections and many potential compounds have associated issues such as toxicity or viral resistance. Picornavirus capsids are

essential for aspects of the virus lifecycle including receptor binding, uncoating, and protection of the viral genome from degradation. Each of these processes is regulated by the structure of the capsid and its individual subunits. Therefore, a comprehensive understanding of the molecular determinants that regulate capsid structure and stability would not only contribute to an improved understanding of the basic biology of these pathogens but would guide the development of novel antiviral agents and stable vaccine antigens.

1.8. Aims and objectives

The overall aim of this thesis was to improve the knowledge regarding the structural stability of picornavirus capsids by examining the molecular determinants of structural stability and integrity in the TMEV GDVII capsid. The first objective of the thesis was to generate and characterise a set of polyclonal antibodies targeting the TMEV GDVII capsid proteins in order to study the capsid using biochemical techniques. The second objective was to develop a simple computational screen to investigate the residues that contribute significantly to the stability and assembly of picornavirus capsids and identify these residues within the subunit interfaces of the TMEV GDVII capsid. The third objective was to determine whether hotspot residues predicted to contribute to the stability of the interpentamer interfaces in TMEV were critical for virus viability and infectivity, using *in vitro* alanine scanning mutagenesis. The final objective was to determine whether the thermostability of TMEV could be improved using heat selection, and to investigate the determinants that likely contributed to this improved stability at the molecular level.

1.9. Overview of chapters

Chapter 2 describes the generation of neutralising polyclonal antibodies targeting the TMEV GDVII capsid. The capsid proteins and regions containing linear epitopes within that were recognised by the antibodies were identified using Western blot experiments combined with a deletion analysis of the VP1 protein. The *in vitro* neutralising ability of the antibodies was

examined using a plaque reduction neutralisation assay. Characterisation of the antibodies prompted an investigation into the potential binding site of the TMEV GDVII secondary receptor, heparan sulphate, using molecular docking experiments, and a potential neutralising mechanism for these antibodies is discussed. The antibodies were optimised for Western analysis and immunofluorescence experiments, providing a useful tool for biochemical experiments later in the thesis.

A novel screen for the prediction of stabilising hotspot residues at the subunit interfaces of a picornavirus capsid is presented in **Chapter 3**. By implementing five readily accessible tools for the prediction of hotspot residues at protein-protein interfaces, the screen was developed to identify the residues that critically contribute to the stability and integrity of the intraprotomer, interprotomer and interpentamer interfaces of the TMEV GDVII capsid. Additional *in-silico* applications were used to examine the interactions formed between each hotspot residue and partner residue(s) across the interface. Finally, structural alignments were included as part of the screen to examine whether the residues identified as hotspots in TMEV were conserved in representative members across the family.

The importance of a subset of hotspot residues identified within the TMEV interpentamer interfaces was further assessed in **Chapter 4**, using a reverse genetics system and site directed mutagenesis. The significance of each selected hotspot to the lifecycle of TMEV was examined by substituting individual hotspot residues to alanine, and the potential effects of these substitutions on virus growth and infectivity was assessed following transfection of mutant RNAs into susceptible cells. Furthermore, the potential effects of the substitutions on RNA replication and protein synthesis were examined using immunofluorescence experiments.

Chapter 5 described the selection of TMEV GDVII virions with improved thermal stability through serial passage of heat exposed virus particles. The thermal tolerance of the wild type

and thermostable TME viruses was assessed using a thermal inactivation assay. The mutations that potentially contributed to improved thermal tolerance were elucidated by sequencing the reverse transcribed P1 capsid encoding regions of the thermostable virions. The potential effects of the mutations on the alteration of protein interactions and changes to subunit interface stability were assessed through *in-silico* analyses.

Chapter 6 provides a summary and discussion of the findings in this thesis. Emphasis is placed on the limitations and implications of each study and how the tools developed in the thesis may be applied to further investigate the structures of TMEV capsids and those belonging to other picornaviruses.

Chapter 2

The generation and characterisation of anti-TMEV capsid antibodies

The work presented in this chapter was published in Virus Research:

Upfold, N., Ross, C., Tastan Bishop, Ö., Luke, G.A., Knox, C. 2018. The generation and characterisation of neutralising antibodies against the Theiler's murine encephalomyelitis virus (TMEV) GDVII capsid reveals the potential binding site of the host cell co-receptor, heparan sulfate. *Virus Research*, 244, 153-163. [10.1016/j.virusres.2017.11.017](https://doi.org/10.1016/j.virusres.2017.11.017).

2.1. Introduction

Picornavirus capsids are highly antigenic (Mateu, 1995; Minor, 1990), often triggering the production of high levels of responding antibodies in the host animal within a matter of days or weeks (Alexandersen et al., 2003; Tsao et al., 2002; Westerhuis et al., 2015; Yang et al., 2011). A subset of these antibodies protect the host by blocking further virus infection through a variety of mechanisms, and are termed neutralising antibodies (nAbs) (Anastasina et al., 2017; Klasse, 2014; Mateu, 1995). Antibodies targeting the picornavirus capsid, its subunits, and end products are not only useful for serological studies (McCray and Werner, 1987; van Dreumel et al., 2015; Veerasami et al., 2008; Yang et al., 2013) but are also valuable reagents for investigating capsid structure, its assembly and uncoating, and the virus-host interactions that mediate these processes. For example, antibodies have been used to map the antigenic sites on the surface of capsids through the generation of nAb escape mutants (Barnett et al., 1989; Bolwell et al., 1989; Huang et al., 2017; Kiener et al., 2014; Mateu, 1995; Sherry et al., 1986), or through the assessment of antibody-capsid complexes (Bannwarth et al., 2015; Hewat and Blaas, 1996; Kiener et al., 2014; Ye et al., 2016; Zheng et al., 2019). Similarly, antibodies have been used for structural and immunogenic comparisons between native and expanded capsids for the purpose of improved vaccine development (Malik et al., 2017; Ren et al., 2015; Wang et al., 2012a). NAbs that trigger structural rearrangements upon binding were recently used in experiments to inspect the specific conformational changes associated with capsid expansion and uncoating of EV-71 and HRV-B14 (Dong et al., 2017; Plevka et al., 2014), providing insights into the uncoating mechanisms of these viruses. A monoclonal antibody recognising the HRV-2 expanded capsid has been extensively used to examine the capsid structural changes associated with uncoating during virus entry (Hewat and Blaas, 2006; Neubauer et al., 1987), and was also used in experiments to confirm that HRV-2 capsids require low pH for the initiation of uncoating (Bayer et al., 1998; Prchla et al., 1994).

Antibodies are also indispensable tools for exploring the molecular determinants of capsid assembly, one of the least understood aspects of the picornavirus lifecycle. Recently, capsid protein specific antibodies were used in studies that examined the residues required for 3C cleavage of the VP1/2A junction in FMDV (Kristensen et al., 2017), and VP0 cleavage during the maturation of EV-71 (Zhang et al., 2017), processes that are vital for capsid assembly. In two separate studies, Mateo et al. (2003) and Rincón et al. (2015) used antibodies against epitopes in the folded protomer to examine whether amino acid substitutions at FMDV capsid subunit interfaces inhibit capsid formation. Similarly, Yuan et al. (2016) used an antibody targeting VP0/VP2 to examine the effects of alanine substitutions in EV-71 VP1 on capsid protein production.

Antibodies targeting the capsid proteins of picornaviruses, such as those belonging to FMDV, CV-B3, EV-71 and PV, have allowed the examination of the subcellular localisation of these proteins within the host cell (Knox et al., 2005; Liu et al., 2013; Wang et al., 2012c; Wychowski et al., 1985), and have been useful in exploring the host-cell factors required for assembly. Pfister et al. (1992) employed antibodies specific to PV pentamers and empty capsids to show that vesicular membranes maintain pentamer concentrations for encapsidation, preventing the formation of empty capsids during assembly. Capsid-specific antibodies were also useful in demonstrating that Hsp90 is required for early stages of capsid assembly in the enteroviruses (Geller et al., 2007; Macejak and Sarnow, 1992). Recently we generated polyclonal antibodies against the N-terminus of VP1 by immunising rabbits with a truncated VP1 peptide (Ross et al., 2016). Using these antibodies in immunofluorescence experiments, it was shown that VP1 localises to the perinuclear region of infected cells where the protein colocalises with Hsp90 during the early stages of capsid assembly, implying a potential role for this chaperone in cardiovirus assembly.

Antibodies targeting the whole picornavirus capsid as opposed to VP1 alone would be useful to extend these studies and investigate the underlying molecular determinants of capsid structure, assembly and uncoating. The overall aim of this study was to generate and characterise antibodies against the TMEV capsid that could be used in biochemical experiments in the chapters that follow. The specific objectives were first to prepare purified TMEV particles for immunisation in rabbits; secondly, to test the serum for antibodies detecting capsid proteins by Western analysis and indirect immunofluorescence; thirdly, to identify linear epitopes recognised by the antibodies; and finally, to characterise the neutralising ability of the resultant antibodies.

2.2. Materials and Methods

2.2.1. Cells and virus

Baby hamster kidney cells, strain 21 (BHK-21) (kindly provided by M. Ryan, University of St Andrews, UK) were maintained in buffered Dulbecco's modified Eagle Medium (DMEM) (Lonza, Switzerland) supplemented with 10 % [v/v] heat-inactivated foetal bovine serum (FBS), 100 U penicillin ml⁻¹, 10 mg streptomycin ml⁻¹ and 25 µg fungizone ml⁻¹, at 37 °C with 5 % CO₂.

TMEV strain GDVII was used to infect cells in all experiments. Virus stocks were prepared by infecting confluent BHK-21 monolayers at a multiplicity of infection (MOI) of 1. Following 24 hours (h) of infection the infected cell lysate was aspirated and stored at -80 °C. Virus titres were determined by plaque assay.

2.2.2. Purification of TMEV GDVII particles for immunisation in rabbits

2.2.2.1. Infection of monolayers

Confluent BHK-21 monolayers grown in T75 cm² flasks were infected with TMEV GDVII in serum free DMEM in a total volume of 2 ml. The virus was left to adsorb for 1 h at room

temperature (RT) with gentle agitation, before the addition of 5 ml serum-free DMEM. The cells were incubated at 37 °C for 24 h to allow the development of cytopathic effect (CPE), before they were frozen at -20 °C.

2.2.2.2. Sucrose cushion purification

TMEV infected cells were freeze-thawed three times to facilitate cell lysis, after which 10 % Nonidet P40 (NP-40) (Roche, Germany) was added to a final concentration of 1 % and allowed to incubate for 2 h at RT, with gentle agitation. Infected cell lysates were clarified by centrifugation at $6\,000 \times g$ for 20 min using a JA20 rotor (Beckman centrifuge, USA) after which 7 % polyethylene glycol (PEG, MW 6000) (Merck, RSA) and NaCl to a final concentration of 0.38 M were added to the supernatant to concentrate the virus particles. Following overnight incubation at 4 °C, virus particles were pelleted by centrifugation at $11\,000 \times g$ at 4 °C for 20 min using a JA20 rotor (Beckman centrifuge, USA). The pellet was resuspended in phosphate buffered saline (PBS) [137 mM NaCl, 2.7 mM KCl, 10 mM Na_2HPO_4 , 2 mM KH_2PO_4 ; pH 7.4] and centrifuged on a 30 % sucrose cushion, prepared in 5 ml Beckman polycarbonate thick walled tubes (Beckman, USA), at $171\,000 \times g$ using a Beckman 70.1Ti rotor (Beckman centrifuge, USA) for 4 h at 4 °C. The pellet was resuspended in 200 μl PBS and stored at -20 °C until sucrose gradient purification.

2.2.2.3. Sucrose density gradient purification

10-40 % sucrose gradients were prepared in 5 ml SW41 tubes (Beckman, USA) using the Biocomp gradient master system (BioComp, Canada). The viral pellet was placed on top of the tubes and centrifuged at $96\,808 \times g$ using the SW41 rotor (Beckman, USA) at 4 °C for 2 h. The resultant virus band was carefully extracted using a 7-gauge syringe needle, washed using PBS and centrifuged at $151\,263 \times g$ in a SW41 rotor (Beckman, USA) for 1 h, at 4 °C. The pellet was resuspended in 250 μl PBS and stored at -20 °C. The virus concentration was determined using a Nanodrop ND-1000 spectrophotometer (Thermo Scientific, USA), and approximately

1 mg of the purified virus sample was used by D. Bellstedt (University of Stellenbosch, South Africa) for the immunisation of rabbits, to generate anti-TMEV capsid antibodies (Bellstedt et al., 1987).

2.2.3. Transmission electron microscopy (TEM)

Sucrose purified virus was prepared for TEM using a method previously described by Lipton and Friedmann (1980) except that sodium phosphotungstate was substituted with a solution of 3 % uranyl acetate. In brief, 5 µl of purified virus sample was placed onto a carbon forvar grid for 1 min. Filter paper was then used to wick away excess liquid and the grid was stained with 3 % uranyl acetate for 1 min. Excess uranyl acetate was removed using filter paper and the grids were left to dry overnight. The grids were viewed using a Libra 120 PLUS transmission electron microscope (Carl Zeiss, Germany) and ITEM software was used to capture and analyse the images (Carl Zeiss, Germany).

2.2.4. Preparation of TMEV infected cell lysate for Western analysis

To produce infected cell lysates for Western blot experiments, 75 cm² flasks containing BHK-21 cells were infected with TMEV in serum-free DMEM. Following a virus adsorption period of 1 h at RT with gentle agitation, virus inoculum was aspirated, and the cells were rinsed twice with PBS before 5 ml DMEM was added. The cells were incubated at 37 °C, harvested at various hours post infection (hpi), pelleted at 1 000 × g and were resuspended in PBS. Control cells were mock-infected with serum free DMEM. Cells that did not exhibit typical signs CPE such as mock infected cells and those harvested early on in the infection cycle were collected following treatment with trypsin before they were pelleted at 1 000 × g and resuspended in PBS.

2.2.5. SDS-PAGE and Western analysis

Samples for analysis by SDS-PAGE were denatured and reduced by heating in 4 × SDS-PAGE loading buffer [62.5 mM Tris HCl (pH 6.8), 10 % glycerol, 1.25 % bromophenol blue, 0.5 % β-mercaptoethanol and 2 % SDS] for 5 min at 95 °C. Acrylamide/bisacrylamide (30:1) gels were prepared using a Mini-Protean 3 gel casting system (Biorad, USA). The 12 % acrylamide resolving gel [1.5M Tris-HCl (pH 8.8)] and 4 % stacking gel [0.5 M Tris-HCl (pH 6.8)] were polymerised by the addition of 10 % [w/v] ammonium persulphate (APS) and TEMED. The gels were electrophoresed for 40 min at 150 V in 1 × SDS running buffer [1.44 % glycine, 25 mM Tris (pH 8.3), 0.1 % SDS] using a Bio-Rad Mini-Protean Tetra cell system (Bio-Rad, USA). Migration and molecular weight estimation of the sample proteins was possible using the PageRuler™ Prestained Protein Ladder (10-170 kDa) (Thermo Scientific, USA). To visualise protein bands gels were stained with Coomassie brilliant blue [6.25 % Coomassie R-250, 50 % methanol, 10 % acetic acid], and then incubated in a destain solution [40 % methanol, 7 % acetic acid, 53 % ddH₂O].

For the detection of specific proteins, samples separated by SDS-PAGE were transferred onto nitrocellulose membranes (Bio-Rad, USA) at 100 volts for 90 min in transfer buffer [25 mM Tris-HCl (pH 8), 192 mM glycine, 20 % [w/v] methanol]. Successful protein transfer was confirmed by staining the nitrocellulose membrane with Ponceau stain [0.5 % [w/v] Ponceau S, 1 % glacial acetic acid] for 1 min. Protein detection was performed using the BM Western blotting kit (chemiluminescence mouse/rabbit kit) (Roche, Germany). Membranes were incubated in blocking buffer [1 % block reagent in Tris-buffered saline (TBS; 50 mM Tris (pH 7.4), 150 mM NaCl)] for 1 h at room temperature. The membranes were transferred into blocking buffer containing primary antibody for 1 h at room temperature with gentle agitation and were subsequently washed three times in TBS-T [50 mM Tris (pH 7.4), 150 mM NaCl, 1 % Tween-20] for 15 min, replacing the TBS-T each time. Secondary POD-labelled

mouse/rabbit antibodies (BM Western blotting kit) (Roche, Germany) diluted 1:20 000 in 0.5 % blocking solution were then applied to the membrane for 30 min at room temperature with gentle agitation, before the membranes were washed three times in TBS-T. Protein detection was performed following incubation of the membrane in premixed detection reagent for 1 min using the ChemiDoc Molecular Imager XRS + (Bio-Rad, USA), and images were analysed using the Image Lab TM software, version 5.1 (Bio-Rad, USA).

2.2.6. Construction of plasmids

Plasmids expressing the TMEV VP1 full-length protein and various VP1 truncations were constructed. The TMEV VP1 sequence was PCR amplified from pGDVIIIFL2, a plasmid that carries the full-length cDNA of TMEV GDVII (Fu et al., 1990), using the KAPA Taq ReadyMix kit (KAPA Biosystems, South Africa). The forward oligonucleotide primer NUVPIF and reverse oligonucleotide primers NUVPIR, NU1-112R, NU1-195R and NU1-221R were used to generate the full length VP1 plasmid pCRVP1 (Full length) and plasmids expressing a series of C-terminal VP1 truncates pVP1^{Δ113-276}, pVP1^{Δ196-276}, pVP1^{Δ222-276} respectively. Primers NU159-276F and NU159-276R were used to generate a plasmid expressing N-terminally truncated VP1 pVP1^{Δ1-158} (Table 2.1). PCR cycles included an initial denaturation step at 95 °C for 1 min, followed by 30 cycles of: denaturation at 95 °C for 1 min, annealing at 60 °C for 1 min and elongation at 72 °C for 1 min, and a final elongation step at 72 °C for 7 min. Thermocycling was performed using a SimpliAmp Thermal Cycler (Thermo Scientific, USA). Resultant products were purified using the GeneJet PCR Purification Kit (Thermo Scientific, USA) according to the manufacturer's instructions, except that the DNA was eluted in 30 µl nuclease free ddH₂O.

Resultant PCR products were ligated into the commercially available plasmid vector pQE-80L (Qiagen, Germany) by restriction with *Bam*HI and *Sal*I (Thermo Scientific, USA), according to the manufacturer's instructions. The restricted inserts were purified using the GeneJet PCR

Purification Kit (Thermo Scientific, USA) as above, prior to ligation reactions. Ligations were performed at 22 °C for 10 min and then overnight at 4 °C in a total volume of 10 µl, containing 1 µl 10X T4 DNA ligase buffer [400 mM Tris-HCl, 100 mM MgCl₂, 100 mM DTT, 5 mM ATP; pH 7.8], 1 U T4 DNA Ligase (5 U/µl) (Thermo Scientific, USA) and plasmid (50-100 ng) and insert DNA at a ratio of 1:3.

Table 2.1 Oligonucleotide primers used to generate plasmids expressing VP1 truncates. Adapted from Upfold et al. (2018)

Primer	Primer sequence 5'→3'	Binding site in genome	Product size (bp)
N-terminal truncations			
NUVP1F	AAA GGA TCC GGA ATT GAC AAT GCT G	3510-3525	-
NUVP1R	AAA GTC GAC <u>TCA</u> CTC AAG CTC AAG AAT G	4323-4338	828
NU1-112R	AAA GTC GAC <u>TCA</u> CTG TTT GGT CAT GAG TGG	3829-3846	336
NU1-195R	AAA GTC GAC <u>TCA</u> CAG AGG GGA ATT GTA AGG	4078-4095	585
NU1-221R	AAA GTC GAC <u>TCA</u> ATC CGA CGT AGG AGC AAC	4156-4173	663
C-terminal truncations			
NU159-276F	AAA GGA TCC GTC ACT GAC CAG CTG ATC	3974-3992	
NU159-276R	AAA GTC GAC <u>TCA</u> CTC AAG CTC AAG AAT G	4321-4337	363

Table 2.1 Footnotes: *Bam*HI and *Sal*I sites are italicised. Stop codons are underlined.

Ligations were transformed by heat-shock into JM109 *E.coli* cells that had been made chemically competent using the CaCl₂ method as described by Chang et al. (2017). Single colonies were inoculated into 5 ml LB supplemented with ampicillin (100 µg/ml) and incubated overnight at 37 °C. Plasmid DNA was subsequently extracted using the GeneJet Plasmid Miniprep kit (Thermo Scientific, USA) according to manufacturer's instructions, except that plasmids were eluted in 50 µl nuclease-free ddH₂O, before analysis by 1 % [w/v] agarose gel electrophoresis. To confirm the presence of inserts and correct open reading frames, the plasmids were sequenced by Inqaba Biotechnical Industries (Pty) Ltd., Pretoria South Africa. Chromatograms were analysed using SnapGene[®] software (GSL Biotech).

2.2.7. Expression of VP1 and truncated VP1 peptides

To express the TMEV VP1 protein and VP1 truncated peptides, JM109 *E. coli* cultures containing the VP1 expression plasmids were grown overnight in LB supplemented with ampicillin (100 µg/ml) at 37 °C with shaking (150 rpm). The cultures were subsequently diluted 1/100 in LB broth and incubated at 37 °C until the OD600 measured between 0.6 and 0.8 AU. To induce expression, 1mM Isopropyl-β-D-thiogalactopyranoside (IPTG; Sigma, USA) was added to the remaining culture and induction was allowed to proceed for 4 h at 37 °C. Cells were pelleted at $11,800 \times g$ for 10 min at 4 °C using a JA20 rotor (Beckman centrifuge, USA) and resuspended to equivalent density in PBS. For induction studies, resuspended pellets were analysed by Western blotting using Anti-His6(2) antibodies (Roche, Germany), that recognised the 6 × histidine tag in pQE-80L, at a dilution of 1:3000.

2.2.8. Indirect immunofluorescence and confocal microscopy

BHK-21 cells grown to 60 % confluency on sterile 13 mm glass coverslips were washed twice with serum-free DMEM before cells were infected with TMEV at a MOI of 1. Following adsorption for 1 h at RT with gentle agitation, the virus inoculum was removed and replaced with DMEM after the cells were rinsed twice using PBS. The cells were incubated at 37 °C and fixed at various time points using 4 % paraformaldehyde for 20 min at RT. Control cells were mock-infected with serum-free DMEM. Following fixation, cells were rinsed twice in PBS and permeabilised using permeabilisation buffer (PB) [10 % sucrose, 0.1 % Triton X- 100 in PBS] for 20 min. Cells were blocked in PB containing 2 % BSA (Block) for 40 min at RT and incubated with polyclonal rabbit antibodies against TMEV GDVII 2C (1:1000) (Jauka et al., 2010), anti-TMEV VP1 antibodies (1:20 000) (Ross et al., 2016) or anti-TMEV capsid antibodies (1:20 000), diluted in block buffer for 1 h with shaking. Cells were washed twice in PBS containing 0.1 % Tween-20 and incubated with species-specific Alexa Fluor 546 or 488-conjugated secondary antibodies (Invitrogen, USA) (1:500) for 30 min. Cells were washed

three times, and 4',6-diamino-2 phenylindole dihydrochloride (DAPI) (Sigma, USA) was added at a final concentration of 0.8 µg/ml in the second wash step to stain cell nuclei. The slides were mounted using Dako fluorescence mounting medium (Dako Inc., USA) and stored at RT. Images were captured using the Zeiss LSM 510- Meta laser scanning confocal microscope and analysed using Zen software (blue edition, Zeiss, Germany). The helium/neon and argon lasers at wavelengths 405, 488 and 543 nm were used to excite DAPI, Alexa-fluor 488 and Alexa-fluor 546 respectively. In order to acquire a representative image for each experiment, between 50 cells were viewed at 63 × magnification. Colocalisation analysis was performed on five randomly selected cells. Immunofluorescence experiments were performed in triplicate.

2.2.9. *In-silico* virus structure assembly and epitope mapping

TMEV virus structure assembly and epitope mapping were performed by C. Ross and were described in detail in Upfold et al. (2018). Briefly, a homology model of TMEV GDVII was obtained from a previous study (Ross et al., 2016) and was solvated and minimised using GROMACS 5.1.2 (Abraham et al., 2015). The complete TMEV capsid was assembled by overlaying 60 copies of the minimised protomer on the biological assembly of TMEV DA (PDB: 1TME) (Grant et al., 1992). To examine the structural locations of the previously identified C- and N-terminal epitope regions (Ross et al., 2016) as well as the suggested heparan sulphate binding domain 240-YKKMKV-245 in VP1 (Reddi and Lipton, 2002), these amino acids were mapped to the full structure of TMEV in PyMOL (Schrodinger, 2010)

2.2.10. Molecular docking

Molecular docking experiments were performed by C. Ross and are described in detail in Upfold et al. (2018). In brief, a complex of two adjacent TMEV protomers was prepared as above (2.2.9). The five-fold interface between the two protomers is the site of the pit involved in receptor binding and was selected for docking of heparan sulphate. Sialic acid and heparan

sulphate compounds were retrieved from the ZINC database (Irwin and Shoichet, 2005), and were individually docked to the protomer-protomer complex using AutoDock4.2 (Morris et al., 2009) and the Lamarckian Genetic Algorithm (LGA). AutoDock Tools (ADT) was used to prepare the protomer complex and the ligands. The sialic acid binding site is known (Tsunoda et al., 2009) and was used as a docking control. As the binding site for heparan sulphate is unknown, four docking simulations were performed using a 35 Å grid box centred at different positions. Finally, the individual amino acid interactions between the TMEV protomer complex and the ligands were determined using LigPlot+ (Laskowski and Swindells, 2011).

2.2.11. Antibody neutralisation assay

A plaque reduction assay was used to examine whether the anti-VP1 (Ross et al., 2016) and anti-capsid antibodies could neutralise virus infection *in vitro*. Antibodies were diluted to 1:50, 1:100, 1:500 and 1:1000 in serum-free DMEM and TMEV stocks were diluted in serum-free DMEM to 1×10^4 PFU/ml. Equal volumes of diluted virus and sera were combined, yielding a final virus dilution of 5×10^3 PFU/ml and serum concentrations of 1:100, 1:200, 1:1000 and 1:2000 (in a total volume of 300 µl). The antibody-sera mixtures were left to co-incubate with gentle agitation for 1.5 h at 37 °C, after which they were added to confluent BHK-21 monolayers in 6-well plates. The plates were incubated for 1 h at RT to allow virus adsorption, before the cells were washed with PBS and overlain with 3 ml of overlay solution [50 % DMEM, 1.25 % methocel, 60 mM NaCl] and incubated at 37 °C for 48 h. Cells were washed and fixed in 4 % paraformaldehyde for 15 min at RT then stained with Coomassie staining solution [45 % methanol, 45 % ddH₂O, 10 % glacial acetic acid and 0.002 % [w/v] Coomassie Brilliant Blue]. Pre-immune serum (final dilution of 1:100) and mock-infected controls were used. The total number of plaques for each well were counted. All experiments were performed in triplicate.

2.3. Results

2.3.1. Sucrose gradient purification of TMEV GDVII virus particles

To purify TMEV virions for immunisation in rabbits, whole virus particles were isolated from GDVII infected BHK-21 cells using a 30 % sucrose cushion followed by a 10-40 % sucrose gradient. Following purification, virus particles were examined by transmission electron microscopy (TEM) and SDS-PAGE (*Figure 2.1*). The micrographs revealed that the sample was relatively pure and that most of virions appeared to be intact with only a few damaged particles (denoted by yellow arrowheads) (*Figure 2.1 A and B*). SDS-PAGE analysis of the purified TMEV sample resolved three protein bands of 37 kDa, 34 kDa and 27 kDa consistent with the known sizes of VP1, VP2 and VP3 respectively (*Figure 2.1 C*), the smallest capsid protein VP4 was not visible due to the small size of this protein.

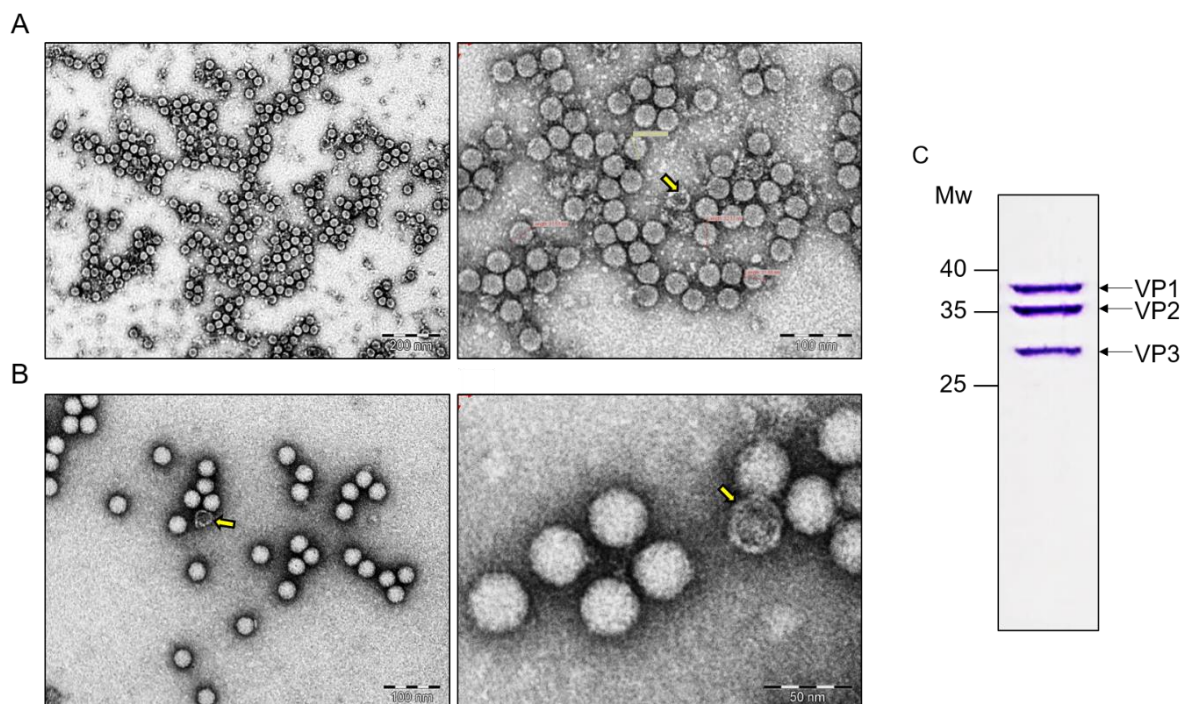


Figure 2.1 TMEV GDVII virus particles following sucrose purification. TEM of GDVII virus particles following sucrose cushion A) and 10-40 % sucrose gradient B) purification. Yellow arrows indicate intact empty capsids. C) GDVII capsid proteins VP1-3 as confirmed by 12 % SDS-PAGE analysis following sucrose gradient purification. MW (molecular weight marker in kDa). Figure adapted from Upfold et al. (2018).

2.3.2. Anti-TMEV capsid antibodies recognise linear epitopes in the VP1 capsid protein

The resultant polyclonal serum was analysed for the presence of antibodies targeting the TMEV capsid proteins (*Figure 2.2*). Sucrose purified TMEV virions and infected BHK-21 cell lysates harvested at 5 hpi were analysed by Western blot in parallel experiments, using decreasing dilutions of serum (*Figure 2.2 A*).

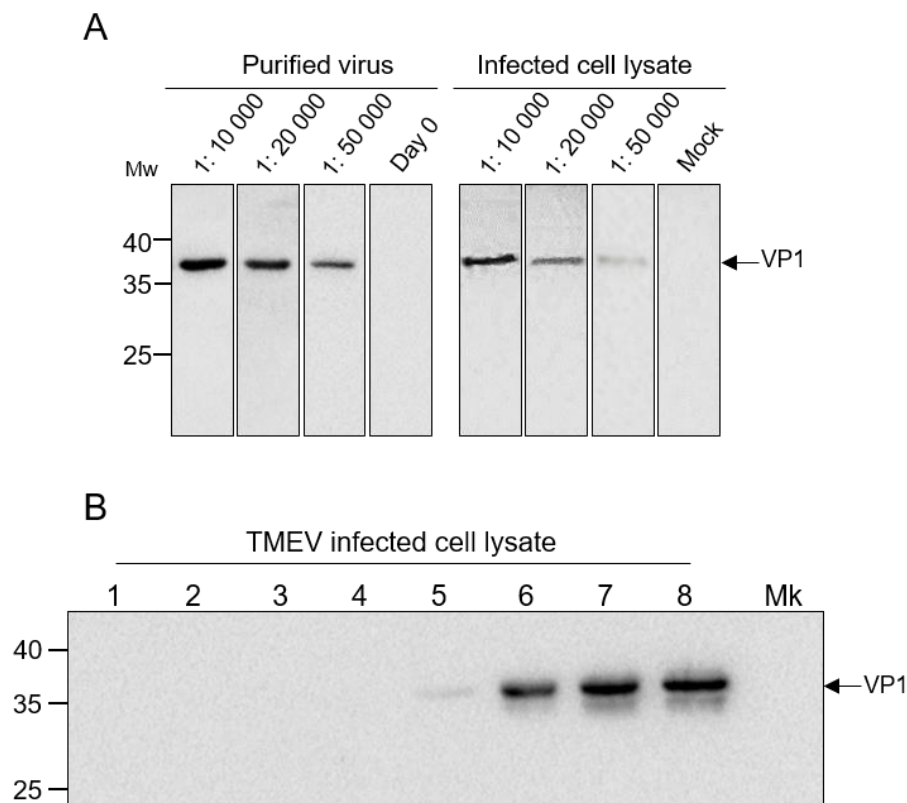


Figure 2.2 Detection of TMEV G DVII VP1 in purified TMEV particles and infected cell lysates. A) Western analysis of purified virus particles and 5-h infected TMEV lysate using decreasing concentrations of anti-capsid serum. B) Western analysis of TMEV infected BHK-21 lysates at various times post infection, using anti-TMEV capsid antibodies. MW (molecular weight marker in kDa). Figure adapted from Upfold et al. (2018).

A single protein band of approximately 37 kDa corresponding to TMEV VP1 was detected in both the sucrose purified virus sample and the 5-h infected cell lysates, while bands

corresponding to the VP2 and VP3 capsid proteins were not detected in any of the samples. Protein bands were absent in mock infected cells or infected cells probed with pre-immune serum, confirming that the 37 kDa band was viral. The antibodies were able to detect the virus and cell lysate samples when diluted at 1:50 000, demonstrating their potency, but the optimal dilution was 1:20 000 as was found previously for the anti-VP1 antibodies (Ross et al., 2016). To investigate the time point at which VP1 could be detected, infected cell lysates were harvested from 1 to 8 h following infection with TMEV stocks and were analysed by Western blot using the capsid antibodies (*Figure 2.2 B*). The VP1 protein appeared from 5 h and increased to 8 hpi, similar to previous findings observed using the anti-VP1 specific antibodies (Ross et al., 2016). Again, no bands were detected in the mock infected cell lysates.

2.3.3. Anti-capsid antibodies detect capsid proteins throughout TMEV infection by immunofluorescence

To examine whether the resultant capsid-antibodies could be used to detect capsid precursors through the course of infection by indirect-immunofluorescence, infected cells were paraformaldehyde fixed at hourly intervals from 4-8 hpi and probed with serum at a dilution of 1:20 000 (*Figure 2.3*). Signal was absent in mock infected cells and TMEV-infected cells probed with secondary antibodies alone as expected (*Figure 2.3 panels a and b*). To confirm that cells were infected, cells were stained using anti-VP1 antibodies and those against 2C (*Figure 2.3 panels c and d*). No signal for TMEV capsid precursors was observed at 4 hpi (*Figure 2.3 panel e*). However, the capsid antibodies recognised proteins in the cytoplasm of 5-h infected cells (*Figure 2.3 panel f*) and the distribution was identical to the signal observed for VP1 (*Figure 2.3 panel c above*), with a cytoplasmic distribution and increased concentration in the juxtannuclear region. From 6-8 hpi the capsid precursors appeared to accumulate in large punctate structures within the cell cytoplasm, and at no time point did the proteins or subunits localise to the nucleus of infected cells (*Figure 2.3 panels g-i*).

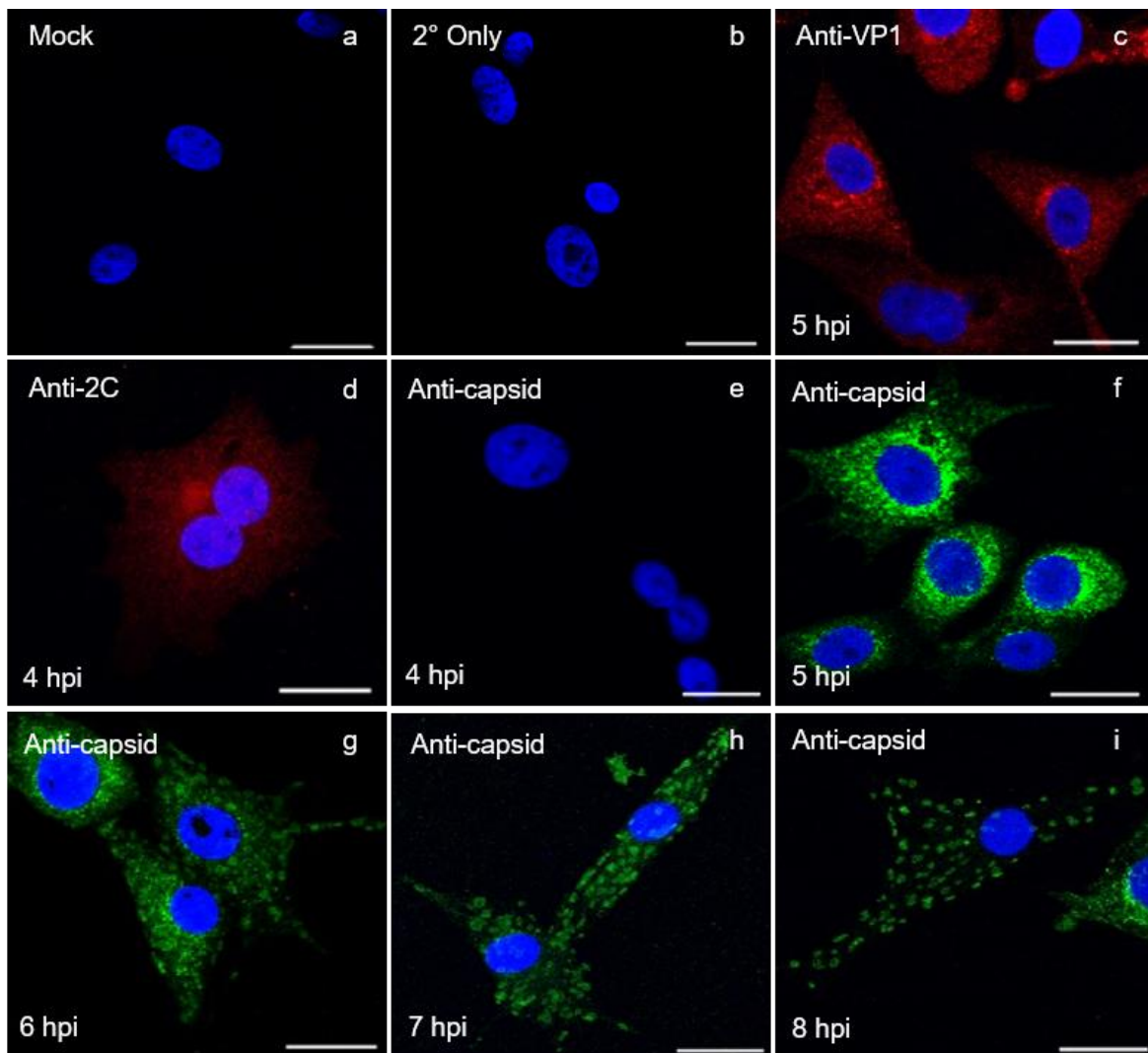


Figure 2.3 Subcellular distribution of capsid proteins during TMEV infection. Cells were mock infected (panel a), or infected with TMEV (panels b-i), fixed with 4 % paraformaldehyde at 4–8 hpi and stained with anti-TMEV VP1 (5 hpi) (panel c), anti-TMEV 2C (4 hpi) (panel d) or anti-TMEV capsid antibodies (4–8 hpi) (panels e-i). Primary antibodies were detected using species specific Alexa Fluor 488-conjugated or 546-conjugated secondary antibodies. Cells in panel b were probed with secondary 488-conjugated antibodies only. Scale bars = 20 μ m. Figure adapted from Upfold et al. (2018).

2.3.4. Anti-TMEV capsid antibodies recognise VP1 C-terminal epitopes

To define the regions containing linear VP1 epitopes recognised by the anti-capsid antibodies during Western analysis, a deletion analysis was performed using a series of truncated VP1 peptides (*Figure 2.4*). The TMEV full-length coding sequence and a series of N- and C-

terminally truncated coding sequences were PCR amplified and cloned into the pQE-80L expression vector. Following transformation, IPTG was used to induce expression for a period of 4 h and whole bacterial lysates were analysed using anti-His6(2) antibodies to confirm protein expression. Western analysis using the anti-capsid antibodies demonstrated that aside from the full-length protein, the antibodies could only recognise the VP1 Δ 1-158 peptide and none of the VP1 C-terminal VP1 Δ 113-276, VP1 Δ 196-276 or VP1 Δ 222-276 truncates.

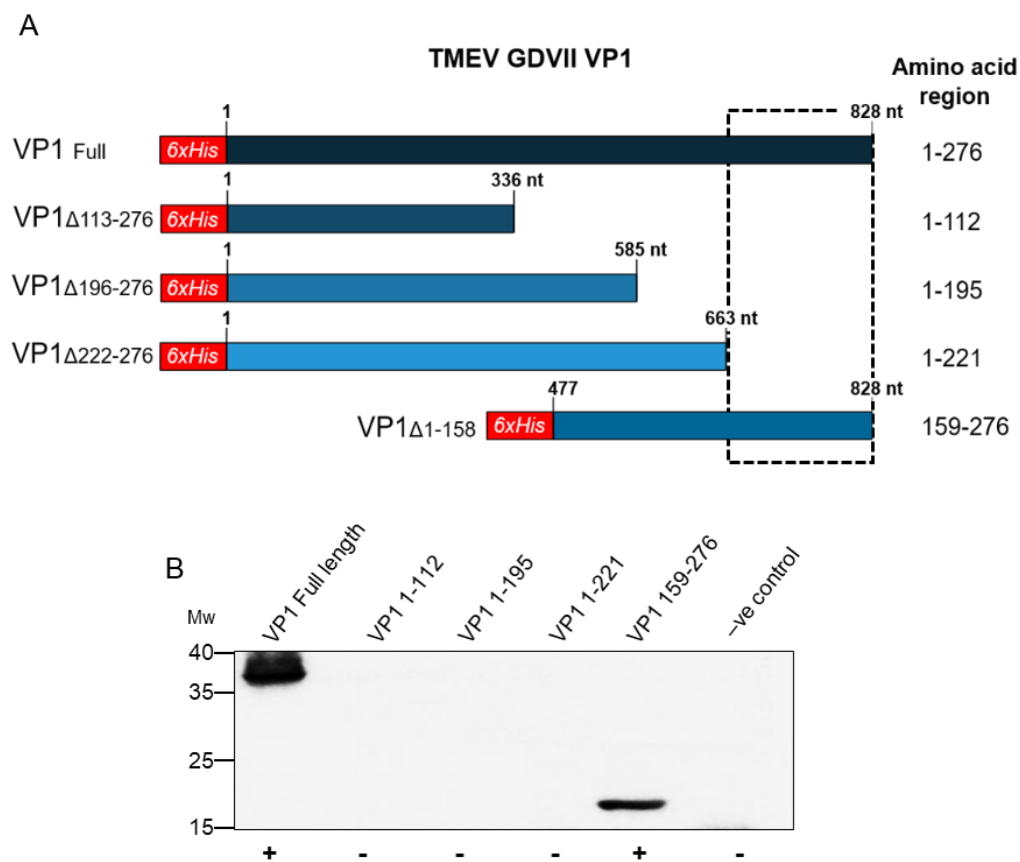


Figure 2.4 Mapping of linear antigenic regions in VP1. A) The strategy used to generate truncated VP1 his-fusion proteins. The red boxes represent the his-coding sequence. The blue boxes represent the truncated regions of VP1. The numbers above the boxes represent the nucleotide locations. Numbers following Δ denote the deleted amino acids. Dashed box highlights the region recognised by anti-capsid antibodies. B) Western blot of bacterially expressed lysates. Cells transformed with VP1 plasmid constructs were induced for 4 h using IPTG. Whole cell lysates were analysed by Western blot using anti-TMEV capsid antibodies to determine the regions of VP1 detected by the antibodies. MW (molecular weight marker in kDa). Figure adapted from Upfold et al. (2018)

These findings indicate that the antibodies recognise linear epitopes within 54 amino acids between residues 222-276 in the C-terminus of VP1. The anti-capsid antibodies did not recognise proteins from cell lysates transformed with the empty pQE-80L vector as anticipated, indicating that no contaminating proteins were present.

2.3.5. C-terminal residues 254–274 reside on a surface exposed loop over the putative receptor binding site

It is likely that the capsid antibodies bind to epitopes exposed on the virion surface, therefore the C-terminal VP1 (222–276) regions were mapped to the TMEV GDVII capsid for further investigation of potential antibody binding sites (*Figure 2.5*). Although the deletion analysis revealed that the anti-capsid antibodies bind to linear epitopes within the last C-terminal residues 222-276 of VP1, it must be noted that antibodies recognising conformational epitopes may also be present as the whole virus particle was used for immunisation (these potential epitopes were not investigated further in this study). Because the N-terminal 1-112 residues recognised by VP1 antibodies in the (Ross et al., 2016) study were only previously modelled on the individual protomer, this region was also mapped to the full TMEV capsid. Mapping these 112 N-terminal residues revealed that three regions 47-57, 79-87 and 95-112 are exposed at the capsid surface. Collectively these residues form a large continuous surface area that extends from the interface between the neighbouring VP1 protein in the adjacent protomer to the interfaces between the VP2 and VP3 proteins of the same protomer (*Figure 2.5 A*). VP1 loop II (98-105) lies within this region and borders puff B in VP2. Within the VP1 C-terminal residues 222-276 recognised by the anti-capsid antibodies, residues 254-272 are surface exposed (*Figure 2.5 B and C*). These residues form part of the protruding C-terminal loop that extends over the putative receptor binding pit.

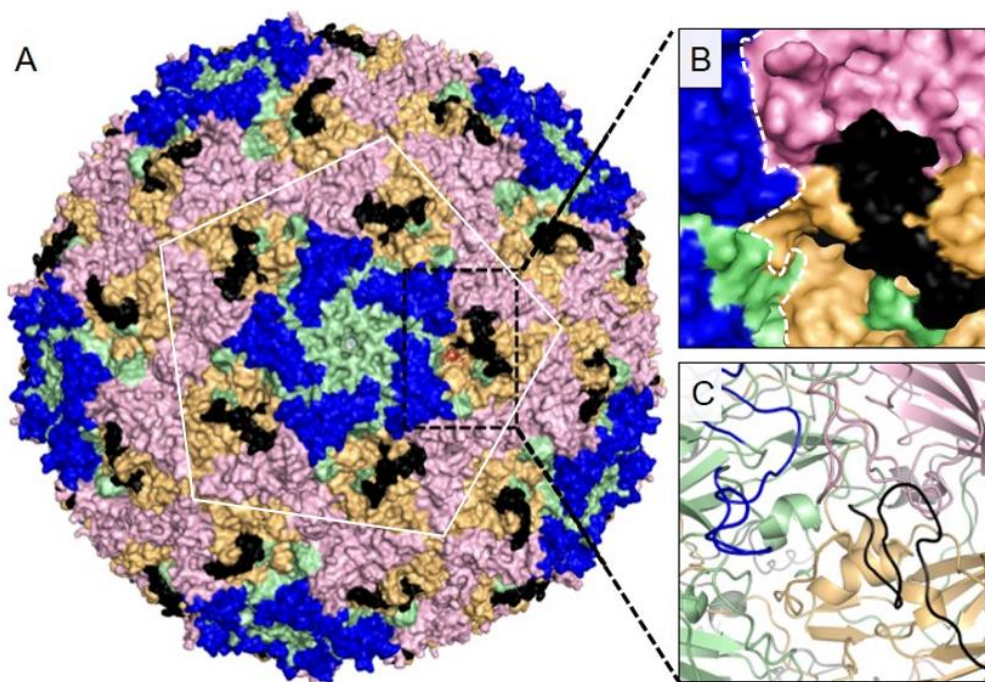


Figure 2.5 Structure of the TMEV capsid showing antigenic regions. A) Homology model of a mature TMEV GDVII capsid. The capsid proteins are coloured green (VP1), pink (VP2) and orange (VP3). Surface exposed residues within the first 112 VP1 N-terminal amino acids are shown in blue (47–57, 79–87 and 95–112). Surface exposed residues within the VP1 C-terminal amino acids 222–276 are shown in black (254–274). A single pentameric subunit is highlighted by white solid lines. B) Local region showing surface of the virus. Dashed white lines indicated the interface between two neighbouring protomers. C) Cartoon depiction of the local capsid region that contains the predicted surface exposed linear epitopes. Adapted from Upfold et al. (2018).

2.3.6. Heparan sulphate, the TMEV co-receptor, docks to the pit below the C-terminal loop

The heparan sulphate co-receptor used by GDVII and sialic acid were docked to a complex of two adjacent protomers, joined at the five-fold interface (*Figure 2.6*). Although the GDVII strain is known to utilise heparan sulphate as a coreceptor, it was previously reported that GDVII is also capable of binding sialic acid (Lipton et al., 2006; Tsunoda et al., 2009). Previous reports have identified the sialic acid binding site between VP1 loop II and VP2 Puff B and so targeted docking of sialic acid to the complex was used as a control for docking experiments.

A grid box spanning a 15 Å was centred over the VP1 loop II and VP2 Puff B and the docking results for sialic acid were consistent with previous findings, confirming the molecule's affinity to this region on the capsid (*Figure 2.6 A*). The capsid binding site for heparan sulphate was previously thought to be a five amino acid motif in the VP1 protein (240-YKKMKV-245) (Reddi and Lipton, 2002). However, this motif appears to be buried deep within the viral capsid and is unlikely the binding site of heparan sulphate (*Figure 2.6 B*). To identify all potential heparan sulphate binding sites, four separate docking simulations were performed across the TMEV protomer, centring the grid boxes in different locations. Each simulation involved two grid boxes, each spanning 15 and 35 Å that were together centred at the same region. Significant results were obtained in one simulation where the grid box was centred on residue L252 of VP1. L252 is located in the pit beneath the C-terminal loop and contains a hydrophobic pocket at the VP1-VP3 interface between two protomers that is thought to form part of receptor binding site. Heparan sulphate docked directly into this pit and interacted with VP1 residues F254 and P257 belonging to the C-terminal loop that is recognised by the capsid antibodies. Moreover, heparan sulphate also interacted with residues that form the hydrophobic pit, specifically VP1 residues P153, A154 and D155 belonging to the neighbouring protomer and VP3 residues VP3 T174, S175 and Y176 of the local protomer (*Figure 2.6 C and D*).

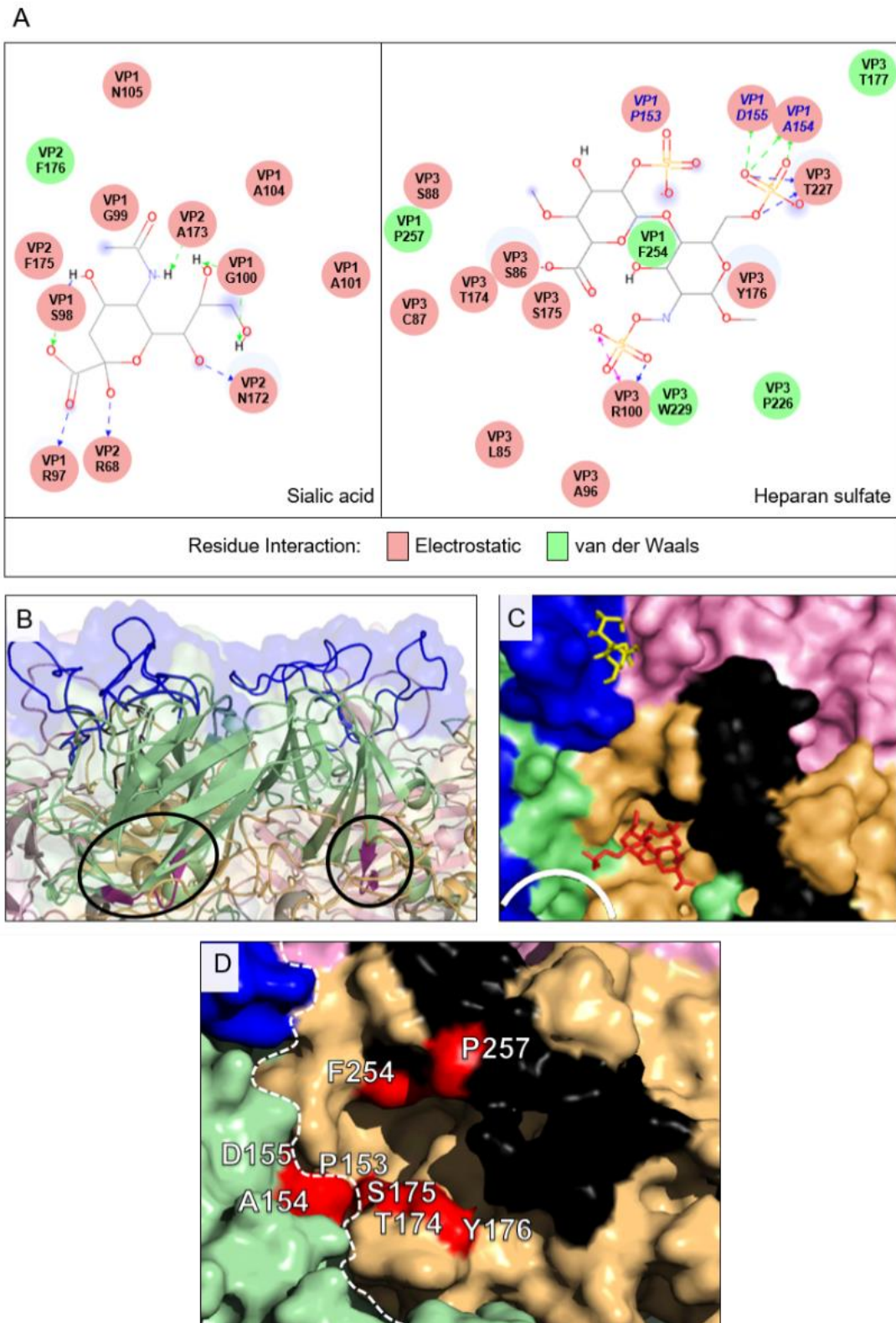


Figure 2.6 The predicted binding of heparan sulphate to the TMEV GDVII capsid. A) Residue interactions between the capsid proteins VP1 and VP2 with sialic acid (left panel), and the capsid proteins VP1 and VP3 with heparan sulphate (right panel). Residues from an adjacent protomer are indicated with italic blue labels. The figures were generated in LigPlot, subsequent to AutoDock

docking simulations. B) Cross-section through the capsid surface. The motif VP1 240-YKKMKV-245 (predicted by Reddi and Lipton, 2002) is mapped in purple (circled in black) and lies deep beneath the surface of the capsid. C) Local region showing docked co-receptors on the surface of the virus. Sialic acid is coloured yellow and heparan sulphate is coloured red. The hydrophobic pocket is indicated by a half white circle. The N- and C-terminal regions recognised by the VP1 and capsid antibodies are coloured blue and black respectively. D) Local region showing the residues that are directly involved in heparan sulphate binding. This figure was adapted from Upfold et al. (2018).

2.3.7. Polyclonal sera containing antibodies that recognise the C-terminus of VP1 neutralise virus infection *in vitro*

The neutralising ability of anti-capsid antibodies was examined alongside that of anti-VP1 antibodies (*Figure 2.7*). Increasing concentrations of sera were incubated with TMEV and the reduction in virus titre was determined by plaque assay. Antibodies recognising the N-terminus of VP1 were not able to inhibit viral infection, even at high concentrations. The anti-TMEV capsid antibodies, however, induced a dramatic neutralising response as a significant decrease in the number of plaques mirrored increasing serum concentrations.

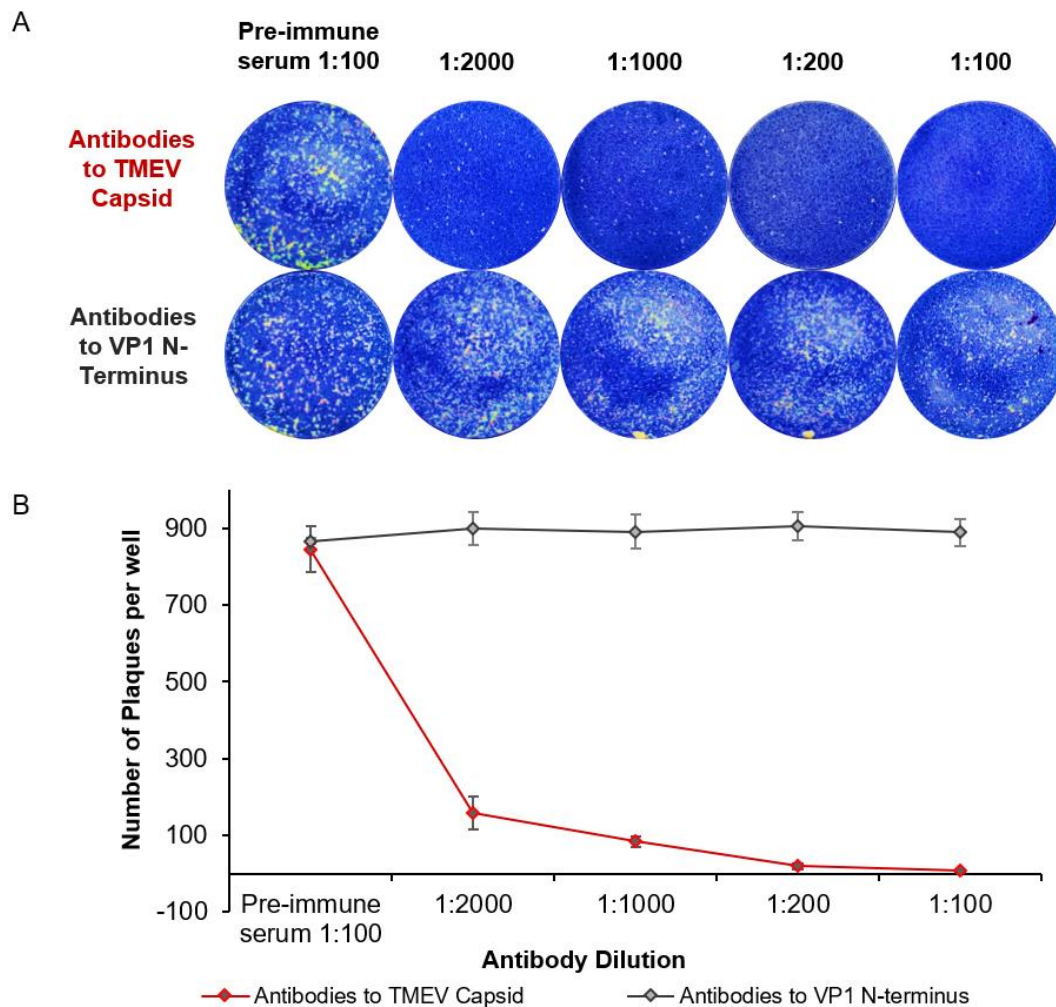


Figure 2.7 The *in vitro* neutralising abilities of polyclonal anti-TMEV capsid and anti-TMEV VP1 antibodies. A) A representative result of three independent experiments for each treatment. B) Quantitative comparison of the neutralising activities of anti-TMEV capsid and anti-TMEV VP1 antibodies at increasing concentrations. Confluent BHK-21 cells were infected with TMEV stocks preincubated with increasing concentrations of anti-capsid and anti-VP1 sera. After removal of virus-serum inoculum, neutralising ability was analysed using a plaque reduction assay. Neutralising ability is expressed as the decrease in plaque number with increasing serum concentration. Pre-immune sera were used as controls for each treatment, at a dilution of 1:100. All experiments were repeated in triplicate. Error bars show standard deviation of the mean. This figure was adapted from Upfold et al. (2018).

2.4. Discussion

The primary aim of this chapter was to generate antibodies recognising the capsid of TMEV, that could be used in conjunction with the existing GDVII replication system to investigate capsid structure and assembly. TMEV particles were used as an antigen for immunisation, and resultant serum contained antibodies that could recognise the 37 kDa VP1 protein in purified virus and infected cell lysates by Western analysis. VP1 is the most surface exposed and immunodominant of the picornavirus capsid proteins (Edlmayr et al., 2011; Meloen et al., 1983; Rossmann et al., 1985), thus it was anticipated that antibodies recognising this protein would be present in the serum. Previous studies isolated antibodies against linear epitopes within VP1 but also the VP2 and VP3 proteins (Crane et al., 1990; Inoue et al., 1994; Kim et al., 1992). It was therefore surprising that antibodies against these proteins were not present in the polyclonal serum, considering that whole TMEV particles were used as an immunogen. Interestingly, another study found that antibodies isolated following the inoculation of mice with DA or GDVII particles could only detect the VP1 protein and capsid particles but not the VP2 or VP3 capsid proteins (Nitayaphan et al., 1985). Previously, Kim et al. (1992) reported that distinct sets of linear epitopes were recognised by antibodies from different mouse strains inoculated with the same antigen, while Inoue et al. (1994) observed that differences in epitope recognition were associated with the route of immunisation and whether intact or inactivated particles were used. Thus, the variation in linear epitopes detected in these studies and in the work presented here is likely a result of differences in the strain of virus used, immunisation scheme, antibody isolation and screening assays, and the animal species used. Moreover, it must be noted that conformational epitopes formed by VP1-3 would not have been detected due to the denaturing of proteins during Western analysis, but the presence of antibodies targeting these epitopes on the virus capsid was not investigated. Their presence is, however, likely considering that whole capsid particles were used as an antigen. The absence of

antibodies targeting the VP4 protein was expected given the internal orientation of the protein, lack of secondary structure, and small size (Jiang et al., 2014; Stanway, 1990).

The next experiments used the anti-capsid antibodies to examine the localisation of capsid proteins during the course of infection. The TMEV lifecycle is complete within 8 h, and previous immunofluorescence experiments using VP1 antibodies detected the protein at 5 hpi (Ross et al., 2016). Thus, TMEV infected BHK-21 cells were analysed from 4 to 8 hpi using the anti-capsid antibodies. Infected cells were paraformaldehyde fixed hourly between these time points and probed with the anti-capsid antibodies. Capsid proteins were detected at 5 hpi and had the same cytoplasmic distribution with increased signal in the juxtannuclear region as previous experiments (Ross et al., 2016). From 6 hpi, the capsid proteins began localising to distinct punctate structures which became more pronounced towards 8 hpi. These punctate structures are similar to those observed by Nedellec et al. (1998) at an earlier time point, and are likely intracytoplasmic crystalline arrays formed by the accumulation of viral capsids prior to host cell death, first observed by Friedmann and Lipton (1980).

Considering that five surface exposed epitopes were previously found within the N-terminus (Ross et al., 2016), it was anticipated that the anti-capsid antibodies would also recognise this highly antigenic region. To test this hypothesis, a deletion analysis was performed on the VP1 protein by generating peptides with N- and C-terminal truncations. Interestingly, the anti-TMEV capsid antibodies could not recognise any linear epitopes within the N-terminal half of VP1 but recognised those within the C-terminal amino acids 159–276 instead.

To better understand the locations of the antigenic region within the C-terminus and the N-terminal epitopes recognised by the anti-VP1 antibodies (Ross et al., 2016), these regions were mapped to the full TMEV capsid surface. The N-terminal residues 47-57, 79-87, and 95-112 were found to form a large region that extended from the VP1-VP1 interface between two

protomers to the VP1-VP3 interface within a single protomer, while residues 98-105 form part of loop II that is located near to VP2 puff B. The C-terminal residues 254-274 reside on a flexible loop that lies at the VP1-VP3 interface within a single protomer. More importantly, this loop extends over the pit believed to be the putative receptor binding site in TMEV (Grant et al., 1992; Luo et al., 1992). Numerous studies investigating picornavirus structure have reported the capsid protein loops as the most surface exposed sites of the capsid but also as major antigenic determinants. The positions of the N-terminal 98-105 and C-terminal 254-274 residues on surface exposed loops were therefore unsurprising. Furthermore, several studies have shown nAbs to recognise epitopes within these loops (Cameron et al., 2001; Inoue et al., 1994; Kim et al., 1992; Luo et al., 1992; Mateu, 1995; Rossmann et al., 1985), thus the next experiments examined the *in vitro* neutralising abilities of the TMEV VP1 and capsid antibodies. Plaque reduction assays demonstrated that while the anti-VP1 antibodies (Ross et al., 2016) could not neutralise virus infection, the anti-TMEV capsid antibodies could. At a dilution of 1:100, the anti-capsid antibodies almost abolished plaque formation entirely. This finding supports previous investigations into the antigenicity of TMEV that found neutralising epitopes exclusively in the C-terminus and not the N-terminus of VP1 (Inoue et al., 1994). Previously, Inoue et al. identified neutralising epitopes within VP1 262-276 in the BeAn strain and it is likely that the anti-capsid antibodies in this study recognise the same epitope in GDVII, given the high sequence similarity between the VP1 proteins of these two strains.

Neutralising antibodies can prevent virus infection through several mechanisms. Antibodies may cross-link virus particles resulting in virus aggregation, thereby preventing virus entry. Antibody binding can also trigger conformational changes that induce premature uncoating (Zheng et al., 2019; Zhu et al., 2018) or conversely, trap the virus in a rigid conformation preventing the conformational rearrangements that lead to uncoating (Ye et al., 2016). Antibody binding may also occlude the receptor binding site thus preventing cell attachment,

and is evidenced by numerous studies (Strauss et al., 2016; Wang et al., 2017; Zheng et al., 2018). The capsid antibodies recognised epitopes within the flexible C-terminal loop that extends over the putative receptor binding site, and thus, disruption of receptor binding may be the mechanism of neutralisation for these nAbs. Host cell receptors have been identified for numerous picornaviruses (as reviewed in chapter one, 1.4.1), yet the identity of the 37 kDa glycoprotein used by both persistent and neurovirulent strains of TMEV remains unknown (Kilpatrick and Lipton, 1991). It is recognised, however, that heparan sulphate and sialic acid mediate receptor binding of neurovirulent and persistent TMEV strains respectively (Fotiadis et al., 1991; Shah and Lipton, 2002). Heparan binding is typically mediated through a motif of hydrophobic residues surrounded by basic amino acids known as a heparan-binding domain (HBD) (Cardin and Weintraub, 1989). Previously, a potential HBD was identified in the C-terminus of VP1 (residues 240-245), although its location in the folded capsid was never investigated (Reddi and Lipton, 2002). This HBD is unlikely to be the heparan binding site in GDVII, as mapping experiments revealed it to be buried deep within the viral capsid. The potential binding site of heparan sulphate was therefore investigated using *in-silico* docking experiments. These simulations suggest that binding likely occurs in the five-fold pit, already known to be associated with receptor binding. Specifically, heparan sulphate interacts with residues within the pocket but also with two residues belonging to the VP1 C-terminus, that is recognised by the capsid nAbs. These results provide further evidence that binding of the capsid antibodies to the C-terminal loop may inhibit or reduce heparan binding and therefore receptor binding, preventing cell attachment and entry.

In conclusion this chapter describes the generation of neutralising polyclonal antibodies targeting the TMEV capsid. Using these antibodies this study is the first to report the distribution of TMEV capsid proteins throughout the progression of infection and demonstrates that these structural proteins behave in a similar manner to those of FMDV and EV-71. The

study also revealed the potential binding site for the TMEV co-receptor heparan sulphate and suggests that the antibodies may neutralise virus infection through prevention of heparan sulphate and/or receptor binding. The generation of neutralising capsid specific polyclonal antibodies and their optimisation by Western blot and indirect immunofluorescence provides valuable reagents with which to further explore the molecular determinants of picornavirus capsid structure, including those involved in capsid assembly, stability, and uncoating. These antibodies are used in the chapters that follow (chapters 4 and 5) to investigate the capsid subunit interface residues required for picornavirus capsid assembly and stability.

Chapter 3

An *in-silico* screen for the prediction of hotspot residues that contribute to the structural stability of subunit interfaces of a picornavirus capsid

3.1. Introduction

The assembly of virus capsids is dependent upon the formation of many non-covalent interactions between capsid protein subunits during the oligomerisation cascade (Mateo et al., 2003; Mateu, 2013; Reguera et al., 2004). Following assembly, the careful modulation of these interactions provides a fine balance between capsid stability and the conformational changes that lead to uncoating. The accumulation of picornavirus capsid structures by X-ray crystallography and high-resolution cryo-electron microscopy has allowed for the theoretical inspection of the specific molecular determinants of capsid assembly and stability (Buchta et al., 2019; Hogle et al., 1985; Kalynych et al., 2016; Lin et al., 2012). To further dissect the contribution of individual residues to assembly, stability or other aspects of the picornavirus lifecycle most studies have relied on *in vitro* mutagenesis analyses of specific amino acids within the capsid (Mateo et al., 2003; Rincón et al., 2015; Yuan et al., 2016). Although limited, these studies have broadened the knowledge surrounding important aspects of picornavirus structure and provide important strategies for the rational design of novel antivirals and the production of stable virus particles for use in biotechnology and medicine (Mateo et al., 2003; Mateo et al., 2008; Mateu, 2011; Wen et al., 2013). The systematic analysis by experimental mutagenesis of large protein interfaces such as those found in virus capsids is, however, not always appropriate. This is because individual mutants must be generated, purified and analysed separately, which is both a costly and prolonged process when many residues are to be analysed (Delano, 2002). Thus, the theoretical prediction of hotspots using computational methods has provided an attractive alternative and is a useful tool to generate a map of specific residues for further experimental analysis (Morrow and Zhang, 2012; Xue et al., 2015). These computational tools employ a variety of methods and models for hotspot prediction.

Energy-based models (Dehouck et al., 2013; Guharoy and Chakrabarti, 2009; Kortemme and Baker, 2002), such as computational alanine scanning (Gao et al., 2004; Guerois et al., 2002;

Huo et al., 2002; Kortemme et al., 2004) use a free energy function to estimate the change in binding energy ($\Delta\Delta G_{\text{binding}}$) between the WT and mutant protein complex upon mutation of individual amino acid residues. Recently, this approach was used to identify residues within conserved motifs across the enterovirus family that are functionally important for uncoating (Ross et al., 2017). A problem facing these models is that they only assess sidechain interactions, thus in cases where the backbone of the residue is mostly involved in the interaction, the residue is ignored. Additionally, alanine scanning can give rise to a small percentage of false positives (Guo et al., 2014). Molecular dynamics (MD) simulations (Huo et al., 2002; Rajamani et al., 2004; Ross et al., 2018; Yogurtcu et al., 2008) can also be used to estimate the free energy of association. Recently, Kotecha et al. (2015) used a MD-based strategy to assess the stability imparted by specific residues at the two-fold axis in FMDV and to identify amino acid substitutions that strengthen interactions across this interface, for the purpose of designing stabilised capsids as candidate vaccines. MD simulations have good predictive power but use computations that are significantly complex and thus are not well suited to large-scale studies of extensive interfaces due to computational cost (Massova and Kollman, 1999; Radom et al., 2018; Rakers et al., 2015; Steinbrecher et al., 2017). Furthermore MD simulations are not easily implemented without an advanced level of skill for their operation (Xia et al., 2010).

Feature-based approaches are typically combined with machine learning models for prediction (Cho et al., 2009; Deng et al., 2013; Geppert et al., 2011; Guney et al., 2008; Moreira et al., 2017; Qiao et al., 2018; Zhu and Mitchell, 2011). These methods consider characteristics such as electrostatics, surface shape (Bradford and Westhead, 2005), number of residue contacts (Assi et al., 2010), residue position, solvent accessible surface area, protrusion index (Xia et al., 2010) and residue conservation (Geng et al., 2019). Feature-based methods are relatively accurate and are computationally efficient (Cukuroglu et al., 2014; Deng et al., 2014) but may

be biased to the features they consider (Zhu and Mitchell, 2011). Each model and approach has caveats that affect their predictive accuracies, however, studies using generic protein interfaces have demonstrated that hotspot prediction with improved accuracy can be achieved through the use of various models and features in combination (Chen et al., 2011b; Lise et al., 2009; Morrow and Zhang, 2012; Qiao et al., 2018; Tuncbag et al., 2009a, 2009b; Wang et al., 2018; Xia et al., 2010)

The work presented in this chapter considers two previous studies conducted by Ross, (2015) and Ross et al. (2017). The former study involved the large-scale analysis of capsid proteins within the picornavirus family and combined phylogenetic analysis and prediction of interacting motifs within individual protomers belonging to CV-24, CV-B3, PV-1, HRV-A16, HRV-B3, FMDV and TMEV. The results demonstrated that a conserved network of subunit-subunit interactions facilitates the folding of picornavirus protomers. The latter study focused on identifying conserved interacting motifs at intraprotomer, interprotomer and interpentamer interfaces of seven enterovirus capsids. These interfaces are associated with conformational changes required for RNA release during enterovirus uncoating. Computational alanine scanning was then used to elucidate hotspot residues within these conserved motifs that are important for capsid stability. The results identified a network of conserved motifs that facilitate stability of mature enterovirus capsids that are likely involved in capsid uncoating.

While the data generated in these studies greatly advanced the understanding of the conserved molecular determinants that modulate enterovirus capsid stability and provided a guide for future mutagenesis experiments examining enterovirus capsids, investigations into the relative importance of individual residues to capsid assembly, disassembly and stability within other picornaviruses remains limited. Given the importance of hotspot residues to the capsids of these economically and medically significant viruses and their relevance to engineering improved viral control strategies, a simplified screen for their detection would be valuable. Furthermore,

while conserved hotspots in picornavirus capsids that are important modulators of stability could be targeted as a broad strategy for therapeutic control, the identification of non-conserved hotspots would provide insight into the molecular regulators of stability that are unique to a particular virus and its lifecycle.

The overall aim of this study was to expand the knowledge surrounding the capsid residues that modulate the stability and assembly of picornavirus capsids. Specifically, the aim was to yield a simple approach for identifying conserved and non-conserved hotspot residues at protein-protein interfaces within the subunits of picornavirus capsids by implementing a combination of easily accessible hotspot prediction tools for analysis of the TMEV capsid. The objectives for this chapter were three-fold; firstly, to identify residues that significantly contribute to the stability of intraprotomer, interprotomer (five-fold) and interpentamer (two-fold) interfaces of TMEV by combining five energy or feature based tools for hotspot prediction. Secondly, to identify interactions formed between these hotspots and partner residues across these respective interfaces using the PIC and jsPISA webservers. Thirdly, to assess the conservation of individual TMEV hotspot residues with other picornaviruses in the family using the ENDscript 2 webserver.

3.2. Materials and Methods

The methodology in this chapter makes use of various webservers for the prediction of hotspot residues, detection of residue-residue interactions and assessment of residue conservation. In combination these tools provide a robust *in-silico* approach for the detection of conserved and non-conserved hotspots at subunit interfaces that are critical to capsid assembly and stability, and identification of their interacting partners. An overview of the methodology is provided in *Figure 3.1*.

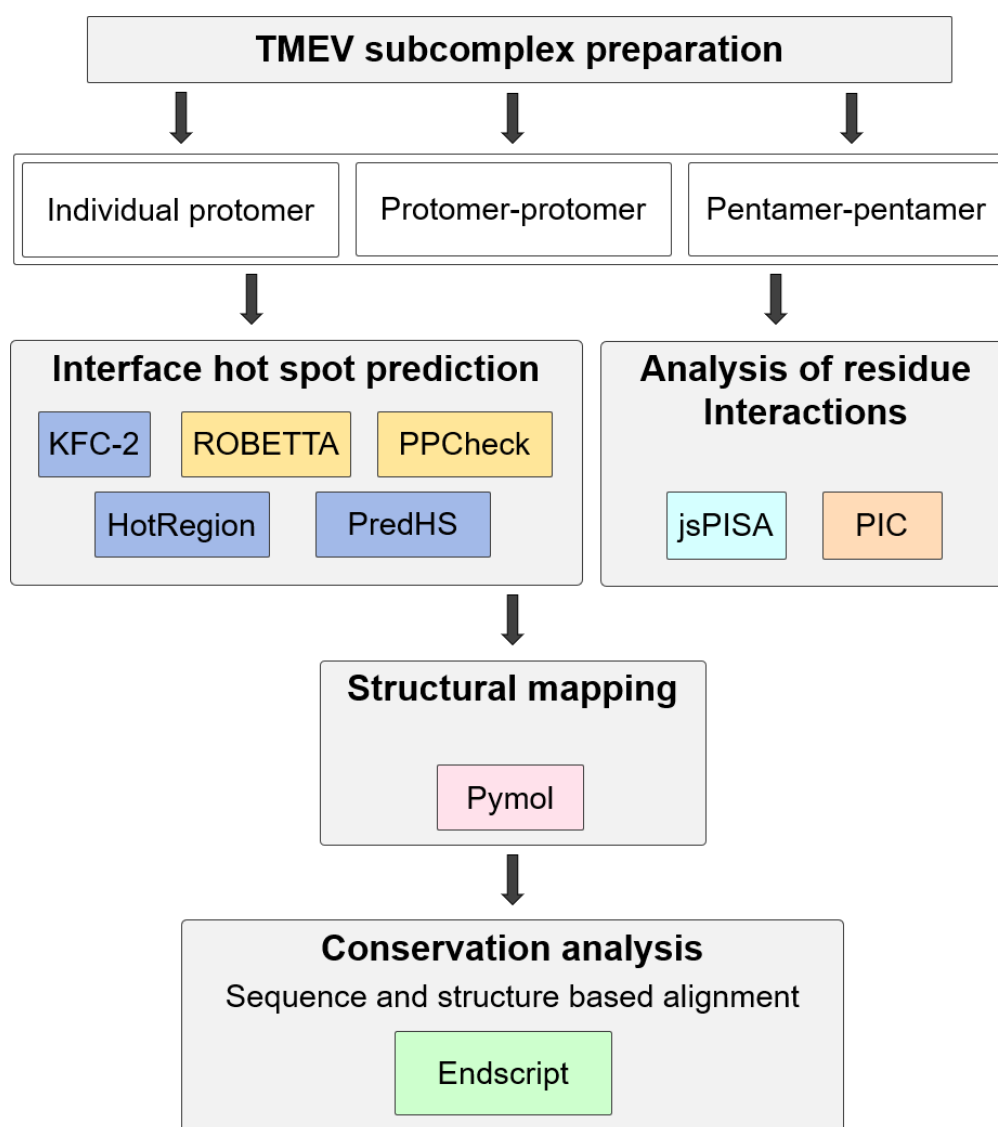


Figure 3.1 Flow diagram of the methodology used to identify conserved and non-conserved hotspot residues and their interacting partners at capsid subunit interfaces. TMEV subcomplexes including the protomer, adjacent protomers at the five-fold axis and neighbouring pentamers at the two-fold axis were extracted from the GDVII PDB file of the full capsid. These complexes were submitted to five hotspot prediction tools for the detection of residues critical to stability of the complex interfaces. The subcomplexes were also submitted to PIC and jsPISA for the analysis of interactions between hotspots and their binding partners. The hotspot residues and their interacting partners were mapped to the capsid complexes using PyMOL for visualisation. Finally, a sequence- and structure-based alignment was performed using ENDscript 2 to assess the conservation of individual hotspot residues in the TMEV capsid with the capsid proteins of other viruses within the picornavirus family.

3.2.1. Preparation of TMEV capsid interface subcomplexes

The TMEV subcomplexes for the analysis of protein-protein interfaces were kindly prepared by C. Ross. Protomer subcomplexes were derived from the PDB file of the assembled TMEV capsid described in chapter two (2.2.9) and in detail in Upfold et al. (2018). The protomers in these complexes were numbered according to their location in the whole TMEV capsid structure which contains P60 protomers. Due to the icosahedral symmetry of the capsid it was unnecessary to examine each interface 60 times, thus each complex was prepared to represent one of the 60 repeating interface complexes within the capsid. To examine the intraprotomer interfaces a single protomer was extracted (P1). To examine interfaces between protomers, two neighbouring protomers surrounding the five-fold axis within an assembled pentamer were extracted (P1 and P2). Finally, to examine the interfaces between pentamers two subunit complexes were created. The first complex, complex A, consisted of two opposing protomers at the two-fold axis of symmetry between pentamers (P1 and P22), the second (complex B) was a complex of two adjacent pentamers located at the pentamer-pentamer interface between the three-fold and two-fold axes of symmetry (P1 and P23). These complexes are shown in *Figure 3.2*.

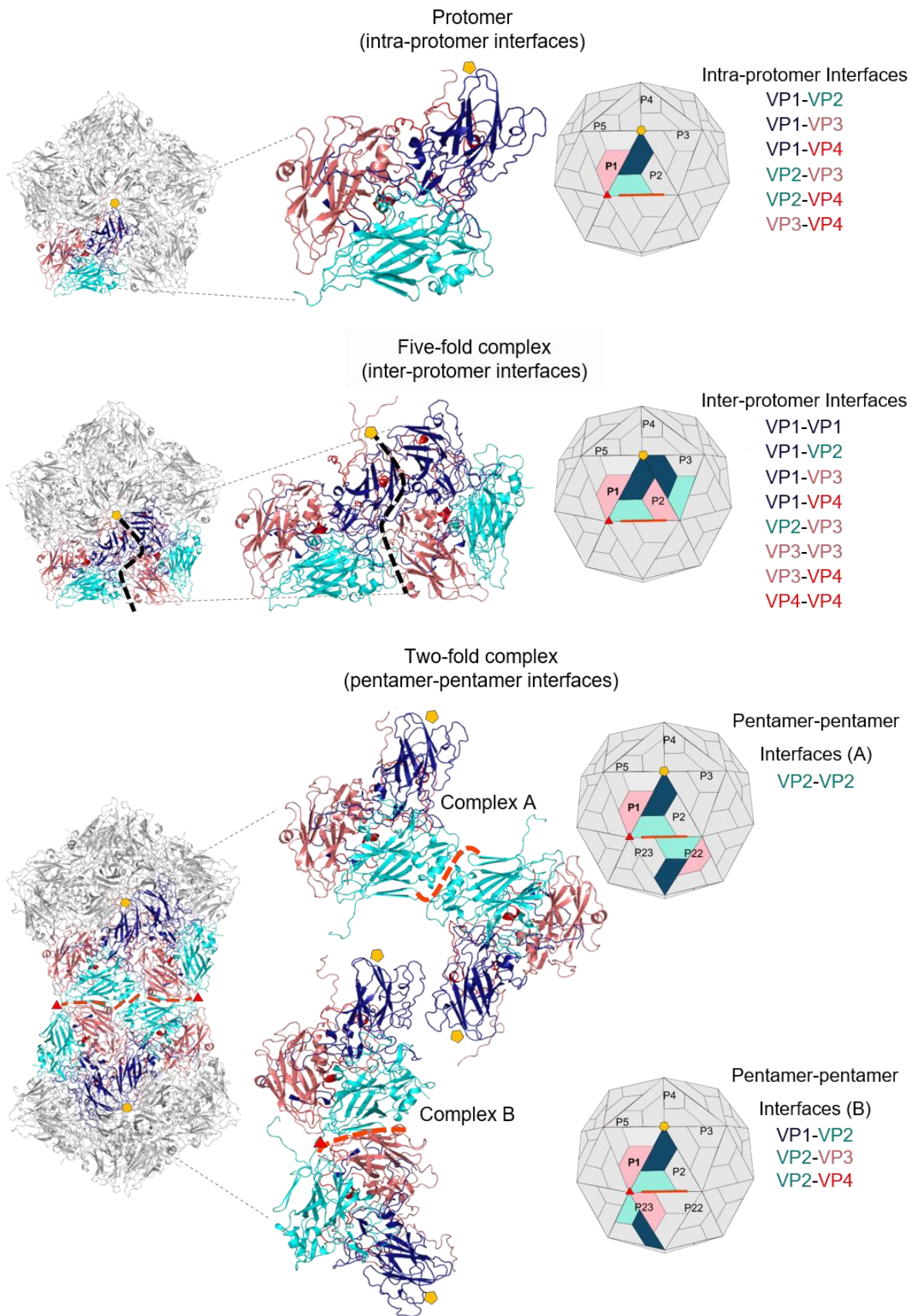


Figure 3.2. TMEV capsid interface subcomplexes for hotspot and protein-protein interaction prediction. The individual subcomplexes were extracted from the PDB file of the full GDVII capsid

generated in chapter two. The interprotomer complex consists of two adjacent protomers at the five-fold axis. The interpentamer complex involves four protomers across the three- and two-fold complexes. Complex A shows the interface formed between two diagonally opposite protomers at the centre of the two-fold axis. Complex B shows the interface formed between VP2 and VP3 from two adjacent protomers belonging to different pentamers. In the interface between two pentamers there are two B complexes (in opposite orientations), but only one A complex, although only one is shown here. Capsid proteins are coloured: navy blue-VP1; cyan-VP2; salmon-VP3; maroon-VP4. Individual protein-protein interfaces that form part of the major interfaces of each complex are listed on the right of the subcomplex structures. Protomers are numbered according to their state in the biological assembly. The five-, three- and two-fold axes have been indicated by yellow pentagons, red triangles and orange lines respectively.

3.2.2. Interface hotspot prediction

Interacting hotspot residues involved in stabilising the capsid subunits were identified using a combination of *in-silico* tools. Each tool was required to be readily accessible and allow the user to submit their own protein complex for analysis. Overall five predictive models based on energy- or feature-related methods were used in combination to allow for cross validation and improved predictive accuracy.

3.2.2.1. Energy-based methods used for analysis

The ROBETTA webserver (<http://robetta.bakerlab.org/alaninescan>) (Kortemme et al., 2004) identifies all residues involved in protein interfaces of a given complex as residues within a 4 Å radius of an atom from a residue belonging to the partner protein. The webserver then substitutes these residues to alanine and calculates the effect of the mutation on the binding free energy of the complex and the change in stability of the protein to which the residue belongs, using a free energy function. ROBETTA classifies hotspot residues as those that are predicted to significantly destabilise the interface following mutation, in energetic terms those that exhibit an increase ≥ 1 kcal/mol in binding free energy.

The PPCheck webserver (<http://caps.ncbs.res.in/ppcheck/>) (Sukhwal and Sowdhamini, 2015) can be used to measure the strength of interactions between two proteins/chains of a given complex and can predict energetically important residues present at these interfaces using pseudoenergies or *in-silico* alanine scanning. PPcheck confers pseudoenergies to protein interfaces based on the sum of non-covalent interaction energies and considers parameters such as extent of residue interaction to predict hotspots.

3.2.2.2. Feature-based methods used for analysis

Knowledge-based FADE and Contacts 2 (KFC2) is an online webserver (https://mitchell-lab.biochem.wisc.edu/KFC_Server/index.php) for the prediction of hotspots in a protein complex given two protein chains in a single PDB file, and uses a machine learning approach that considers biochemical and structural features (Zhu and Mitchell, 2011). KFC originally examined these features and used decision trees to predict hotspot residues (Darnell et al., 2008, 2007). The updated KFC2 method combines two models that are trained using a support vector machines and considers additional features relating to interface position, residue size, packing density, solvent accessibility, local residue plasticity and the hydrophobicity and flexibility of surrounding residues (Zhu and Mitchell, 2011).

PredHS (Prediction of hotspots) is an online webserver (<http://predhs.denglab.org/>) that employs a machine learning based method to predict hotspots at protein-protein interfaces of a given protein complex in the PDB format with at least two chains (Deng et al., 2014). PredHS extracts all the available sequence-, structure- and energetic-based features of the complex and selects the optimal subset of features for consideration, then uses Euclidian and Voronoi neighbourhoods to generate individual residue scores. Residues with scores larger than zero are rated as hotspots.

HotRegion is an online database of predicted clusters (<http://prism.cccb.ku.edu.tr/hotregion>) (Cukuroglu et al., 2012). When a PDB file containing a protein complex and two chain identifiers is uploaded, HotRegion will predict hotspots in the protein interfaces of the complex using HotPoint (Tuncbag et al., 2010), which considers solvent accessibility and energetic contribution of each residue. A network of hotspot residues is constructed, and hotspots found to be involved in contacts with other hotspot residues are defined as members of a hot region within the interface and are highlighted on a 3D structure of the protein complex.

The TMEV protomer, interprotomer and interpentamer (A and B) subcomplexes (*Figure 3.2*) were individually submitted to each of the selected prediction webservers for analysis. A residue was only considered to be a hotspot if identified by at least two of the five prediction methods. The results were mapped to the crystal structures of the individual TMEV subcomplexes for visualisation in PyMOL (Schrodinger, 2010).

3.2.3. Prediction of interacting residues

Interprotein interactions were calculated using the Protein Interaction Calculator (PIC) (<http://pic.mbu.iisc.ernet.in/>) (Tina et al., 2007) and the Protein Interactions, Surfaces and Assemblies (jsPISA) webserver (<http://www.ccp4.ac.uk/pisa>) (Krissinel, 2015). The TMEV capsid intraprotomer, interprotomer and interpentamer (A and B) subcomplexes (*Figure 3.2*) were individually submitted to PIC and jsPISA for analysis. PIC calculates various protein-protein interactions including hydrophobic interactions within 5 Å; mainchain-mainchain, mainchain-sidechain and sidechain-sidechain hydrogen bonds; cation-pi and ionic interactions within 6 Å; disulphide bonds, aromatic-aromatic interactions between 4.5 and 7 Å and aromatic-sulphur interactions between 5.3 Å using the coordinates of a given PDB file. jsPISA uses a thermodynamic approach to detect macromolecular assemblies using the coordinates of a PDB file, then calculates the solvation energy, binding energy, hydrophobic P-value, number of hydrogen bonds, salt bridges and disulphide bonds of a macromolecular interface and lists

the exact residue pairs involved in these interactions (Krissinel, 2015; Krissinel and Henrick, 2007). The results generated by the two webservers were then used to generate interacting network diagrams of the hotspots and their interacting partners.

3.2.4. Identification of conserved hotspot residues

The ENDscript 2 server (<http://endscript.ibcp.fr>) (Robert and Gouet, 2014) was used to determine the degree of conservation of each of the hotspot residues identified at each interface. The PDB file of a single TMEV protomer was uploaded, and individual protein chains (A, B, C and D representing VP1-4) were analysed separately. ENDscript 2 considers the conservation of a protein's sequence and structure. Given a specified chain in a PDB file, ENDscript extracts the amino acid sequence to perform a PDBAA BLAST search. The homologous sequences are aligned using Clustal Omega and a multiple sequence alignment is generated that also includes secondary structure information. Additionally, a 3D structure of the PDB file superimposed with all homologous protein structures is created and the conserved residues are highlighted (Gouet et al., 2003; Robert and Gouet, 2014).

3.3. Results

3.3.1. Hotspot residues predicted within the intraprotomer interfaces of TMEV

To identify residues that contribute to the structural integrity of interfaces within the TMEV protomer, the protomer complex was submitted to the five hotspot prediction webservers. Six interfaces are formed between the individual capsid proteins upon folding of the protomer. Together, 72 residues were identified as hotspots within these interfaces (*Figure 3.3 A and B*), by two or more of the hotspot prediction tools (Table S1). 32 of these residues belong to VP1, 20 to VP2 and 20 to VP3. No hotspot residues were detected in the VP4 protein. The PIC and jsPISA analyses confirmed that all 72 hotspot residues are involved in interactions across the six interfaces (*Figure 3.3 C*).

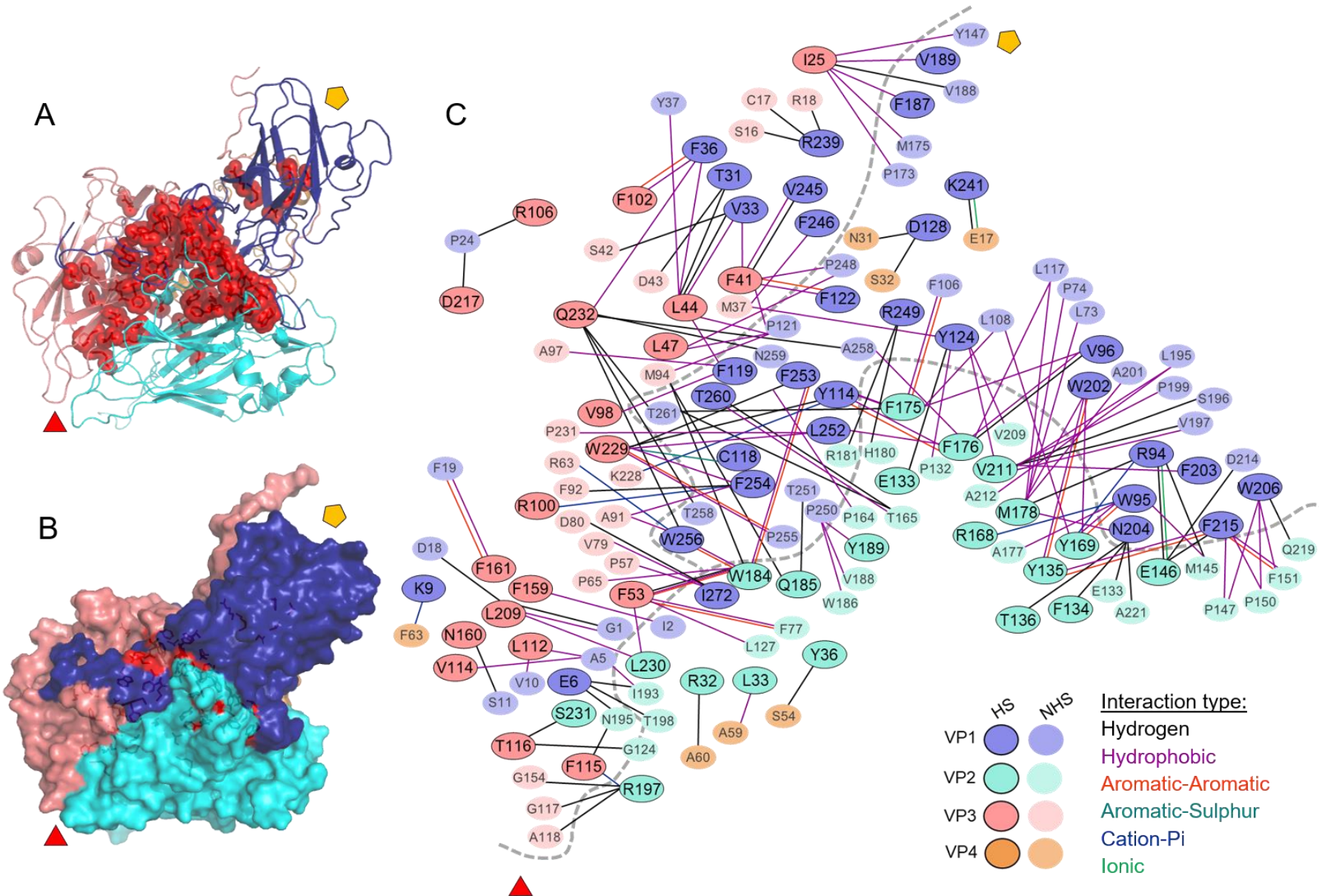


Figure 3.3 Identification of hotspot residues and their interacting partners within intraprotomer interfaces of the TMEV capsid. A) Cartoon mapping of predicted hotspot residues (shown as red spheres) at the six intraprotomer interfaces in TMEV. B) Surface exposure of the predicted hotspots. C) Schematic network of hotspot residues and the interactions between their binding partners within the intraprotomer interfaces. HS – hotspot residue. NHS – Null hotspot residue (hotspot interacting partner). Capsid proteins are coloured: navy blue-VP1; cyan-VP2; salmon-VP3 and orange-VP4. five-fold and three-fold axes are indicated by yellow pentagons and red triangles respectively.

While most of the hotspot residues are involved in interactions across only one interface, residue Q185 belonging to VP2 forms hydrogen bonds with residues T251 and M94 from VP1 and VP3 respectively and was predicted to contribute to the stability of both interfaces. 44 of the hotspot residues were predicted to form interactions with at least one other hotspot residue across the interface and 33 hotspots were predicted to form interactions with only one other residue across the interface. Most of the hotspot residues at the VP1-VP3 and VP2-VP3 interfaces were shown to be involved in hydrophobic interactions or hydrogen bonds with partner residues, however, hydrophobic interactions are dominant at the VP1-VP2 interface. Aromatic interactions were shown to be relatively common throughout the interface and are twice as likely to be found between two interacting hotspot residues than between a hotspot and non-hotspot residue.

Sequence and structure conservation analysis of the hotspot residues revealed that 57 of the residues are conserved in the capsid proteins of other picornaviruses. Two of the 32 hotspots belonging to VP1, six of the 20 residues identified as hotspots in VP2 and three out of the 20 in VP3 are conserved in only the coronaviruses (*Table 3.1*). Several of the hotspot residues detected in the interfaces of the TMEV protomer were previously suggested to be important for the stability of the virus, others were found to correlate to residues previously reported to be important for virus growth, receptor binding. These residues of interest are highlighted in bold and will be discussed subsequently.

Table 3.1 Hotspot residues in the TMEV intraprotomer interfaces and their conservation within the picornavirus family.

TMEV Hotspot Residue		Conservation Analysis									
		MEV	SAFV	SVV	FMDV		ERAV	EV71	HRV		CAV-9
					Type C	SAT2			3	2	
VP1	E6										
	K9										
	T31										
	V33										
	F36										
	R94										
	W95			F							
	V96										
	Y114		W	F			W				
	C118										
	F119										
	F122										
	Y124										
	D128										
	F187										
	V189		I	L							
	W202						Y				
	F203	Y									
	N204							D			
	W206										
	F215					Y					
	R239									K	K
	K241									H	H
	V245			W			Y				
	F246			W				W	W	W	W
	R249										
	L252										
F253											
F254											
W256			Y								
T260											
I272											
VP2	R32										
	L33						I	I	I	V	
	Y36		F								
	E133										
	F134	Y									
	Y135										
	T136										
	E146										
	R168										
	Y169										
	F175										

F176										
M178										
W184										
Q185							N	N	N	
Y189		F			F		F	F		
R197										
V211	I					A				
L230	V		V			I	I			
S231										
VP3	I25	V	A	A		L		A	A	A
	F41	Y			Y					
	L44								M	
	L47	I		V	V	V		I		I
	F53									
	V98	L	I	L	L	L	L	I	I	I
	R100									
	F102			Y	Y		Y	Y	Y	Y
	R106									
	L112									
	V114			M	M	I	M	M	L	M
	F115				Y			Y		
	T116									
	F159	Y								
	N160	S	T	T	T	S	T		T	
	F161									
	L209			V	V		I			M
	D217									
	W229									
	Q232									

Table 3.1 Footnotes:

Hotspot residue conservation analysis as determined using the ENDScript 2 webserver. Individual proteins were submitted to the webserver and compared against picornavirus capsid proteins from other genera. Cardiovirus: SAFV (PDB: 5CFC/5A8F); Senecavirus: SSV-1 (PDB: 3CJI); Aphthovirus: FMDV type C, FMDV SAT2, ERAV (PDB: 1FMD, 5ACA, 2WFF); Enterovirus: EV-71, HRV-3, HRV-2 CAV-9 (PDB: 3VBS, 1RHI, 1FPN, 1D4M). Red blocks indicate residues that are 100 % conserved, orange blocks denote conservative substitutions. Hotspots highlighted in bold are those that correspond to residues previously reported to be important for picornavirus structure or stability. Full alignments are included in figures S1-S6.

3.3.2. Destabilising residues at interprotomer interfaces

The TMEV interprotomer interfaces are formed between two adjacent protomers within the same pentamer. A total of 34 residues were identified by two or more prediction models (Table S2) as hotspots within these eight interfaces (*Figure 3.4 A-C*). 13 hotspot residues were identified in the VP1 protein, five in VP2, 12 in VP3 and four in VP4. The VP1-VP3 interface

had the highest number of hotspot residues, followed by the VP2-VP3 interface and the interface between two VP1 proteins (*Figure 3.4 D*).

Analysis of interactions across these interfaces using PIC and jsPISA confirmed that all hotspot residues detected are involved in non-covalent interactions with residues from partner proteins across the interface (*Figure 3.4 D*). 16 of the hotspots form interactions with other hotspots and 13 of the hotspots form interactions with only one other residue. Hotspot residue Y29 belonging to VP4 was predicted to be important for the stability of both the VP1-VP4 and VP3-VP4 interfaces (Table S2). Analysis of residue interactions revealed that hydrophobic interactions and hydrogen bonds are equally abundant across the interface, however, hydrophobic interactions are mostly formed between the VP1-VP1 and VP2-VP3 interfaces, and hydrogen bonds are more common across the VP1-VP3 interface (*Figure 3.4 D*). VP1 residues R171 and W176 were predicted as hotspots in the VP1-VP3 and VP1-VP1 interfaces (Table S2) respectively, however, these residues are also involved in non-covalent interactions with proteins at other interfaces. R171 is involved in hydrogen bonds with residues G101, I224 and G225 in VP3, but also with residue F36 of the neighbouring VP1 protein. W176 is involved in hydrogen bonds and cation-pi interactions with residues A135 and R237 of the adjacent VP1 protein but is also involved in hydrogen bonds and hydrophobic interactions with residue F14 in VP2. Similarly, VP4 residues Y25 and Y29 are hotspots in the VP4-VP4 and VP4-VP3 interfaces respectively, but also form bonds with residues from capsid proteins at other interfaces where they are not important for stability (*Figure 3.4 D*).

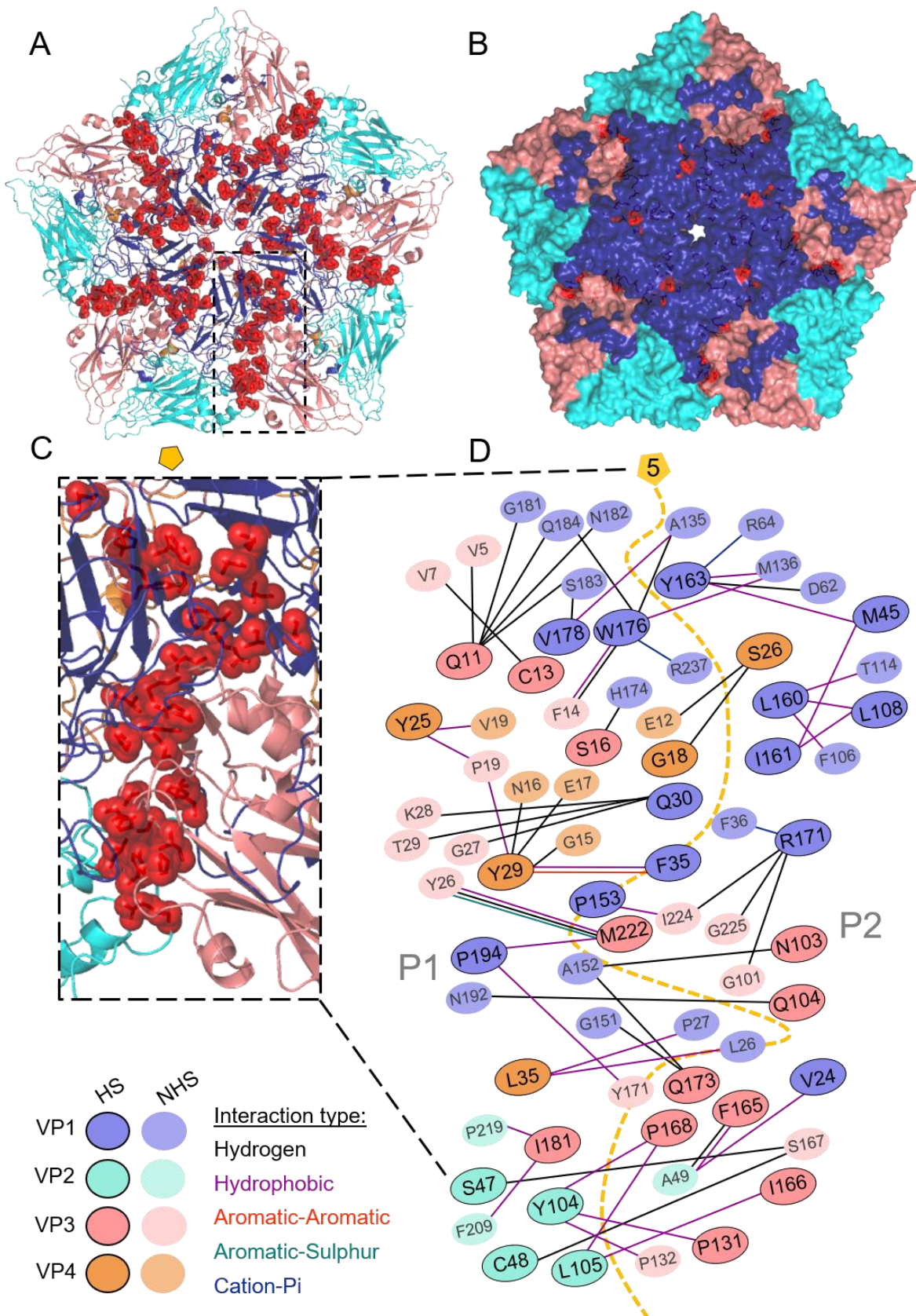


Figure 3.4 Network of hotspot residues and their interacting partners between two protomers of TMEV. A) Cartoon mapping of predicted hotspot residues (shown as red spheres) at the interprotamer

interfaces of the TMEV capsid. B) Surface exposure of the predicted hotspots. C) Close view of predicted hotspots (shown as red spheres). D) Schematic network of hotspot residues and the interactions between their binding partners within interprotomer interfaces. HS – hotspot residue. NHS – Null hotspot residue (hotspot interacting partner). Capsid proteins are coloured: navy blue-VP1; cyan-VP2; salmon-VP3 and orange-VP4. Five-fold and three-fold axes are indicated by yellow pentagons and red triangles respectively. Protomers are numbered according to their biological state in the complete capsid.

Sequence and structure conservation analysis using ENDscript 2 revealed that 32 of the 34 of the interprotomer hotspot residues are conserved with residues in the capsid proteins of other picornaviruses (*Table 3.2*), and only ten residues are conserved in the cardioviruses alone. Several of the hotspot residues detected in the TMEV interprotomer interfaces were also previously reported to be important for the receptor binding and stability of TMEV, while others correlate to residues that are reported to be required for virus growth and stability in related picornaviruses. These residues of interest are highlighted in bold and will be discussed subsequently.

Table 3.2 Hotspot residues in the TMEV interprotomer interfaces and their conservation within the picornavirus family.

TMEV Hotspot Residue		Conservation Analysis								
		MEV	SAFV	SVV	FMDV		ERAV	EV-71	HRV-3	PV-1
					Type C	SAT 2				
VP1	V24			A						
	Q30									
	F35									
	M45	A	V	V						
	L108									
	P153									
	L160									
	I161	L								
	Y163									
	R171									
	W176	Y		F			F			
	V178	A					I			
	P194									
	VP2	S47						T	T	
C48										
Y104				F						
L105										
VP3	Q11			S			S	T	S	S
	C13									
	S16				T	N		T	T	T
	N103				T			T	T	T
	Q104			N						
	P131									
	F165			Y	Y	Y	Y	W	W	W
	I166					V				
	P168									
	Q173									
	I181									
M222			L	L			L	L	L	
VP4	G18									
	Y25									
	S26									
	Y29									
	L35									

Table 3.2 Footnotes:

Hotspot residue conservation analysis as determined using the ENDscript 2 webserver. Individual proteins were submitted to the webserver and compared against picornavirus capsid proteins from other genera. Cardiovirus: SAFV (PDB: 5CFC/5A8F); Senecavirus: SSV-1 (PDB: 3CJI); Aphthovirus: FMDV type C, FMDV SAT2, ERAV (PDB: 1FMD, 5ACA, 2WFF/2XB0); Enterovirus: EV-71, HRV-3, PV-1 (PDB: 3VBS, 1RHI, 2PLV). Red blocks indicate residues that are 100 % conserved, orange blocks denote conservative substitutions. Hotspots highlighted in bold are those that correspond to residues previously

reported to be important for picornavirus structure or stability. Alignments are included in figures S1-S6.

3.3.3. Destabilising residues at pentamer-pentamer interfaces

The pentamer-pentamer interface is formed through the interaction of four protomers across two adjacent pentamers and extends between two 3-fold axes (*Figure 3.2*). Interactions across this interface primarily involve residues between VP2 and VP3 proteins from separate pentamers near the three-fold axes. The same VP2 protein forms interactions with the VP2 protein from one of the protomers in the opposite pentamer. These proteins meet diagonally across the interface at the centre of the two-fold axis. 24 residues were predicted to be hotspots across these interfaces (*Figure 3.5 A-C*), by two or more of the prediction models (Table S3). The 24 hotspots are, however, doubled across the entire pentamer interface as four protomers are involved. 18 of the 24 hotspots were identified across the VP2-VP3 interface, with seven belonging to VP2 and the remaining 11 to VP3. Six residues were predicted to be hotspots between the VP2-VP2 proteins; this interface involves identical residues from the VP2 proteins running in opposite directions, thus the six hotspot residues would be doubled across the interface (as shown in *Figure 3.5 D*). No hotspot residues were predicted at the VP2-VP4 interface.

Interaction analysis using PIC and jsPISA confirmed that all hotspot residues are involved in non-covalent interactions across the pentameric interface (*Figure 3.5 D*). Most hotspot residues form hydrogen bonds with partner residues, although some residues are involved in a few hydrophobic interactions closer to the two-fold axis. None of the hotspot residues are involved in interactions with residues belonging to proteins at other protein-protein interfaces, unlike some hotspots in the intra- and interprotomer interfaces. Interestingly, hotspot residues T53, L57 and R102 belonging to VP2 and D152 and L153 belonging to VP3 only form interactions

with non-hotspot residues, and 13 of the hotspot residues are only involved in interactions with one other residue across the interface.

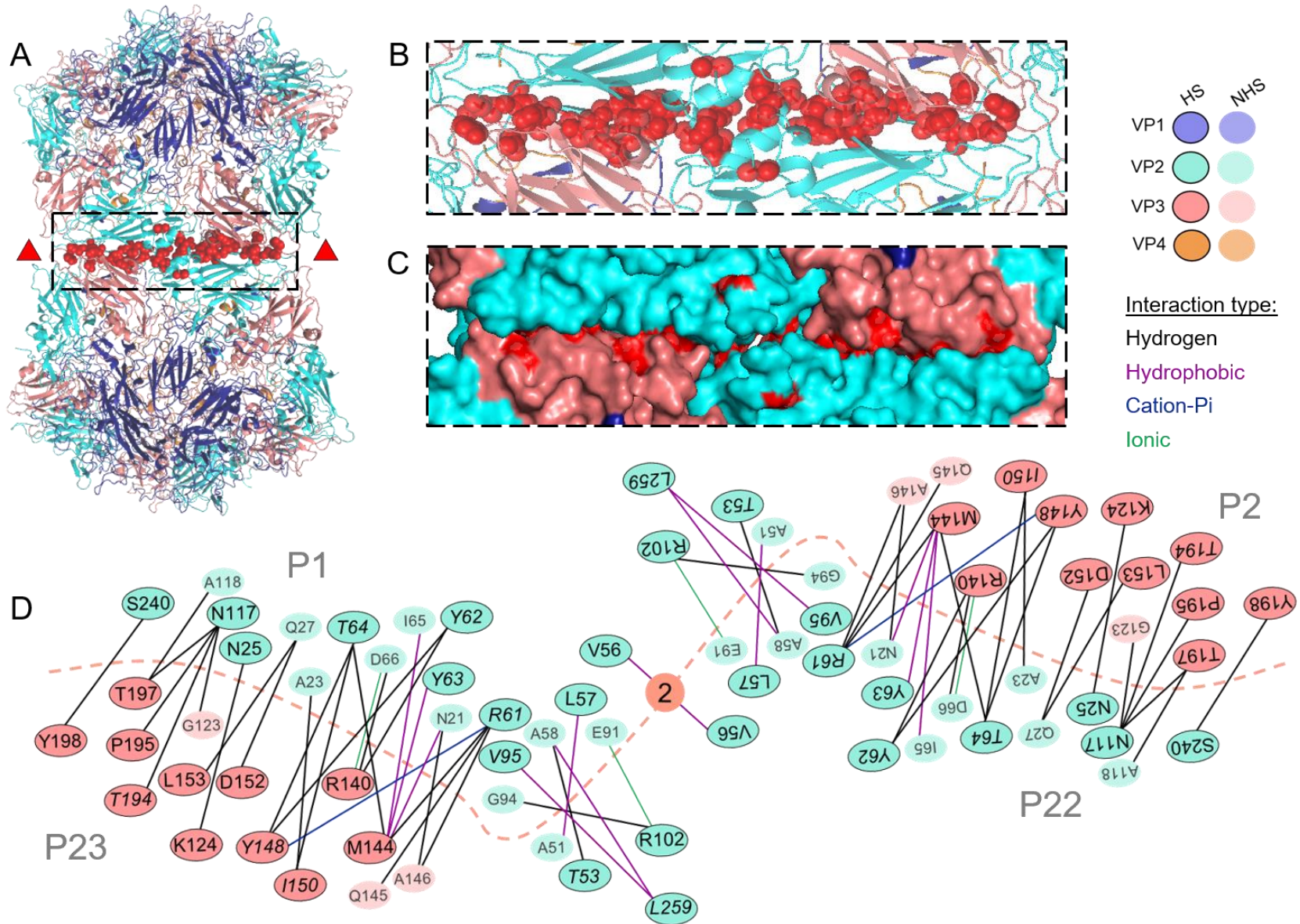


Figure 3.5 Network of hotspot residues and their interacting partners at the pentamer-pentamer interface. A) Cartoon mapping of predicted hotspot residues (shown as red spheres) at the interpentamer interfaces of the TMEV capsid. B) Close view of predicted hotspots (shown as red spheres). C) Surface exposure of the predicted hotspots. D) Schematic network of hotspot residues and the interactions between their binding partners within interpentamer interfaces. HS – hotspot residue. NHS – Null hotspot residue (hotspot interacting partner). Capsid proteins are coloured: navy blue-VP1; cyan-VP2; salmon-VP3 and orange-VP4. Two-fold and three-fold axes are indicated by dotted orange lines and red triangles respectively. Protomers are numbered according to their biological state in the complete capsid.

Conservation analysis using the ENDscript 2 webserver revealed that all hotspot residues are conserved in at least one other virus within the family and that only two residues -VP3 P195 and Y198 are conserved in the cardioviruses alone (*Table 3.3*). Several of the hotspot residues detected in the TMEV interpentamer interfaces correlate to residues that are reported to be required for stability and uncoating in related picornaviruses. These residues of interest are highlighted in bold and will be discussed subsequently.

Table 3.3 Hotspot residues in TMEV interpentamer interfaces and their conservation within the picornavirus family.

TMEV Hotspot Residue		Conservation Analysis										
		MEV	SAFV	SWV	FMDV		ERAV	EV-71	HRV		EV-D68	PV-1
					Type C	SAT2			B 14	2		
VP2	N25				T	T		T	T	T		T
	T53	S							S			
	V56	I										
	L57						V					V
	R61											
	Y62			W	F	F		F	F	F	F	F
	Y63				F	F						
	T64											
	V95			A		I			I	I	M	L
	R102											
	N117					T						
	S240			T				T	T			
	L259								I	A		
	VP3	K124				R						
R140												
M144					A	A						
Y148												
I150							V		V		V	
D152												
L153				I			V		V	V		I
T194												
P195												
T197												
Y198												

Table 3.3 Footnotes:

Hotspot residue conservation analysis as determined using the EndScript 2 webserver. Individual proteins were submitted to the webserver and compared against picornavirus capsid proteins from other genera. Cardiovirus: SAFV (PDB: 5CFC/5A8F); Senecavirus: SSV-1 (PDB: 3CJI); Aphthovirus: FMDV type C, FMDV SAT2, ERAV (PDB: 1FMD, 5ACA, 2WFF/2XB0); Enterovirus: EV-71, HRV-B14, PV-1 (PDB: 3VBS, 1R08 4RHV, 2PLV). Red blocks indicate residues that are 100 % conserved, orange blocks denote conservative substitutions. Hotspots highlighted in bold are those that correspond to residues previously reported to be important for picornavirus structure or stability. Full alignments are included in figures S1-S6.

3.4. Discussion

The primary aim of this study was to develop a simple approach for the prediction of hotspot residues at protein-subunit interfaces within picornavirus capsids. Unlike a previous study examining enterovirus interfaces (Ross et al., 2017), this study did not limit hotspot prediction to conserved motifs, but instead identified hotspots throughout a protein-protein interface and conservation was determined as a *post hoc* analysis. This approach was chosen to identify non-conserved hotspots that have evolved to stabilise the interfaces of TMEV in a manner unique to the virus' lifecycle, but also to identify conserved stabilising residues throughout the family that may provide insights into conserved mechanisms of capsid stability within the picornaviruses as a whole. Also unique to this screen was the use of multiple prediction tools in combination. This approach was used as studies identifying hotspot residues in generic protein interfaces have reported that prediction accuracy is significantly improved when methods are combined (Morrow and Zhang, 2012; Tuncbag et al., 2009b). Two energy-based and three structure-based prediction methods were chosen. Each tool was selected because it was readily accessible, can be implemented by users without prior advanced bioinformatic knowledge and can accept PDB files provided by the user.

The first analysis explored the residues that contribute significantly to the stability of interfaces within the TMEV protomer complex. These six interfaces are formed following the folding of the four capsid proteins into the stable protomer subunit, which occurs immediately following P1 processing (Jiang et al., 2014). In total, 72 residues were identified as hotspots contributing significantly to the binding specificity and energy of the complex, by two or more of the webservers. Interestingly most of the hotspot residues were identified to form interactions across the VP1-VP2 and VP1-VP3 interfaces within a protomer. Sixty-one percent of the hotspot residues were predicted to form interactions with at least one other hotspot residue and, 45 % of the hotspots were predicted to form interactions with only one other residue across the

interface. Most of the hotspot residues at the VP1-VP3 and VP2-VP3 interfaces were shown to be involved in hydrophobic interactions or hydrogen bonds with partner residues. However, most hotspot residues at the VP1-VP2 interface form contacts with partner residues through hydrophobic interactions, consistent with the fact that most of this interface is buried beneath the capsid surface.

Several of the hotspot residues predicted at the intraprotomer interfaces were previously suggested to stabilise the TMEV capsid under changing pH conditions, based on structural studies of TMEV (Luo et al., 1992). TMEV is more resistant to variable pH conditions than many other coronaviruses, including mengo virus (MEV) (Luo et al., 1992). Hotspot residues VP1 W202, W206, F215 and VP2 Y135 that were identified to interact with residues across the VP1-VP2 interface, reside on the TMEV VP1 FMDV loop and Puff B of VP2 respectively. These residues are four out of five aromatic residues that are thought to form a hydrophobic core that imparts a stable conformation to the TMEV VP1 FMDV loop, allowing it to maintain stability under a broad range of pH conditions (Luo et al., 1992). This stabilising core is absent in most other coronaviruses and consequently the VP1 FMDV loops in these viruses readily change conformation at a mild pH. In MEV these conformational changes expose the receptor binding site and weaken the capsid, making it unstable and susceptible to dissociation in the presence of 0.15 M Cl⁻ or Br⁻ (Luo et al., 1992). Furthermore, the screen detected residue VP2 E146 as a hotspot. This residue is known to interact with non-hotspot residue D214 in VP1 through hydrogen bonds, as was also suggested in this study using PIC and jsPISA. These residues also contribute the stability of the VP1 FMDV loop of TMEV under changing pH conditions (Luo et al., 1992). The identification of these residues as hotspots in this study supports the previous suggestions that they are responsible for the stability of TMEV under changing pH conditions (Luo et al., 1992; Zurbriggen et al., 1989). Moreover, very few of these hotspot residues were conserved in the other picornaviruses, including the coronavirus

MEV, further supporting their role in modulating the unique pH stability of TMEV. Hotspot residues R94, W95 and V96 in VP1 were identified to form interactions with hotspot residues F176 and M178 in VP2. These residues reside on loop II of VP1 and Puff A of VP2 and it has been speculated that interactions between these residues contribute to the conformational stability of these loops (Luo et al., 1992). Substitution of amino acid A101 at the surface of loop II VP1 to a bulkier hydrophobic residue was previously reported to disrupt interactions between these residues, in turn reducing both loop stability and viral persistence (Zurbriggen et al., 1989). The prediction of these residues as hotspots further supports the previous reports that they stabilise the conformation of the surface loops upon which they reside and are important for capsid stability.

Hotspot residues VP1 F254 and VP3 R100 were predicted to form cation- π interaction across the VP1-VP3 interface. These residues reside in the putative receptor binding pit of TMEV and were also predicted to be directly involved in heparan sulphate binding as shown in docking experiments performed in chapter two and Upfold et al. (2018). Moreover, hotspot residues VP1 V245, F246, R249, L252, F253, F254, W256, T260 and I272 form part of the VP1 C-terminal loop that extends over the pit. This is the same C-terminal loop that was recognised by the anti-TMEV capsid antibodies produced in chapter two and Upfold et al. (2018). The results demonstrated these hotspot residues to be involved in numerous interactions with residues belonging to VP2 and VP3, which may help to maintain the structural integrity of the loop that forms the wall of the receptor binding pit. Furthermore, almost all of these hotspot residues were not conserved in viruses belonging to other genera, an unsurprising finding given that picornaviruses have evolved a variety of residues and topological features for receptor binding (Tuthill et al., 2010).

Of the 72 predicted hotspots, 63 % were conserved in at least one virus from another genus. Several of these conserved residues were previously reported to be functionally important in

viruses belonging to different genera. Hotspot residues, K241 and R249 in TMEV VP1 correspond to residues K256 and R264 in EV-71 that were reported to be critical for virus growth and replication (Yuan et al., 2016). *In vitro* substitution of these residues to alanine proved lethal as the resultant virions could not be recovered following serial passaging (Yuan et al., 2016). Analysis of residue conservation in this study revealed these two residues to be highly conserved in other enteroviruses as well as in FMDV type C and SAT2. Residue R249 was conserved in all viruses analysed except for SVV-1. Recently Ross et al. (2017) identified a network of interacting motifs within regions of enterovirus capsids that were associated with RNA release. Computational alanine scanning of residues within these motifs revealed several hotspot residues that likely contribute to enterovirus capsid stability and uncoating, including residue R264 in EV-71 that corresponds to hotspot residue R249 in TMEV (Ross et al., 2017). Both residues R249 in TMEV and R246 in the enteroviruses form interactions with residues belonging to the VP2 protein (residues H180 and R181 in TMEV, that are not hotspots). TMEV VP1 hotspot residues Y124, N204 and F246 were also found to be conserved with energetically important VP1 residues Y128, D206 and W261 in EV-71 (Ross et al., 2017). The conservation of these TMEV hotspots with residues previously reported to be important for growth and stability in other viruses implies their importance to intraprotomer interface stability across the picornaviruses.

Hotspot residue K241 (VP1) corresponding to residue K256 in EV-71 (Yuan et al., 2016) was predicted to be involved in interactions with VP4, a protein known to make contacts with the RNA genome (Butan et al., 2014; Lyu et al., 2014). Several studies have reported that interactions between the viral RNA genome, the N-terminal extensions of VP1-VP3 and the VP4 protein stabilise picornavirus capsids and influence both pH and thermal stability (Curry et al., 1997; Shakeel et al., 2016). Moreover, recent studies have speculated that these RNA-protein interactions located below the capsid surface may exert enough force as to significantly

contribute to genome uncoating under particular physiological conditions (Buchta et al., 2019; Lyu et al., 2014). Hotspot residue VP1 K241 also corresponds to residue R202 in the VP1 protein of HPV-3 that is known to be involved in interactions with the viral genome (Shakeel et al., 2013). Furthermore, residue T47 in HPV-3 VP3 is also involved in RNA-interactions. This residue is conserved with TMEV VP3 S16, a residue that is not a hotspot residue at the intraprotomer interface but is at the interprotomer interface (Figure S7) (Shakeel et al., 2013). Whether these hotspot residues interact with RNA in TMEV is not known, however, their conservation in two separate genera suggests a common function. Furthermore, it is tempting to speculate that conformational changes to the viral RNA genome under altered physiological conditions during uncoating may infer changes upon these hotspots, in turn destabilising the interfaces they maintain.

Next, the screen was applied to identify hotspot residues contributing to the stability of the interprotomer interfaces. These interfaces are formed between five protomer complexes of the assembled pentamer and begin at the five-fold axis and extend vertically towards the two-fold axis. Pentamers have been reported as very stable intermediates during assembly and uncoating (Arkhipov et al., 2006; Reddy et al., 1998). It has been tentatively suggested that evolution has selected strong interactions across the interprotomer interfaces because dissociation of pentamers into protomer subunits is not necessary for the virus lifecycle, and strong interactions between protomers would ensure the increased concentration of intact pentamers for the efficient assembly of virus capsids (Mateu, 2017). To identify residues that contribute to critical stabilising interactions between the protomers that form the pentamer, a complex of two adjacent protomers was submitted to five hotspot prediction tools.

The analysis identified 34 residues as hotspots, with the majority being located at the VP1-VP3 interface. 47 % of the hotspots formed interactions with other hotspots and 50 % of residues formed interactions with only one other residue. Hotspot residue Y29 belonging to VP4 was

predicted to be important for stability of both the VP1-VP4 and VP3-VP4 interfaces. No other hotspot was predicted to be important for the stability of multiple interfaces between the protomers. Analysis of residue interactions revealed that hydrophobic interactions and hydrogen bonds were equally abundant across the interface.

In many picornaviruses the receptor binding sites also involve residues located at or adjacent to the protomer-protomer interfaces. For example, the canyons of enteroviruses surround the five-fold axes and traverse the protomeric interfaces (Rossmann, 1989; Smyth and Martin, 2002). This is no different for TMEV, where the receptor binding pit involves residues belonging to VP1 from one protomer and VP3 from the neighbouring protomer (Luo et al., 1996) that interact across the interface. Two hotspot residues identified at this interface in TMEV are residues P153 and I181 belonging to VP1 and VP3 respectively. These residues are exposed at the bottom of the TMEV receptor binding pit and analysis of residue interactions revealed that they form interactions with VP3 I224, VP2 F209 and VP2 P219 across the interprotomer VP1-3, VP1-VP2 and VP3-2 interfaces respectively. P153 was previously shown to be directly involved in binding to the unknown glycoprotein receptor of the TMEV BeAn strain, as substitution of this residue to alanine significantly reduced binding affinity to BHK-21 cells while substitution to threonine or aspartic acid completely abolished viral infectivity (Hertzler et al., 2000). Moreover, docking experiments performed in chapter two revealed that VP1 P153 is likely involved in binding of TMEV GDVII to the co-receptor heparan sulphate (Upfold et al., 2018). The identification of P153 as a residue contributing significantly to the binding and stability of the protomer-protomer interface in this study supports the suggestion by Hertzler et al. (2000) that this residue is important for receptor interactions and capsid assembly in TMEV.

With most picornaviruses, receptor binding alone or in combination with low pH triggers conformational changes that result in the controlled destabilisation of the capsid and uncoating

of the RNA genome (Baggen et al., 2018a), thus receptor binding and the stability of the capsid are closely linked. The uncoating process in TMEV is poorly studied and made more ambiguous as the primary receptor is yet to be identified (Reddi et al., 2004). Cardiovirus uncoating, like that of FMDV, is thought to be triggered by a drop in pH, however, it has been speculated that the insensitivity of TMEV to low pH could indicate that uncoating of this virus is induced by receptor binding instead (Luo et al., 1992). The identification of hotspot residues at the intra- and inter-protomer interfaces in and surrounding the putative receptor binding site and the fact that some of these residues are also predicted to bind the co-receptor supports this suggestion. Moreover, it can be further speculated that binding of the receptor and/or heparan to these specific energetically important hotspots may destabilise the intra- and inter-protomer interfaces substantially to induce the necessary cascade of conformational changes that contribute to genome release. Alternatively, hotspot residues at these positions may be important for maintaining the structural conformations necessary for receptor binding but may not be significantly destabilised upon receptor binding to stimulate uncoating.

It was recently reported that the cardiovirus SAFV-3 forms an intermediate A-particle during uncoating and then rapidly dissociates into pentamer subunits (Mullapudi et al., 2016). These expanded particles were observed to contain pores extending from the five-fold to the two-fold axes that the authors speculate might serve as channels for the release of VP4, the N-termini of VP1 and the RNA genome during uncoating. Uncoating intermediates have not been observed during the uncoating of other coronaviruses including TMEV, but experiments have not yet ruled out their formation. TMEV hotspots VP1 W176, V178, VP2 S47, Y104, L105, VP3 S16, P131, F165, I166 and P168 are conserved with residues in SAFV-3 at the protomer-protomer interface. In the crystal structure of the SAFV-3 A-particle these residues maintain their interactions and conformation and are located on either edge of the five-fold pore. In TMEV these residues predominantly form hydrophobic bonds across the interface. Interestingly,

hotspot residues VP1 P153, VP3 N103, Q104, Q173, I181 and M222 are conserved with residues in SAFV-3 that undergo conformational rearrangement to form the pore at the protomer-protomer interface. In TMEV these residues predominantly form hydrogen bonds across the interface.

In total 64 % of the hotspot residues identified at the inter-protomer interfaces were conserved in viruses belonging to other genera of the family. Residues extending between the protomer interfaces and the quazi fold axes are highly variable, forming a variety of topological features in the different genera that are sometimes the sites of receptor binding (Luo et al., 1992; Rossmann et al., 2002; Suomalainen and Greber, 2013). Despite these topological differences, the conservation of many of the hotspot residues at these interfaces may suggest that similar mechanisms contribute to the stability of the interfaces between protomers in picornavirus capsids.

Finally, the screen was applied to identify hotspot residues at the interpentamer interfaces of TMEV, located between the three- and two-fold axes of symmetry. Numerous studies have implicated these interfaces in major structural rearrangements associated with genome release and capsid dissociation. For example, structural studies on enterovirus uncoating intermediates have demonstrated the formation of large pores at the two- and three-fold axes (Bostina et al., 2011; Butan et al., 2014; Dong et al., 2017; Lee et al., 2016; Liu et al., 2018; Lyu et al., 2014; Pickl-Herk et al., 2013; Ren et al., 2013; Shakeel et al., 2013; Wang et al., 2012a), suggesting that RNA release may be between pentamer subunits. Furthermore, recent investigation has revealed that the loss of one or more pentamers may also be critical for the release of RNA in echoviruses (EV) and HRV-2 (Buchta et al., 2019; Harutyunyan et al., 2013), and while it is still unknown whether all aphtho- and cardioviruses form intermediate structures during genome release (Mullapudi et al., 2016; Tuthill et al., 2009), studies have identified pentamer subunits as the end products of uncoating in these viruses (Tuthill et al., 2007). These

observations provide strong evidence that the pentameric interfaces are important for RNA release and dissociation and must therefore undergo structural rearrangements or encounter conditions that severely weaken the interactions to allow for pore formation or dissociation. To further understand the residues that modulate the assembly and stability of the pentameric interfaces in TMEV, complexes of two opposing protomers (VP2-VP2) and two adjacent protomers (VP2-VP3) were submitted to the five webservers for hotspot prediction.

In total, 24 hotspot residues were identified, and all belonged to the VP2 and VP3 proteins of opposing pentamers, that make up the bulk of this interface. Because the entire interface between pentamers involves four protomers, the 24 hotspots are repeated to yield 48 hotspot residues between two pentamers. 75 % of the hotspot residues formed interactions with other hotspots, and 54 % formed interactions with only one other residue across the interface. Most hotspot residues formed hydrogen bonds with partner residues, although some residues were involved in a few hydrophobic interactions closer to the two-fold axis. This finding is consistent with the report that weak non-covalent interactions are important for the assembly of pentamers into the picornavirus capsid (Li et al., 2012; Mateu, 2017). Except for 2 of the 24 hotspots, all were conserved in at least one representative virus from another genus, suggesting a conserved function for these residues in viruses throughout the family.

Interestingly, 17 of the 24 hotspot residues predicted at the TMEV pentamer interface correspond to residues that were suggested to form interactions across the pentamer-pentamer interfaces of the SVV-1 mature capsid (Cao et al., 2018). These residues include N25, R61, Y62 (W in SVV-1), Y63, T64, V95 (A in SVV-1), R102, N117, S240 (T in SVV-1) in VP2 and M144, Y148, I150, D152, L153 (I in SVV-1), T194, T197 in VP3. Hotspot residues R61 (VP2), K124 and D152 (both in VP3) at the TMEV pentamer interfaces were conserved within almost all picornaviruses analysed, including FMDV. Previously Mateo et al. (2003) examined the importance of residues at pentamer interfaces to FMDV growth and stability. Mutation of

the FMDV residues R60, R120 and D148 corresponding to TMEV hotspots R61 in VP2 and K124 and D152 in VP3 had deleterious effects on the resulting mutant virions. The substitution R60A proved lethal as the virus could not be recovered following 90 h post transfection with mutant RNA. Residue substitutions R120A and D152A were recovered post transfection, however virus growth, yield and plaque size were significantly attenuated (Mateo et al., 2003). Furthermore, the authors found that substitution of residue T190 in FMDV VP3 to alanine resulted in revertant mutants, implying the reduced fitness of the alanine mutant. This residue corresponds to the hotspot residue T194 in TMEV VP3, which is highly conserved within other members of the picornavirus family. Additionally, the authors found substitutions V112A (VP2) and H144 (VP3) to be lethal, while K193A (VP3) reduced virus yield and K63A (VP2), E146A (VP3) and E213A (VP2) mutants could only be recovered following genotypic reversions or forward mutations (Mateo et al., 2003). Interestingly none of amino acids are conserved in TMEV, however, structurally these residues align with N117 (VP2), Y148 (VP3), T197 (VP3), T64 (VP2), I150 (VP3) and L259 (VP2) respectively and were all predicted to be hotspots at the pentameric interfaces of TMEV. In a recent study, the stability of FMDV Type O and SAT particles was greatly improved through the amino acid substitution F62Y in the VP2 protein (Scott et al., 2017). This residue corresponds to the stabilising hotspot residue Y63 in the TMEV pentamer interface.

Ross et al. (2017) previously identified energetically important residues in conserved interacting motifs within the two-fold interfaces of the enteroviruses. Several of the hotspot residues in this study correspond to those identified by Ross et al. (2017). Hotspot VP2 R61 in TMEV was conserved with a residue that was also predicted to be important for maintaining the stability of the pentamer interfaces in EV-71, PV-1, HEV-D68, HRV-2A and HRV-B3, while T64, also in VP2, corresponded to a residue that was predicted to be important for the stability of PV-1, HEV-D68, HRV-B3. Furthermore, residues M144 and D152 in VP3

corresponded with residues that were also predicted to be energetically important to the two-fold axes in most of the enteroviruses analysed. Hotspot residue I150 in TMEV VP3 corresponds to a residue within a conserved motif in enteroviruses. The same motif contains the energetically important residues corresponding to the TMEV hotspot residues M144, Y148 and D152. This Isoleucine residue was, however, not predicted to destabilise the interface upon substitution to alanine in the enteroviruses (Ross et al., 2017).

The finding that most of the hotspot residues at TMEV pentamer interfaces are conserved in viruses of different genera implies their biological importance. Moreover, the fact that corresponding conserved residues were predicted to be stabilising in other viruses, were reported to be involved in pentamer-pentamer contacts, or have been reported to be important for virus growth in other genera implies that they may have been conserved because of a shared role in structural stability of this interface. The importance of two- and three-fold pore formation and separation of the pentameric interfaces to the picornavirus uncoating process is widely known (Bostina et al., 2011; Buchta et al., 2019; Tuthill et al., 2007; Wang et al., 2012a), thus the conservation of specific hotspot residues in the pentamer interfaces of TMEV with residues that are important for stability in other viruses is not surprising. Previously Garriga et al. (2012) identified a region of VP3 located at the interface between pentamers that becomes disordered during HRV-2 RNA release. TMEV hotspot residues M144, I150, D152 and L153 are conserved with HRV-2 residues in this region. Furthermore, hotspot residues R61 in VP2 and K124 in VP3 are conserved with interpentamer residues in HRV-B14 that were shown to become destabilised upon acidification at a pH of 5 (Warwicker, 1989). Unlike TMEV, HRVs are known to be sensitive to low pH (Garriga et al., 2012) and histidine residues at the pentamer interface are thought to play a role in this sensitivity (Warwicker, 1989). Importantly, HRV-B14 residues corresponding to R61 and K124 form interactions with histidine residues across the interface (Warwicker, 1989), but in TMEV these residues form interactions with amino

acids that are not protonated in conditions below neutral pH, which may explain in part TMEV's increased resistance to acidic conditions. Interestingly, R61 forms cation- π interactions with hotspot residue Y148 in VP3 which corresponds structurally to the acid sensitive H150 in HRV-B14.

In conclusion, the work presented in this chapter aimed to further the understanding of capsid residues that modulate the stability and assembly of picornavirus capsids. This was achieved through the development and implementation of a simple *in-silico* approach using readily accessible tools for the prediction of conserved and non-conserved hotspot residues and the interactions they form at capsid protein subunit interfaces. Collectively this methodology provides a rapid approach for identifying the hotspot residues that significantly contribute to the stability of the intraprotomer, interprotomer and interpentamer interfaces that must be formed upon the assembly of subunits into the picornavirus capsid. The intraprotomer and interpentamer interfaces contained hotspot residues unique to TMEV and the coronaviruses that were previously reported to be involved in pH stability and receptor binding. However, these interfaces also contained many hotspots that were conserved with residues in picornaviruses belonging to other genera, some of which were reported to be important for virus growth or stability, suggesting that molecular determinants of capsid stability may be somewhat conserved across the family. Almost all hotspot residues at pentamer-pentamer interfaces were conserved in the coronaviruses and viruses belonging to other genera. Many of these residues were previously linked to stability or uncoating in other picornaviruses, providing a rationale for investigating these hotspots further. Thus, the next chapter further examines the importance of pentameric hotspots by substituting selected hotspot residues to alanine in the TMEV cDNA. Monitoring of cytopathic effect and analysis of protein expression using the capsid antibodies generated in chapter two are then used to examine the potential implications of the hotspot residue substitutions.

Chapter 4

The *in vitro* mutagenesis of hotspot residues within the interpentamer interfaces of the TMEV capsid

4.1. Introduction

In the previous chapter the *in-silico* analysis of hotspot residues at the intra-, interprotomer and interpentamer interfaces of the TMEV capsid presented a vast amount of data surrounding the residues that likely contribute significantly to the stability of the capsid. These data provide a series of testable hypotheses that must be further validated using an *in vitro* system to confirm the role of these residues as hotspots. The work presented in this chapter, aimed to further dissect the importance of a select subset of these hotspots *in vitro*, using reverse genetics in combination with mutagenesis. This approach has previously been implemented for the elucidation of residues that are functionally important for capsid assembly, stability and viral infectivity in several other picornaviruses (Biswal et al., 2016; Mateo et al., 2003; Yuan et al., 2016), and has been used to engineer picornavirus particles with improved thermostability (Adeyemi et al., 2017; Kotecha et al., 2015; Mateo et al., 2008; Rincón et al., 2014; Scott et al., 2017). Many of these studies have relied on *in vitro* alanine scanning mutagenesis (Mateo et al., 2003; Rincón et al., 2015; Yuan et al., 2016). The rationale for substituting residues with alanine is two-fold; firstly, all atoms in the sidechain beyond the β -carbon are removed upon mutation allowing the role of sidechain functional group to be determined and secondly, alanine's methyl functional group is both chemically inert and non-bulky, but also lacks angle preferences (unlike glycine or proline) and therefore does not alter the secondary structure of the protein (Cunningham and Wells, 1989; Morrow and Zhang, 2012).

Two separate studies used *in vitro* alanine scanning to assess the importance of individual residues at FMDV capsid subunit interfaces to virus infectivity and particle formation. These studies revealed that although most residues involved in noncovalent interactions between protomers are not individually required for completion of the FMDV virus lifecycle (Rincón et al., 2015), most residues forming interactions between pentameric subunits are (Mateo et al., 2003). The authors speculated that pentamer interfaces were less tolerant to the loss of

individual residue sidechains because relatively few, weak, noncovalent interactions are formed between pentamers, unlike the many buried, strong, protein interactions between protomers (Rincón et al., 2015). In the current study, residues that were previously predicted as hotspots at the interpentamer interfaces of TMEV were analysed using *in vitro* alanine scanning mutagenesis. The rationale for selecting residues at this interface is three-fold. Firstly, it is widely accepted that pentameric interfaces are the sites of major structural rearrangements during picornavirus genome release and capsid dissociation, which are essential for virus infectivity (Bostina et al., 2011; Buchta et al., 2019; Butan et al., 2014; Dong et al., 2017; Harutyunyan et al., 2013; Lee et al., 2016; Liu et al., 2018; Lyu et al., 2014; Pickl-Herk et al., 2013; Ren et al., 2013; Shakeel et al., 2013; Tuthill et al., 2007; Wang et al., 2012a). An improved understanding of the residues directly involved in modulating these interfaces would likely add to the knowledge surrounding capsid stability, assembly and uncoating, and may elucidate potential targets for the development of antivirals that interfere with these processes. Secondly, almost all pentameric hotspot residues predicted by the screen were conserved in at least one representative virus from another genus, suggesting a shared biological function for these residues in viruses throughout the family. Moreover, most of the hotspots corresponded to residues previously reported or predicted to be important for picornavirus structure or stability in other viruses. Thus, further analysis of these hotspots in TMEV would likely provide information that could also be applicable to other members of the picornaviruses. Thirdly, these residues are located away from receptor binding sites and antigenic regions of the TMEV capsid (Hertzler et al., 2000; Jnaoui et al., 2002; Luo et al., 1992; Upfold et al., 2018), thus any mutagenesis effects would likely not be a result of unwanted disruptions to other aspects of the virus lifecycle such as attachment and entry.

The overall aim of this study was to evaluate the importance of previously predicted interpentamer hotspot residues to TMEV virus infection by mutating each hotspot residue to

alanine and examining the effects on the TMEV lifecycle. The first objective was to select a subset of pentamer hotspot residues for analysis and secondly, to develop a site directed mutagenesis strategy for introducing the alanine substitutions into the TMEV cDNA. Using this system, the third objective was to engineer individual alanine substitutions into the TMEV cDNA, thus individually replacing the chosen hotspots. The final objective was to assess the importance of the individual hotspot residues by transfecting corresponding *in vitro* transcribed mutant RNAs into susceptible cells and to examine the potential effects on virus infectivity, replication and protein synthesis.

4.2. Materials and Methods

4.2.1. Cells and plasmids

BHK-21 cells were maintained as described in section 2.2.1. pGDVIIFL2 (Figure S8) contains the full-length cDNA of TMEV GDVII inserted into the pBlueScript[®] SK II- Phagemid Vector (Fu et al., 1990; Roos et al., 1989), and was used as a template for the generation of WT TMEV GDVII transcripts and for the generation of mutant TMEVs. pJET1.2/blunt (Thermo Scientific, USA) is a commercially available linearised cloning vector, that can accept inserts from 6 bp to 10 kb and was used as a subcloning vector in this study. A list of the individual plasmids generated in this study is provided in *Table 4.1*.

Table 4.1 Recombinant plasmids generated in this study

Plasmid	Description/Amino acid substitution	Purpose
pJetP1/P2/HindIII-1	Recombinant plasmid containing the TMEV P1 and partial P2 sequences in the pJET1.2/blunt cloning vector. A <i>HindIII</i> site at nucleotide position 223 of the VP2 coding sequence was removed by altering the <i>HindIII</i> sequence through site directed mutagenesis.	Template for site directed mutagenesis experiments to introduce individual alanine substitutions into the P1 coding region of TMEV.
The plasmids listed below consist of pGDVIIIFL2 containing the <i>HindIII</i> -negative P1/P2 insert and additional amino acid substitutions in the P1 coding region of TMEV as indicated:		
pGDVII/HindIII-1	<i>HindIII</i> -negative P1/P2 from pJetP1/P2/ <i>HindIII</i> -1	Template for mutant <i>HindIII</i> -1 TMEV transcripts.
pGDVII/R61A/H-1	R to A substitution at amino acid 61 in VP2	Templates for <i>in vitro</i> transcription of hotspot mutant RNAs
pGDVII/Y62A/H-1	Y to A substitution at amino acid 62 in VP2	
pGDVII/Y63A/H-1	Y to A substitution at amino acid 63 in VP2	
pGDVII/T64A/H-1	T to A substitution at amino acid 64 in VP2	
pGDVII/V95A/H-1	V to A substitution at amino acid 95 in VP2	
pGDVII/L259A/H-1	L to A substitution at amino acid 259 in VP2	
pGDVII/Y148A/H-1	Y to A substitution at amino acid 148 in VP3	
pGDVII/I150A/H-1	I to A substitution at amino acid 150 in VP3	
pGDVII/T194A/H-1	T to A substitution at amino acid 194 in VP3	Templates for <i>in vitro</i> transcription of non-hotspot (neutral) mutant RNAs
pGDVII/K18A/H-1	K to A substitution at amino acid 18 in VP2	
pGDVII/G94A/H-1	G to A substitution at amino acid 94 in VP2	
pGDVII/D242A/H-1	D to A substitution at amino acid 242 in VP2	

4.2.2. Generation of recombinant pGDVIIIFL2 mutants

A total of 12 amino acids were individually substituted to alanine in the full-length cDNA of TMEV GDVII (Table 4.1) using site directed mutagenesis. Figure 4.1 shows an overview of the cloning and mutagenesis strategy used to generate the pGDVIIIFL2 mutants.

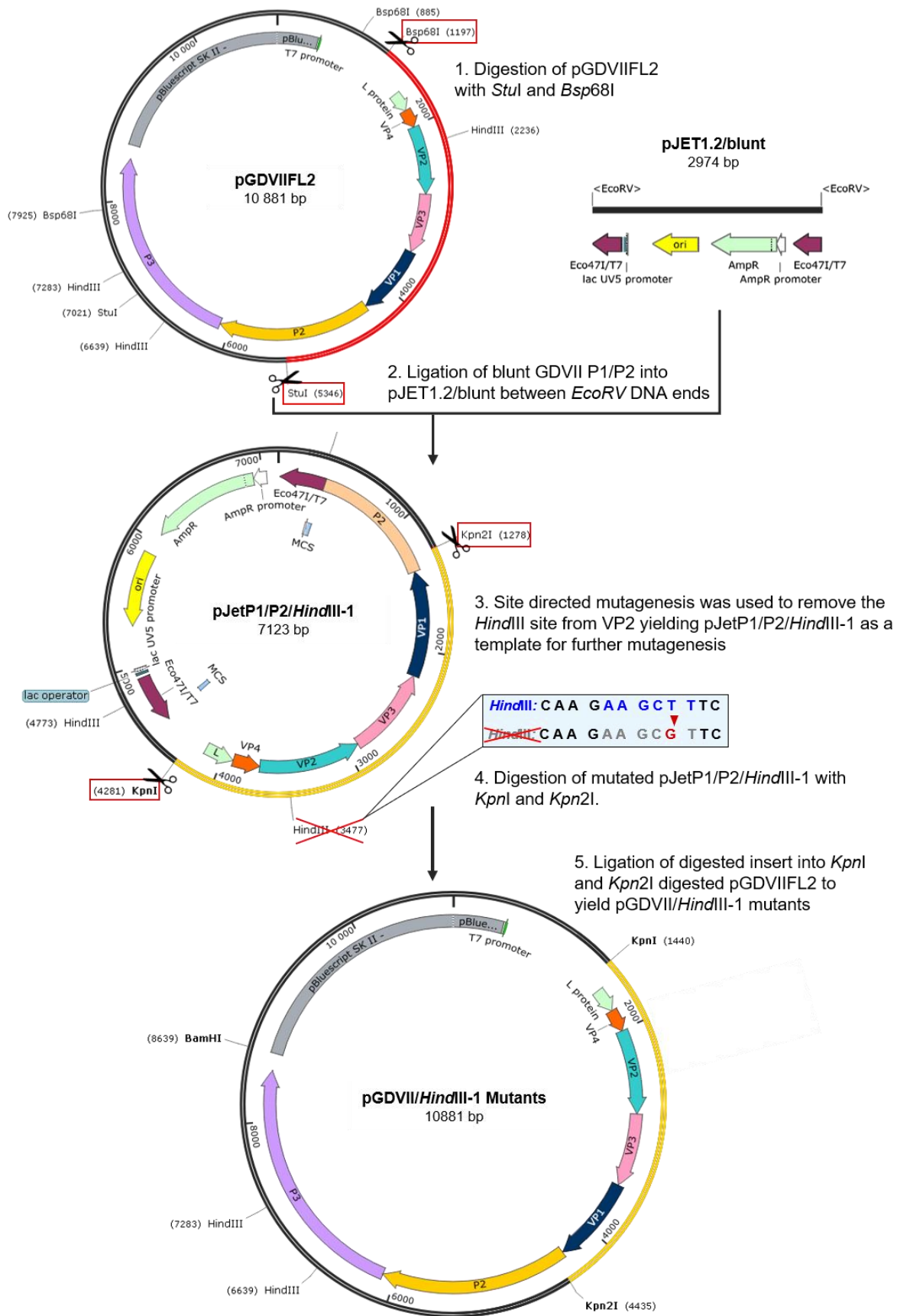


Figure 4.1 Schematic overview of strategy used to engineer alanine substitutions into the TMEV cDNA. The P1/P2 region of the TMEV genome was isolated by digestion with *StuI* and *Bsp68I* and cloned into pJET1.2 blunt to yield pJetP1/P2. Site directed mutagenesis was used to alter the *HindIII* restriction site in the VP2 coding sequence in pJetP1/P2 to yield pJetP1/P2/*HindIII*-1, the template used for further mutagenesis experiments. This was done to be able to distinguish the genome from the wild type TMEV. Following site directed mutagenesis to introduce individual alanine substitutions into the coding sequences of VP2 and VP3, the mutant inserts were digested using *KpnI* and *Kpn2I* and ligated into pGDVIIFL2 backbone that had been digested with the same enzymes, yielding infectious mutant TMEV cDNAs.

4.2.2.1. Preparation of vector pJetP1/P2/*HindIII*-1 for site-directed mutagenesis

The size of pGDVIIFL2 (10.8 kb) prevented its use as a template for site directed mutagenesis reactions, thus the smaller 7.12 kb pJetP1/P2/*HindIII*-1 vector was generated as a mutagenesis template (*Figure 4.1*). To this end a 4.15 kb region of the plasmid pGDVIIFL2 encompassing the capsid-coding region and partial coding sequence of P2 (P1-P2) was digested with the endonucleases *Bsp68I* and *StuI* and the blunt fragment was cloned into the pJET1.2/blunt (2.97 kb) cloning vector (Thermo Scientific, USA). 5 µg of pGDVIIFL2 plasmid was initially digested using *Bsp68I* at 37 °C for 2 h in a total volume of 50 µl containing 5 µl 10X Buffer O (Thermo Scientific, USA) and 30 U *Bsp68I* 10 U/µl (Thermo Scientific, USA). The 6.7 kb band containing the P1-P2 coding regions was gel purified using the GeneJET Gel purification kit (Thermo Scientific, USA), according to the manufacturer's instructions except that DNA was eluted in a final volume of 30 µl. The fragment was then digested with *StuI* at 37 °C for 3 h, in a 40 µl reaction containing the 30 µl of gel purified DNA, 4 µl 10X NEB Buffer 4 and 20 U *StuI* 10U/µl (New England Biolabs). The 4.15 kb fragment was gel purified as above and ligated into the pJET1.2/blunt vector using the CloneJET PCR Cloning Kit (Thermo Scientific, USA), according to the manufacturer's instructions. The ligated plasmid (pJetP1/P2) was transformed into DH5α *E. coli* cells that had been made chemically competent using the CaCl₂ method as described by Chang et al. (2017). Individual colonies were cultured in LB

supplemented with ampicillin (100 $\mu\text{g/ml}$) and incubated overnight at 37 $^{\circ}\text{C}$. Plasmid DNA was subsequently extracted using the GeneJet Plasmid Miniprep kit (Thermo Scientific, USA) according to manufacturer's instructions, except that the plasmid was eluted in 50 μl nuclease-free ddH₂O.

4.2.2.2. Site directed mutagenesis

To generate pJetP1/P2/*Hind*III-1, the *Hind*III restriction site was altered in the sequence encoding VP2 in pJetP1/P2, by substituting the second last thymine of the *Hind*III restriction site to guanine using the Phusion Site-Directed Mutagenesis Kit (Thermo Scientific, USA). This approach was also used to introduce point mutations into the VP2 and VP3 coding regions of pJetP1/P2/*Hind*III-1. An overview of this process is shown in Figure 4.2. Primer pairs were designed in a back-to-back fashion and point mutations were created by including mismatched bases within the middle of one of the primers in the pair (Table S4).

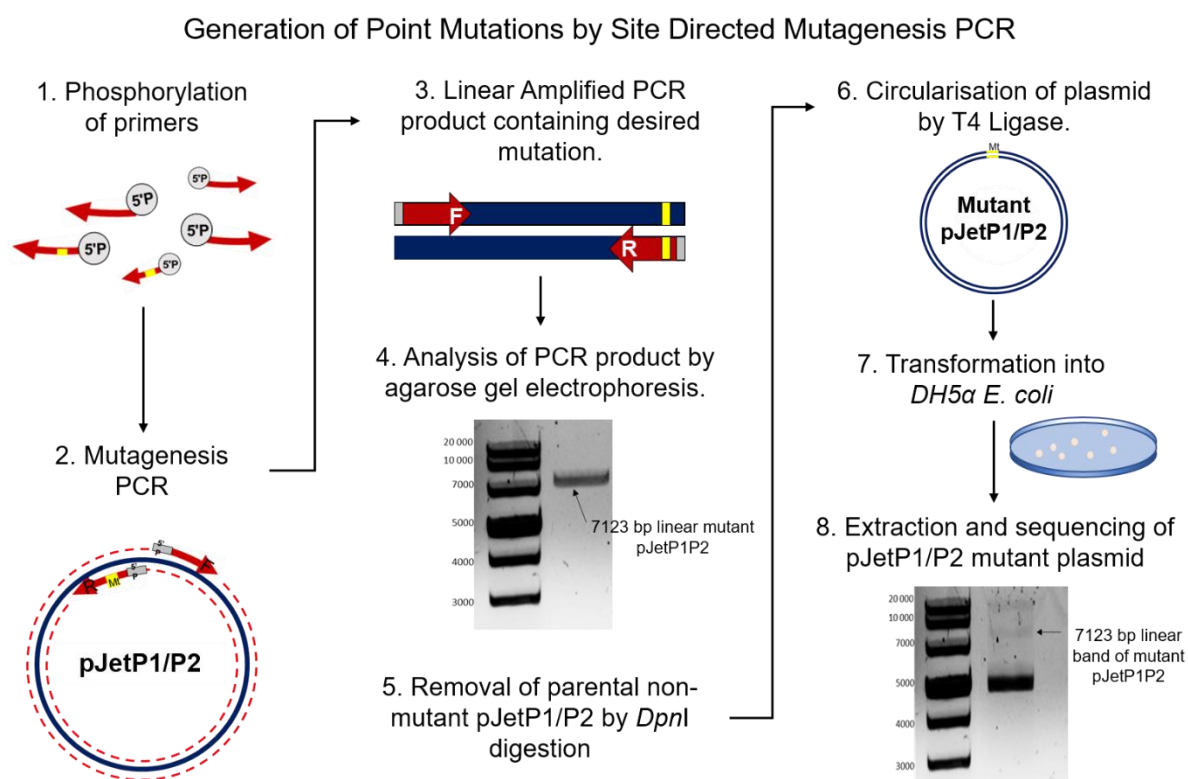


Figure 4.2 Schematic diagram of the site directed mutagenesis procedure used to engineer specific alanine substitutions into the P1 region of pJetP1/P2/*Hind*III-1. Two back-to-back primers were

designed, with one primer containing mismatched nucleotides to be mutated in the centre of the primer. The primers were phosphorylated prior to PCR amplification of the entire target plasmid. *DpnI* was then used to digest the parental Dam-methylated plasmid, before the linear PCR product was circularised in a rapid ligation reaction. The plasmid was then transformed into *E. coli* cells, and the resultant mutant plasmid was extracted and sequenced to ensure that the desired mutation was present.

The oligonucleotide primers were individually phosphorylated prior to PCR using T4 polynucleotide kinase (PNK) (Thermo Scientific, USA). Each reaction contained 125 pmol of oligonucleotide primer, 2.5 μ l of 10X reaction buffer A, 2.5 μ l of 10 mM ATP (Sigma, USA) and 1 U of T4 PNK (10 U/ μ l) in a total volume of 25 μ l. Phosphorylation was allowed to proceed at 37 °C for 30 min before the reaction was terminated by heating to 75 °C for 5 min. Each PCR reaction (50 μ l) included 10 μ l of 5X Phusion HF buffer, 200 μ M dNTP mix, 0.5 μ M of each phosphorylated non-overlapping forward and reverse primer, 0.1 ng of pJetP1/P2/*HindIII*-1 and 0.02 U Phusion Hot Start DNA polymerase (0.02 U/ μ l). Two-step PCR cycling was performed using a SimpliAmp Thermal Cycler (Thermo Scientific, USA) with the following conditions: 98 °C for 30 seconds; 25 cycles of 98 °C for 10 seconds and 72 °C for 4 min; and a final elongation step of 72 °C for 10 min.

To remove Dam-methylated parental plasmid DNA following PCR, 10 U of *DpnI* (10 U/ μ l) (Thermo Scientific, USA) was added directly to each reaction mixture. The PCR products were circularised using T4 DNA ligase in a reaction containing 20 ng of *DpnI* treated PCR product, 2 μ l 5X Rapid Ligation Buffer, 0.5 μ l T4 DNA ligase and ddH₂O to a final volume of 10 μ l. Reactions were incubated at 25 °C for 5 min before 10 μ l was transformed into chemically competent *E. coli* DH5 α cells. Derived clones were grown in 10 ml LB supplemented with ampicillin (100 μ g/ml) at 37 °C overnight, and plasmids were extracted using the GeneJET Plasmid miniprep Kit (Thermo Scientific, USA). Derived clones were sequenced (Inqaba Biotechnical Industries (Pty) Ltd., Pretoria, South Africa) to confirm the presence of the desired

point mutations. The mutated capsid-coding regions (P1-P2) of pJetP1/P2/*HindIII*-1 were digested with the endonucleases *KpnI* and *Kpn2I* and cloned back into pGDVIIFL2 which was digested with the same endonucleases. Each restriction reaction contained 1 µg of pGDVIIFL2 or mutant pJetP1/P2/*HindIII*-1, 6 µl of 10X Multicore Buffer (Promega), 4 µl of Fast Digest® *KpnI* (Thermo Scientific, USA) and 20 U of *Kpn2I* (10 U/µl) (Thermo Scientific, USA) in a total volume of 60 µl. The reactions were incubated using a SimpliAmp Thermal Cycler (Thermo Scientific, USA) at 37 °C for 2.5 h before the reaction temperature was increased to 55 °C for 2 h. The 3 kb mutant inserts and 7.8 kb pGDVIIFL2 backbone were gel purified using the Monarch® DNA Gel Extraction Kit (New England Biolabs) according to the manufacturer's instructions. The inserts were ligated back into the pGDVIIFL2 vector in reaction mixtures containing insert to vector ratios of 3:1 (not exceeding 100 ng of total DNA), 2 µl 5X Rapid Ligation Buffer, 0.5 µl T4 DNA ligase and ddH₂O to a final volume of 10 µl. Reactions were incubated at 25 °C for 5 min followed by 4 °C overnight and were transformed into chemically competent DH5α cells. Selected colonies were cultured, and plasmids were extracted as described above. The P1 regions of the pGDVIIFL2/*HindIII*-1 mutants were sequenced (Inqaba Biotechnical Industries (Pty) Ltd., Pretoria South Africa) to ensure that no unwanted mutations were introduced during the mutagenesis or cloning procedures.

4.2.3. Production and transfection of infectious wild type and mutant TMEV

RNAs

4.2.3.1. *In vitro* synthesis of GDVII mutant RNA

Mutant or WT pGDVIIFL2/*HindIII*-1 plasmids were each linearised by digestion with *BamHI*. The digestion reaction mixtures contained 5 µg of plasmid DNA, 6 µl of 10X Buffer E and 30 U of *BamHI* (10 U/µl) (Promega) and were incubated at 37 °C for 2 h. Following the incubation, 2 µl of each reaction mixture was analysed by 1 % [w/v] agarose gel electrophoresis to confirm complete digestion of each plasmid. Linearised plasmids were gel purified using the

Monarch[®] DNA Gel Extraction Kit (New England Biolabs), according to the manufacturer's instructions. The linearised recombinant plasmids were used as templates to synthesize T7 transcripts using the TranscriptAid T7 High Yield Transcription Kit (Thermo Scientific, USA), according to the manufacturer's instructions. For synthesis of transcripts, each reaction contained 0.5 µg of linearised DNA template, 4 µl of 5X TranscriptAid Reaction Buffer, 8 µl of ATP/CTP/GTP/UTP mix, 2 µl of TranscriptAid Enzyme Mix and DEPC-treated ddH₂O to a final volume of 20 µl. The reaction mixtures were incubated at 37 °C for 2 h. Following RNA synthesis, the DNA template was removed by the addition of 4 U of RNase-free DNase I (1 U/µl) incubated at 37 °C for 15 min. To stop the reaction, 2 µl of 0.5 M EDTA, (pH 8.0) was added and incubated at 65 °C for 10 min. The RNA transcripts were purified using the GeneJET RNA Cleanup and Concentration Micro Kit (Thermo Scientific, USA) according to the manufacturer's instructions and RNA concentrations were determined using a Nanodrop ND-1000 spectrophotometer (Thermo Scientific, USA).

4.2.3.2. Transfection of BHK-21 cells with wild type and mutant GDVII RNAs

In vitro transcribed RNA was transfected into BHK-21 cells using the TransFectin[™] Lipid Reagent (BioRad). Transfection mixtures comprising 50 µl serum free DMEM, 1 µg WT or mutant viral RNA and 1 µl TransFectin[™] Lipid Reagent were combined in nuclease-free microcentrifuge tubes and were incubated for 30 min at RT. Medium was aspirated from 70-80 % confluent monolayers of BHK-21 cells grown overnight in 24-well tissue culture plates. 300 µl serum-free DMEM was added into each well and transfection mixtures were added dropwise. The cells were incubated at 37 °C with a 5 % influx of CO₂. Following 6 h of incubation, the transfection medium was removed and replaced with 500 µl complete DMEM (5 % FCS, 1 % PSF). The transfected cells were monitored for signs of CPE every 12 h. Following 96 hours post transfection (hpt) infected cells were aspirated and frozen at -80 °C.

Where no CPE was observed, cells were passaged up to nine times on fresh BHK-21 monolayers.

4.2.4. Titration of replicating wild type and mutant TMEV by plaque assay

The number of resultant infectious virus particles following the transfection of cells with infectious WT and mutant RNAs was determined as plaque forming units (PFU) per ml by plaque assay. Eight 10-fold dilutions of WT and mutant transfected cell lysates were made in serum-free DMEM. Confluent BHK-21 monolayers were washed with 1 × PBS (pH 7.4) and 0.2 or 0.05 ml of each virus dilution was added to individual wells of 6 or 24-well plates respectively. Virus adsorption was allowed to proceed for 1.5 h at 37 °C with gentle agitation, before the cells were washed with 1 × PBS and overlain with 3 or 1 ml of overlay solution [50 % DMEM, 1.25 % methocel, 60 mM NaCl] per individual 6 and 24-well respectively. The cells were incubated for 48 h, or longer if no plaques were visible, before the cells were washed with 1 × PBS and fixed with 4 % paraformaldehyde at RT for 20 min. Fixed cells were washed with 1 × PBS and stained with Coomassie staining solution (45 % methanol, 45 % ddH₂O, 10 % glacial acetic acid and 0.002 % [w/v] Coomassie Brilliant Blue) for 1 h at RT. The number of plaques was counted, and the titre of each virus was calculated in terms of PFU/ml of the original stock, taking both the dilution factor and volume plated into account. Each plaque assay was repeated in triplicate.

4.2.5. *Hind*III restriction analysis of RT-PCR products

Viral RNA was extracted from the supernatants of the transfected cell lysates that exhibited CPE, using the QIAamp Viral RNA Mini Kit (Qiagen, Germany), according to the manufacturer's instructions. The viral RNA was used as a template for the reverse-transcription PCR (RT-PCR) of a 1124 bp product spanning the coding sequences of the Leader, VP4 and VP2 proteins. cDNA synthesis was performed using the RevertAid First Strand cDNA Synthesis Kit (Thermo Scientific, USA) as per the manufacturer's instructions. Each 20 µl

cDNA synthesis reaction contained 0.5 µg of total viral RNA, 4 µl of 5X Reaction buffer, 2 µl 10 mM dNTP Mix, 200 U RevertAid M-MuLV Reverse Transcriptase (200 U/µl) and 20 µM of the VP2NU-Rev reverse primer (5' TTGCGCAAGCACAGTTTCG) that recognises the last 19 bp of the sequence encoding the VP2 capsid protein (*Figure 4.4 D*). The reaction was incubated at 42 °C for 1 h, before the reaction was terminated by heating to 70 °C for 5 min. The resultant cDNA was used as a template for PCR using the Q5[®] High-Fidelity PCR Kit. PCR reactions contained 5 µl cDNA template, 1.25 µl of 10 µM L/VP4-For forward primer (5' GACGATGACGTCTTCTGGCCTTC) recognising 23 bp in the centre of the L protein (*Figure 4.4 D*), 1.25 µl of 10 µM VP2NU-Rev reverse primer and 12.5 µl Q5[®] High-Fidelity 2X Master Mix in a total reaction volume of 25 µl. PCR cycles included an initial denaturation step at 98 °C 30 seconds, followed by 25 cycles of: denaturation at 98 °C for 10 seconds, annealing at 62 °C for 30 seconds and elongation at 72 °C for 1 min, and a final elongation step at 72 °C for 5 min. Thermocycling was performed using a SimpliAmp Thermal Cycler (Thermo Scientific, USA).

Resultant L-VP4-VP2 RT-PCR products were subjected to restriction digestion using *HindIII*. Each reaction contained 3 µl PCR product, 3 µl 10X Fast Digest[®] Green buffer and Fast Digest[®] *HindIII* enzyme (both Thermo Scientific, USA), in a total volume of 30 µl. The reactions were incubated at 37 °C for 1 h before the DNA was analysed by 1 % agarose gel electrophoresis.

4.2.6. SDS-PAGE and Western analysis

Equal volumes of transfected cell lysate were pelleted by centrifugation at 13 000 × g, pellets were resuspended in 20 µl PBS and equal volumes were used for Western blot experiments. SDS-PAGE and Western analysis were carried out as described in section 2.2.5. Anti-capsid (Upfold et al., 2018) and anti-2C (Jauka et al., 2010) antibodies were used to probe for TMEV capsid proteins and the non-structural 2C protein, both at a dilution of 1:20 000.

4.2.7. Immunofluorescence experiments

BHK-21 cells grown to 70 % confluency on glass coverslips were transfected with mutant and WT viral RNAs as described above. Cells were fixed in 4 % paraformaldehyde for 20 min at RT following 14 and 24 hpt. Following fixation, cells were rinsed twice in PBS and permeabilised using permeabilisation buffer (PB) [10 % sucrose, 0.1 % Triton X- 100 in PBS] for 20 min. Cells were blocked in PB containing 2 % BSA (Block) for 40 min at RT and incubated with anti-TMEV capsid antibodies (1:20 000) (Upfold et al., 2018) generated in chapter two, and mouse monoclonal anti-dsRNA (English & Scientific Consulting; 10020500) (1:3000), diluted in block buffer for 1 h with gentle agitation. Cells were washed twice in PBS containing 0.1 % Tween-20 and incubated with goat-anti-rabbit Alexa Fluor 488-conjugated and goat-anti-mouse Alexa Fluor 546-conjugated secondary antibodies (Invitrogen, USA) (1:500) for 30 min. Cells were washed three times, and 4',6-diamino-2 phenylindole dihydrochloride (DAPI) (Sigma, USA) was added at a final concentration of 0.8 µg/ml in the second wash step to stain the nucleus. The slides were mounted using Dako fluorescence mounting medium (Dako Inc., USA) and stored at RT. The cells were visualised using an Olympus BX60 fluorescence microscope (Olympus, Japan) equipped with a colour view Olympus DP72 camera (Olympus, Japan), and images were analysed using CellSens Entry software, version 1.9 (Olympus, Germany). The number of nuclei was quantified using ImageJ, the number of infected cells was quantified visually. The percentage of infected cells was calculated for three separate images generated from three separate transfections for each virus.

4.2.8. *In-silico* figure preparation, graph generation and statistical analysis

In-silico visualisation of the pentamer interfaces and image generation was performed using PyMOL (Schrodinger, 2010). GraphPad Prism 8 was used to plot data and to perform statistical analysis in conjunction with RStudio. Plasmid maps were generated in SnapGene® v.4.2.4.

4.3. Results

4.3.1. Selection of hotspot residues for mutational analysis

Nine hotspot residues were selected for *in vitro* alanine scanning mutagenesis (*Figure 4.3*). These residues include R61, Y62, Y63, T64, V95, L259 in the TMEV VP2 protein and Y148, I150 and T194 in the VP3 protein. Three residues that form interactions across the pentamer interface, but were not predicted as hotspot residues, were selected as non-hotspot (neutral) controls. These residues include K18, G94 and D242 in the TMEV VP2 protein.

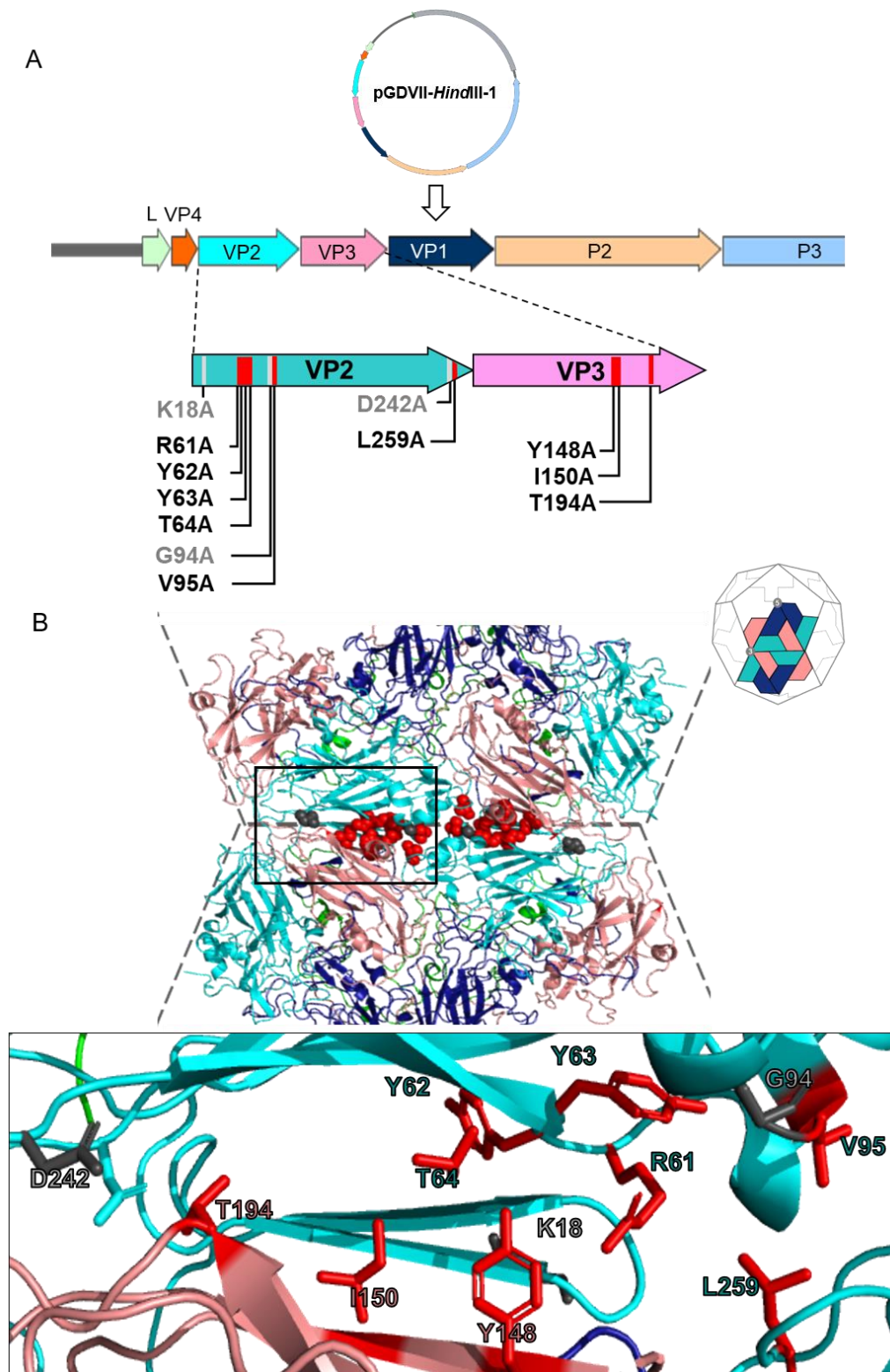


Figure 4.3 Pentamer-pentamer interface hotspot residues selected for mutagenesis experiments.

A) Location of hotspot residues for alanine mutagenesis within the TMEV cDNA. B) Cartoon representation of the TMEV pentamer-pentamer interface showing the residues selected for mutagenesis. Residues coloured red indicate those that were predicted as hotspots, residues coloured grey are interface residues that were selected as non-hotspot (neutral) controls.

4.3.2. Alteration of the *HindIII* restriction site in TMEV VP2 does not impact virus yield or protein synthesis

Following the generation of pGDVIIFL2-*HindIII*-1, sequencing confirmed that site directed mutagenesis had successfully altered the *HindIII* restriction site (*Figure 4.4 A*). To demonstrate that neither the loss of the *HindIII* restriction site nor the mutagenesis procedure itself could negatively affect the production or yield of TME virions, equal volumes of *in vitro* transcribed WT and *HindIII* mutant RNAs were transfected into BHK-21 cells. The onset of CPE was clearly visible from 24 hpt, for both viruses, and Western analysis of 48-h transfected cell lysates revealed the presence of similar levels of the non-structural 2C and structural capsid proteins (*Figure 4.4 B*), indicating that viral protein expression was not disrupted in the *HindIII*-negative mutant. Plaque assays revealed no significant difference in virus titres between the WT and mutant viruses (T-Test *P value* = 0.7105) (*Figure 4.4 C*), demonstrating that the alteration of the *HindIII* restriction site using the mutagenesis procedure did not affect virus function or growth.

To confirm that the resultant TMEV virions were indeed a result of transfection with infectious mutant RNA and not contamination of WT virions, viral RNA was extracted, and RT-PCR was performed to amplify the L-VP4-VP2 region of the WT and mutant TMEV genomes (*Figure 4.4 D*). Equal volumes of resultant PCR products were subjected to *HindIII* restriction digestion which revealed different digest patterns as expected, confirming that the resultant virions were mutant (*Figure 4.4 E*). Restriction of the *HindIII* mutant resulted in a single 1124 bp band consistent with failed cleavage due to removal of the restriction site, while two products of 536 and 588 bp were visible following digestion of the WT product, consistent with successful *HindIII* cleavage. pJetP1/P2/*HindIII*-1 was therefore used as a template for further mutagenesis experiments.

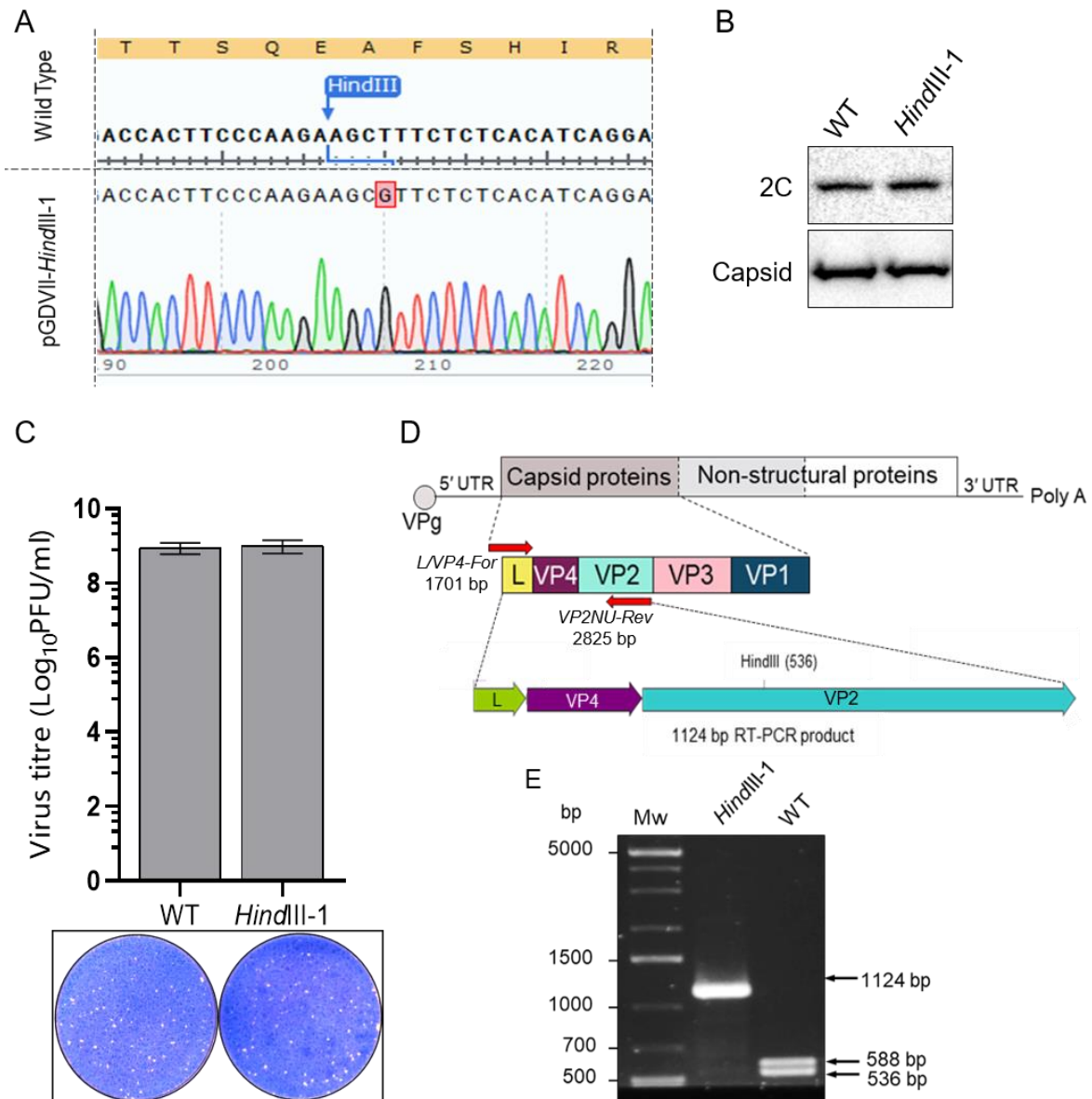


Figure 4.4 The *HindIII-1* control mutant behaves like wild type TMEV. A) The *HindIII* endonuclease restriction site in VP2 was altered by mutation of the second last thymine within the palindromic site to guanine, using site directed mutagenesis. Sequencing of the pGDVIIIFL2-*HindIII-1* plasmid confirmed that mutagenesis was successful (the guanine substitution is highlighted in red), and that no unwanted mutations were present. B) Western analysis of WT and *HindIII* mutant transfected cell lysates following 48 hpt. C) The yields of WT and *HindIII-1* control viruses in 48-h transfected cell lysates were titred by plaque assay on BHK-21 cell monolayers. Error bars indicate standard deviation (SD). D) Schematic view of the TMEV L-VP4-VP2 coding region amplified by RT-PCR. Following transfection with equal concentrations of viral RNAs, total viral RNA was extracted from the infected cell lysates and used as a template for RT-PCR of a 1124 bp region of P1, covering the L, VP4 and VP2 coding sequences. E) *HindIII* restriction analysis of the 1124 bp RT-PCR product. To confirm that no contamination of WT virus had occurred, RT-PCR products were subjected to restriction digestion

using *HindIII*. The *HindIII*-1 control mutant RT-PCR product was not successfully digested, confirming that the resultant virus was the mutant control, while the fragment belonging to the WT virus was cleaved by the endonuclease into two fragments of 536 and 588 bp as expected.

4.3.3. Monitoring cytopathic effect of mutant viruses

To examine the potential effects of the amino acid substitutions on virus infectivity, *in vitro* transcribed mutant and WT TMEV RNA was transfected into BHK-21 cells (*Figure 4.5 A*). CPE was not observed in any of the cells mock transfected with transfection mixtures lacking viral RNA, demonstrating that none of the transfection reagents were toxic or induced the false appearance of CPE. The onset of CPE was apparent in cells transfected with WT RNA at 24 hpt as expected, with 100 % CPE observed after 48 h. CPE was completely absent in cells transfected with any of the nine hotspot-to-alanine mutants at all time points observed, and the cell monolayers were comparable to those in the mock transfected control. The serial passage of the mutant transfected cell supernatants on fresh BHK-21 cell monolayers did not lead to the onset of CPE, even following nine passages.

Three residues, K18, G94 and D242 in VP2 that were also predicted to form interactions between TMEV pentamers but were not predicted as hotspots, were individually mutated to alanine as neutral controls. As observed in WT transfected cells, transfection of corresponding control mutant RNAs induced CPE at 24 hpt, demonstrating that these alanine substitutions had not disrupted virus infectivity. To confirm that the CPE observed in the K18A, G94A and D242A mutant transfected cells was a result of infection with these mutant viruses and not cross contamination with WT virus, mutant and WT viral RNA was extracted and RT-PCR was performed, amplifying the 1124 bp fragment of the RNA genome spanning the L-VP4-VP2 proteins. The resultant PCR products were subjected to restriction analysis using *HindIII* (*Figure 4.5 B*). As expected, the WT virus was successfully cleaved into two

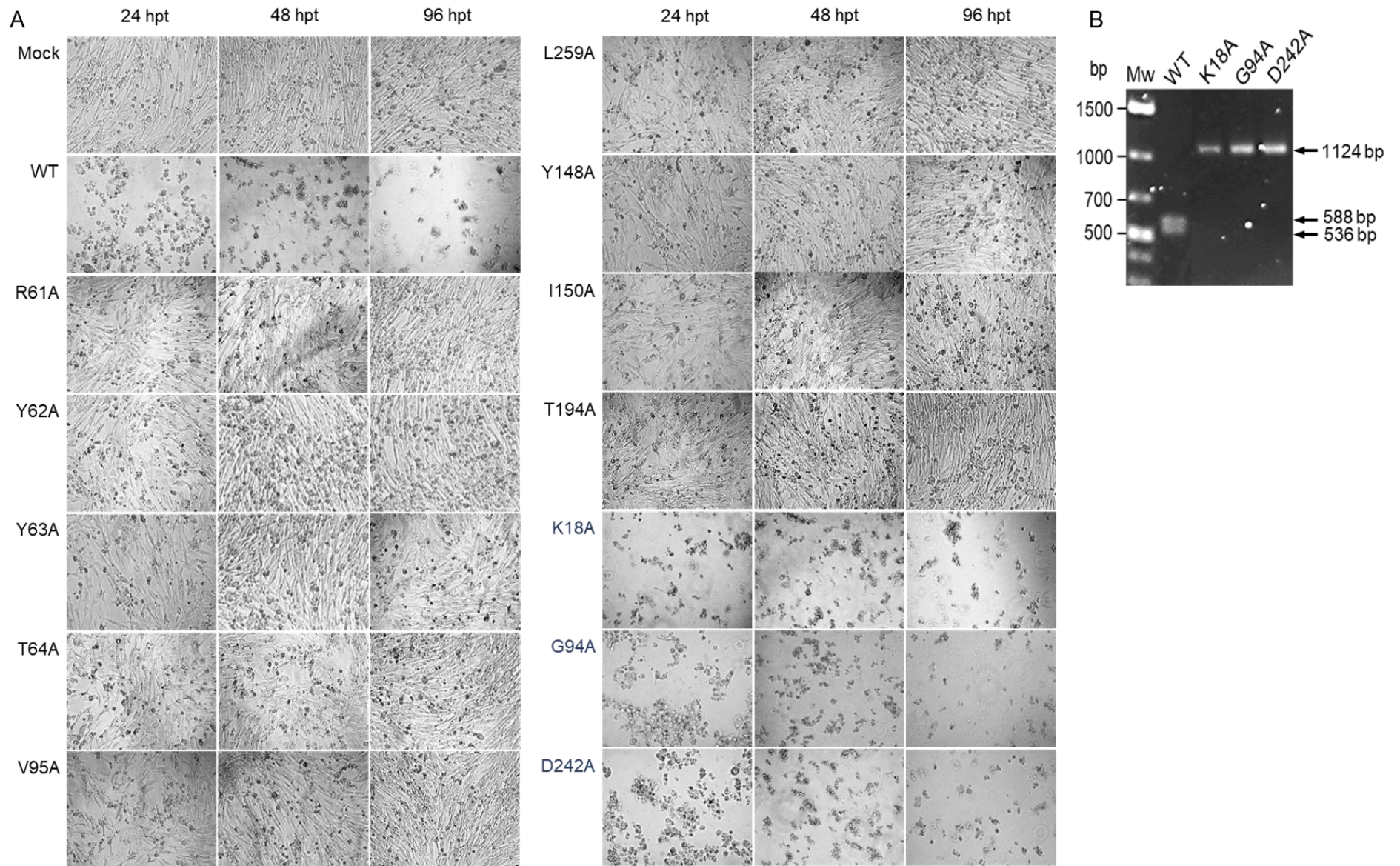


Figure 4.5 Comparison of the cytopathic effects induced by transfection of hotspot mutant, non-hotspot mutant and wild type TMEV RNAs. A) Following the transfection of individual mutant or WT RNAs onto 70 % confluent BHK-21 cell monolayers, the cells were monitored for the appearance of CPE at 24, 48 and 96 hpt. Transfections were performed in triplicate. B) *HindIII* restriction analysis of RT-PCR products generated from viral RNA that was extracted from transfected cell supernatants following the onset of CPE.

fragments. Bands of 1124 bp were observed for K18A, G94A and D242A demonstrating that *HindIII* was not able to digest the PCR product, proving that the CPE observed was a result of infection with these viruses and not due to cross contamination with WT virus.

4.3.4. The absence of CPE is a result of the loss of individual hotspot residues and not defective viral RNA

To ensure that no unwanted mutations were introduced during the site directed mutagenesis reactions or subsequent cloning of the mutant P1/P2 fragments back into the WT backbone, 6 of the hotspot-to-alanine mutant plasmids were randomly selected and sequenced from the *KpnI* to the *Kpn2I* restriction sites, between which the mutant P1/P2 fragments were re-inserted (*Figure 4.6*). Sequencing revealed that the mutant inserts were in frame with the rest of the TMEV ORF (*Figure 4.6 A*) and that no unwanted mutations were present in the mutant viruses. Furthermore, replacement of the insert from one of the mutant plasmids with the WT insert restored infectivity, as CPE was observed from 24 hpt following transfection with corresponding RNA (*Figure 4.6 B*) and plaque assays demonstrated no significant difference between the titres of the restored virus and the WT virus (T-test: *P value* = 0.8134). These experiments confirmed that the lack of CPE in the hotspot-to-alanine mutants was not due to unanticipated mutations in the TMEV cDNA.

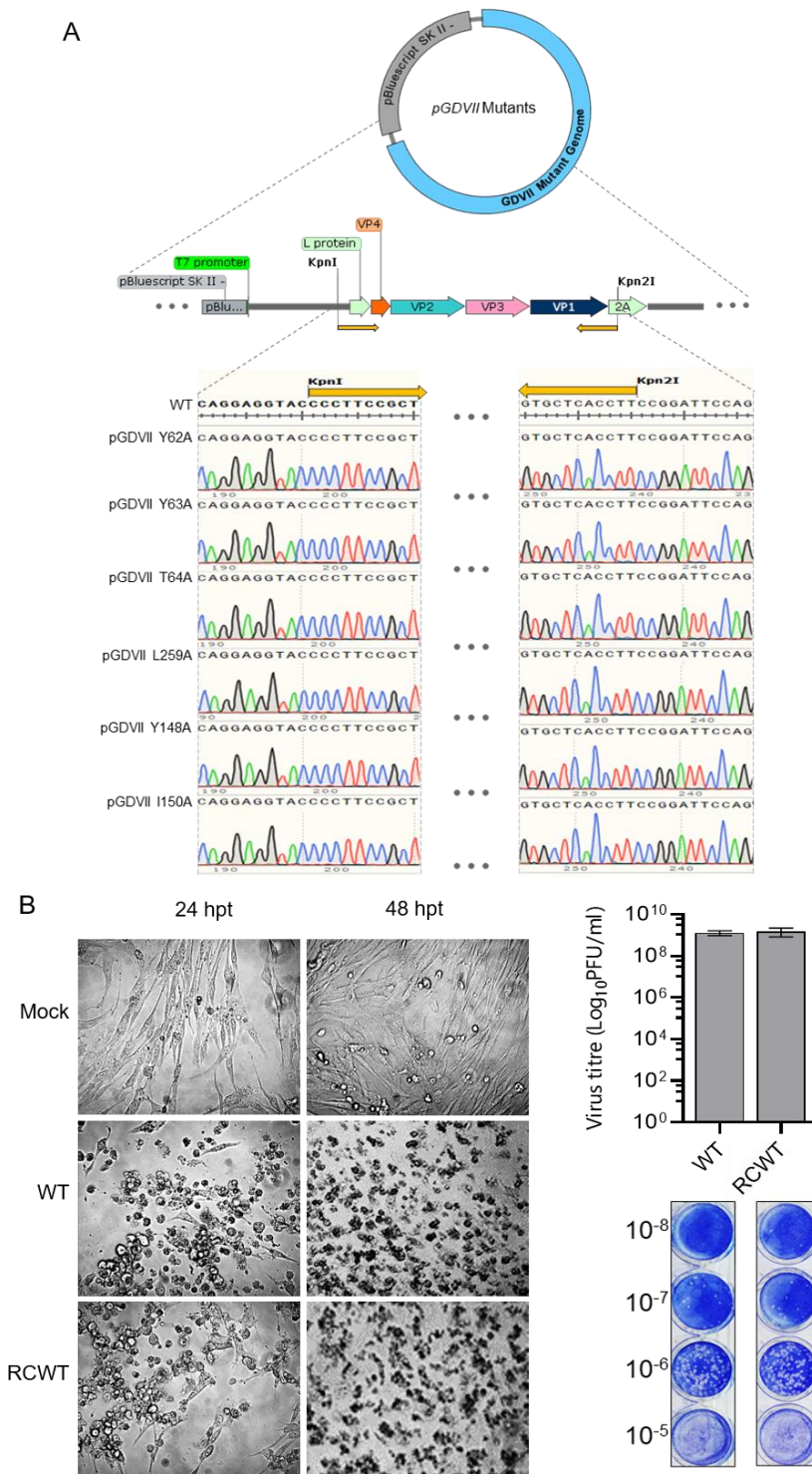


Figure 4.6 Controls to demonstrate that the lack of CPE was not due to defective mutant viral RNA. A) Sequencing of the mutant pGDVII/H-1 plasmids revealed that the mutant inserts were in frame with the TMEV ORF. To demonstrate that the pGDVIIIFL2 backbone was not altered during the generation of the mutants, the mutant insert from one plasmid was replaced with the WT fragment. B) Transfection of the restored WT virus (RCWT) results in CPE. C) No significant difference in viral titres was observed between the two viruses. Error bars indicate standard deviation (SD).

4.3.5. TMEV replication and viral protein synthesis are not inhibited by substitution of the hotspot residues to alanine

Immunofluorescence analyses were carried out on the mutant RNA transfected cells firstly, to exclude the possibility that the absence of CPE was a consequence of failed transfection, and secondly, to examine whether the loss of the individual hotspot residues affected other aspects of the TMEV lifecycle, including replication or protein synthesis. Equal concentrations of mutant and WT RNA were used for transfections. At 14 and 24 hpt cells were paraformaldehyde fixed before they were stained using the anti-capsid antibodies, and dsRNA monoclonal antibodies specific for replicating viral RNA (*Figure 4.7*). Cells that stained positive for TMEV capsid proteins and dsRNA were detected following the transfection of all mutant and WT RNAs, indicating that the lack of CPE in mutant transfected cells (observed in *Figure 4.5*) was not a result of failed transfections. Furthermore, this demonstrated that the substitution of individual hotspot and non-hotspot (neutral) residues to alanine did not inhibit TMEV replication or protein synthesis.

At 14 h post transfection, the percentage of TMEV infected cells was not significantly different between the hotspot mutant viruses, non-hotspot (neutral) mutant viruses and the WT virus (*Figure 4.7*). In all transfection experiments at 14 hpt, less than 3 % of the transfected cells were positive for TMEV capsid protein or replicating RNA. At 24 hpt the number of TMEV infected cells was markedly different between the hotspot mutants, WT and non-hotspot control mutants. 76 % of the WT transfected cells were positive for TMEV, consistent with the previous observation of CPE at 24 hpt (*Figure 4.5*). The number of cells positive for TMEV capsid proteins or replicating RNA in cells transfected with hotspot mutant viral RNAs was completely different to the WT transfected cells (*Figure 4.7*). No significant increase was observed between 14 and 24 h for any of the hotspot-mutant viruses (Adjusted *P-values* are

displayed following a Two-Way ANOVA and Turkey's post hoc test in supplementary table S5).

The number of TMEV positive cells transfected with non-hotspot (neutral) control virus RNA increased in the same manner as the WT transfected cells. Statistical analysis demonstrated that the number of TMEV positive cells was not significantly different between the three neutral mutants and the WT virus (adjusted *P-values* available in supplementary table S5) and is consistent with the pattern of CPE observed at 24 hpt in previous experiments (*Figure 4.5*). This result demonstrates that substitution of the K18, G94 and D242 non-hotspot residues to alanine did not disrupt the virus lifecycle and resulted in the generation of virions that could infect neighbouring cells.

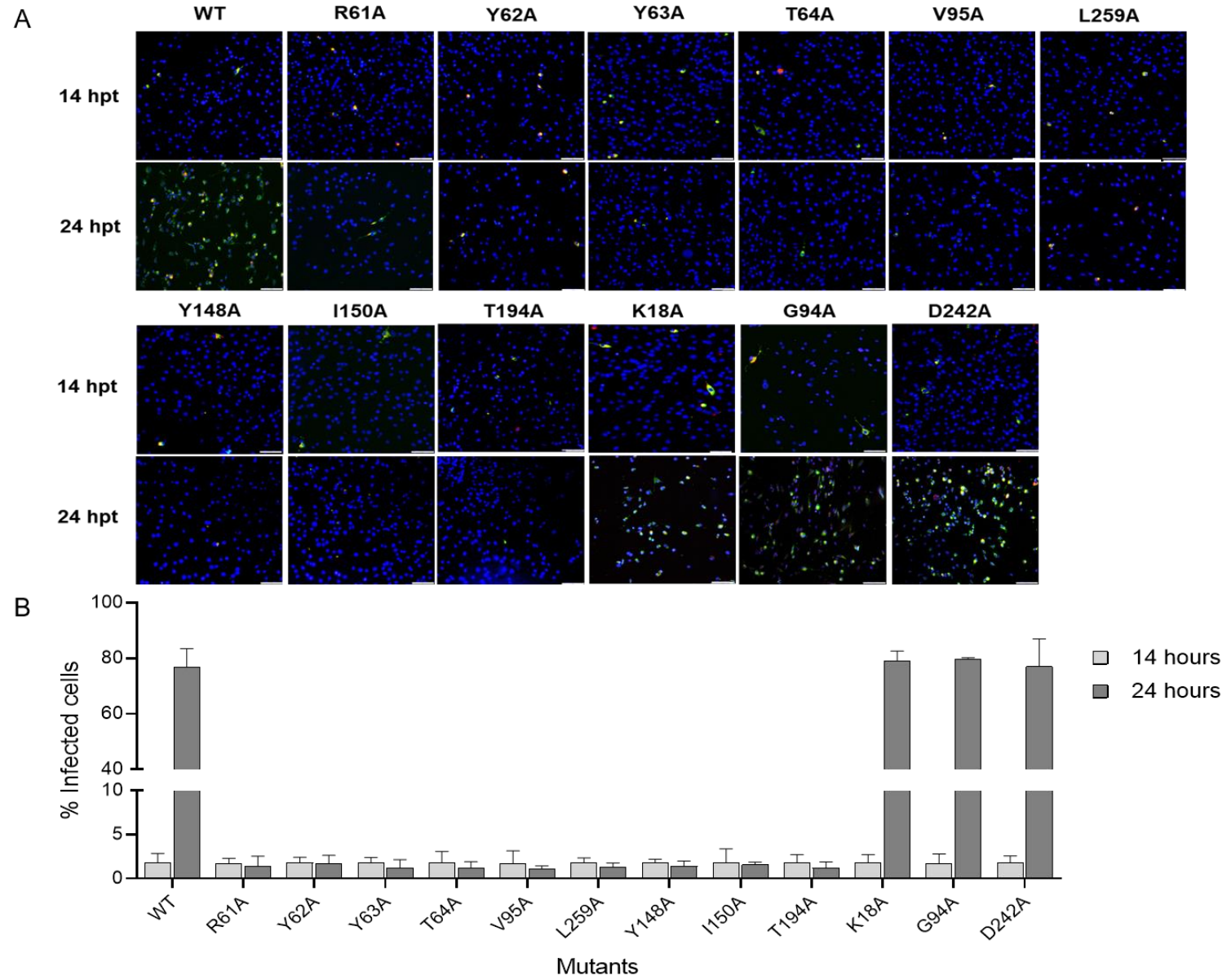


Figure 4.7 Immunofluorescence analysis of cells transfected with mutant and wild type TMEV RNAs. A) BHK-21 cells were transfected with 1 μ g of WT or mutant viral RNAs and were analysed by immunofluorescence at 14- and 24-h post infection, using polyclonal rabbit anti-TMEV capsid and mouse monoclonal dsRNA primary antibodies. Primary antibodies were detected using species specific Alexa Fluor 488 (green)- and 546 (red)-conjugated secondary antibodies respectively. Scale bars = 100 μ m. B) The percentage of infected cells at 14 and 24 hpt represented in A. Error bars represent the SD of three replicate images from three separate transfections (Supplementary Figures S9 & S10). A two-way ANOVA followed by a Tukey's post hoc analysis showed that there was no significant difference between the number of infected cells at 14 hpt, that there was a significant difference between the number of infected cells between the hotspot mutants and the non-hotspot (neutral) and WT viruses at 24 hpt, but that there was no significant difference between the number of infected cells in the non-hotspot mutant and WT transfected cells (Table S5).

4.4. Discussion

The aim of this chapter was to assess the importance of *in-silico* predicted hotspot residues at the pentamer-pentamer interfaces of TMEV to virus infectivity, using an *in vitro* system. Nine of the 24 interpentamer residues predicted as hotspots in chapter three were selected for mutagenesis. These hotspots include amino acids R61, Y62, Y63, T64, V95 and L259 in VP2, and Y148, I150 and T194 in VP3. The rationale for selecting these residues was threefold; firstly, these residues were found to be highly conserved in other genera and many correspond to residues that have previously been shown or predicted to be important for capsid assembly or stability in other viruses of the family. Secondly, the sidechains but not the mainchains of the selected residues were predicted to be involved in the stabilising interaction. This is important because substitution to alanine removes the residue's sidechain but does not alter the mainchain, thus, only hotspots forming stabilising interactions through their sidechains could be analysed using this method. Thirdly, primers with appropriate melting temperatures could be designed for mutation of these hotspots as they were not found in regions with high G-C content.

Three residues that form part of the interface but were not predicted to be important for interface stability, were selected as non-hotspot residue (neutral) controls. These residues include K18, G94 and D242 belonging to VP2. K18 and D242 sidechains form hydrogen bonds with non-hotspot residues F19 and N71 in VP1 and VP3 across the pentamer interface respectively. The sidechain of G94 is predicted to interact with the mainchain of R102 in VP2 via hydrogen bonds. Although R102 is predicted to be a hotspot (Chapter three, *Figure 3.5*), the stabilising ionic interactions are predicted between the sidechains of R102 and E91 in the VP2 protein of the opposing pentamer. G94 is conserved in the VP2 proteins of representatives from the cardio-, aphtho-, entero- and senecavirus, but residues K18 and D242 are not (Supplementary Figure S3).

Previous mutagenesis studies on TMEV have largely made use of overlap PCR as described by Ho et al. (1989) to introduce point mutations into the cDNA of the virus (Basta and Palmenberg, 2014; Finch et al., 2015; Murray et al., 2009; Pavelko et al., 2011). More recently, a simpler strategy combining site directed mutagenesis PCR and directional subcloning has been used to engineer mutations into the P1 coding regions of FMDV (Caridi et al., 2015; Kotecha et al., 2018, 2015; Kristensen et al., 2017; Luna et al., 2009; Mateo et al., 2008, 2003; Rincón et al., 2015), EMCV (Zhu et al., 2011) and TMEV DA (Bell et al., 2014; Stavrou et al., 2010). This approach involves subcloning the P1 coding region of the virus into a smaller vector, which is used as a template for PCR amplification of the entire plasmid, using the QuikChange system (Stratagene) and a single pair of overlapping mutagenic primers. Subsequently, the mutant insert is cloned back into the parental plasmid, yielding viral cDNA containing the mutation of interest. Advantages of this method are that only one set of primers is needed for a single PCR reaction and mutants can be engineered rapidly (Xia and Xun, 2017). In this study, a similar approach was used in which the P1 and partial P2 sequences of TMEV GDVII were subcloned into a smaller vector, yielding a 7.12 kb plasmid for site directed

mutagenesis. Instead of the QuikChange system, the Phusion Site Directed Mutagenesis Kit was used. Unlike the former system, phosphorylated back-to-back primers containing mismatched nucleotides near the centre of one of the primers are used in an inverse PCR. The resultant product is the linear PCR amplified plasmid that must be circularised before it is transformed into *E. coli*. The resultant mutant insert is then removed from the mutant vector and ligated into the parental plasmid, yielding the mutant viral cDNA. Using back-to-back or partially overlapping primers has significant advantages compared to the completely overlapping primers used in the QuikChange system. Firstly, non-overlapping primers reduce the likelihood of primer-dimer formation during PCR. Secondly, partially overlapping or back-to-back primers yield exponentially more product following PCR. Thirdly, the increased concentration of PCR product improves the efficiency of downstream applications, including transformation (Hemsley et al., 1989; Xia et al., 2015).

To demonstrate the viability of this approach for generating the mutant TMEV cDNAs, a control mutant was generated in which the *HindIII* restriction site was altered by mutation of the second last thymine in the restriction motif to a guanine nucleotide. Sequencing of pGDVII/*HindIII*-1 demonstrated that alteration of the *HindIII* site was successful. Transfection of corresponding mutant and WT RNA revealed that neither the point mutation nor the mutagenesis procedure itself affected TMEV protein synthesis or virus yield, confirming that this method was appropriate for the generation of subsequent mutants. Furthermore, *HindIII* restriction analysis of RT-PCR products generated using RNA from resultant *HindIII*-1 mutant and WT virions produced different restriction patterns. This demonstrated that mutant and WT RNA could be rapidly distinguished without DNA sequencing. The pJetP1/P2/*HindIII*-1 plasmid rather than pJetP1/P2 was used as a template into which the individual alanine substitutions were introduced, so that any mutant virions formed following transfection could be rapidly distinguished from the WT virus.

Transfection of the *in vitro* transcribed hotspot mutant RNAs into BHK-21 cells did not result in the onset of CPE, even after 96 h post transfection. CPE, however, was observed upon transfection of the non-hotspot (neutral) mutant control K18A, G94A and D242A RNAs, and was consistent with that observed following transfection with WT RNA. *HindIII* restriction digest of resultant RT-PCR products demonstrated that the CPE observed was due to transfection with the non-hotspot (neutral) mutant RNA and not contaminating WT virus. Unlike other reports in similar studies, none of the hotspot-to-alanine mutants were able to induce CPE following transfection of viral RNA. For example, Mateo et al. (2003) examined the effects of alanine substitutions on residues involved in interactions between pentamers of the FMDV capsid and found that 80 % of the residues were critical. Although the largest proportion of the mutants could also not be recovered following electroporation with mutant viral RNA, some of the mutants exhibited highly reduced viral titres and small plaque phenotypes, while others acquired compensatory mutations or reversions that restored infectivity of the mutant (Mateo et al., 2003). An important difference between the analysis presented here and the study by Mateo and co-authors is that the TMEV interpentamer residues mutated to alanine were already predicted as hotspots important for capsid formation and virus stability, while Mateo and colleagues examined all possible amino acids involved in interactions across the interface. This may explain why deleterious effects were observed following substitution of each TMEV hotspot residue to alanine in this study, and why a broader range of effects was observed for the FMDV mutants in the Mateo et al. (2003) analysis.

One residue examined by Mateo and colleagues, T190, corresponds to the TMEV hotspot residue T194. The authors found that only the WT FMDV genotype was present following transfection of T190A RNA, indicating that the residue had reverted to threonine. However, in this study reversion of A194 to threonine was not observed. In a follow up study by Luna et al.

(2009), the serial passage of many of the deleterious FMDV mutants generated by Mateo et al. (2003) yielded virions with second-site substitutions that restored virus infectivity. In this study, the passage of mutant transfected cell lysate did not result in the restoration of any of the original residues, or the emergence of variants with additional mutations that could restore infectivity, even following a series of nine passages. In the Luna et al. study, most of the substitutions that restored virus infectivity in FMDV were found at the capsid interpentamer interfaces and involved amino acids near to the originally substituted residue. However, the TMEV hotspot residues analysed in this study are surrounded by and directly interact with many other hotspot residues, thus, the non-specific mutation of these neighbouring hotspot residues may have potentially compounded any deleterious effects instead of restoring virus infectivity. Furthermore, the hotspot residues R61, Y62, Y63, T64 in VP2 and Y148 and I150 in VP3 form part of an interacting hotspot sub-network within the interface. Any destabilising effects from the substitution of one of these hotspot residues may have critically affected the interacting partner residues in this network, potentially amplifying any destabilising effects at the interface.

It was necessary to confirm that the absence of CPE was not due to failed transfections or nonviable mutant RNAs. To this end, cells were transfected with equal concentrations of mutant and WT RNAs and were examined in immunofluorescence experiments. At 14 hpt there was no significant difference in the percentage of cells positive for TMEV capsid protein or replicating RNA between the hotspot mutants, non-hotspot (neutral) mutants and WT transfected cells in three replicates. At 24 hpt the percentage of cells positive for TMEV had increased to numbers greater than 76 % in WT and non-hotspot (neutral) transfected experiments, but the percentage of TMEV positive cells did not increase in cells transfected with hotspot-mutant RNA, demonstrating that the virus lifecycle was disrupted. It is unlikely

that differences in transfection efficiency contributed to the observed differences in CPE as the number of TMEV positive cells was equal at 14 hpt.

The lack of CPE combined with the observation of similar numbers of TMEV positive cells at 14 and 24 hpt strongly suggests that the amino acid substitutions prevented completion of the TMEV lifecycle and subsequent infection of new cells. A possible but unlikely explanation is that the mutations could have disrupted viral protein synthesis. The residues that were individually substituted to alanine are, however, situated away from the known picornavirus polyprotein cleavage sites (Kristensen and Belsham, 2019; Palmenberg, 1990), and so it is unlikely that polyprotein processing was affected. Furthermore, the detection of capsid proteins using TMEV specific anti-capsid antibodies (Upfold et al., 2018), following the transfection of mutant RNAs, demonstrated that the individual amino acid substitutions did not prevent viral protein synthesis. A second explanation is that replication was affected by the residue substitutions, however, the positive staining for dsRNA during immunofluorescence experiments is consistent with the replicating RNA of positive sense RNA viruses such as TMEV (Son et al., 2015; Weber et al., 2006), indicating that replication was not likely inhibited in the mutants.

The interfaces between pentamers are the known sites of pore formation or dissociation, required for genome release in the picornaviruses (Bostina et al., 2011; Buchta et al., 2019; Tuthill et al., 2007; Wang et al., 2012a), but are also the sites of contact during the assembly of pentamers into viral capsids. With this in mind, one of two possible explanations seem more appropriate. Either substitution of these residues (i) prevented the assembly of stable capsids inside cells or (ii) capsids did assemble but could not survive cell egress or the extracellular environment due to decreased stability against dissociation, preventing the infection of new cells. Despite the observation that capsid proteins were being synthesised in the mutant transfected cells, it is plausible that their subsequent assembly into viable capsids was

significantly affected by the substitutions. TMEV hotspot residue R61 corresponds to residue R60 in FMDV that also abolished viral infection upon substitution to alanine (Mateo et al., 2003). Using antibodies specific for folded protomers and the full capsid, the authors demonstrated that assembly was likely affected by this residue change. Considering the conservation of this residue in both viruses it is likely that TMEV capsid assembly may also be affected by substitution of R61 residue in this study. Since these substituted residues are located at the TMEV pentamer interfaces, it is likely that the stages of capsid assembly from protomer folding to pentamer formation proceeded without disruption, but that the assembly of pentamers into provirions was directly affected. Alternatively, the residue substitutions at the pentamer interfaces could have resulted in the formation of capsids with significantly reduced stability compared to the WT capsid. This is a highly plausible suggestion given that substituted residues were predicted as hotspot residues important for capsid stability (chapter three). These particles may have been more sensitive to stresses during cell egress or those found in the extracellular environment, leading to premature dissociation and the prevention of subsequent rounds of infection. Finally, it is unlikely that substitution of the hotspots affected the TMEV lifecycle by preventing entry. Even if virions were capable of assembling into stable capsids, the TMEV pentameric interfaces are located far away from residues demonstrated or predicted to be involved in receptor binding (Hertzler et al., 2000; Jnaoui et al., 2002; Luo et al., 1992; Upfold et al., 2018), thus it is unlikely that the lack of CPE was due to prevention of mutant virions from binding to new cells.

In conclusion the overall aim of this study was to evaluate the importance of previously predicted interpentamer hotspot residues to TMEV virus infection. Nine hotspot and three non-hotspot (neutral) residues were selected and individually mutated to alanine, using a novel and appropriate site directed mutagenesis system for this virus. Following the generation of the mutant cDNAs, transfection of the corresponding hotspot mutant RNAs into susceptible cells

demonstrated the importance of these residues to TMEV infectivity as no CPE was observed. Immunofluorescence experiments indicated that the amino acid substitutions likely had no effect on virus replication or protein synthesis. Further experiments are needed confirm whether capsid assembly is disrupted by the residue substitutions or whether capsids are formed that rapidly disassemble due to decreased stability against dissociation. Non-hotspot (neutral) residues involved in interpentamer interactions were also mutated to alanine and had no effect on viral function. Collectively the work presented in this chapter demonstrates that these hotspot residues are important for the TMEV lifecycle.

Chapter 5

The selection of TMEV GDVII virions
with increased thermal tolerance

5.1. Introduction

The replication of picornaviruses is characterised by high mutation rates, resulting in quasispecies populations that comprise highly similar but non-identical genomes, and is a consequence of their error-prone nonproofreading RNA-dependent RNA polymerases (Domingo, 1997; Domingo et al., 2012). Predisposition to rapid mutation has been a major driving force in picornavirus evolution and has allowed virions to overcome a variety of selection pressures (Domingo et al., 2008; Pfeiffer and Kirkegaard, 2005), resulting in the continued emergence of antigenic variants (Reeve et al., 2016; Waman et al., 2014). Despite this adaptability, picornavirus capsids have evolved under stringent and conflicting constraints; the capsid must be strong enough to withstand dissociation in the extracellular environment, but must not be so strong as to impede delivery of the genome to the host cell (Mateo et al., 2003). These limitations combined with the requirements of an individual virus's lifecycle have resulted in the evolution of metastable capsids with different biophysical stabilities (Mateo, 2013; Scott et al., 2019; Yuan et al., 2017).

The thermostability of virus particles is an important consideration for the development of stable vaccines. Picornavirus particles used as vaccine antigens are often susceptible to heat-induced structural rearrangements that alter virus antigenicity, thereby preventing the induction of appropriate immune responses following immunisation (Doel and Baccarini, 1981; Mateo et al., 2008; Wang et al., 2013). VLPs and empty capsids are even less thermostable and rapidly lose antigenic potency, which is a major obstacle to their development as vaccine candidates (Adeyemi et al., 2017; Basavappa et al., 1994; Fox et al., 2017; Kotecha et al., 2015). Identifying the genetic basis of improved thermal tolerance would not only provide a better understanding of picornavirus capsid assembly, genome uncoating and capsid structure (Rincón et al., 2014), but could inform the design of vaccine antigens with improved

thermostability (Adeyemi et al., 2017; Kotecha et al., 2015; Mateo et al., 2008; Porta et al., 2013).

Several approaches have been implemented to yield picornavirus particles with improved stability. Authors have generated capsid particles or VLPs with improved thermal tolerance by inspecting picornavirus crystal structures and introducing appropriate amino acid substitutions that, for example, alter electrostatic interactions or introduce stabilising disulphide bonds across pentameric interfaces of the capsid (López-Argüello et al., 2019; Mateo et al., 2008; Porta et al., 2013; Rincón et al., 2014). Alternatively, authors have employed *in-silico* calculations to identify potential residue substitutions that would increase capsid stability (Kotecha et al., 2015; Scott et al., 2017). More recently, authors have exploited the adaptability of picornaviruses to various stresses to select virions with improved stability. Studies have generated EV-71 and PV virions with improved thermal tolerance following the heating of virus particles to non-physiological temperatures and passaging the remaining virions (Adeyemi et al., 2017; Kelly, 2015). Few studies have examined the inherent thermostabilities of cardioviruses. Although these viruses are not major human pathogens, understanding the underlying genetic mechanisms that contribute to increased stability in these viruses may help to advance the knowledge surrounding capsid structure and thermal tolerance within the family.

The overall aim of this study was to examine the thermal tolerance of TMEV GDVII by recurrent passage of the virus following exposure to non-physiological temperatures, and to elucidate the genetic basis for increased thermal tolerance in the resultant isolates. The first objective was to assess the inherent thermostability of TMEV GDVII following the short-term exposure of the virus to temperatures above 37 °C. The second objective was to select thermal tolerant GDVII isolates by passaging the virus at 37 °C following exposure of the virus to temperatures above 50 °C. The final objective was to identify and examine potential mutations

within the P1 capsid encoding regions of the heat-selected isolates that contributed to increased thermal tolerance.

5.2. Materials and Methods

An overview of the methodology used in this study to generate and assess TMEV GDVII virions with improved thermal tolerance is given in *Figure 5.1*.

5.2.1. Cells and virus

BHK-21 cells were maintained as described in section 2.2.1. TMEV strain GDVII was used to infect cells in all experiments, and virus stocks were prepared as described in section 2.2.1.

5.2.2. Short-term thermal inactivation assays

Thermal inactivation assays were performed as described by Adeyemi et al., (2017) with minor adaption. 200 µl of WT virus or mutant virus stocks were heated to a range of temperatures from 45 to 60 °C for 30 min using a SimpliAmp Thermal Cycler (Thermo Scientific, USA), before the temperature was cooled to 4 °C for 5 min. The surviving virions were titrated by plaque assay on BHK-21 monolayers grown in 24-well plates, as described in section 4.2.4. To calculate the log reduction in virus titre the following formula was used:

$$\text{Log Reduction} = \text{Log}_{10} \left(\frac{A}{B} \right)$$

To calculate the percentage reduction in virus titre the following formula was used:

$$\text{Percentage reduction} = \frac{(A - B) \times 100}{A}$$

Where: *A* is the number of plaque-forming virions prior to heat exposure, *B* is the number of plaque-forming virions post heat exposure.

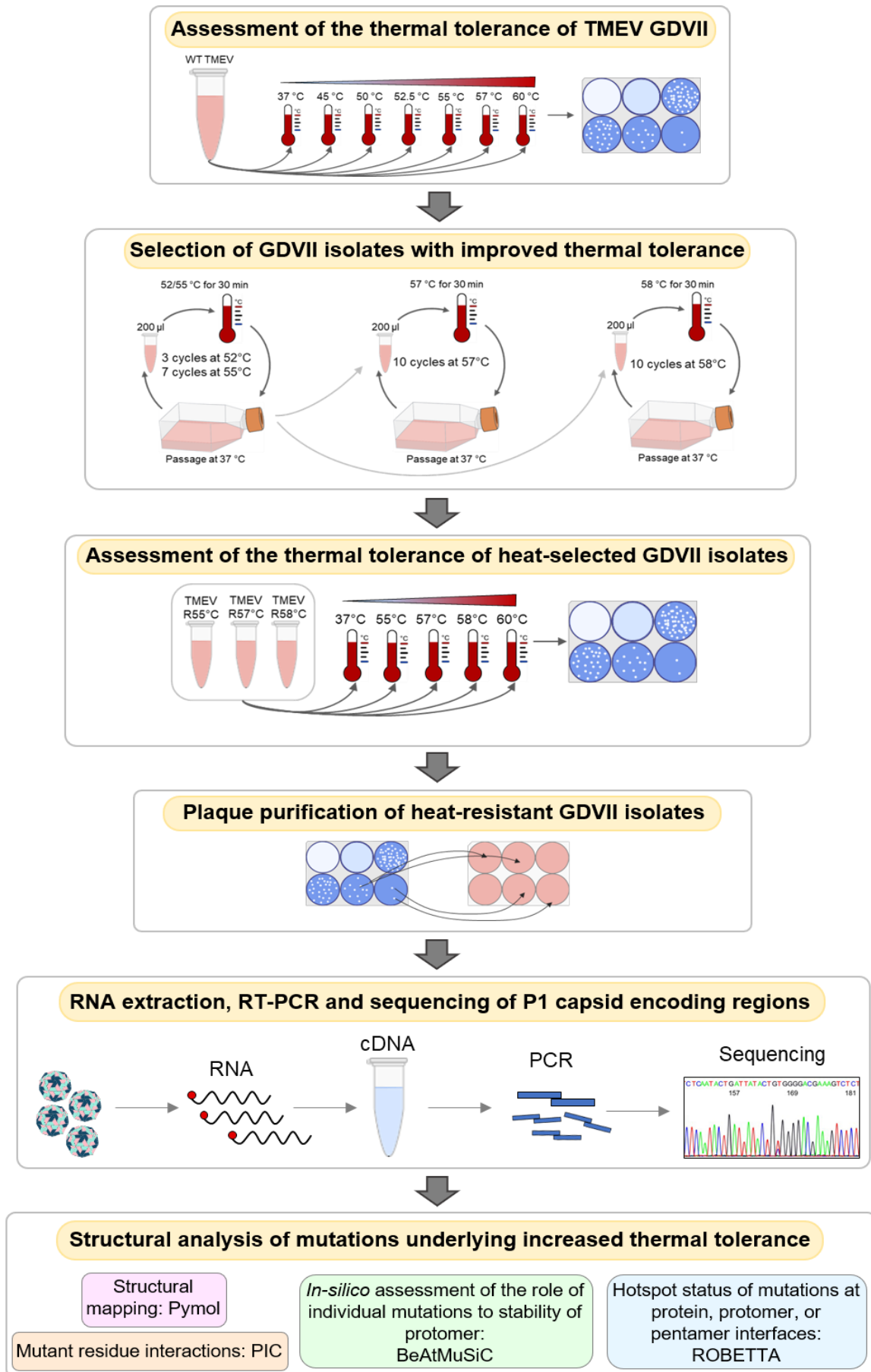


Figure 5.1 Flow diagram of the methodology to select TMEV GDVII isolates with improved thermal resistance and to assess the underlying mutations that contribute to this improved tolerance. The inherent thermal tolerance of TMEV was assessed using a short-term thermal inactivation assay. TMEV isolates with improved resistance to 55 °C, 57 °C and 58 °C were selected by continuous cycles of heat-exposure and passage of remaining virions. The selection of isolates with improved tolerance to these temperatures was confirmed using short-term thermal inactivation assays. Individual isolates within the three virus pools were plaque-purified. The P1 segments of these virions were reverse-transcribed following virus RNA extraction, and sequencing was performed to identify mutations within this capsid encoding region of the genome. The potential effects of the mutations on the structure of the virus capsid were assessed by *in-silico* investigation.

5.2.3. Selection of virions with increased thermostability

WT TMEV GDVII stocks diluted to 2.8×10^6 PFU/ml in DMEM to a final volume of 200 μ l were used for the initial heat shock. This is approximately enough virus to infect a monolayer of BHK-21 cells in a T25 cm² flask at a MOI of 1. The virus was heated to 52.5 °C for 30 min in a SimpliAmp Thermal Cycler (Thermo Scientific, USA), before the temperature was decreased to 4 °C for 5 min. The surviving virions were amplified on a monolayer of BHK-21 cells in a T25 cm² flask until CPE was observed. 200 μ l of the crude infected lysate was heated again to 52.5 °C. This cycle was repeated three times, after which the temperature was increased to 55 °C for an additional seven heat passages. Following the passages and heat exposure to 55 °C, 10 more passage cycles were completed at 57 °C and 58 °C in simultaneous experiments. Where no CPE was observed, virus was amplified on another monolayer before the heat shock was repeated. WT virus that was not heated was also passaged alongside every cycle as a control.

5.2.4. Plaque purification of heat selected virions

A series of ten-fold dilutions of heat passaged virus was made in serum-free DMEM. Confluent BHK-21 monolayers were washed with $1 \times$ PBS (pH 7.4) and 0.05 ml of each virus dilution was added to individual wells of a 24-well plate. Virus adsorption was allowed to proceed for

1.5 h at 37 °C with gentle agitation, before the cells were washed with 1 × PBS and overlain with 1 ml agarose overlay solution [DMEM containing agarose to a final volume of 1 %] per individual well. The cells were incubated until individual plaques were visible ~48 hpi. Plaques were carefully isolated and used to inoculate fresh BHK-21 monolayers grown in individual wells of a 24 well plate. The cells were incubated until CPE was visible, and the infected cell lysates were frozen at -80 °C as individual virus stocks.

5.2.5. RNA extraction and RT-PCR

Viral RNA was extracted from 140 µl of mutant virus stock using the QIAamp Viral RNA Mini Kit (Qiagen, Germany), according to the manufacturer's instructions. The viral RNA was used as a template for the reverse-transcription PCR (RT-PCR) of two products spanning the P1 region of the TMEV genome (*Figure 5.2*). The first 1124 bp product spanned the sequences encoding the VP4 and VP2 capsid proteins, while the second larger product (1732 bp) included the last 99 bp of the VP2 coding sequence, and the full sequences encoding VP3 and VP1.

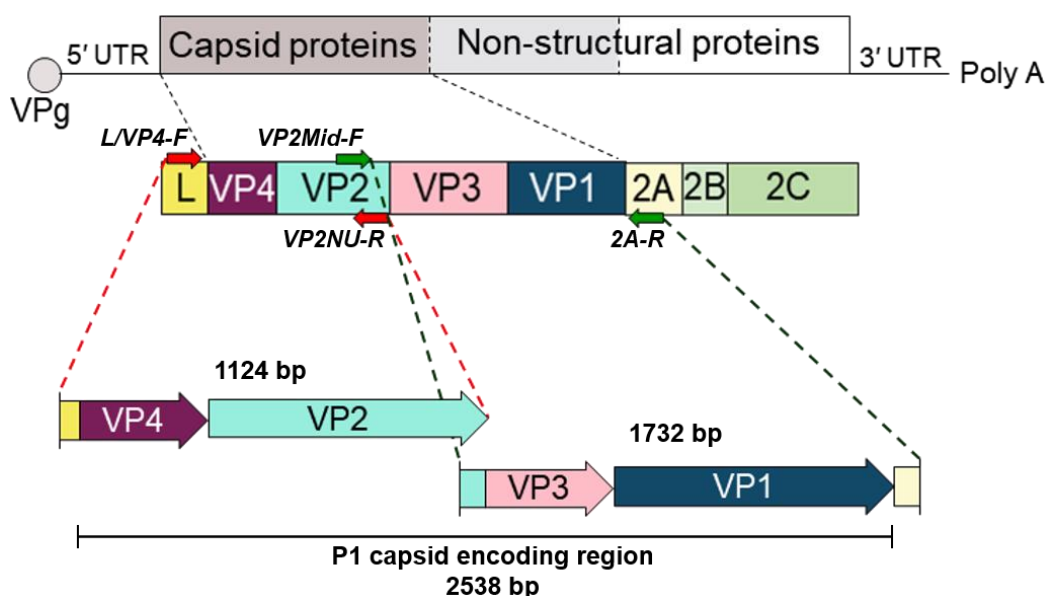


Figure 5.2 Schematic diagram of the strategy used to RT-PCR amplify the TMEV P1 capsid encoding region of thermostable mutants. The P1 region was amplified as two overlapping products. The first consisting of a 1124 bp product containing the VP4 and VP2 coding sequences, and the second

a 1732 bp product encompassing the VP3 and VP1 coding sequences. The products overlap by the last 99 bp of VP2.

cDNA synthesis was performed using the RevertAid First Strand cDNA Synthesis Kit (Thermo Scientific, USA) as per the manufacturer's instructions. Each 20 μ l cDNA synthesis reaction contained 0.5 μ g of total viral RNA, 4 μ l of 5X Reaction buffer, 2 μ l 10 mM dNTP Mix, 200 U RevertAid M-MuLV Reverse Transcriptase (200 U/ μ l) and 20 μ M of either the VP2NU-Rev reverse primer or the 2A-Rev reverse primer (Table 5.1).

Table 5.1 Primers used for RT-PCR of the TMEV P1 capsid encoding region.

Primer	Primer sequence 5'→3'	Binding site in genome	Product size (bp)
L/VP4-For	GACGATGACGTCTTCTGGCCTTC	1701-1723	1124
VP2NU-Rev	AAATCTAGAGCTTGC GCAAGCACAGTTTCG	2795-2813	
VP2-Mid-For	TACGCCACCGGTTCTTCACCG	2715-2735	1732
2A-Rev	CTGGAATCCGGAAGGTGAGCAC	4425-4446	

The reactions were incubated at 42 °C for 1 h, before they were terminated by heating to 70 °C for 5 min. The resultant cDNAs were used as templates for PCR using the Q5[®] High-Fidelity PCR Kit (New England Biolabs). PCR reactions to a final volume of 50 μ l contained 5 μ l cDNA template, 25 μ l Q5[®] High-Fidelity 2X Master Mix and either 2.5 μ l of 10 μ M L/VP4-For forward primer and 2.5 μ l of 10 μ M VP2NU-Rev reverse primer or 2.5 μ l 10 μ M VP2-Mid-For forward primer and 2.5 μ l of 10 μ M 2A-Rev reverse primer. PCR cycles included an initial denaturation step at 98 °C for 30 seconds, followed by 25 cycles of: denaturation at 98 °C for 10 seconds, annealing at 62 °C for 30 seconds and elongation at 72 °C for 1 min (VP4-VP2 product) or 1.5 min (VP3-VP1 product), and a final elongation step at 72 °C for 5 min. Thermocycling was performed using a SimpliAmp Thermal Cycler (Thermo Scientific, USA). The resultant PCR products were sequenced (Inqaba Biotechnical Industries (Pty) Ltd.,

Pretoria, South Africa) to identify mutations in the P1 capsid encoding region. Chromatograms were analysed using SnapGene[®] software (GSL Biotech).

5.2.6. *In-silico* figure preparation, graph generation and statistical analysis

In-silico visualisation of the pentamer interfaces and image generation was performed using PyMOL (Schrodinger, 2010). GraphPad Prism 8 was used to plot data and to perform statistical analysis in conjunction with RStudio. To assess the effects of the individual mutations on residue-residue interactions, the Protein Interactions Calculator (PIC) (Tina et al., 2007) was used (Chapter three, 3.2.3). TMEV PDB files containing the individual mutations for PIC analysis were prepared using the mutagenesis wizard embedded in PyMOL. To assess the effect of the individual mutations on the binding free energy of the protomer/pentamer complex by *in-silico* analysis, the BeAtMuSiC webserver (<http://babylone.ulb.ac.be/beatmusic/>) (Dehouck et al., 2013) was used. BeAtMuSiC predicts the changes in binding free energy of a protein complex induced by specific point mutations, using a coarse-grained approach. An increase in the binding free energy (kcal/mol) indicates that a specific mutation stabilised the complex. The hotspot status of only the substitutions located within interfaces between proteins, protomers or pentamers were assessed as previously described (3.2.2.1), using the ROBETTA webserver (<http://www.rosetta.org/alascansubmit.jsp>) (Kortemme et al., 2004). To analyse the hotspot status using alanine scanning in ROBETTA, protomer/pentamer complexes containing the individual interfacial mutations were prepared using the embedded mutagenesis wizard in PyMOL.

5.3. Results

5.3.1. Thermostability of the TMEV GDVII capsid

The thermal tolerance of WT TMEV GDVII was assessed by heating the virus to a range of temperatures for 30 min. The remaining virus was titrated by plaque assay and is shown in *Figure 5.3*. Virus was incubated at 37 °C as a control. Heating to 45 °C significantly decreased

the virus yield by 3 logs (99.9 %), however, complete inactivation was only observed following exposure to 55 °C. A temperature of 52.5 °C reduced the virus titre by 6 logs or 99.9999 %, and was the temperature chosen for initial rounds of heat-selection. This was followed by 7 further cycles of heat-exposure at 55 °C. The TMEV virus pool selected at 55 °C was then subjected to further rounds of heat-selection at 57 °C and 58 °C in simultaneous experiments.

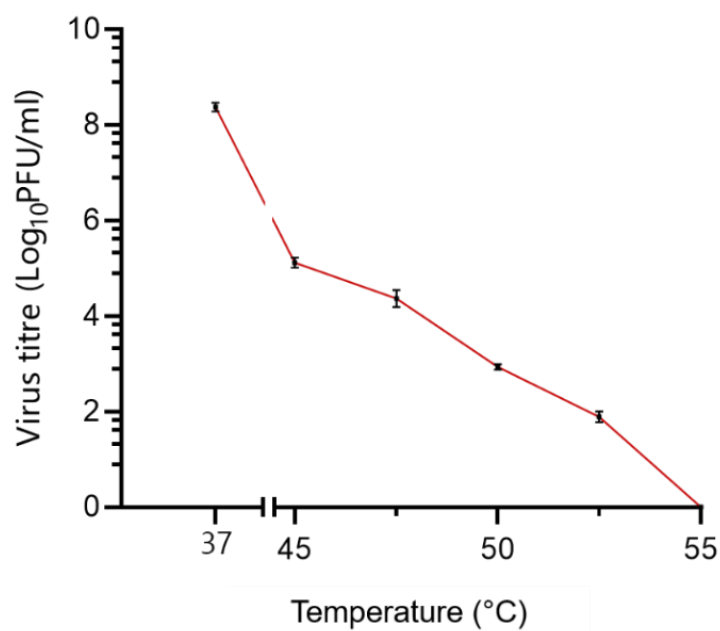


Figure 5.3 Thermal tolerance of TMEV GDVII. WT GDVII virus stocks were heated to a range of temperatures for 30 min and cooled to 4 °C. The surviving virions were titrated by plaque assay on BHK-21 cells. (n=3. Error bars indicate SD).

5.3.2. Thermal tolerance of heat-selected virions

The ability of the heat-selected isolates to withstand a range of temperatures was assessed using a thermal inactivation assay. Following exposure of the mutant viruses to various temperatures, the remaining infectious virions were titrated by plaque assay (*Figure 5.4*). No virus could be recovered following the heating of the passaged WT TMEV to 55 °C, 57 °C and 58 °C. The heat-selected viruses were more tolerant and could be recovered following exposure to higher

temperatures. There was no significant difference between the titres of TMEV selected at 55 °C (TMEV R55 °C) and the WT passaged virus following exposure to the control temperature of 37 °C ($P = 0.1848$). Unlike the WT virus, TMEV R55 °C was not inactivated following exposure to 55 °C. However, a 1.6 log reduction in the titre of TMEV R55 °C was observed, yielding approximately 3.7×10^6 PFU/ml. Following exposure to 57 °C, TMEV R55 °C decreased substantially by ~4 logs, but the virus was only inactivated after heating to 58 °C. Following exposure to 37 °C, the titres of TMEV R57 °C and TMEV R58 °C were significantly reduced from WT and TMEV R55 °C ($P < 0.005$), but not each other ($P = 0.0088$). A temperature of 55 °C did not significantly reduce the yield of these two viruses, and the titres of the three heat-selected viruses were similar following incubation at this temperature ($P > 0.005$). Following exposure to 57 °C, the titre of TMEV R57 °C decreased by 0.3 logs (59 %), while the titre of TMEV R58 °C only decreased by 0.1 logs (21 %). There was no significant difference between the TMEV R57 and R58 °C virus titres following exposure to 57 °C ($P = 0.5390$). Incubation at 58 °C substantially reduced the yield of TMEV R57 °C, and the virus was completely inactivated after heating to 60 °C. Following exposure to the same temperature, the titre of TMEV R58 °C decreased by 0.9 logs (89 %) but was significantly higher than the titres for the other viruses ($P < 0.005$). Heating to 60 °C completely inactivated TMEV R58 °C.

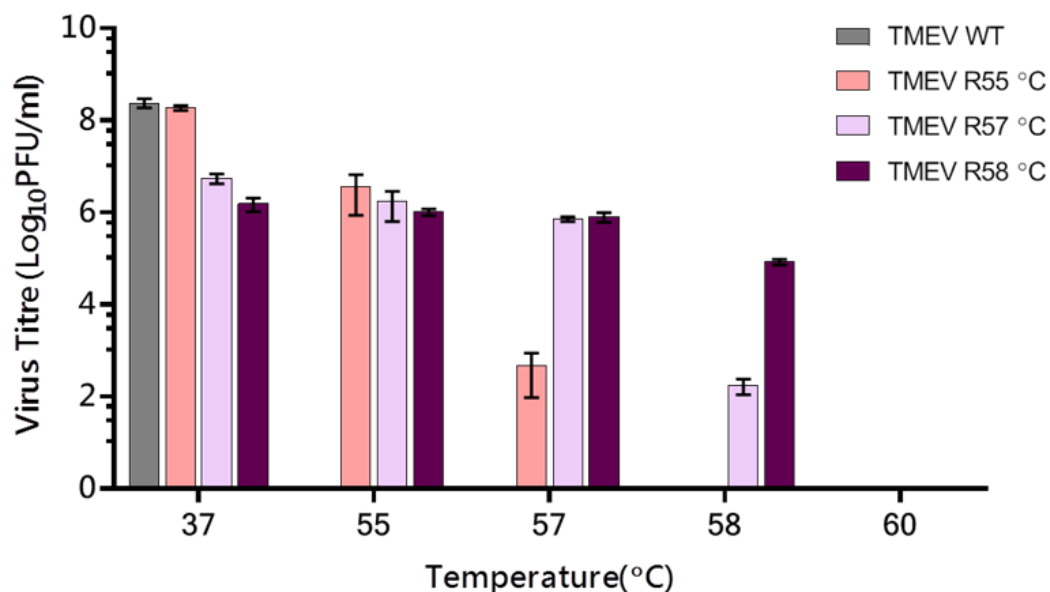


Figure 5.4 Thermal-tolerance assay of heat-selected TMEV isolates. TMEV GDVII isolates selected at 55 °C (TMEV R55 °C), 57 °C (TMEV R57 °C), and 58 °C (TMEV R58 °C) were incubated at 37, 55, 57 and 58 °C for 30 min and immediately cooled to 4 °C. The remaining virus was titrated by plaque assay on monolayers of BHK-21 cells. (n=3. Error bars indicate SD).

5.3.3. Identification of underlying mutations following thermal selection

To identify potential mutations that evolved during heat-selection, the entire P1 capsid encoding regions of plaque-purified TMEV isolates were sequenced. In total, 7 amino acid substitutions were identified and are presented in *Table 5.2*. Four separate plaque-purified virions derived from each temperature pool were sequenced. Three of the four 55 °C selected isolates shared the same amino acid substitutions (R55 °C 1), while the fourth contained the same mutations but also an additional substitution (R55 °C 2). The four plaque-purified R57 °C isolates shared the same amino acid substitutions. This was also observed for the isolates plaque-purified from the R58 °C virus pool. Collectively, two amino acid substitutions were found in VP1, one in VP2, three in VP3 and one in VP4. WT TMEV that had been passaged without heat exposure was also sequenced, and no mutations resulting in amino acid changes were present.

Table 5.2 Amino acid substitutions within the capsid coding regions of TME virions with increased thermal tolerance

Virus	Amino acid substitution(s)
55 °C	1 A201V; E262K; D216N
	2 V141I; A201V; E262K; D216N
57 °C	1 A201V; E262K; A96T; D216N; M66T
58 °C	1 A201V; V114I; D216N

Table 5.2. Mutations are coloured according to the protein in which they are located. VP1 (Blue), VP2 (Cyan), VP3 (Salmon), VP4 (Green).

The individual mutations were mapped onto the structural model of the TMEV pentamer (prepared in chapter three) using PyMOL (Figure 5.5), which revealed that five of the residues were surface exposed, while the remaining mutant residues were buried beneath the surface. Two substitutions A201V and D216N in VP1 and 3 respectively, were present in all of the mutant P1 regions sequenced. Mapping of the mutant residues to the TMEV crystal structure revealed that both residues were present within the interprotomer interfaces.

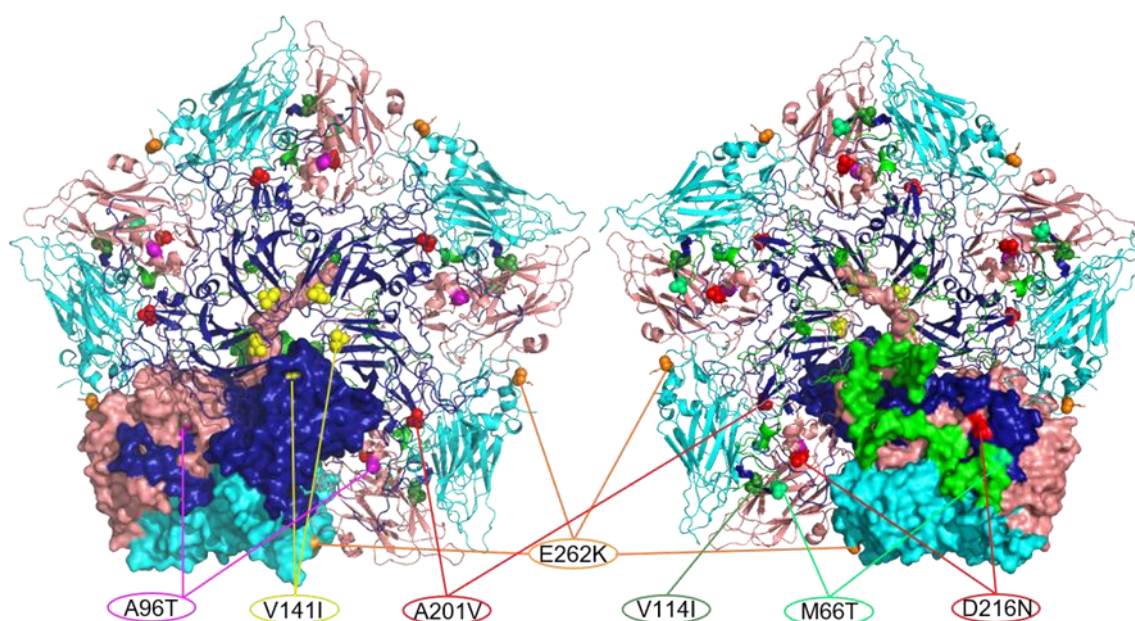


Figure 5.5 Positions of the individual mutations in the TMEV pentamer. Red coloured mutations are those found in all mutants sequenced. The front view of the pentamer is shown on the left, the

reverse view of the pentamer is shown on the right. Capsid proteins are coloured: navy blue-VP1; cyan-VP2; salmon-VP3 and green-VP4.

Amino acid substitution A201V within VP1

Residue A201 is buried within the intraprotomer interface between VP1 and VP2 (*Figure 5.6 A*) and interacts with VP2 M178 through hydrophobic interactions. Furthermore, A201 is predicted to form intraprotein hydrophobic interactions with the adjacent residues A200 and W202 (*Figure 5.6 A*). Predictive modelling of the A201V substitution, and subsequent analysis of the mutant protomer revealed that the hydrophobic interactions established between A201 and partner residues are not altered upon substitution to valine (*Figure 5.6 B*). It was previously found that A201 was a non-hotspot residue and was therefore not energetically important for capsid stability (Chapter three, *Figure 3.3*). *In-silico* analysis following substitution to valine indicated that the residue substitution increased the binding free energy and likely increased the stability of the protomer. Moreover, *in-silico* alanine scanning of the protomer following introduction of the valine mutation revealed that the residue was now considered a hotspot that was important for the stability of the protomer.

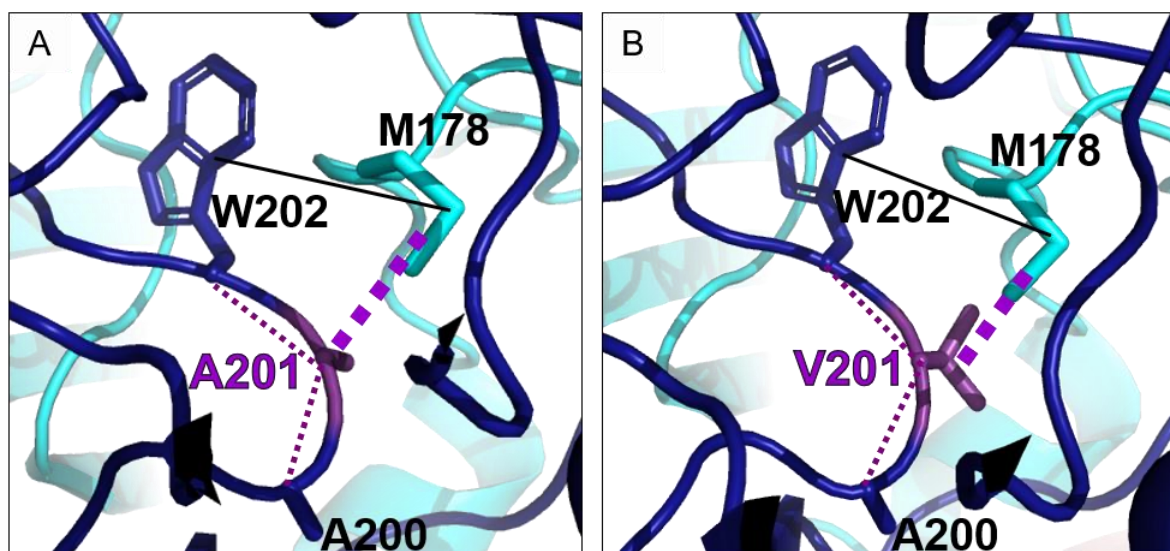


Figure 5.6 Location of the mutation A201V within the VP1 protein at the VP1-VP2 intraprotomer interface and interactions between this residue and neighbouring residues within the protein and protomer. A) Wild type TMEV cartoon of the protomer showing interactions between A201 and partner residues. B) Mutant TMEV cartoon of the protomer showing interactions between V201 and partner residues. VP1 is shown in navy blue, VP2 is coloured cyan. Solid black lines indicate hydrogen bonds, thin dashed purple lines indicate hydrophobic interactions between residues of the same protein and thick dashed purple lines indicate hydrophobic interactions between residues belonging to different proteins within the protomer.

Amino acid substitution D216N within VP3

Amino acid substitution D216N (VP3) is located at the VP3-VP1 intraprotomer interface. Unlike A201, this residue is not buried, and is instead exposed to the interior surface of the capsid (*Figure 5.7 A and B*). Interaction analysis revealed that D216 forms intraprotomer mainchain-mainchain and mainchain-sidechain hydrogen bonds with residues D13 and N12 (both VP1) respectively. Furthermore, the analysis revealed that the negatively charged D216 forms ionic interactions with the positively charged K25 VP1 residue (*Figure 5.7 C*). Following substitution of the negatively charged aspartate residue to the neutral asparagine, the ionic interactions are abolished but the hydrogen bonds between the D13 and N12 VP1 residues are maintained (*Figure 5.7 D*). Furthermore, an additional sidechain-sidechain hydrogen bond is

formed between the two asparagine residues (N216 and N12). D216 was not previously predicted to be a hotspot residue and was also not predicted to interact with any hotspot residue (Chapter three, *Figure 3.3*). *In-silico* analysis following substitution of D216 to asparagine revealed no change in the binding free energy of the complex, suggesting that the mutation did not increase the stability of the protein-protein interface within the protomer. Computational alanine scanning mutagenesis confirmed that the mutant residue remained a non-hotspot.

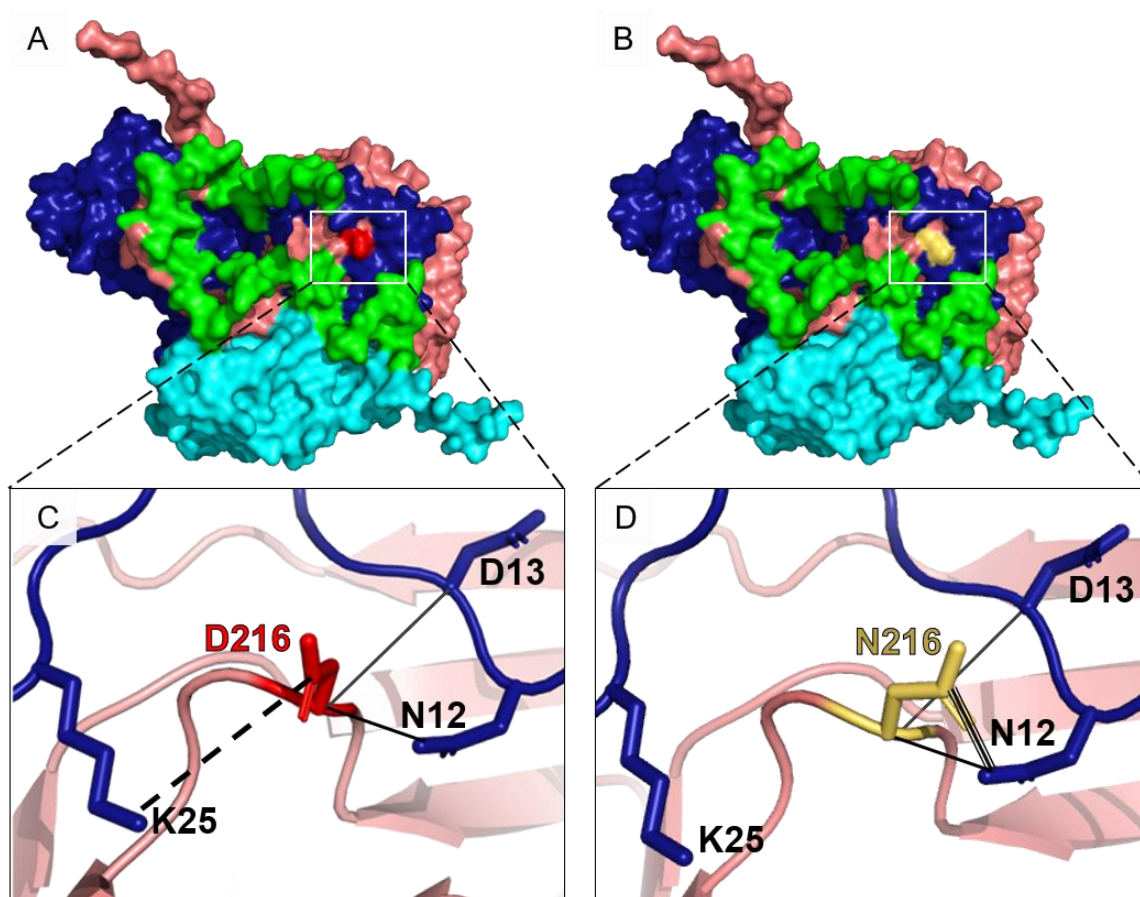


Figure 5.7 Location of the mutation D216N within the VP3 protein at the VP3-VP1 intraprotomer interface and interactions between this residue and neighbouring VP1 residues within the protomer. A) Internal surface view of the wild type TMEV protomer showing surface exposed D216. B) Internal surface view of the mutant TMEV protomer showing surface exposed N216. C) Cartoon of the VP3-VP1 interface showing the wild type residue D216 and the interactions formed between this VP3 residue and partner VP1 residues. D) Cartoon of the VP3-VP1 interface showing the mutant residue N216 and the interactions formed between the mutant VP3 residue and neighbouring VP1 partner residues. Capsid proteins are coloured: navy blue-VP1; cyan-VP2; salmon-VP3 and green-VP4. Red coloured residues are negatively charged, yellow coloured residues have neutral charge. Solid black

lines indicate mainchain-mainchain and mainchain-sidechain hydrogen bonds. Thick dashed lines indicate ionic interactions between positive and negatively charged residues. Triple lines indicate hydrogen bonds formed between residue sidechains.

Amino acid substitution E262K within VP2

The amino acid substitution E262K within VP2 was observed in TMEV R55 °C and R57 °C mutants but not those isolated from the R58 °C pool. E262 is located at the interpentamer interface between two VP2 proteins and forms part of an alpha-helix. Analysis of electrostatic interactions using PyMOL revealed that substitution of the negatively charged glutamate to the positively charged lysine increased the overall positive charge of the two-fold interface (*Figure 5.8 A and B*). The two alpha-helices at the two-fold axis run in opposite directions and are adjacent to each other. This allows E262 to form ionic interactions with two R101 residues, one across the two-fold axis belonging to the opposing VP2 protein, and the other within the same VP2 protein (*Figure 5.8 C*). Furthermore, mainchain-mainchain hydrogen bonds are also formed between the E262 and R101 residues within the same protein. Interaction analysis following substitution to lysine revealed that the ionic interactions between R101 residues are abolished, instead residue K262 forms ionic interactions with E91 across the interface (*Figure 5.8 D*). E262 was not previously recognised as a hotspot residue (Chapter three, *Figure 3.5*), and *in-silico* analysis following substitution to lysine revealed no change in the binding free energy of the complex, suggesting that the mutation did not directly alter the stability of the pentamer interface. Furthermore, *in-silico* alanine scanning mutagenesis of the K262 mutant protomer suggested that the neighbouring hotspot, R102 (Chapter three, *Figure 3.5*), became a non-hotspot, while residue H103 became a hotspot.

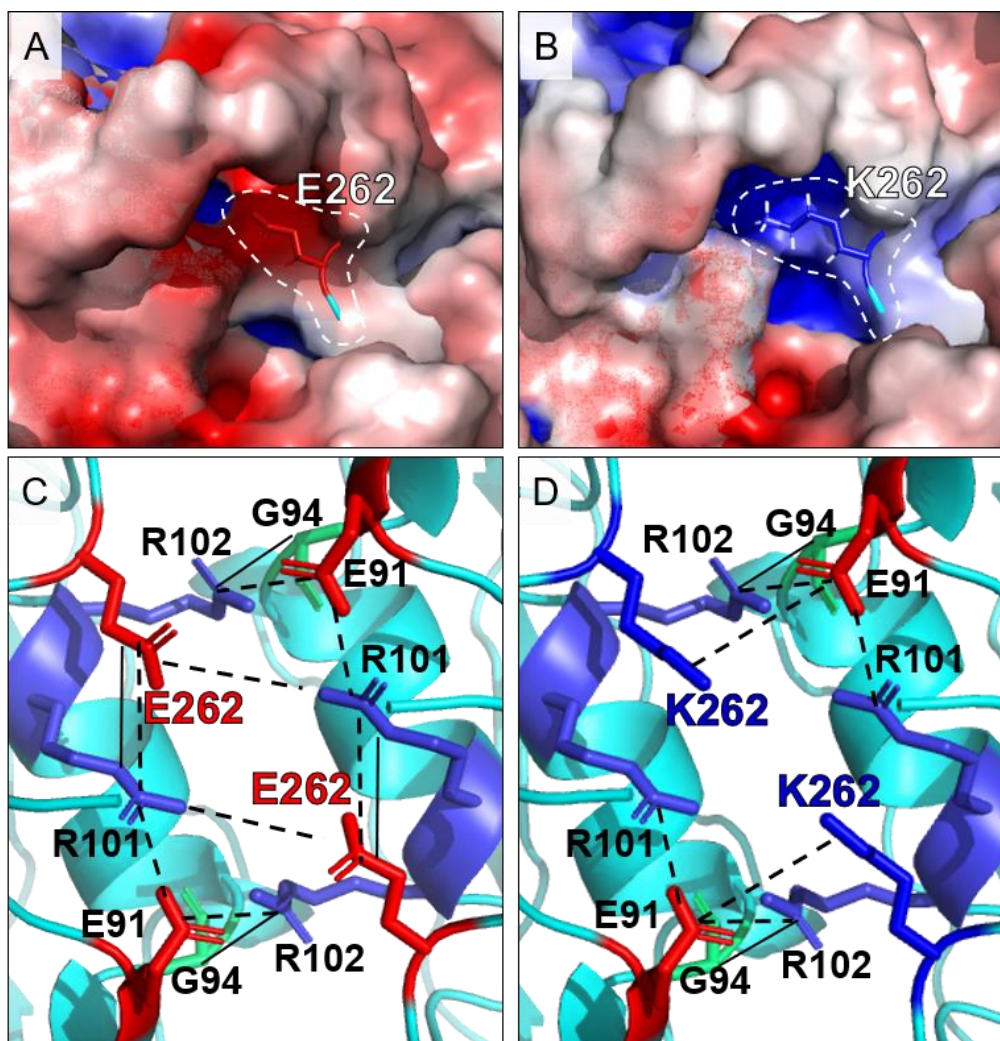


Figure 5.8 Location of the mutation E262K within the VP2 protein at the VP2-VP2 interpentamer two-fold interface and interactions formed between this mutant residue and neighbouring residues within the protein and across the interface. A) Electrostatic potential of wild type virus showing charge distribution at the two-fold axis. B) Electrostatic potential of mutant virus showing charge distribution at the two-fold axis following in-silico mutation of E262 to lysine. Electrostatic potential was calculated using the APBS plugin embedded within Pymol. The colouring represents positive charge (blue), negative charge (red) and neutral (white). C) Cartoon view of the two-fold interface showing the wild type E262 residue (VP2) and the interactions formed between this residue and partner residues of the same VP2 protein and the VP2 protein belonging to the opposing pentamer. D) Cartoon view of the two-fold interface showing the mutant K262 residue (VP2) and the interactions formed between this residue and partner residues of the same VP2 protein and the VP2 protein belonging to the opposing pentamer. Solid black lines indicate mainchain-sidechain hydrogen bonds and black dashed lines indicate ionic interactions formed between residues of opposing charges. VP2 is coloured cyan. Red residues indicate those with negative charge, blue residues indicate those with positive charge. Other residues of interest with no charge are coloured green.

Amino acid substitution V141I within VP1

Amino acid substitution V141I in the VP1 protein was only observed in one of the heat-selected mutants isolated following repeated exposure to 55 °C. This residue is located near to the five-fold axis when the pentamer is assembled but is not located at an interface. V141 was predicted to form intraprotein contacts within VP1 alone. The analysis revealed that mainchain-mainchain hydrogen bonds are formed between V141 and two glycine residues at positions 139 and 179, and that hydrophobic interactions are formed between V141 and residues A135 and I177 (*Figure 5.9 A*). Predictive modelling of the I141 mutant combined with interaction analysis suggested that substitution to isoleucine did not alter any of the interactions (*Figure 5.9 B*). Furthermore, *in-silico* analysis suggested that the substitution did not alter the binding free energy of the protomer complex and thus did not likely improve the stability of the protomer subunit.

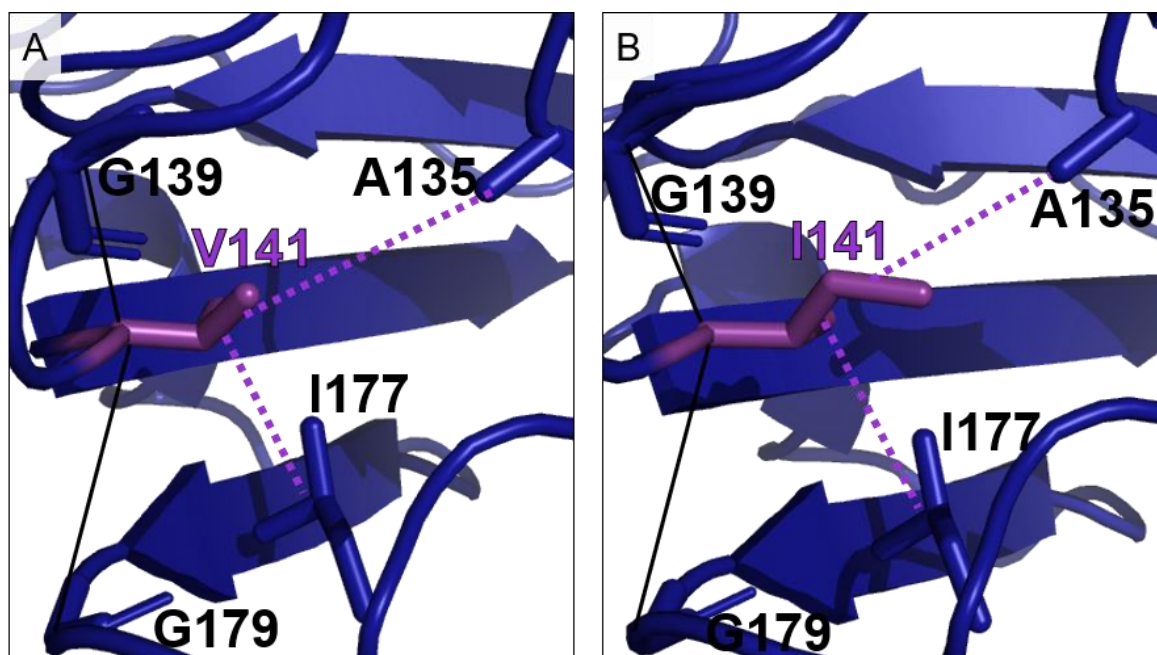


Figure 5.9 Location of the mutation V141I within the VP1 protein near the five-fold axis and interactions formed between this residue and neighbouring residues within the same protein. A) Cartoon view of the wild type VP1 protein showing the V141 residue near the five-fold axis. B) Cartoon view of the mutant V141I VP1 protein showing the I141 residue near the five-fold axis. The VP1 protein

is coloured blue. Hydrophobic residues are coloured purple. Solid black lines indicate mainchain-mainchain hydrogen bonds between neighbouring residues within the same protein. Purple dashed lines denote hydrophobic interactions formed between residues within the same protein.

Amino acid substitution A96T within VP3

The amino acid substitution A96T in VP3 was unique to one of TMEV R57 °C mutants. A96 is located within an alpha-helix of the VP3 protein at the bottom of the putative receptor binding pit (*Figure 5.10*). Interaction analysis revealed that A96 forms a single mainchain-mainchain hydrogen bond with S93 in the same VP3 protein (*Figure 5.10 A*). Predictive modelling and interaction analysis of the threonine substitution suggested that additional hydrogen bonds were formed with the adjacent VP3 residues T90 and S93 (*Figure 5.10 B*). *In-silico* analysis suggested that substitution to threonine did not alter the binding free energy of the protomer complex. A96 is located next to the residues V98 and R100 that were previously predicted as hotspots (Chapter three, *Figure 3.3*). Although A96 is not an interfacial residue, *in-silico* alanine scanning was performed on the TMEV protomer to assess the status of the neighbouring hotspot residues, and indicated that no change had occurred. Finally, because threonine introduced a sidechain beyond the β -carbon, the surface depth of protomers pre and post substitution were analysed in Pymol. This suggested that the sidechain of threonine protruded further to the surface, creating a slightly shallower pocket within the pit than the WT alanine residue (*Figure 5.10 C-F*).

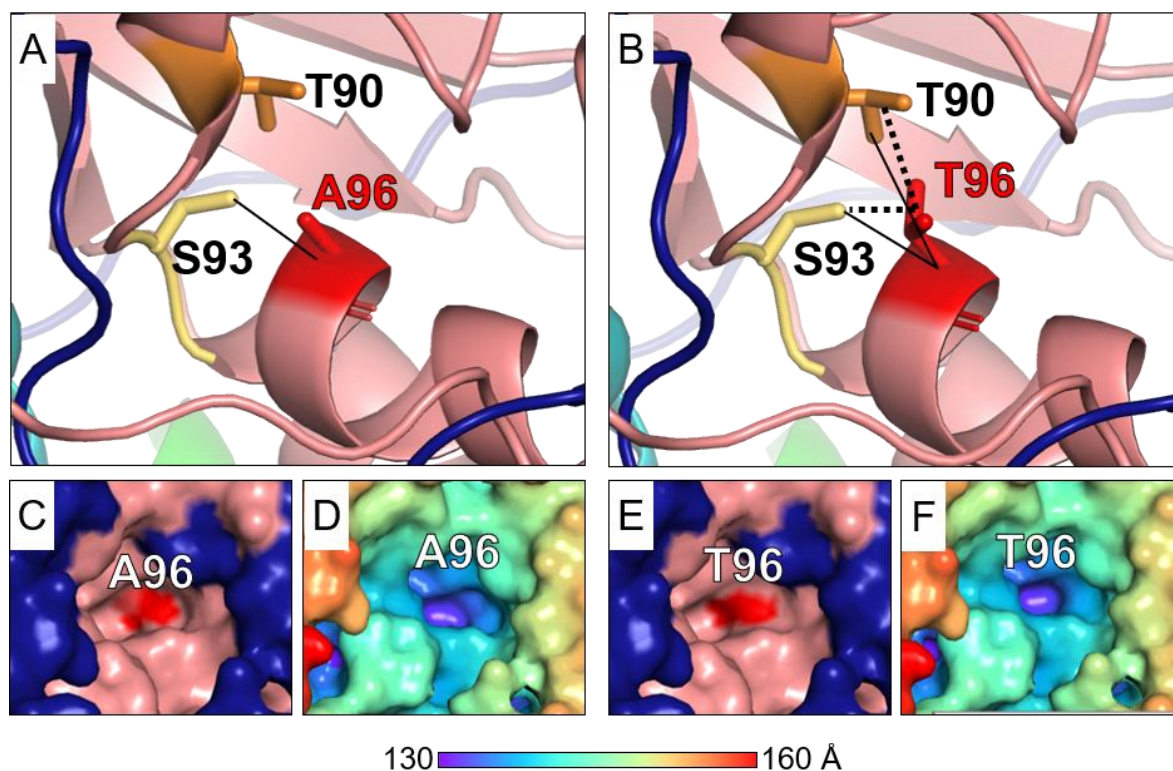


Figure 5.10 The location of the A96T mutation within the VP3 protein at the base of the putative TMEV receptor binding site. A) Cartoon diagram of the wild type VP3 alpha-helix at the base of the putative receptor binding site showing wild type residue A96 and the interactions formed between this residue and partners within the same protein. B) Cartoon diagram of the mutant VP3 alpha-helix at the base of the putative receptor binding site showing the mutant T96 residue and the interactions formed between this residue and neighbouring residues within the same protein. Solid black lines indicate mainchain-sidechain hydrogen bonds, while black dashed lines indicate sidechain-sidechain hydrogen bonds. C) surface view of the pocket within the receptor binding pit showing the A96 wild type residue (shown in red). D) Surface depth cue of the surface of the wild type receptor binding pit. E) Surface view of the pocket within the receptor binding pit showing the mutant T96 residue (shown in red). F) Surface depth cue of the surface of the mutant T96 receptor binding pit. In cartoon and surface view diagrams VP1, VP2, VP3 and VP4 are coloured blue, cyan, salmon and green respectively. A96T residues are coloured red. Other VP2 residues of interest are highlighted in orange or yellow.

Amino acid substitution M66T within VP4

Following thermal selection, M66T was the only amino acid substitution observed within the VP4 protein and was unique to TMEV R57 °C. M66 is located at the surface of the protomer and is oriented internally within the capsid (*Figure 5.11 A and B*). Although the residue is located close to the two-fold axis, it is not predicted to interact with residues belonging to the adjacent pentamer. M66 forms mainchain-mainchain hydrogen bonds with residue A64 within the same VP4 protein and hydrophobic interactions with residue V17 belonging to VP1 within the same protomer (*Figure 5.11 C*). Analysis of the interactions formed upon substitution from the hydrophobic methionine to the neutral threonine revealed that while the mainchain-mainchain hydrogen bonds were unaltered, the hydrophobic interactions between this residue and V17 were abolished (*Figure 5.11 D*). No change in the binding free energy of the protomer complex was predicted upon substitution of M66 to threonine, suggesting that the mutation did not increase the stability of the protein-protein interface within the protomer. Computational alanine scanning mutagenesis confirmed that the substituted residue remained a non-hotspot.

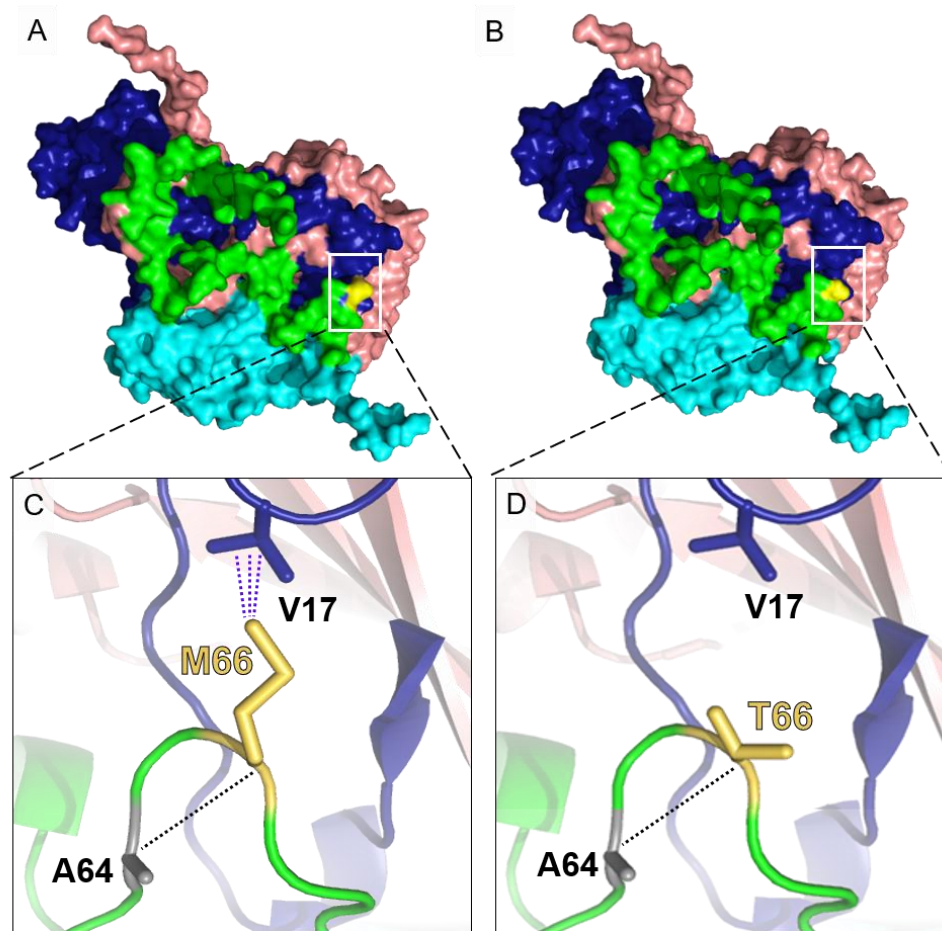


Figure 5.11 The location of the mutation M66T within the VP4 protein at the VP4-VP1 intraprotomer interface of the TMEV protomer. A) Internal surface view of the TMEV protomer showing the M66 wild type residue. B) Internal surface view of the mutant TMEV protomer showing the T66 mutation. C) Cartoon view of the VP4-VP1 interface at the internal surface of the TMEV wild type protomer. The wild type M66 residue is highlighted in yellow and interactions between residues in the same protein and those in the adjacent VP1 protein are indicated. D) Cartoon view of the VP4-VP1 interface at the internal surface of the TMEV mutant protomer. The mutant T66 residue is highlighted in yellow and interactions formed between partner residues are indicated. VP1-VP4 are coloured as blue, cyan, salmon and green/grey respectively. Mainchain-mainchain hydrogen bonds between residues of the same protein are indicated by black dotted lines. Hydrophobic interactions are indicated by three dashed purple lines.

Amino acid substitution V114I within VP3

The substitution V114I in VP3 was the only unique mutation in the R58 °C mutant pool. V114 is buried within the intraprotomer interface between VP3 and VP1. Analysis of residue interactions revealed that V114 forms mainchain-mainchain hydrogen bonds with residue T116 and hydrophobic interactions with residue L112 (both in the same VP3 protein) (*Figure 5.12 A*). Furthermore, V114 forms hydrophobic interactions with A5 from the VP1 protein within the same protomer. Analysis of interactions upon substitution of V114 to isoleucine suggested that none of the interactions are altered, but that an additional hydrophobic interaction is formed with the neighbouring VP2 I193 residue across the VP3-VP2 interface (*Figure 5.12 B*). Assessment of the binding free energy post substitution suggested that the amino acid replacement did not alter the binding free energy of the protomer. Previously, V114 was predicted as a hotspot residue (Chapter three, *Figure 3.3*), computational alanine scanning of the I114 mutant protomer revealed that the residue remained a hotspot post substitution. Additionally, *in-silico* alanine scanning suggested that in the WT protomer residue I193 is not a hotspot, but upon mutation of V114 to isoleucine and the establishment of hydrophobic interactions with I193, it becomes an energetically important hotspot to the VP3-VP2 interface.

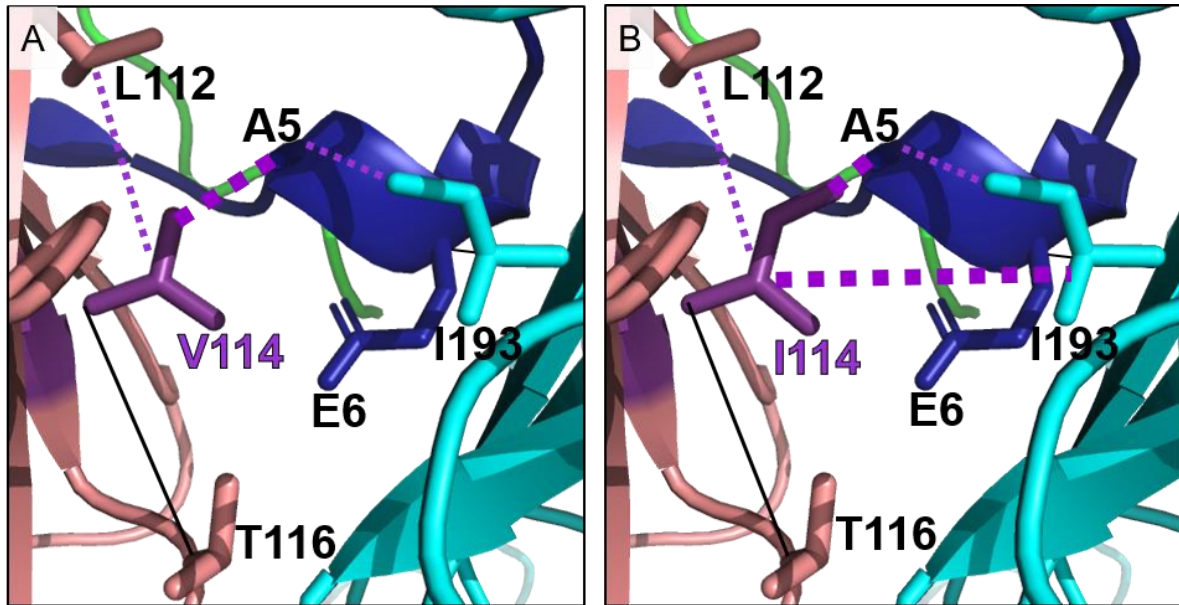


Figure 5.12 The location of the V114I mutation within the VP3 protein at VP3-VP1 intraprotomer interface. A) Cartoon diagram of the wild type intraprotomer interface showing the V114 wild type residue and interactions formed between this residue and partners belonging to the same VP3 protein and the neighbouring VP1 protein in the same protomer. B) Cartoon diagram of the mutant intraprotomer interface showing the I114 mutant residue and the interactions formed between this residue and adjacent residues within the same protein, as well as partner residues in the neighbouring VP1 and VP2 proteins within the same protomer. V114I residues are highlighted in purple. VP1, VP2, VP3 and VP4 are coloured blue, cyan, salmon and green respectively. Black solid lines denote mainchain-mainchain hydrogen bonds, purple dashed lines indicate hydrophobic interactions.

5.4. Discussion

The aim of this chapter was to improve the thermal tolerance of TMEV GDVII through natural selection and continued exposure of the virus to non-physiological temperatures. To examine the inherent thermal tolerance of WT GDVII, the virus was heated to a range of temperatures between 45 and 60 °C. Following exposure to 45 °C the virus titre decreased dramatically by ~3 logs or 99.9 %. Thereafter, the virus titre decreased approximately 10-fold with every 2.5 °C increase in temperature, until the virus was completely inactivated at 55 °C. Few studies have directly examined the thermal sensitivities of cardioviruses (Speir, 1962). Two studies assessed the long term stabilities of different TMEV strains at or slightly above physiological

temperatures (33-39.8 °C) (Calenoff et al., 1990; Pritchard et al., 1992), and found GDVII to be less temperature sensitive than the BeAn strain. A third study reported that GDVII also was more stable than the DA strain following exposure of the virus to 42 °C for 5 min (McCright et al., 1999). Previous studies have not, however, reported the thermal sensitivity of TMEV GDVII over a range of non-physiological temperatures. In this study, the temperature that initially reduced the yield of TMEV by 99.9 % (45 °C) was much lower than the temperatures of 51 °C and 50 °C observed to reduce titres of PV-1 (Adeyemi et al., 2017) and EV-71 (Kelly, 2015) by 99.9 % in similar studies. Despite this difference, TMEV was inactivated at 55 °C while PV-1 and EV-71 were reported to be completely inactivated at lower temperatures of 52 °C and 53 °C respectively (Adeyemi et al., 2017; Kelly, 2015). It must be noted that the temperature at which complete inactivation of TMEV occurred may be within the range of 52.5 and 55 °C, as temperatures between these points were not evaluated in this study.

To generate thermostable particles in previous studies, Adeyemi et al. (2017) and Kelly (2015) heated PV-1 and EV-71 to temperatures that reduced the virus by 99.9 % for initial cycles of heat selection. In this study, it was decided to use 52.5 °C which reduced TMEV titres by 99.9999 % but did not completely inactivate the virus. Following seven additional cycles at 55 °C and ten more cycles at 57 °C and 58 °C in separate experiments, three virus pools were derived (TMEV R55 °C, TMEV R57 °C and TMEV R58 °C). As anticipated these viruses could tolerate the temperatures to which they had been repeatedly exposed. Virus titres between the WT virus and TMEV R55 °C mutants were similar following heat exposure to the control temperature of 37 °C. However, the virus titres of TMEV R57 and R58 °C after exposure to 37 °C were substantially lower. This finding suggests that adaption of the virus to higher temperatures may have attenuated virus growth or another aspect of the virus lifecycle leading to lower yields and is consistent with previous studies that have also observed improved thermal tolerance at the expense of other aspects of the virus lifecycle. For example, McCright

et al. (1999) demonstrated that introduction of the amino acid substitution T81D into the DA VP1 protein yielded a mutant with increased thermostability at 42 °C, but with a slower replication cycle. Similarly, Hertzler et al. (2000) generated a panel of BeAn mutants containing mutations in the putative receptor binding pit, and found that some of the mutants exhibited increased thermostability at 40 °C, but had reduced receptor binding and delayed replication kinetics. More recently, FMDV mutants with attenuated virus growth or reduced plaque size were observed among a panel of engineered virions with increased thermal tolerance. The authors speculated that this trade-off was due to delayed uncoating and replication (Scott et al., 2017). It is possible that some of the mutations within P1 that imparted improved thermal tolerance to the capsid may have had deleterious effects on the virus lifecycle. However, potential mutations within the P2 or P3 regions of these viruses that were not sequenced may have also contributed to reduced virus titres.

To elucidate the genetic basis for improved thermal tolerance, the entire P1 capsid encoding regions of plaque-purified virions were sequenced. The amino acid substitutions A201V in VP1 and D216N in VP3 were observed in all mutants sequenced, indicating that these mutations evolved during the early cycles of heat selection and were maintained in subsequent virus populations with increased thermal resistance. Their presence in all succeeding mutants strongly suggests that these substitutions were important for improving the tolerance of TMEV particles to higher temperatures. A201 is located at the base of the VP1 FMDV loop and forms interactions with residues within the same loop, as well as with residues of VP2 puff B. These residues include W202 (VP1) and M178 (VP2) which were previously identified as hotspots (Chapter three, *Figure 3.3*), and have been implicated in maintaining the conformation of these loops under a broad range of pH conditions (Luo et al., 1992). Studies have shown that disruption of these interactions leads to reduced loop stability and viral persistence (Zurbriggen et al., 1989), but whether these loops also play an important role in maintaining the thermal

stability of the TMEV capsid has not been investigated. Substitution of A201 to valine was not predicted to alter any of these important interactions but was predicted to increase the binding free energy of the intraprotomer interface, likely improving the overall stability of the VP1 and VP2 loops but also the protomer. It is tempting to speculate that the conformation of these loops could also be important for thermal stability of the capsid, and that substitution to valine could increase the binding free energy substantially to improve the conformational rigidity of the loops and reduce protomer dissociation at increased temperatures. However, this would require further investigation.

The amino acid substitution D216N (VP3) is located within the VP3-VP1 intraprotomer interface. Residue D216 in the WT virus is predicted to form ionic interactions with the positively charged K25 residue belonging to VP1 as well as hydrogen bonds with VP1 residues N12 and D13. Substitution of the negatively charged aspartate residue to the neutral asparagine (D216N) abolished ionic interactions between this residue and K25 as expected, although an additional hydrogen bond was predicted between the N216 mutant residue and N12 sidechains. Following the *in-silico* substitution of the residue to asparagine, no significant increase in the binding free energy was predicted, suggesting that the mutation did not stabilise the protein-protein interface within the protomer. D216N and K25 are exposed to the inside of the capsid. The interaction of positive residues inside the capsid with the RNA genome can substantially neutralise RNA charge and promote encapsidation of RNA during the assembly of ssRNA icosahedral viruses, as well as stability of the resultant virions (Carrillo et al., 2018; Shakeel et al., 2017; Zhu et al., 2015). The identity and nature of capsid protein-RNA interactions remain unknown for most picornaviruses. However, it was previously reported that electrostatic interactions dominate contacts between capsid residues and the RNA-stem loop in Ljungan virus (Zhu et al., 2015). Considering the internal position of D216N and K25 it is plausible that substitution of aspartate to asparagine (D216N) and the subsequent loss of ionic interactions

between the two residues may have allowed K25 to form strong ionic interactions with the negatively charged viral RNA, thereby increasing stability of the capsid through RNA-protein interactions instead of protein-protein interactions.

E262K in VP2 also evolved during the early cycles of thermal selection, as the substitution was present in mutants following exposure to 55 and 57 °C, but not within the mutant populations following exposure to 58 °C. Interestingly, E262K was the only amino acid substitution observed at the pentamer interfaces following thermal selection. Previous studies have revealed that the pentameric interfaces are far less tolerant to mutation than the intraprotomer or interprotomer interfaces (Mateo et al., 2003; Rincón et al., 2015), and may explain why additional mutants with substitutions within these interfaces did not emerge. Substitution of the negatively charged glutamate residue to a positively charged lysine, and the subsequent rearrangement of ionic interactions across the interface increased the positive charge of the two-fold axis. This alteration of charge dynamics may have affected the thermal tolerance of the capsid, as recently Yuan et al., (2016) demonstrated that thermostable mutants can be generated by altering the charge characteristics of the capsid proteins of EV-71. However, it must be noted that the amino acid substitution itself was not predicted to increase the binding free energy of the complex or alter the residue's non-hotspot status, and thus did not likely further stabilise the complex. This finding may explain why the substitution was not maintained in the population of virions selected following exposure to 58 °C.

The amino acid substitution V141I in the VP1 protein was unique to a single population of virions that evolved following passage at 55 °C. This residue is located within the VP1 protein at a loop that protrudes to the five-fold axis. V141 was predicted to form interactions with residues in the same VP1 protein alone and was not located at a protein interface. Following the *in-silico* substitution of this residue to isoleucine, no alterations in interactions were predicted. Furthermore, no change in binding free energy was observed in the protomer

following the substitution, suggesting that the substitution did not alter stability of the protomer or capsid. It is plausible that because the mutation did not provide any advantage, it was not further maintained in TMEV 57 °C and 58 °C virion populations.

Two amino acid substitutions were unique to the P1 regions of 57 °C selected virions. One substitution, A96T, was located at the bottom of the putative receptor binding pit. Although this residue was predicted to only form interactions with neighbouring residues in the same protein, substitution to threonine was predicted to increase the number of hydrogen bonds to the adjacent S93 and T90 residues. This substitution was not predicted to result in a change in the binding free energy of the protomer. Alanine residues lack sidechains past the β -carbon and so the mutation to threonine introduced a sidechain (Betts and Russell, 2003). Surface depth analysis in PyMol revealed that the substitution altered the pit by filling in the pocket and making it slightly shallower. In PV and EV-71 mutants with improved thermostability, mutations were also observed within the receptor binding pocket of these viruses (Adeyemi et al., 2017; Kelly, 2015). In most enteroviruses these pockets are known to bind lipid moieties known as pocket factors which stabilise the virus capsid (Baggen et al., 2018a). The amino acid substitutions identified in the PV and EV-71 thermostable virions were predicted to increase the size of the hydrophobic pocket allowing for improved binding of the pocket factor, which may have assisted the capsids in retaining these stabilising lipids at increased temperatures (Adeyemi et al., 2017; Kelly, 2015). Conversely, the structures of coronaviruses lack deep canyons with hydrophobic pockets and lipid factors. Instead, these viruses possess smaller analogous pits (Grant et al., 1992; Luo et al., 1992, 1987; Mullapudi et al., 2016). Thus, if the A96T substitution was able to contribute to improved thermostability of TMEV in this study, then the mechanism would have been completely different to that observed in the enteroviruses. Considering that the A96T substitution resides in the receptor pit that was predicted to be the site of heparan sulphate binding (Upfold et al., 2018), it is possible that the mutation altered

this binding site or affected the manner in which the co-receptor binds to this pocket. This in turn could have delayed attachment and uncoating. A previous study investigating residues within the receptor binding site of the BeAn strain found that many of the mutations in the pit dramatically reduce binding affinity but increase thermal tolerance of the virions (Hertzler et al., 2000). In this study, it is plausible that substitution of A96 in the GDVII receptor binding pit had a similar effect, and could potentially explain the attenuated virus yields observed for the TMEV R57 °C mutants following exposure to the control temperature of 37 °C.

The second amino acid substitution unique to TMEV R57 °C was M66T in VP4. This was the only substitution in the VP4 protein observed in any of the mutants. Like D216N, this residue forms part of the internal surface of the protomer. Substitution of this residue from a hydrophobic amino acid to a neutral polar residue abolished hydrophobic interactions that were formed between M66 and V17 (VP1). Upon *in-silico* mutation no change in the binding free energy of the complex was predicted, suggesting that this substitution did not further stabilise the protein-protein interface within the protomer. If the substitution M66T affected the tolerance of TMEV to non-physiological temperatures, the mechanism is not clear. However, it could be speculated that the amino acid substitution may have altered the dynamics of the internal surface of the capsid, which could have altered protein-RNA interactions thereby increasing the capsid thermostability.

The only amino acid substitution unique to the 58 °C selected mutants was V114I in the VP3 protein. V114 is buried within the VP3-VP1 intraprotomer interface and was predicted to be involved in hydrogen bonds and hydrophobic interactions within the same protein as well as a single hydrophobic interaction with A5 in the neighbouring VP1 protein. Mutation of valine to isoleucine is a highly favoured substitution in general proteins (Betts and Russell, 2003), and it was predicted that this substitution did not alter any of the interactions involving the WT residue. Interestingly, an additional hydrophobic interaction was predicted to form between the

mutant residue and the VP2 residue I193 across the VP3-VP2 interface. V114 was previously predicted as a hotspot (Chapter three, *Figure 3.3*), but *in-silico* mutation to isoleucine did not result in a change in the binding free energy of the complex, and I114 was still considered to be a hotspot. Notably, I193 was not previously predicted to be a hotspot residue, however, analysis of the mutant V114I protomer suggested that I193 was now considered energetically important and thus a hotspot residue following alanine scanning mutagenesis. Based on this finding, it is likely that the hydrophobic interaction formed between I193 did stabilise the protomer, even if the V114I substitution itself did not directly alter stability of the protomer.

In conclusion, the work presented in this chapter aimed to improve the thermal tolerance of TMEV GDVII by natural selection following repeated exposure of the virus to non-physiological temperatures. This was achieved through the continued passage of viruses at 52.5/55 °C, 57 °C and 58 °C resulting in three pools of virions that could tolerate these temperatures. Identification of the underlying genetic basis for increased thermal tolerance, revealed a pair of amino acid substitutions that were present in all subsequent mutants and several other substitutions that were mostly unique to the different virus pools. Although it is likely that many of these residues contribute to improved thermal tolerance, it would be useful to introduce these amino acid substitutions individually or together into an infectious clone of WT TMEV to confirm their effects on thermostability of the virus. In conclusion this study provides the first analysis of the tolerance of TMEV GDVII to a range of non-physiological temperatures and the genetic basis for improved thermal resistance, adding to the knowledge surrounding picornavirus capsid stability.

Chapter 6

General Discussion and future prospective

6.1. Summary and future prospective

Picornaviruses are a family of significant disease-causing pathogens for which no antivirals and few vaccines are commercially available (Baggen et al., 2018a; Cathcart et al., 2014). These small RNA viruses are non-enveloped and rely on their capsids for critical aspects of their lifecycles including receptor binding, uncoating, and protection of the viral genome from degradation (Ehrenfeld et al., 2010; Stanway, 1990; Tuthill et al., 2010, 2007). The structure of the picornavirus capsid and the individual subunits that constitute it are fundamental to each of these processes. Increased knowledge of the molecular determinants that regulate capsid structure and stability is not only required for an improved understanding of the basic biology of these important viruses, but is applicable to the development of novel antiviral agents (De Colibus et al., 2014) and improved vaccine antigens (Mateo et al., 2008, 2003; Mateu, 2011). The primary focus of this thesis was broadening the understanding of picornavirus capsid structure and stability using TMEV GDVII, a cardiovirus which can be manipulated without biosafety concerns.

The purpose of the first part of the thesis was to generate necessary reagents to study the TMEV GDVII capsid, which could be used in conjunction with the available replication system. To this end, polyclonal antibodies that could recognise TMEV by Western analysis and immunofluorescence were generated by immunising rabbits with purified TMEV particles. A deletion analysis revealed that the antibodies were able to detect VP1 linear epitopes in the C-terminus of the protein, but not those in VP2 or VP3. Furthermore, a plaque reduction assay demonstrated that the antibodies were able to neutralise virus infection, unlike antibodies that had previously been generated against the N-terminus of the VP1 protein (Ross et al., 2016). Not only were these antibodies a valuable tool for subsequent experiments within this thesis, but they provide an important reagent for future investigations into TMEV capsid assembly, stability and uncoating. For example, host cell factors are known to be required for picornavirus

morphogenesis (Jiang et al., 2014), but further studies are necessary to fully understand their specific functions. Previous studies have demonstrated roles for the heat-shock protein Hsp90 in PV P1 processing and capsid maturation (Geller et al., 2007), and in FMDV P1 processing and pentamer formation (Newman et al., 2017). The role of Hsp90 in cardiovirus assembly remains unknown; however, it was previously shown that VP1 colocalises with the chaperone during the early stages of assembly (Ross et al., 2016). The antibodies produced in this thesis provide a valuable tool for biochemical experiments such as co-immunoprecipitation assays and high-resolution confocal analyses to further examine the role of Hsp90 and other host factors in the TMEV lifecycle.

Structural mapping revealed that the VP1 C-terminal residues detected by the anti-capsid antibodies form part of a loop over the putative receptor binding pit, which led to speculation that the antibodies neutralise virus infection by preventing receptor attachment. This precipitated an investigation into the potential binding site of the GDVII co-receptor, heparan sulphate (Lipton et al., 2006; Reddi et al., 2004; Reddi and Lipton, 2002), which was selected because the primary receptor for TMEV remains unidentified (Kilpatrick and Lipton, 1991; Zhou et al., 2000). It was previously suggested that the binding site consisted of a series of residues belonging to VP1 (Reddi and Lipton, 2002), however, these residues were found to be buried following inspection of the GDVII model, challenging this suggestion. Instead it was shown through docking experiments performed in this study that heparan sulphate likely binds to residues within the receptor binding pit and on the C-terminal loop. These predictions have provided the starting point for future studies to investigate the co-receptor binding site of TMEV. Possible experiments could include mutagenesis of these residues and analysis of subsequent effects on the virus lifecycle, such as host cell binding and uncoating. Furthermore, the antibodies provide a tool to further investigate aspects of TMEV antigenicity and neutralisation. Possible experiments to further examine the neutralising mechanism could

involve the selection of neutralisation-resistant escape mutants and identification of mutations that confer resistance to neutralisation.

The next part of the thesis focused on the development of an *in-silico* screen for the prediction of stabilising hotspot residues at the intraprotomer, interprotomer and interpentamer interfaces of a picornavirus capsid. The few studies that have previously attempted to identify these important residues have relied on the systematic mutational analysis of every interfacial amino acid (Mateo et al., 2003; Reguera et al., 2004; Rincón et al., 2015), which can be lengthy and resource-intensive when many residues are analysed. Alternatively, *in-silico* calculations and molecular dynamics simulations have been implemented to predict the most stabilising residues for further analysis (Kotecha et al., 2015; Warwicker, 1989), but they require substantial computing time and prior bioinformatic knowledge. The screen in this study made use of a collection of readily accessible *in-silico* tools to identify hotspot residues, those that contribute significantly to the binding free energy of a protein-protein complex, from other interface residues. This screen can be applied to any virus capsid with relative ease, providing that the structure of the virion has been determined and that the biological assembly of the virus is available on the protein data bank (Berman et al., 2000). Considering the availability of many picornavirus structures from different genera (Hadfield et al., 1997; Kalynych et al., 2016; Lea et al., 1994; Luo et al., 1992; Miller et al., 2001; Muckelbauer et al., 1995; Mullapudi et al., 2016; Venkataraman et al., 2008; Wang et al., 2015; Wang et al., 2012a; Zhu et al., 2015), this screen could be applied broadly across the family as a first step for the identification of residues that contribute significantly to stability of the capsid.

In this thesis the screen was applied to TMEV GDVII, revealing numerous conserved and non-conserved hotspot residues within the respective interfaces of the capsid, and provided a large amount of data which may form the basis of future structural studies. The literature regarding the structure of TMEV is limited; nevertheless, many of the non-conserved hotspots were

identified as residues that were previously reported to be important for various aspects of the virus lifecycle. For example, hotspot residues VP1 W202, W206, F215 and VP2 Y135 were suggested by Luo et al. (1992) to form a stabilising core of protein interactions between the VP1 FMDV and VP2 EF (puff A) loops that are proposed to provide stability to the TMEV capsid under a broad range of pH conditions (Luo et al., 1992; Zurbriggen et al., 1989). Their identification as stabilising hotspots provides further support for this hypothesis. Another example includes hotspot residues P153, F254 (VP1), R100 and I181 (VP3) that have also been linked to host cell attachment (Hertzler et al., 2000), or heparan sulphate binding (Upfold et al., 2018). It was previously speculated that TMEV uncoating is receptor mediated and not induced by low pH (Luo et al., 1992). Considering that receptor binding induces uncoating by destabilising important residue interactions to trigger a cascade of conformational rearrangements that culminate in pore formation or dissociation (Baggen et al., 2018a; Tuthill et al., 2010, 2007), the overlap of receptor binding sites and stabilising hotspots provides support for the hypothesis that receptor binding modulates TMEV uncoating.

Many of the hotspots identified in the TMEV capsid corresponded to residues that were conserved in picornaviruses of economic or clinical significance. Furthermore, in many of these viruses, the corresponding residues were either i) reported to form stabilising interactions at capsid subunit interfaces (Cao et al., 2018; Ross et al., 2017), ii) implicated in conformational rearrangements during uncoating and genome release (Garriga et al., 2012; Mullapudi et al., 2016; Warwicker, 1989), or iii) were shown to be necessary for virus growth and infectivity (Mateo et al., 2003; Rincón et al., 2015; Yuan et al., 2016). Taken together this suggests that the molecular determinants of capsid stability may be somewhat conserved across the picornavirus family. This hypothesis could be tested in future studies by applying the *in-silico* screen to other picornaviruses across different genera to examine the conserved hotspots that

contribute to stability across the family; if found to be correct, then conserved stabilising residues may provide ideal candidates as possible broad-spectrum drug targets.

It is important to stress that the screen is based on *in-silico* predictions and that the functional importance of any hotspot requires confirmation by *in vitro* analysis. Thus, the next part of the thesis examined further a subset of the hotspots predicted at pentamer interfaces of the TMEV capsid. Nine hotspots conserved with residues in clinically or economically significant picornaviruses were selected as they had previously been shown to be important for capsid stability or assembly, or the lifecycles of these viruses. Additionally, the sidechain of each selected residue was involved in the stabilising contact(s) and could be analysed by substitution to alanine using the selected mutagenesis method. For comparison, three interpentamer interface residues that had been predicted as non-hotspots were randomly selected for analysis. Following the introduction of each alanine substitution into the full-length TMEV cDNA clone and transfection of corresponding RNA transcripts, CPE was observed in WT and non-hotspot mutant transfected cells, but was completely absent in hotspot mutant transfected cells, suggesting that the hotspot residues were required for some aspect of the TMEV lifecycle. Further examination by immunofluorescence demonstrated that at 14 hpt a similar percentage of cells were positive for capsid proteins and replicating viral RNA in all transfected cells, indicating that the hotspot mutations did not likely disrupt protein synthesis and RNA replication. Following another 10 h, the percentage of cells positive for TMEV capsid proteins and RNA dramatically increased in the WT and non-hotspot mutant transfected cells but remained the same in cells transfected with hotspot mutant RNA, indicating that no new cells were infected. Although the meaning of these results is not fully understood, it is suspected that substitution of the individual hotspot residues either prevented the assembly of stable capsids, or that less stable capsids could assemble, but not survive cell exit or the extracellular environment. Further experiments to examine whether assembly is disrupted by these

mutations could involve sucrose density fractionation combined with scintillation counting to assess sedimentation values associated with the TMEV capsid and subunits following transfection. Versions of this method have been applied extensively to studies investigating various aspects of picornavirus capsid assembly (Ansardi et al., 1992; Arslan et al., 2016; Compton et al., 1990; Grubman, 1984; Newman et al., 2017; Thibaut et al., 2014; Yafal and Palma, 1979). Additionally, purified fractions could be analysed by TEM to determine whether intact particles are present. To examine whether mutant particles could assemble, exit the host cell and enter the cell supernatant, immunoprecipitation experiments using the anti-capsid antibodies could be performed to concentrate potential particles. Similar methods have been used to purify and concentrate particles during picornavirus morphogenesis studies (Steurbaut and Vrijssen, 2003; Thibaut et al., 2014). Moreover, RNA extraction and RT-PCR of genome regions from precipitated particles would be useful to examine whether potential virions are intact.

The conformation by *in vitro* mutagenesis that interpentamer hotspot residues are required for the TMEV lifecycle and infectivity, but that non-hotspot residues are not, supports the robustness of the screen; however, additional hotspot residues should be examined to determine the broader accuracy of the *in-silico* screen. Nevertheless, of the nine hotspots that were found to be required for the TMEV lifecycle, residues R61, Y62, Y63 and T64 in VP2, and Y148 and I150 in VP3 form a concentrated and interconnected network of interactions in the centre of the VP3-VP2 interpentamer interface. This observation, combined with their conservation and importance in clinically significant picornaviruses, makes these residues worthy of further investigation as potential broad-spectrum antiviral targets. This potential could be assessed using docking simulations to identify potential compounds and small peptides that bind to this network of residues that could potentially affect stability or inhibit assembly. Similar approaches have been used to identify capsid-targeting molecules as drug candidates for other

viruses (Chen et al., 2019; De Colibus et al., 2014; Jain et al., 2017; Lin et al., 2018; Quintero-Gil et al., 2017; Sierra et al., 2018).

The final part of this thesis sought to increase the thermal stability of TMEV GDVII and investigate the genetic basis for improved thermal tolerance. Three virus pools were derived by serial passage following selection at increasing temperatures of 52/55 °C, 57 °C and 58 °C. Thermal-inactivation assays confirmed that the viruses could tolerate these respective temperatures, unlike the WT virus, which was completely inactivated following incubation at 55 °C. An interesting finding was that, following exposure to the control temperature of 37 °C, the viruses selected at 57 and 58 °C had reduced titres compared to the WT virus, suggesting that adaptation to higher temperatures negatively affected virus fitness. Similar studies have observed this trade-off in other viruses (Hertzler et al., 2000; McCright et al., 1999; Scott et al., 2017). In one of these studies the authors speculated that the mutations that resulted in increased thermal tolerance delayed uncoating and replication, thereby affecting virus growth (Scott et al., 2017).

The amino acid substitutions that likely contributed to the improved thermal tolerance of these TMEV mutants were identified by sequencing the entire P1 capsid coding regions of individual plaque-purified virions. Seven substitutions, V141I, A201V in VP1; E262K in VP2; A96T, V114I and D216N in VP3; and M44T in VP4, were identified across the three thermostable virus pools, and most were mapped to the intraprotomer interfaces of the capsid. This finding is noteworthy because previous studies found that amino acids linked to the thermal tolerance of enteroviruses are mainly located between the protomers or in the binding pocket at the surface of these virions (Adeyemi et al., 2017; Filman et al., 1989; Kelly, 2015; Kelly et al., 2015). This difference is likely attributed to the fact that, unlike coronaviruses, enterovirus receptor pockets can bind to stabilising lipid molecules that have been shown to increase thermostability (Katpally and Smith, 2007).

Following the *in-silico* analysis of the potential changes in binding free energy induced by these mutations, only one substitution, A201V, was predicted to stabilise the capsid through protein-protein interactions. This residue forms part of the VP1 FMDV loop and interacts with previously identified hotspots in the VP1 FMDV and VP2 EF loops. These loops are implicated in maintaining the stability of the TMEV capsid under variable pH conditions (Luo et al., 1992). Further research is required to determine whether these loops can modulate thermostability of the capsid. Nucleic acid-protein interactions have also been shown to regulate virus capsid stability (Carrillo et al., 2018; Mateu, 2013; Reguera et al., 2005; Shakeel et al., 2017; Zhu et al., 2015). Two mutations, D216N and M44T, were identified at the internal surface of the capsid. While these residue substitutions were not predicted to increase stability of protein-protein interfaces, they may have directly or indirectly contributed to stronger RNA-protein interactions. For example, substitution of the negatively charged aspartic acid to the neutral polar asparagine was predicted to abolish ionic interactions with the neighbouring lysine residue in VP1 (K25). This in turn may have allowed the positive lysine to interact more freely with the negatively charged RNA. Such interactions were shown to be important for RNA-protein binding in parechovirus B (Zhu et al., 2015). Only one amino acid substitution, E262K, was observed at the pentamer interfaces. This is consistent with the previous suggestion that these interfaces are not tolerant to mutation (Mateo et al., 2003). Although this residue was not predicted to increase stability of the interface upon mutation, substitution to lysine was predicted to alter the ionic bonds across the interface which could have affected thermostability, as was a reported implication of altering charged residues in EV-71 (Yuan et al., 2016). One substitution, A96T, was present in the receptor binding site. A previous study showed that in the BeAn virus, some mutations in the receptor binding site increase virus thermostability, but attenuate host cell binding (Hertzler et al., 2000). In this study, substitution of the A96 residue may have also affected cell binding, which would explain the reduced virus

yield for the 57 °C mutants. It is less clear how the last two residue substitutions V114I and V141I may have affected stability. However, V114I may have indirectly improved stability of the protomer, as following heat exposure and substitution of this residue, hydrophobic interactions were predicted to form between I114 and the adjacent VP2 residue, I193. Furthermore, in the WT virus, I193 was not identified as a hotspot residue, but in V114I mutant virus, the *in-silico* screen predicted this residue as a stabilising hotspot in the VP2-VP3 intraprotomer interface.

To further elucidate which of the identified substitutions are responsible for increased thermal tolerance and/or attenuated virus growth, and to further examine any of the possible stabilising mechanisms discussed above, each substitution should be individually introduced into the GDVII infectious clone. The site-directed mutagenesis protocol developed to assess the individual hotspot residues in chapter four provides an excellent approach to do so. To assess the individual effects of the substitutions on thermal tolerance, each engineered mutant could be re-subjected to the thermal inactivation assays used in this study, which would also provide information on infectivity and virus fitness. The Particle Stability Thermal Release Assay (PaSTRy) (Walter et al., 2012) could be used to directly assess the effect of the substitutions on capsid stability under increasing thermal stress. This method has been applied extensively to examine the thermostabilities of WT and engineered picornavirus particles (Adeyemi et al., 2017; Nguyen et al., 2019; Scott et al., 2019, 2017; Zhu and Zhang, 2015) and vaccine antigens (Kotecha et al., 2018, 2016, 2015). Furthermore this method can be applied to investigate picornavirus uncoating (Liu et al., 2018; Walter et al., 2012) and could be used to examine potential delays in uncoating in the mutant virions, particularly in individually engineered D216N and M44T mutants, where it is suspected that capsid-RNA interactions are altered by these amino acid substitutions. The potential effects of the substitution A96T on host cell binding and attachment could be analysed using a binding assay as described by Hertzler et al.

(2000). Moreover, as it is not known whether individual or combined mutations are responsible for the altered thermostability, the effects of the amino acid substitutions should also be assessed in combination.

6.2. Concluding remarks

This thesis focused on broadening the understanding of picornavirus capsid structure and stability. The development of neutralising antibodies has provided a valuable tool to further investigate the TMEV capsid. The development of a novel *in-silico* screen for the prediction of hotspot residues that contribute to the stability of the TMEV capsid has improved the understanding of the structure of this cardiovirus. Furthermore, the screen demonstrated that structurally important residues such as those involved in receptor binding and capsid antigenicity may be important for capsid stability. This screen can be applied to any picornavirus to elucidate hotspot residues at subunit interfaces that contribute substantially to the stability of the capsid and is therefore appropriate for future studies exploring the structures of these important viruses. The *in vitro* analysis of hotspot residues involved in subunit-subunit interactions of the TMEV capsid is the first analysis of this type in this virus and the cardioviruses, and adds to the small number of studies that have experimentally assessed the importance of subunit interface residues and their relevance to the picornavirus lifecycle (Mateo et al., 2003; Rincón et al., 2015). The investigation into the thermal tolerance of TMEV and the genetic basis for improved thermostability is also novel for this virus. Previous studies have largely focused on the enteroviruses and FMDV (Adeyemi et al., 2017; Nguyen et al., 2019; Scott et al., 2019, 2017; Zhu and Zhang, 2015) because of their clinical and economic importance, however, a broader understanding of thermal tolerance across the family may elucidate both unique and conserved mechanisms of stability in these viruses. Such studies are of critical importance because not only do they contribute to a better understanding of virus capsids and structure-function relationships (Mateu, 2011; Reguera et al., 2004), but they may

offer potential guidelines for the design of capsid-specific antiviral agents (Bocanegra et al., 2012, 2011) and for the development of particles as improved vaccine antigens (Mateo et al., 2008; Mateu, 2011). Therefore, it is hoped that the findings from this thesis and future studies using the tools generated here may not only lead to a broader understanding of picornavirus structure but may contribute to the design of novel strategies which are urgently needed for disease prevention and control.

References

- Abraham, J.M., Murtola, T., Schulz, R., Pall, S., Smith, J.C., Hess, B., Lindahl, E., 2015. GROMACS: High performance molecular simulations through multi-level parallelism from laptops to supercomputers. *SoftwareX* 1–2, 19–25. doi:10.1016/j.softx.2015.06.001
- Abzug, M.J., Michaels, M.G., Wald, E., Jacobs, R.F., Romero, J.R., Sánchez, P.J., Wilson, G., Krogstad, P., Storch, G.A., Lawrence, R., Shelton, M., Palmer, A., Robinson, J., Dennehy, P., Sood, S.K., Cloud, G., Jester, P., Acosta, E.P., Whitley, R., Kimberlin, D., 2015. A randomized, double-blind, placebo-controlled trial of pleconaril for the treatment of neonates with enterovirus sepsis. *J. Pediatric Infect. Dis. Soc.* 5, 53–62. doi:10.1093/jpids/piv015
- Acharya, R., Fry, E., Stuart, D., Fox, G., Rowlands, D., Brown, F., 1989. The three-dimensional structure of foot-and-mouth disease virus at 2.9 Å resolution. *Nature* 337, 709–716. doi:10.1038/337709a0
- Adeyemi, O.O., Nicol, C., Stonehouse, N.J., Rowlands, D.J., 2017. Increasing Type 1 Poliovirus Capsid Stability by Thermal Selection. *J. Virol.* 91, 1–17. doi:10.1128/JVI.01586-16
- Adeyemi, O.O., Sherry, L., Ward, J.C., Pierce, D.M., Herod, M.R., Rowlands, D.J., Stonehouse, N.J., 2019. Involvement of a Nonstructural Protein in Poliovirus Capsid Assembly. *J. Virol.* 93, 1–15. doi:10.1128/JVI.01447-18.
- Airaksinen, A., Roivainen, M., Hovi, T., 2001. Coxsackievirus A9 VP1 Mutants with Enhanced or Hindered A Particle Formation and Decreased Infectivity. *J. Virol.* 75, 952–960. doi:10.1128/jvi.75.2.952-960.2001
- Alexandersen, S., Zhang, Z., Donaldson, A.I., Garland, A.J.M., 2003. The pathogenesis and diagnosis of foot-and-mouth disease. *J. Comp. Pathol.* 129, 1–36. doi:10.1016/S0021-9975(03)00041-0
- Anastasina, M., Domanska, A., Palm, K., Butcher, S., 2017. Human picornaviruses associated with neurological diseases and their neutralization by antibodies. *J. Gen. Virol.* 98, 1145–1158. doi:10.1099/jgv.0.000780
- Andino, R., Rieckhof, G.E., Baltimore, D., 1990. A functional ribonucleoprotein complex forms around the 5' end of poliovirus RNA. *Cell* 63, 369–380. doi:10.1016/0092-8674(90)90170-J
- Ansardi, D.C., Morrow, C.D., 1995. Amino Acid Substitutions in the Poliovirus Maturation Cleavage Site Affect Assembly and Result in Accumulation of Provirions. *J. Virol.* 69, 1540–1547. doi:0022-538X/95/\$04.00+0
- Ansardi, D.C., Porter, D.C., Anderson, M.J., Morrow, C.D., 1996. Poliovirus assembly and encapsidation of genomic RNA. *Adv. Virus Res.* 46, 1–68. doi:10.1016/S0065-3527(08)60069-X
- Ansardi, D.C., Porter, D.C., Morrow, C.D., 1992. Myristylation of poliovirus capsid precursor P1 is required for assembly of subviral particles. *J. Virol.* 66, 4556–4563. doi:0022-538X/92/074556-08\$02.00/0

- Arkhipov, A., Freddolino, P.L., Schulten, K., 2006. Stability and Dynamics of Virus Capsids Described by Coarse-Grained Modeling. *Structure* 14, 1767–1777. doi:10.1016/j.str.2006.10.003
- Arslan, S.Y., Son, K., Lipton, H.L., 2016. During Infection, Theiler's Virions Are Cleaved by Caspases and Disassembled into Pentamers. *J. Virol.* 90, 3573–3583. doi:10.1128/JVI.03035-15
- Assi, S.A., Tanaka, T., Rabbitts, T.H., Fernandez-fuentes, N., 2010. PCRPI: Presaging Critical Residues in Protein interfaces, a new computational tool to chart hot spots in protein interfaces. *Nucleic Acids Res.* 38, 1–11. doi:10.1093/nar/gkp1158
- Atmar, R.L., Piedra, P.A., Patel, S.M., Greenberg, S.B., Couch, R.B., Glezen, W.P., 2012. Picornavirus, the Most Common Respiratory Virus Causing Infection among Patients of All Ages Hospitalized with Acute Respiratory Illness. *J. Clin. Microbiol.* 50, 506–508. doi:10.1128/JCM.05999-11
- Baggen, J., Hurdiss, D.L., Zocher, G., Mistry, N., Roberts, R.W., Slager, J.J., Guo, H., van Vliet, A.L.W., Wahedi, M., Benschop, K., Duizer, E., de Haan, C.A.M., de Vries, E., Casanovas, J.M., de Groot, R.J., Arnberg, N., Stehle, T., Ranson, N.A., Thibaut, H.J., van Kuppeveld, F.J.M., 2018a. Role of enhanced receptor engagement in the evolution of a pandemic acute hemorrhagic conjunctivitis virus. *Proc. Natl. Acad. Sci.* 115, 397–402. doi:10.1073/pnas.1713284115
- Baggen, J., Thibaut, H.J., Strating, J.R.P.M., Kuppeveld, F.J.M., 2018b. The life cycle of non-polio enteroviruses and how to target it. *Nat. Rev. Microbiol.* 16, 368–381. doi:10.1038/s41579-018-0005-4
- Bahadur, R.P., Janin, J., 2008. Residue conservation in viral capsid assembly. *Proteins* 71, 407–414. doi:10.1002/prot.21710
- Bakker, S.E., Gropelli, E., Pearson, A.R., Stockley, P.G., Rowlands, D.J., Ranson, N.A., 2014. Limits of Structural Plasticity in a Picornavirus Capsid Revealed by a Massively Expanded Equine Rhinitis A Virus Particle. *J. Virol.* 88, 6093–6099. doi:10.1128/JVI.01979-13
- Bandyopadhyay, A.S., Garon, J., Seib, K., Orenstein, W.A., 2015. Polio vaccination: past, present and future. *Future Microbiol.* 10, 791–808. doi:10.2217/fmb.15.19
- Banerjee, K., Bhat, R., Bhaskara Rao, V.U., Nain, A., Rallapalli, K.L., Gangopadhyay, S., Singh, R.P., Banerjee, M., Jayaram, B., 2019. Toward development of generic inhibitors against the 3C proteases of picornaviruses. *FEBS J.* 286, 765–787. doi:10.1111/febs.14707
- Bannwarth, L., Girerd-chambaz, Y., Arteni, A., Guigner, J., Ronzon, F., Manin, C., Vénien-Bryan, C., 2015. Mapping of the epitopes of poliovirus type 2 in complex with antibodies. *Mol. Immunol.* 67, 233–239. doi:10.1016/j.molimm.2015.05.013
- Barnard, D.L., 2006. Current Status of Anti-Picornavirus Therapies. *Curr. Pharm. Des.* 12, 1379–1390. doi:1381-6128/06 \$50.00+.00
- Barnett, P. V., Ouldrige, E.J., Rowlands, D.J., Brown, F., Parry, N.R., 1989. Neutralizing Epitopes of Type O Foot-and-Mouth Disease Virus. I. Identification and Characterization of Three Functionally Independent, Conformational Sites. *J. Gen. Virol.* 70, 1483–1491. doi:10.1099/0022-1317-70-6-1483

- Basavappa, R., Syed, R., Flore, O., Icenogle, J.P., Filman, D.J., Hogle, J.M., 1994. Role and mechanism of the maturation cleavage of VP0 in poliovirus assembly: Structure of the empty capsid assembly intermediate at 2.9 Å resolution. *Protein Sci.* 3, 1651–1669. doi:10.1002/pro.5560031005
- Basta, H.A., Palmenberg, A.C., 2014. AMP-activated protein kinase phosphorylates EMCV, TMEV and SafV leader proteins at different sites. *Virology* 462–463, 236–240. doi:10.1016/j.virol.2014.06.026
- Batson, S., Rundell, K., 1991. Proteolysis at the 2A/2B Junction in Theiler's Murine Encephalomyelitis Virus. *Virology* 181, 764–767. doi:10.1016/0042-6822(91)90914-W
- Bayer, N., Schober, D., Prchla, E., Murphy, R.F., Blaas, D., Fuchs, R., 1998. Effect of Bafilomycin A1 and Nocodazole on Endocytic Transport in HeLa Cells: Implications for Viral Uncoating and Infection. *J. Virol.* 72, 9645–55.
- Bazanów, B., Fracka, A., Jackulak, N., Romuk, E., Gębarowski, T., Owczarek, A., Stygar, D., 2018. Viral, Serological, and Antioxidant Investigations of Equine Rhinitis A Virus in Serum and Nasal Swabs of Commercially Used Horses in Poland. *Biomed Res. Int.* 2018, 1–6. doi:10.1155/2018/8719281
- Bedard, K.M., Semler, B.L., 2004. Regulation of picornavirus gene expression. *Microbes Infect.* 6, 702–713. doi:10.1016/j.micinf.2004.03.001
- Bell, M.P., Renner, D.N., Johnson, A.J., Pavelko, K.D., 2014. An Elite Controller of Picornavirus Infection Targets an Epitope That is Resistant to Immune Escape. *PLoS One* 9, 1–12. doi:10.1371/journal.pone.0094332
- Bellstedt, D.U., Human, P.A., Rowland, G.F., Van der Merwe, K.J., 1987. Acid-treated, naked bacteria as immune carriers for protein antigens. *J. Immunol. Methods* 98, 249–255. doi:10.1016/0022-1759(87)90012-3
- Belnap, D.M., McDermott, B.M.J., Filman, D.J., Cheng, N., Trus, B.L., Zuccola, H.J., Racaniello, V.R., Hogle, J.M., Steven, A.C., 2000. Three-dimensional structure of poliovirus receptor bound to poliovirus. *Proc. Natl. Acad. Sci. United States Am.* 97, 73–78. doi:10.1073/pnas.97.1.73
- Benschop, K.S.M., Van Der Avoort, H.G., Duizer, E., Koopmans, M.P.G., 2015. Antivirals against enteroviruses: A critical review from a public-health perspective. *Antivir. Ther.* 20, 121–130. doi:10.3851/IMP2939
- Bergelson, J.M., Chan, M., Solomon, K.R., St. John, N.F., Lin, H., Finberg, R.W., 1994. Decay-accelerating factor (CD55), a glycosylphosphatidylinositol-anchored complement regulatory protein, is a receptor for several echoviruses. *Proc. Natl. Acad. Sci.* 91, 6245–6248. doi:10.1073/pnas.91.13.6245
- Berman, H.M., Westbrook, J., Feng, Z., Gilliland, G.L., Bhat, T.N., Weissig, H., Shindyalov, I.N., Bourne, P.E., 2000. The Protein Data Bank. *Nucleic Acids Res.* 28, 235–242. doi:10.1093/nar/28.1.235
- Berryman, S., Clark, S., Monaghan, P., Jackson, T., 2005. Early events in integrin $\alpha\beta 6$ -mediated cell entry of Foot-and-Mouth Disease Virus. *J. Virol.* 79, 8519–8534. doi:10.1128/JVI.79.13.8519–8534.2005
- Betts, M.J., Russell, R.B., 2003. Amino acid properties and consequences of substitutions, in: Barnes, M.R., Gray, I.C. (Eds.), *Bioinformatics for Geneticists*. John Wiley and Sons Inc.,

Hoboken, NJ.

- Bhasin, V.K., 2008. Problems with the oral polio vaccine. *Nat. Med.* 14, 9. doi:10.1038/nm0108-9.
- Biswal, J.K., Das, B., Sharma, G.K., Khulape, S.A., Pattnaik, B., 2016. Role of a single amino acid substitution of VP3 H142D for increased acid resistance of foot-and-mouth disease virus serotype A. *Virus Genes* 52, 235–243. doi:10.1007/s11262-016-1294-1
- Blair, W.S., Pickford, C., Irving, S.L., Brown, D.G., Anderson, M., Bazin, R., Cao, J., Ciaramella, G., Isaacson, J., Jackson, L., Hunt, R., Kjerrstrom, A., Nieman, J.A., Patick, A.K., Perros, M., Scott, A.D., Whitby, K., Wu, H., Butler, S.L., 2010. HIV Capsid is a Tractable Target for Small Molecule Therapeutic Intervention. *PLoS Pathog.* 6, 1–10. doi:10.1371/journal.ppat.1001220
- Bocanegra, R., Nevot, M., Doménech, R., López, I., Abián, O., Rodríguez-Huete, A., Cavasotto, C.N., Velázquez-Campoy, A., Gómez, J., Martínez, M.Á., Neira, J.L., Mateu, M.G., 2011. Rationally Designed Interfacial Peptides Are Efficient In Vitro Inhibitors of HIV-1 Capsid Assembly with Antiviral Activity. *PLoS One* 6, 1–14. doi:10.1371/journal.pone.0023877
- Bocanegra, R., Rodríguez-Huete, A., Fuertes, Ángel, M., del Álamo, M., Mateu, M.G., 2012. Molecular recognition in the human immunodeficiency virus capsid and antiviral design. *Virus Res.* 169, 388–410. doi:10.1016/j.virusres.2012.06.016
- Bogan, A.A., Thorn, K.S., 1998. Anatomy of Hot Spots in Protein Interfaces. *J. Mol. Biol.* 280, 1–9.
- Bolwell, C., Clarke, B.E., Parry, N.R., Ouldrige, E.J., Brown, F., Rowlands, D.J., 1989. Epitope Mapping of Foot-and-Mouth Disease Virus with Neutralizing Monoclonal Antibodies. *J. Gen. Virol.* 70, 59–68. doi:10.1099/0022-1317-70-1-59
- Borghese, F., Michiels, T., 2011. The Leader Protein of Cardioviruses Inhibits Stress Granule Assembly. *J. Virol.* 85, 9614–9622. doi:10.1128/JVI.00480-11
- Bostina, M., 2019. Monoclonal antibodies point to Achilles' heel in picornavirus capsid. *PLOS Biol.* 17, 1–8. doi:10.1371/journal.pbio.3000232
- Bostina, M., Levy, H., Filman, D.J., Hogle, J.M., 2011. Poliovirus RNA Is Released from the Capsid near a Twofold Symmetry Axis. *J. Virol.* 85, 776–783. doi:10.1128/jvi.00531-10
- Bourne, C., Lee, S., Venkataiah, B., Lee, A., Korba, B., Finn, M.G., Zlotnick, A., 2008. Small-Molecule Effectors of Hepatitis B Virus Capsid Assembly Give Insight into Virus Life Cycle. *J. Virol.* 82, 10262–10270. doi:10.1128/JVI.01360-08
- Boyd, K.J., Bansal, P., Feng, J., May, E.R., 2015. Stability of Norwalk Virus Capsid Protein Interfaces Evaluated by in Silico Nanoindentation. *Front. Bioeng. Biotechnol.* 3, 1–8. doi:10.3389/fbioe.2015.00103
- Bradford, J.R., Westhead, D.R., 2005. Improved prediction of protein-protein binding sites using a support vector machines approach. *Bioinformatics* 21, 1487–1494. doi:10.1093/bioinformatics/bti242
- Brandenburg, B., Lee, L.Y., Lakadamyali, M., Rust, M.J., Zhuang, X., Hogle, J.M., 2007. Imaging Poliovirus Entry in Live Cells. *PLoS Biol.* 5, 1543–1555. doi:10.1371/journal.pbio.0050183

- Brown, J.D., Ryan, M.D., 2010. Ribosome “Skipping”: “Stop-Carry On” or “StopGo” Translation, in: Atkins, J.F., Gesteland, R.F. (Eds.), *Recoding: Expansion of Decoding Rules Enriches Gene Expression*. Springer, Heidelberg, pp. 101–121. doi:10.1007/978-0-387-89382-2_5
- Bruneau, P., Blondel, B., Crainic, R., Horodniceanu, F., Girard, M., 1983. Poliovirus Type 1 Capsid Polypeptides: Absence of a Free Form In The Cytoplasm of Infected HeLa Cells. *Ann. Virol.* 134, 151–164.
- Buchta, D., Füzik, T., Hrebík, D., Levdansky, Y., Sukeník, L., Mukhamedova, L., Moravcová, J., Vácha, R., Plevka, P., 2019. Enterovirus particles expel capsid pentamers to enable genome release. *Nat. Commun.* 10, 1–9. doi:10.1038/s41467-019-09132-x
- Butan, C., Filman, D.J., Hogle, J.M., 2014. Cryo-Electron Microscopy Reconstruction Shows Poliovirus 135S Particles Poised for Membrane Interaction and RNA Release. *J. Virol.* 88, 1758–1770. doi:10.1128/JVI.01949-13
- Calenoff, M.A., Faaberg, K.S., Lipton, H.L., 1990. Genomic regions of neurovirulence and attenuation in Theiler murine encephalomyelitis virus. *Proc. Natl. Acad. Sci.* 87, 978–982. doi:10.1073/pnas.87.3.978
- Cameron, K., Zhang, X., Seal, B., Rodriguez, M., Njenga, M.K., 2001. Antigens to viral capsid and non-capsid proteins are present in brain tissues and antibodies in sera of Theiler’s virus-infected mice. *J. Virol. Methods* 91, 11–19. doi:10.1016/S0166-0934(00)00246-9
- Cao, L., Zhang, R., Liu, T., Sun, Z., Hu, M., Sun, Y., Cheng, L., Guo, Y., Fu, S., Hu, J., Li, Xiangmin, Yu, C., Wang, H., Chen, H., Li, Xueming, Fry, E.E., Stuart, D.I., Qian, P., Lou, Z., Rao, Z., 2018. Seneca Valley virus attachment and uncoating mediated by its receptor anthrax toxin receptor 1. *Proc. Natl. Acad. Sci.* 115, 13087–13092. doi:10.1073/pnas.1814309115
- Cardin, A.D., Weintraub, H.J.R., 1989. Molecular Modeling of Protein-Glycosaminoglycan Interactions. *Arteriosclerosis* 9, 21–32. doi:10.1161/01.ATV.9.1.21
- Caridi, F., Vázquez-Calvo, A., Sobrino, F., Martín-Acebes, M.A., 2015. The pH Stability of Foot-and-Mouth Disease Virus Particles Is Modulated by Residues Located at the Pentameric Interface and in the N Terminus of VP1. *J. Virol.* 89, 5633–5642. doi:10.1128/JVI.03358-14
- Carocci, M., Bakkali-kassimi, L., 2012. The encephalomyocarditis virus. *Virulence* 3, 351–367. doi:10.4161/viru.20573
- Carrillo, P.J.P., Hervás, M., Rodríguez-Huete, A., Pérez, R., Mateu, M.G., 2018. Systematic analysis of biological roles of charged amino acid residues located throughout the structured inner wall of a virus capsid. *Sci. Rep.* 8, 1–13. doi:10.1038/s41598-018-27749-8
- Cathcart, A.L., Baggs, E.L., Semler, B.L., 2014. Picornaviruses: Pathogenesis and Molecular Biology, Reference Module in Biomedical Research. UC Irvine. doi:10.1016/B978-0-12-801238-https://escholarship.org/uc/item/9gk1997c
- Chang, A.Y., Chau, V.W.Y., Landas, J.A., Pang, Y., 2017. Preparation of calcium competent *Escherichia coli* and heat-shock transformation. *JEMI methods* 1, 22–25.
- Chen, J., Ye, X., Zhang, X.Y., Zhu, Z., Zhang, X., Xu, Z., Ding, Z., Zou, G., Liu, Q., Kong, L., Jiang, W., Zhu, W., Cong, Y., Huang, Z., 2019. Coxsackievirus A10 atomic structure

- facilitating the discovery of a broad-spectrum inhibitor against human enteroviruses. *Cell Discov.* 5, 1–15. doi:10.1038/s41421-018-0073-7
- Chen, R., Chen, W., Yang, S., Wu, D., Wang, Y., Tian, Y., Shi, Y., 2011. Rigorous assessment and integration of the sequence and structure based features to predict hot spots. *BMC Bioinformatics* 12, 1–14. doi:10.1186/1471-2105-12-311
- Chen, X., Fernando, G.J.P., Crichton, M.L., Flaim, C., Yukiko, S.R., Fairmaid, E.J., Corbett, H.J., Primiero, C.A., Ansaldo, A.B., Frazer, I.H., Brown, L.E., Kendall, M.A.F., 2011. Improving the reach of vaccines to low-resource regions, with a needle-free vaccine delivery device and long-term thermostabilization. *J. Control. Release* 152, 349–355. doi:10.1016/j.jconrel.2011.02.026
- Cheng, S., Brooks, C.L., 2015. Protein-protein interfaces in viral capsids are structurally unique. *J. Mol. Biol.* 427, 3613–3624. doi:10.1016/j.jmb.2015.09.008
- Cho, K., Kim, D., Lee, D., 2009. A feature-based approach to modeling protein-protein interaction hot spots. *Nucleic Acids Res.* 37, 2672–2687. doi:10.1093/nar/gkp132
- Chong, P., Guo, M.S., Lin, F.H.Y., Hsiao, K.N., Weng, S.Y., Chou, A.H., Wang, J.R., Hsieh, S.Y., Su, I.J., Liu, C.C., 2012. Immunological and Biochemical Characterization of Coxsackie Virus A16 Viral Particles. *PLoS One* 7, e49973. doi:10.1371/journal.pone.0049973
- Chow, M., Newman, J.F.E., Filman, D., Hogle, J.M., Rowlands, D.J., Brown, F., 1987. Myristylation of picornavirus capsid protein VP4 and its structural significance. *Nature* 327, 482–486. doi:10.1038/327482a0
- Cifuentes, J.O., Lee, H., Yoder, J.D., Shingler, K.L., Carnegie, M.S., Yoder, J.L., Ashley, R.E., Makhov, A.M., Conway, J.F., Hafenstein, S., 2013. Structures of the Procapsid and Mature Virion of Enterovirus 71 Strain 1095. *J. Virol.* 87, 7637–7645. doi:10.1128/JVI.03519-12
- Clackson, T., Wells, J., 1995. A hot spot of binding energy in a hormone-receptor interface. *Science* (80-.). 267, 383–386.
- Collen, T., Dimarchi, R., Doel, T.R., 1991. A T cell epitope in VP1 of foot-and-mouth disease virus is immunodominant for vaccinated cattle. *J. Immunol.* 146, 749–755.
- Compton, S.R., Nelsen, B., Kirkegaard, K., 1990. Temperature-Sensitive Poliovirus Mutant Fails To Cleave VP0 and Accumulates Provirions. *J. Virol.* 64, 4067–4075. doi:0022-538X/90/094067-09\$02.00/0
- Couderc, T., Delpeyroux, F., Le Blay, H., Blondel, B., 1996. Mouse Adaptation Determinants of Poliovirus Type 1 Enhance Viral Uncoating. *J. Virol.* 70, 305–312. doi:0022-538X/96/\$04.00+0
- Coyne, C.B., Bergelson, J.M., 2006. Virus-Induced Abl and Fyn Kinase Signals Permit Coxsackievirus Entry through Epithelial Tight Junctions. *Cell* 124, 119–131. doi:10.1016/j.cell.2005.10.035
- Crane, M.A., Jue, C., Mitchell, M., Lipton, H., Kim, B.S., 1990. Detection of restricted predominant epitopes of Theiler's murine encephalomyelitis virus capsid proteins expressed in the λ gt11 system: differential patterns of antibody reactivity among different mouse strains. *J. Neuroimmunol.* 27, 173–186. doi:10.1016/0165-5728(90)90067-W

- Cukuroglu, E., Engin, H.B., Gursoy, A., Keskin, O., 2014. Hot spots in protein-protein interfaces: Towards drug discovery. *Prog. Biophys. Mol. Biol.* 116, 165–173. doi:10.1016/j.pbiomolbio.2014.06.003
- Cukuroglu, E., Gursoy, A., Keskin, O., 2012. HotRegion: A database of predicted hot spot clusters. *Nucleic Acids Res.* 40, D829–D833. doi:10.1093/nar/gkr929
- Cunningham, B.C., Wells, J.A., 1989. High-resolution epitope mapping of hGH-receptor interactions by. *Science* (80-.). 244, 1081–1085.
- Curry, S., Fry, E., Blakemore, W., Abu-Ghazaleh, R., Jackson, T., King, A., Lea, S., Newman, J., Stuart, D., 1997. Dissecting the Roles of VP0 Cleavage and RNA Packaging in Picornavirus Capsid Stabilization: the Structure of Empty Capsids of Foot-and-Mouth Disease Virus. *J. Virol.* 71, 9743–9752. doi:0022-538X/97/\$04.00+0
- Dang, M., Wang, X., Wang, Q., Wang, Y., Lin, J., Sun, Y., Li, X., Zhang, L., Lou, Z., Wang, J., Rao, Z., 2014. Molecular mechanism of SCARB2-mediated attachment and uncoating of EV71. *Protein Cell* 5, 692–703. doi:10.1007/s13238-014-0087-3
- Darnell, S.J., LeGault, L., Mitchell, J.C., 2008. KFC Server: interactive forecasting of protein interaction hot spots. *Nucleic Acids Res.* 36, 265–269. doi:10.1093/nar/gkn346
- Darnell, S.J., Page, D., Mitchell, J.C., 2007. An automated decision-tree approach to predicting protein interaction hot spots. *Proteins* 68, 813–823. doi:10.1002/prot.21474
- De Colibus, L., Wang, X., Spyrou, J.A.B., Kelly, J., Ren, J., Grimes, J., Puerstinger, G., Stonehouse, N., Walter, T.S., Hu, Z., Wang, J., Li, X., Peng, W., Rowlands, D.J., Fry, E.E., Rao, Z., Stuart, D.I., 2014. More powerful virus inhibitors from structure-based analysis of HEV71 capsid-binding molecules. *Nat. Struct. Mol. Biol.* 21, 282–288. doi:10.1038/nsmb.2769
- De Jesus, N.H., 2007. Epidemics to eradication: the modern history of poliomyelitis. *Virol. J.* 4, 1–18. doi:10.1186/1743-422X-4-70
- Debing, Y., Neyts, J., Thibaut, H.J., 2014. Molecular Biology and Inhibitors of Hepatitis A Virus. *Med. Res. Rev.* 34, 895–917. doi:10.1002/med.21292
- Dehouck, Y., Kwasigroch, J.M., Rooman, M., Gilis, D., 2013. BeAtMuSiC: Prediction of changes in protein-protein binding affinity on mutations. *Nucleic Acids Res.* 41, 333–339. doi:10.1093/nar/gkt450
- Delano, W.L., 2002. Unraveling hot spots in binding interfaces: progress and challenges. *Curr. Opin. Struct. Biol.* 12, 14–20. doi:10.1016/S0959-440X(02)00283-X
- Delhaye, S., van Pesch, V., Michiels, T., 2004. The Leader Protein of Theiler's Virus Interferes with Nucleocytoplasmic Trafficking of Cellular Proteins. *J. Virol.* 78, 4357–4362. doi:10.1128/JVI.78.8.4357-4362.2004
- Deng, L., Guan, J., Wei, X., Yi, Y., Zhang, Q.C., Zhou, S., 2013. Boosting Prediction Performance of Protein-Protein Interaction Hot Spots by Using Structural Neighborhood Properties. *J. Comput. Biol.* 20, 333–344. doi:10.1089/cmb.2013.0083
- Deng, L., Zhang, Q.C., Chen, Z., Meng, Y., Guan, J., Zhou, S., 2014. PredHS: a web server for predicting protein-protein interaction hot spots by using structural neighborhood properties. *Nucleic Acids Res.* 1, 1–6. doi:10.1093/nar/gku437

- Doel, T.R., Baccharini, P.J., 1981. Thermal Stability of Foot-and-Mouth Disease Virus. *Arch. Virol.* 70, 21–32.
- Domingo, E., 1997. RNA Virus Mutations and Fitness for Survival. *Annu. Rev. Microbiol.* 51, 151–178. doi:10.1146/annurev.micro.51.1.151
- Domingo, E., Martin, V., Perales, C., Escarmis, C., 2008. Coxsackieviruses and Quasispecies Theory: Evolution of Enteroviruses. *Curr. Top. Microbiol. Immunol.* 323, 3–32.
- Domingo, E., Sheldon, J., Perales, C., 2012. Viral Quasispecies Evolution. *Microbiol. Mol. Biol. Rev.* 76, 159–216. doi:10.1128/MMBR.05023-11
- Dong, Y., Liu, Y., Jiang, W., Smith, T.J., Xu, Z., Rossmann, M.G., 2017. Antibody-induced uncoating of human rhinovirus B14. *Proc. Natl. Acad. Sci.* 114, 8017–8022. doi:10.1073/pnas.1707369114
- Donnelly, M.L.L., Hughes, L.E., Luke, G., Mendoza, H., ten Dam, E., Gani, D., Ryan, M.D., 2001. The ‘cleavage’ activities of foot-and-mouth disease virus 2A site-directed mutants and naturally occurring ‘2A-like’ sequences. *J. Gen. Virol.* 82, 1027–1041. doi:10.1099/0022-1317-82-5-1027
- Dove, A.W., Racaniello, V.R., 2000. An Antiviral Compound That Blocks Structural Transitions of Poliovirus Prevents Receptor Binding at Low Temperatures. *J. Virol.* 74, 3929–3931. doi:10.1128/jvi.74.8.3929-3931.2000
- Dvorak, C.M.T., Hall, D.J., Hill, M., Riddle, M., Pranter, A., Dillman, J., Deibel, M., Palmenberg, A.C., 2001. Leader Protein of Encephalomyocarditis Virus Binds Zinc, Is Phosphorylated during Viral Infection, and Affects the Efficiency of Genome Translation. *Virology* 290, 261–271. doi:10.1006/viro.2001.1193
- Edlmayr, J., Niespodziana, K., Popow-Kraupp, T., Krzyzanek, V., Focke-Tejkl, M., Blaas, D., Grote, M., Valenta, R., 2011. Antibodies induced with recombinant VP1 from human rhinovirus exhibit cross-neutralisation. *Eur. Respir. J.* 37, 44–52. doi:10.1183/09031936.00149109
- Ehrenfeld, E., Domingo, E., Roos, R.P. (Eds.), 2010. *The Picornaviruses*. ASM Press, Washington, DC. doi:10.1128/isbn978-1-55581-603-2
- Ellard, F.M., Drew, J., Blakemore, W.E., Stuart, D.I., King, A.M.Q., 1999. Evidence for the role of His-142 of protein 1C in the acid-induced disassembly of foot-and-mouth disease virus capsids. *J. Gen. Virol.* 80, 1911–1918. doi:10.1099/0022-1317-80-8-1911
- Fernandez-Tomas, C.B., Baltimore, D., 1973. Morphogenesis of poliovirus. II. Demonstration of a New Intermediate, the Provirus. *J. Virol.* 12, 1122–1130.
- Filman, D.J., Syed, R., Chow, M., Macadam, A.J., Minor, P.D., Hogle, J.M., 1989. Structural factors that control conformational transitions and serotype specificity in type 3 poliovirus. *EMBO J.* 8, 1567–79. doi:10.1002/j.1460-2075.1989.tb03541.x
- Finch, L.K., Ling, R., Naphine, S., Olsper, A., Michiels, T., Lardinois, C., Bell, S., Loughran, G., Brierley, I., Firth, A.E., 2015. Characterization of Ribosomal Frameshifting in Theiler’s Murine Encephalomyelitis Virus. *J. Virol.* 89, 8580–8589. doi:10.1128/jvi.01043-15
- Fotiadis, C., Kilpatrick, D.R., Lipton, H.L., 1991. Comparison of the Binding Characteristics to BHK-21 Cells of Viruses Representing the Two Theiler’s Virus Neurovirulence

- Groups. *Virology* 182, 365–370. doi:10.1016/0042-6822(91)90683-3
- Fox, H., Knowlson, S., Minor, P.D., Macadam, A.J., 2017. Genetically Thermo-Stabilised, Immunogenic Poliovirus Empty Capsids; a Strategy for Non-replicating Vaccines. *PLoS Pathog.* 13, 1–14. doi:10.1371/journal.ppat.1006117
- Freundt, E.C., Drappier, M., Michiels, T., 2018. Innate Immune Detection of Cardioviruses and Viral Disruption of Interferon Signaling. *Front. Microbiol.* 9, 1–12. doi:10.3389/fmicb.2018.02448
- Fricks, C.E., Hogle, J.M., 1990. Cell-induced conformational change in poliovirus: externalization of the amino terminus of VP1 is responsible for liposome binding. *J. Virol.* 64, 1934–1945. doi:0022-538X/90/051934-12\$02.00/0
- Fry, E.E., Knowles, N.J., Newman, J.W.I., Wilsden, G., Rao, Z., King, A.M.Q., Stuart, D.I., 2003. Crystal Structure of Swine Vesicular Disease Virus and Implications for Host Adaptation. *J. Virol.* 77, 5475–5486. doi:10.1128/JVI.77.9.5475–5486.2003
- Fry, E.E., Lea, S.M., Jackson, T., Newman, J.W.I., Ellard, F.M., Blakemore, W.E., Abu-Ghazaleh, R., Samuel, A., King, A.M.Q., Stuart, D.I., 1999. The structure and function of a foot-and-mouth disease virus-oligosaccharide receptor complex. *EMBO J.* 18, 543–554. doi:10.1093/emboj/18.3.543
- Fu, J., Stein, S., Rosenstein, L., Bodwell, T., Routbort, M., Semler, B.L., Roos, R.P., 1990. Neurovirulence Determinants of Genetically Engineered Theiler Viruses. *Proc. Natl. Acad. Sci.* 87, 4125–4129.
- Gao, Y., Wang, R., Lai, L., 2004. Structure-based method for analyzing protein-protein interfaces. *J. Molecular Model.* 10, 44–54. doi:10.1007/s00894-003-0168-3
- Garriga, D., Pickl-Herk, A., Luque, D., Wruss, J., Castón, J.R., Blaas, D., Verdaguer, N., 2012. Insights into Minor Group Rhinovirus Uncoating: The X-ray Structure of the HRV2 Empty Capsid. *PLoS Pathog.* 8, 1–14. doi:10.1371/journal.ppat.1002473
- Geller, R., Taguwa, S., Frydman, J., 2012. Broad action of Hsp90 as a host chaperone required for viral replication. *Biochim. Biophys. Acta* 1823, 698–706. doi:10.1016/j.bbamcr.2011.11.007
- Geller, R., Vignuzzi, M., Andino, R., Frydman, J., 2007. Evolutionary constraints on chaperone-mediated folding provide an antiviral approach refractory to development of drug resistance. *Genes Dev.* 21, 195–205. doi:10.1101/gad.1505307
- Geng, C., Vangone, A., Folkers, G.E., Xue, L.C., Bonvin, A.M.J.J., 2019. iSEE: Interface structure, evolution, and energy-based machine learning predictor of binding affinity changes upon mutations. *Proteins* 87, 110–119. doi:10.1002/prot.25630
- Geppert, T., Hoy, B., Wessler, S., Schneider, G., 2011. Context-Based Identification of Protein-Protein Interfaces and “Hot-Spot” Residues. *Chem. Biol.* 18, 344–353. doi:10.1016/j.chembiol.2011.01.005
- Gerhauser, I., Hansmann, F., Ciurkiewicz, M., Löscher, W., Beineke, A., 2019. Facets of Theiler’s Murine Encephalomyelitis Virus-Induced Diseases: An Update. *Int. J. Mol. Sci.* 20, 448. doi:10.3390/ijms20020448
- Gouet, P., Robert, X., Courcelle, E., 2003. ESPript/ENDscript: extracting and rendering sequence and 3D information from atomic structures of proteins. *Nucleic Acids Res.* 31,

- 3320–3323. doi:10.1093/nar/gkg556
- Grant, R.A., Filman, D.J., Fujinami, R.S., Icenogle, J.P., Hogle, J.M., 1992. Three-dimensional structure of Theiler virus. *Proc. Natl. Acad. Sci.* 89, 2061–2065. doi:10.1073/pnas.89.6.2061
- Greve, J.M., Davis, G., Meyer, A.M., Forte, C.P., Yost, S.C., Marlor, C.W., Kamarck, M.E., McClelland, A., 1989. The Major Human Rhinovirus Receptor Is ICAM-1. *Cell* 56, 839–847. doi:10.1016/0092-8674(89)90688-0
- Grubman, M.J., 1984. In Vitro Morphogenesis of Foot-and-Mouth Disease Virus. *J. Virol.* 49, 760–765.
- Grubman, M.J., Morgan, D.O., Kendall, J., Baxt, B., 1985. Capsid Intermediates Assembled in a Foot-and-Mouth Disease Virus Genome RNA-Programmed Cell-Free Translation System and in Infected Cells. *J. Virol.* 56, 120–6. doi:0022-538X/85/100120-07\$02.00/0
- Guerois, R., Nielsen, J.E., Serrano, L., 2002. Predicting Changes in the Stability of Proteins and Protein Complexes: A Study of More Than 1000 Mutations. *J. Mol. Biol.* 320, 369–387. doi:10.1016/S0022-2836(02)00442-4
- Guharoy, M., Chakrabarti, P., 2009. Empirical estimation of the energetic contribution of individual interface residues in structures of protein-protein complexes. *J. Comput. Aided. Mol. Des.* 23, 645–654. doi:10.1007/s10822-009-9282-3
- Gulbahar, M.Y., Davis, W.C., Guvenc, T., Yarim, M., Parlak, U., Kabak, Y.B., 2007. Myocarditis Associated with Foot-and-Mouth Disease Virus Type O in Lambs. *Vet. Pathol.* 44, 589–599. doi:10.1354/vp.44-5-589
- Guney, E., Tuncbag, N., Keskin, O., Gursoy, A., 2008. HotSprint: database of computational hot spots in protein interfaces. *Nucleic Acids Res.* 36, 662–666. doi:10.1093/nar/gkm813
- Guo, C., Zhang, C., Zheng, H., Huang, Y., 2013. Recombinant adenovirus expression of FMDV P1-2A and 3C protein and its immune response in mice. *Res. Vet. Sci.* 95, 736–741. doi:10.1016/j.rvsc.2013.05.001
- Guo, W., Wisniewski, J.A., Ji, H., 2014. Hot spot-based design of small-molecule inhibitors for protein-protein interactions. *Bioorg. Med. Chem. Lett.* 24, 2546–2554. doi:10.1016/j.bmcl.2014.03.095
- Guttman, N., Baltimore, D., 1977. Morphogenesis of Poliovirus. IV. Existence of Particles Sedimenting at 150S and Having the Properties of Provirion. *J. Virol.* 23, 363–367.
- Hadfield, A.T., Lee, W., Zhao, R., Oliveira, M.A., Minor, I., Rueckert, R.R., Rossmann, M.G., 1997. The refined structure of human rhinovirus 16 at 2.15 Å resolution: implications for the viral life cycle. *Structure* 5, 427–441. doi:10.1016/S0969-2126(97)00199-8
- Harutyunyan, S., Kumar, M., Sedivy, A., Subirats, X., Kowalski, H., Köhler, G., Blaas, D., 2013. Viral Uncoating Is Directional: Exit of the Genomic RNA in a Common Cold Virus Starts with the Poly-(A) Tail at the 3'-End. *PLoS Pathog.* 9, 1–14. doi:10.1371/journal.ppat.1003270
- Hause, B.M., Collin, E.A., Anderson, J., Hesse, R.A., Anderson, G., 2015. Bovine Rhinitis Viruses Are Common in U.S. Cattle with Bovine Respiratory Disease. *PLoS One* 10, 1–12. doi:10.1371/journal.pone.0121998

- Hayden, F.G., Herrington, D.T., Coats, T.L., Kim, K., Cooper, E.C., Villano, S.A., Liu, S., Hudson, S., Pevear, D.C., Collett, M., McKinlay, M., 2003. Efficacy and Safety of Oral Pleconaril for Treatment of Colds Due to Picornaviruses in Adults: Results of 2 Double-Blind, Randomized, Placebo-Controlled Trials. *Clin. Infect. Dis.* 36, 1523–1532. doi:10.1086/375069
- He, Y., Chipman, P.R., Howitt, J., Bator, C.M., Whitt, M.A., Baker, T.S., Kuhn, R.J., Anderson, C.W., Freimuth, P., Rossman, M.G., 2001. Interaction of coxsackievirus B3 with the full length coxsackievirus-adenovirus receptor. *Nat. Struct. Mol. Biol.* 8, 874–878. doi:10.1038/nsb1001-874
- Hemsley, A., Arnheim, N., Toney, D.M., Cortopassi, G., Galas, D.J., 1989. A simple method for site-directed mutagenesis using the polymerase chain reaction. *Nucleic Acids Res.* 17, 6545–6551. doi:10.1093/nar/17.16.6545
- Hendry, E., Hatanaka, H., Fry, E., Smyth, M., Tate, J., Stanway, G., Santti, J., Maaronen, M., Hyypiä, T., Stuart, D., 1999. The crystal structure of coxsackievirus A9: new insights into the uncoating mechanisms of enteroviruses. *Structure* 7, 1527–1538. doi:10.1016/S0969-2126(00)88343-4
- Hertzler, S., Luo, M., Lipton, H.L., 2000. Mutation of Predicted Virion Pit Residues Alters Binding of Theiler's Murine Encephalomyelitis Virus to BHK-21 Cells. *J. Virol.* 74, 1994–2004. doi:10.1128/JVI.74.4.1994-2004.2000
- Hewat, E.A., Blaas, D., 2006. Nonneutralizing Human Rhinovirus Serotype 2-Specific Monoclonal Antibody 2G2 Attaches to the Region That Undergoes the Most Dramatic Changes upon Release of the Viral RNA. *J. Virol.* 80, 12398–12401. doi:10.1128/jvi.01399-06
- Hewat, E.A., Blaas, D., 1996. Structure of a neutralizing antibody bound bivalently to human rhinovirus 2. *EMBO J.* 15, 1515–1523. doi:10.1002/j.1460-2075.1996.tb00495.x
- Hewat, E.A., Neumann, E., Conway, J.F., Moser, R., Ronacher, B., Marlovits, T.C., Blaas, D., 2000. The cellular receptor to human rhinovirus 2 binds around the 5-fold axis and not in the canyon: a structural view. *EMBO J.* 19, 6317–6325. doi:10.1093/emboj/19.23.6317
- Hindiyeh, M., Li, Q.H., Basavappa, R., Hogle, J.M., Chow, M., 1999. Poliovirus Mutants at Histidine 195 of VP2 Do Not Cleave VP0 into VP2 and VP4. *J. Virol.* 73, 9072–9079.
- Ho, S.N., Hunt, H.D., Horton, R.M., Pullen, J.K., Pease, L.R., 1989. Site-directed mutagenesis by overlap extension using the polymerase chain reaction. *Gene* 77, 51–59.
- Hober, D., Sauter, P., 2010. Pathogenesis of type 1 diabetes mellitus: interplay between enterovirus and host. *Nat. Rev. Endocrinol.* 6, 279–289. doi:10.1038/nrendo.2010.27
- Hofer, F., Gruenberger, M., Kowalski, H., Machat, H., Huettinger, M., Kuechler, E., Blaas, D., 1994. Members of the low density lipoprotein receptor family mediate cell entry of a minor-group common cold virus. *Proc. Natl. Acad. Sci.* 91, 1839–1842. doi:10.1073/pnas.91.5.1839
- Hogle, J.M., 2002. Poliovirus Cell Entry: Common Structural Themes in Viral Cell Entry Pathways. *Annu. Rev. Microbiol.* 56, 677–702. doi:10.1146/annurev.micro.56.012302.160757
- Hogle, J.M., Chow, M., Filman, D.J., 1985. Three-Dimensional Structure of Poliovirus at 2.9 Å Resolution. *Science* (80-.). 229, 1358–1365. doi:10.1126/science.2994218

- Horsington, J.J., Gilkerson, J.R., Hartley, C.A., 2012. Mapping B-cell epitopes in equine rhinitis B viruses and identification of a neutralising site in the VP1 C-terminus. *Vet. Microbiol.* 155, 128–136. doi:10.1016/j.vetmic.2011.08.022
- Huang, K.Y.A., Chen, M.F., Huang, Y.C., Shih, S.R., Chiu, C.H., Lin, J.J., Wang, J.R., Tsao, K.C., Lin, T.Y., 2017. Epitope-associated and specificity-focused features of EV71-neutralizing antibody repertoires from plasmablasts of infected children. *Nat. Commun.* 8, 1–14. doi:10.1038/s41467-017-00736-9
- Huber, S.A., 1994. VCAM-1 Is a Receptor for Encephalomyocarditis Virus on Murine Vascular Endothelial Cells. *J. Virol.* 68, 3453–3458. doi:0022-538X/94/\$04.00+0
- Huo, S., Massova, I., Kollman, P.A., 2002. Computational Alanine Scanning of the 1:1 Human Growth Hormone-Receptor Complex. *J. Comput. Chem.* 23, 15–27. doi:10.1002/jcc.1153
- Inoue, A., Choe, Y.K., Kim, B.S., 1994. Analysis of Antibody Responses to Predominant Linear Epitopes of Theiler's Murine Encephalomyelitis Virus. *J. Virol.* 68, 3324–3333. doi:10.1016/0165-5728(94)90367-0
- Irwin, J.J., Shoichet, B.K., 2005. ZINC - A Free Database of Commercially Available Compounds for Virtual Screening. *J. Chem. Inf. Model.* 45, 177–182. doi:10.1021/ci049714
- Jackson, T., Clark, S., Berryman, S., Burman, A., Cambier, S., Mu, D., Nishimura, S., King, A.M.Q., 2004. Integrin $\alpha\beta 8$ Functions as a Receptor for Foot-and-Mouth Disease Virus: Role of the β -Chain Cytodomain in Integrin-Mediated Infection. *J. Virol.* 78, 4533–4540. doi:10.1128/jvi.78.9.4533-4540.2004
- Jackson, T., Mould, A.P., Sheppard, D., King, A.M.Q., 2002. Integrin $\alpha\beta 1$ Is a Receptor for Foot-and-Mouth Disease Virus. *J. Virol.* 76, 935–941. doi:10.1128/JVI.76.3.935–941.2002
- Jackson, T., Sheppard, D., Denyer, M., Blakemore, W., King, A.M.Q., 2000. The Epithelial Integrin $\alpha\beta 6$ Is a Receptor for Foot-and-Mouth Disease Virus. *J. Virol.* 74, 4949–4956. doi:10.1128/JVI.74.11.4949-4956.2000
- Jacobson, M.F., Baltimore, D., 1968. Morphogenesis of Poliovirus. I. Association of the Viral RNA with Coat Protein. *J. Mol. Biol.* 33, 369–378. doi:10.1016/0022-2836(68)90195-2
- Jain, J., Kumari, A., Somvanshi, P., Grover, A., Pai, S., Sunil, S., 2017. In silico analysis of natural compounds targeting structural and nonstructural proteins of chikungunya virus. *F1000 Res.* 6, 1–26. doi:10.12688/f1000research.12301.2
- Jauka, T., Mutsvunguma, L., Boshoff, A., Edkins, A.L., Knox, C., 2010. Localisation of Theiler's murine encephalomyelitis virus protein 2C to the Golgi apparatus using antibodies generated against a peptide region. *J. Virol. Methods* 168, 162–169. doi:10.1016/j.jviromet.2010.05.009
- Jayawardena, N., Burga, L.N., Easingwood, R.A., Takizawa, Y., Wolf, M., Bostina, M., 2018. Structural basis for anthrax toxin receptor 1 recognition by Seneca Valley Virus. *Proc. Natl. Acad. Sci.* 115, E10934–E10940. doi:10.1073/pnas.1810664115
- Jiang, P., Liu, Y., Ma, H.C., Paul, A., Wimmer, E., 2014. Picornavirus Morphogenesis. *Microbiol. Mol. Biol. Rev.* 78, 418–437. doi:10.1128/MMBR.00012-14
- Jnaoui, K., Minet, M., Michiels, T., 2002. Mutations That Affect the Tropism of DA and

- GDVII Strains of Theiler's Virus In Vitro Influence Sialic Acid Binding and Pathogenicity. *J. Virol.* 76, 8138–8147. doi:10.1128/JVI.76.16.8138-8147.2002
- Kalynych, S., Palkova, L., Plevka, P., 2016. The Structure of Human Parechovirus 1 Reveals an Association of the RNA Genome with the Capsid. *J. Virol.* 90, 1377–1386. doi:10.1128/JVI.02346-15
- Katen, S.P., Chirapu, S.R., Finn, M., Zlotnick, A., 2010. Trapping of Hepatitis B Virus Capsid Assembly Intermediates by Phenylpropenamide Assembly Accelerators. *ACS Chem. Biol.* 5, 1125–1136. doi:10.1021/cb100275b
- Katpally, U., Smith, T.J., 2007. Pocket Factors Are Unlikely To Play a Major Role in the Life Cycle of Human Rhinovirus. *J. Virol.* 81, 6307–6315. doi:10.1128/jvi.00441-07
- Kelly, J.T., 2015. The enterovirus 71 particle: An evolutionary approach to investigate structure and function with implications for drug and vaccine development. The University of Leeds School.
- Kelly, J.T., De Colibus, L., Elliott, L., Fry, E.E., Stuart, D.I., Rowlands, D.J., Stonehouse, N.J., 2015. Potent antiviral agents fail to elicit genetically-stable resistance mutations in either enterovirus 71 or Coxsackievirus A16. *Antiviral Res.* 124, 77–82. doi:10.1016/j.antiviral.2015.10.006
- Keskin, O., Ma, B., Nussinov, R., 2005. Hot Regions in Protein – Protein Interactions : The Organization and Contribution of Structurally Conserved Hot Spot Residues. *J. Mol. Biol.* 345, 1281–1294. doi:10.1016/j.jmb.2004.10.077
- Kiener, T.K., Jia, Q., Meng, T., Chow, V.T.K., Kwang, J., 2014. A Novel Universal Neutralizing Monoclonal Antibody against Enterovirus 71 That Targets the Highly Conserved “Knob” Region of VP3 Protein. *PLoS Negl. Trop. Dis.* 8, e2895. doi:10.1371/journal.pntd.0002895.t001
- Kilpatrick, D.R., Lipton, H.L., 1991. Predominant Binding of Theiler's Viruses to a 34-Kilodalton Receptor Protein on Susceptible Cell Lines. *J. Virol.* 65, 5244–5249. doi:0022-538X/91/105244-06\$02.00/0
- Kim, B.S., Choe, Y.K., Crane, M.A., Jue, C.R., 1992. Identification and localization of a limited number of predominant conformation-independent antibody epitopes of Theiler's murine encephalomyelitis virus. *Immunol. Lett.* 31, 199–205. doi:10.1016/0165-2478(92)90146-F
- King, A.M.Q., Lefkowitz, E.J., Mushegian, A.R., Adams, M.J., Dutilh, B.E., Gorbalenya, A.E., Harrach, B., Harrison, R.L., Junglen, S., Knowles, N.J., Kropinski, A.M., Krupovic, M., Kuhn, J.H., Nibert, M.L., Rubino, L., Sabanadzovic, S., Sanfaçon, H., Siddell, S.G., Simmonds, P., Varsani, A., Zerbini, F.M., Davison, A.J., 2018. Changes to taxonomy and the International Code of Virus Classification and Nomenclature ratified by the International Committee on Taxonomy of Viruses (2018). *Arch. Virol.* 163, 2601–2631. doi:10.1007/s00705-018-3847-1
- Klasse, P.J., 2014. Neutralization of Virus Infectivity by Antibodies: Old Problems in New Perspectives. *Adv. Biol.* 2014, 1–24. doi:10.1155/2014/157895
- Knox, C., Moffat, K., Ali, S., Ryan, M., Wileman, T., 2005. Foot-and-mouth disease virus replication sites form next to the nucleus and close to the Golgi apparatus, but exclude marker proteins associated with host membrane compartments. *J. Gen. Virol.* 86, 687–

696. doi:10.1099/vir.0.80208-0
- Koch, F., Koch, G., 1985. *The Molecular Biology of Poliovirus*, 1st ed. Springer-Verlag/Wien, New York. doi:10.21775/9781910190517.02
- Kolatkar, P.R., Bella, J., Olson, N.H., Bator, C.M., Baker, T.S., Rossmann, M.G., 1999. Structural studies of two rhinovirus serotypes complexed with fragments of their cellular receptor. *EMBO J.* 18, 6249–6259. doi:10.1093/emboj/18.22.6249
- Korant, B., Lonberg-Holm, K., Yin, F., Noble-Harvey, J., 1975. Fractionation of biologically active and inactive populations of human rhinovirus type 2. *Virology* 394, 384–394. doi:10.1016/0042-6822(75)90311-6
- Kortemme, T., Baker, D., 2002. A simple physical model for binding energy hot spots in protein-protein complexes. *Proc. Natl. Acad. Sci.* 99, 14116–14121. doi:10.1073/pnas.202485799
- Kortemme, T., Kim, D.E., Baker, D., 2004. Computational Alanine Scanning of Protein-Protein Interfaces. *Sci. STKE* 219, 1–8. doi:10.1126/stke.2192004pl2
- Kotecha, A., Perez-Martin, E., Harvey, Y., Zhang, F., Ilca, S.L., Fry, E.E., Jackson, B., Maree, F., Scott, K., Hecksel, C.W., Harmsen, M.M., Mioulet, V., Wood, B., Juleff, N., Stuart, D.I., Charleston, B., Seago, J., 2018. Chimeric O1K foot-and-mouth disease virus with SAT2 outer capsid as an FMD vaccine candidate. *Sci. Rep.* 8, 1–12. doi:10.1038/s41598-018-31856-x
- Kotecha, A., Seago, J., Scott, K., Burman, A., Loureiro, S., Ren, J., Porta, C., Ginn, H.M., Jackson, T., Perez-Martin, E., Siebert, C.A., Paul, G., Huiskonen, J.T., Jones, I.M., Esnouf, R.M., Fry, E.E., Maree, F.F., Charleston, B., Stuart, D.I., 2015. Structure-based energetics of protein interfaces guides foot-and-mouth disease virus vaccine design. *Nat. Struct. Mol. Biol.* 22, 788–794. doi:10.1038/nsmb.3096
- Kotecha, A., Zhang, F., Juleff, N., Jackson, T., Perez, E., Stuart, D., Fry, E., Charleston, B., Seago, J., 2016. Application of the thermofluor PaSTRy technique for improving foot-and-mouth disease virus vaccine formulation. *J. Gen. Virol.* 97, 1557–1565. doi:10.1099/jgv.0.000462
- Krissinel, E., 2015. Stock-based detection of protein oligomeric states in jsPISA. *Nucleic Acids Res.* 43, W314–W319. doi:10.1093/nar/gkv314
- Krissinel, E., Henrick, K., 2007. Inference of Macromolecular Assemblies from Crystalline State. *J. Mol. Biol.* 372, 774–797. doi:10.1016/j.jmb.2007.05.022
- Kristensen, T., Belsham, G.J., 2019. Identification of a short, highly conserved, motif required for picornavirus capsid precursor processing at distal sites. *PLoS Pathog.* 15, 1–22. doi:10.1371/journal.ppat.1007509
- Kristensen, T., Normann, P., Gullberg, M., Fahnøe, U., Polacek, C., Rasmussen, T.B., Belsham, G.J., 2017. Determinants of the VP1/2A junction cleavage by the 3C protease in foot-and-mouth disease virus-infected cells. *J. Gen. Virol.* 98, 385–395. doi:10.1099/jgv.0.000664
- Ku, Z., Ye, X., Shi, J., Wang, X., Liu, Q., Huang, Z., 2015. Single Neutralizing Monoclonal Antibodies Targeting the VP1 GH Loop of Enterovirus 71 Inhibit both Virus Attachment and Internalization during Viral Entry. *J. Virol.* 89, 12084–12095. doi:10.1128/jvi.02189-15

- Laskowski, R.A., Swindells, M.B., 2011. LigPlot+: Multiple Ligand-Protein Interaction Diagrams for Drug Discovery. *J. Chem. Inf. Model.* 51, 2778–2786. doi:10.1021/ci200227u
- Lea, S., Hernandez, J., Blakemore, W., Brocchi, E., Curry, S., Domingo, E., Fry, E., Abu-Ghazaleh, R., King, A., Newman, J., Stuart, D., Mateu, M., 1994. The structure and antigenicity of a type C foot-and-mouth disease virus. *Structure* 2, 123–139.
- Lee, H., Shingler, K.L., Organtini, L.J., Ashley, R.E., Makhov, A.M., Conway, J.F., Hafenstein, S., 2016. The novel asymmetric entry intermediate of a picornavirus captured with nanodiscs. *Sci. Adv.* 2, 1–10. doi:10.1126/sciadv.1501929
- Lemon, S.M., Ott, J.J., Van Damme, P., Shouval, D., 2018. Type A viral hepatitis: A summary and update on the molecular virology, epidemiology, pathogenesis and prevention. *J. Hepatol.* 68, 167–184. doi:10.1016/j.jhep.2017.08.034
- Lentz, K.N., Smith, A.D., Geisler, S.C., Cox, S., Buontempo, P., Skelton, A., DeMartino, J., Rozhon, E., Schwartz, J., Girijavallabhan, V., O’Connell, J., Arnold, E., 1997. Structure of poliovirus type 2 Lansing complexed with antiviral agent SCH48973: Comparison of the structural and biological properties of the three poliovirus serotypes. *Structure* 5, 961–978. doi:10.1016/S0969-2126(97)00249-9
- Lewis, J.K., Bothner, B., Smith, T.J., Siuzdak, G., 1998. Antiviral agent blocks breathing of the common cold virus. *Proc. Natl. Acad. Sci.* 95, 6774–6778. doi:10.1073/pnas.95.12.6774
- Li, C., Wang, J.C.Y., Taylor, M.W., Zlotnick, A., 2012. In Vitro Assembly of an Empty Picornavirus Capsid follows a Dodecahedral Path. *J. Virol.* 86, 13062–13069. doi:10.1128/JVI.01033-12
- Li, Q., Yafal, A.G., Lee, Y.M., Hogle, J., Chow, M., 1994. Poliovirus Neutralization by Antibodies to Internal Epitopes of VP4 and VP1 Results from Reversible Exposure of These Sequences at Physiological Temperature. *J. Virol.* 68, 3965–3970.
- Li, Y., Zhou, Z., Post, C.B., 2005. Dissociation of an antiviral compound from the internal pocket of human rhinovirus 14 capsid. *Proc. Natl. Acad. Sci.* 102, 7529–7534. doi:10.1073/pnas.0408749102
- Lim, X.F., Jia, Q., Khong, W.X., Yan, B., Premanand, B., Alonso, S., Chow, V.T.K., Kwang, J., 2012. Characterization of an Isotype-Dependent monoclonal antibody against linear neutralizing epitope effective for prophylaxis of enterovirus 71 infection. *PLoS One* 7, 1–11. doi:10.1371/journal.pone.0029751
- Lin, C.J., Liu, C.H., Wang, J.Y., Lin, C.C., Li, Y.F., Richardson, C.D., Lin, L.T., 2018. Small molecules targeting coxsackievirus A16 capsid inactivate viral particles and prevent viral binding. *Emerg. Microbes Infect.* 7, 1–11. doi:10.1038/s41426-018-0165-3
- Lin, J., Lee, L.Y., Roivainen, M., Filman, D.J., Hogle, J.M., Belnap, D.M., 2012. Structure of the Fab-Labeled “Breathing” State of Native Poliovirus. *J. Virol.* 86, 5959–5962. doi:10.1128/JVI.05990-11
- Lipton, H.L., 1975. Theiler’s Virus Infection in Mice: an Unusual Biphasic Disease Process Leading to Demyelination. *Infect. Immun.* 11, 1147–1155.
- Lipton, H.L., Calenoff, M., Bandyopadhyay, P., Miller, S.D., Dal Canto, M.C., Gerety, S., Jensen, K., 1991. The 5’Noncoding Sequences From a Less Virulent Theilers Virus

- Dramatically Attenuate Gdvii Neurovirulence. *J. Virol.* 65, 4370–4377. doi:0022-538X/91/084370-08\$02.00/0
- Lipton, H.L., Friedmann, A., 1980. Purification of Theiler's Murine Encephalomyelitis Virus and Analysis of the Structural Virion Polypeptides: Correlation of the Polypeptide Profile with Virulence. *J. Virol.* 33, 1165–1172. doi:0022-538X/80/03-1165/08\$02.00/0
- Lipton, H.L., Kumar, A.S.M., Hertzler, S., Reddi, H. V., 2006. Differential usage of carbohydrate co-receptors influences cellular tropism of Theiler's murine encephalomyelitis virus infection of the central nervous system. *Glycoconj. J.* 23, 39–49. doi:10.1007/s10719-006-5436-x
- Lise, S., Archambeau, C., Pontil, M., Jones, D.T., 2009. Prediction of hot spot residues at protein-protein interfaces by combining machine learning and energy-based methods. *BMC Bioinformatics* 10, 1–17. doi:10.1186/1471-2105-10-365
- Liu, Q., Huang, X., Ku, Z., Wang, T., Liu, F., Cai, Y., Li, D., Leng, Q., Huang, Z., 2013. Characterization of enterovirus 71 capsids using subunit protein-specific polyclonal antibodies. *J. Virol. Methods* 187, 127–131. doi:10.1016/j.jviromet.2012.09.024
- Liu, Y., Sheng, J., Baggen, J., Meng, G., Xiao, C., Thibaut, H.J., Van Kuppeveld, F.J.M., Rossmann, M.G., 2015a. Sialic acid-dependent cell entry of human enterovirus D68. *Nat. Commun.* 6, 1–7. doi:10.1038/ncomms9865
- Liu, Y., Sheng, J., Fokine, A., Meng, G., Shin, W., Long, F., Kuhn, R., Kihara, D., Rossmann, M., 2015b. Structure and inhibition of EV-D68, a virus that causes respiratory illness in children. *Science (80-.)*. 347, 71–74. doi:10.1126/science.1261962 Targeting
- Liu, Y., Sheng, J., van Vliet, A.L.W., Buda, G., van Kuppeveld, F.J.M., Rossmann, M.G., 2018. Molecular basis for the acid-initiated uncoating of human enterovirus D68. *Proc. Natl. Acad. Sci.* 115, E12209–E12217. doi:10.1073/pnas.1803347115
- Liu, Y., Wang, C., Mueller, S., Paul, A. V., Wimmer, E., Jiang, P., 2010. Direct Interaction between Two Viral Proteins, the Nonstructural Protein 2CATPase and the Capsid Protein VP3, Is Required for Enterovirus Morphogenesis. *PLoS Pathog.* 6, 75–76. doi:10.1371/journal.ppat.1001066
- Logan D, Abu-Ghazaleh, R., Blakemore, W., Curry, S., Jackson, T., King, A., Lea, S., Lewis, R., Newman, J., Parry, N., Rowlands, D.J., Stuart, D., Fry, E.E., 1993. Structure of a major immunogenic site on foot-and-mouth disease virus. *Nature* 362, 566–568.
- Logan, G., Newman, J., Wright, C.F., Lasecka-Dykes, L., Haydon, D.T., Cottam, E.M., Tuthill, T.J., 2018. Deep Sequencing of Foot-and-Mouth Disease Virus Reveals RNA Sequences Involved in Genome Packaging. *J. Virol.* 92, 1–11. doi:10.1128/jvi.01159-17
- López-Argüello, S., Rincón, V., Rodríguez-Huete, A., Martínez-Salas, E., Belsham, G.J., Valbuena, A., Mateu, M.G., 2019. Thermostability of the Foot-and-Mouth Disease Virus Capsid Is Modulated by Lethal and Viability-Restoring Compensatory Amino Acid Substitutions. *J. Virol.* 93, 2293–2318. doi:10.1128/jvi.02293-18
- Loughran, G., Libbey, J.E., Uddowla, S., Scallan, M.F., Ryan, M.D., Fujinami, R.S., Rieder, E., Atkins, J.F., 2013. Theiler's murine encephalomyelitis virus contrasts with encephalomyocarditis and foot-and-mouth disease viruses in its functional utilization of the StopGo non-standard translation mechanism. *J. Gen. Virol.* 94, 348–353. doi:10.1099/vir.0.047571-0

- Luna, E., Rodríguez-Huete, A., Rincón, V., Mateo, R., Mateu, M.G., 2009. Systematic Study of the Genetic Response of a Variable Virus to the Introduction of Deleterious Mutations in a Functional Capsid Region. *J. Virol.* 83, 10140–10151. doi:10.1128/JVI.00903-09
- Luo, M., He, C., Toth, K.S., Zhang, C.X., Lipton, H.L., 1992. Three-dimensional structure of Theiler murine encephalomyelitis virus (BeAn strain). *Proc. Natl. Acad. Sci.* 89, 2409–2413. doi:10.1073/pnas.89.6.2409
- Luo, M., Toth, K.S., Zhou, L., Pritchard, A., Lipton, H.L., 1996. The Structure of a Highly Virulent Theiler's Murine Encephalomyelitis Virus (GDVII) and Implications for Determinants of Viral Persistence. *Virology* 220, 246–250. doi:10.1006/viro.1996.0309
- Luo, M., Vriend, G., Kamer, G., Minor, I., Arnold, E., Rossmann, M.G., Boege, U., Scraba, D.G., Duke, G.M., Palmenberg, A.C., 1987. The atomic structure of Mengo virus at 3.0 Å resolution. *Science* (80-.). 235, 182–191. doi:10.1126/science.3026048
- Lyu, K., Ding, J., Han, J., Zhang, Y., Wu, X., He, Y., Qin, C., Chen, R., 2014. Human Enterovirus 71 Uncoating Captured at Atomic Resolution. *J. Virol.* 88, 3114–3126. doi:10.1128/JVI.03029-13
- Ma, H.C., Liu, Y., Wang, C., Strauss, M., Rehage, N., Chen, Y.H., Altan-Bonnet, N., Hogle, J., Wimmer, E., Mueller, S., Paul, A. V., Jiang, P., 2014. An Interaction between Glutathione and the Capsid Is Required for the Morphogenesis of C-Cluster Enteroviruses. *PLoS Pathog.* 10, 1–17. doi:10.1371/journal.ppat.1004052
- Macejak, D.G., Sarnow, P., 1992. Association of Heat Shock Protein 70 with Enterovirus Capsid Precursor P1 in Infected Human Cells. *J. Virol.* 66, 1520–1527. doi:0022-538X/92/031520-08\$02.00/0
- Malik, N., Kotecha, A., Gold, S., Asfor, A., Ren, J., Huiskonen, J.T., Tuthill, T.J., Fry, E.E., Stuart, D.I., 2017. Structures of foot and mouth disease virus pentamers: Insight into capsid dissociation and unexpected pentamer reassociation. *PLoS Pathog.* 13, 1–15. doi:10.1371/journal.ppat.1006607
- Maree, F.F., Blignaut, B., de Beer, T.A.P., Rieder, E., 2013. Analysis of SAT Type Foot-And-Mouth Disease Virus Capsid Proteins and the Identification of Putative Amino Acid Residues Affecting Virus Stability. *PLoS One* 8, 1–12. doi:10.1371/journal.pone.0061612
- Marongiu, M., Pani, A., Corrias, M., Sau, M., La Colla, P., 1981. Poliovirus morphogenesis. I. Identification of 80S dissociable particles and evidence for the artifactual production of procapsids. *J. Virol.* 39, 341–347. doi:0022-538X/81/080341-07\$02.00/0
- Marsian, J., Fox, H., Bahar, M.W., Kotecha, A., Fry, E.E., Stuart, D.I., Macadam, A.J., Rowlands, D.J., Lomonosoff, G.P., 2017. Plant-made polio type 3 stabilized VLPs-A candidate synthetic polio vaccine. *Nat. Commun.* 8, 1–9. doi:10.1038/s41467-017-00090-w
- Martikainen, M., Salorinne, K., Lahtinen, T., Malola, S., Permi, P., Häkkinen, H., Marjomäki, V., 2015. Hydrophobic pocket targeting probes for enteroviruses. *Nanoscale* 7, 17457–17467. doi:10.1039/c5nr04139b
- Martino, T.A., Petric, M., Weingartl, H., Bergelson, J.M., Opavsky, M.A., Richardson, C.D., Modlin, J.F., Finberg, R.W., Kain, K.C., Willis, N., Gauntt, C.J., Liu, P.P., 2000. The coxsackie-adenovirus receptor (CAR) is used by The Coxsackie-Adenovirus Receptor (CAR) Is Used by Reference Strains and Clinical Isolates Representing All Six Serotypes

- of Coxsackievirus Group B and by Swine Vesicular Disease Virus. *Virology* 271, 99–108. doi:10.1006/viro.2000.0324
- Massova, I., Kollman, P.A., 1999. Computational Alanine Scanning To Probe Protein-Protein Interactions: A Novel Approach To Evaluate Binding Free Energies. *J. Am. Chem. Soc.* 121, 8133–8143. doi:10.1021/ja990935j
- Mateo, R., Diaz, A., Baranowski, E., Mateu, M.G., 2003. Complete Alanine Scanning of Intersubunit Interfaces in a Foot-and-Mouth Disease Virus Capsid Reveals Critical Contributions of Many Side Chains to Particle Stability and Viral Function. *J. Biol. Chem.* 278, 41019–41027. doi:10.1074/jbc.M304990200
- Mateo, R., Luna, E., Rincon, V., Mateu, M.G., 2008. Engineering Viable Foot-and-Mouth Disease Viruses with Increased Thermostability as a Step in the Development of Improved Vaccines. *J. Virol.* 82, 12232–12240. doi:10.1128/JVI.01553-08
- Mateu, M.G., 2017. The Foot-and-mouth Disease Virion: Structure and Function, in: Sobrino, F.S., Domingo, E. (Eds.), *Foot-and-Mouth Disease Virus: Current Research and Emerging Trends*. Caister Academic Press, Norfolk, UK, pp. 61–106. doi:10.21775/9781910190517.02
- Mateu, M.G., 2013. Assembly, stability and dynamics of virus capsids. *Arch. Biochem. Biophys.* 531, 65–79. doi:10.1016/j.abb.2012.10.015
- Mateu, M.G., 2011. Virus engineering: functionalization and stabilization. *Protein Eng. Des. Sel.* 24, 53–63. doi:10.1093/protein/gzq069
- Mateu, M.G., 2009. The capsid protein of human immunodeficiency virus: Intersubunit interactions during virus assembly. *FEBS J.* 276, 6098–6109. doi:10.1111/j.1742-4658.2009.07313.x
- Mateu, M.G., 1995. Antibody recognition of picornaviruses and escape from neutralization: a structural view. *Virus Res.* 38, 1–24. doi:10.1016/0168-1702(95)00048-8
- McCray, J., Werner, G., 1987. Different rhinovirus serotypes neutralized by antipeptide antibodies. *Nature* 329, 736–738.
- McCright, I.J., Tsunoda, I., Whitby, F.G., Fujinami, R.S., 1999. Theiler's Viruses with Mutations in Loop I of VP1 Lead to Altered Tropism and Pathogenesis. *J. Virol.* 73, 2814–2824.
- Mello, C., Aguayo, E., Rodriguez, M., Lee, G., Jordan, R., Cihlar, T., Birkus, G., 2014. Multiple classes of antiviral agents exhibit in vitro activity against human rhinovirus type C. *Antimicrob. Agents Chemother.* 58, 1546–1555. doi:10.1128/AAC.01746-13
- Meloen, R.H., Briare, J., Woortmeyer, R.J., van Zaane, D., 1983. The Main Antigenic Determinant Detected by Neutralizing Monoclonal Antibodies on the Intact Foot-and-Mouth Disease Virus Particle is Absent from Isolated VP1. *J. Gen. Virol.* 64, 1193–1198. doi:10.1099/0022-1317-64-5-1193
- Mendelsohn, C.L., Wimmer, E., Racaniello, V.R., 1989. Cellular Receptor for Poliovirus: Molecular Cloning, Nucleotide Sequence, and Expression of a New Member of the Immunoglobulin Superfamily. *Cell* 56, 855–865.
- Merilahti, P., Tauriainen, S., Susi, P., 2016. Human Parechovirus 1 Infection Occurs via α V β 1 Integrin. *PLoS One* 11, 1–17. doi:10.1371/journal.pone.0154769

- Miller, S.T., Hogle, J.M., Filman, D.J., 2001. Ab initio Phasing of High-symmetry Macromolecular Complexes: Successful Phasing of Authentic Poliovirus Data to 3.0 Å Resolution. *J. Mol. Biol.* 307, 499–512. doi:10.1006/jmbi.2001.4485
- Minor, P.D., 1990. Antigenic Structure of Picornaviruses, in: Racaniello, V.R. (Ed.), *Picornaviruses*. Springer Berlin Heidelberg, Berlin, Heidelberg, pp. 121–154. doi:10.1007/978-3-642-75602-3_5
- Monaghan, P., Gold, S., Simpson, J., Zhang, Z., Weinreb, P.H., Violette, S.M., Alexandersen, S., Jackson, T., 2005. The $\alpha\beta 6$ integrin receptor for Foot-and-mouth disease virus is expressed constitutively on the epithelial cells targeted in cattle. *J. Gen. Virol.* 86, 2769–2780. doi:10.1099/vir.0.81172-0
- Moreira, I.S., Fernandes, P.A., Ramos, M.J., 2007. Hot spots—A review of the protein – protein interface determinant amino-acid residues. *Proteins Struct. Funct. Bioinforma.* 68, 803–812. doi:10.1002/prot.21396
- Moreira, I.S., Koukos, P.I., Melo, R., Almeida, J.G., Preto, A.J., Schaarschmidt, J., Trellet, M., Gümüş, Z.H., Costa, J., Bonvin, Alexandre, M.J.J., 2017. SpotOn: High Accuracy Identification of Protein-Protein Interface Hot-Spots. *Sci. Rep.* 7, 1–11. doi:10.1038/s41598-017-08321-2
- Morris, G.M., Huey, R., Lindstrom, W., Sanner, M.F., Belew, R.K., Goodsell, D.S., Olson, A.J., 2009. AutoDock4 and AutoDockTools4: Automated Docking with Selective Receptor Flexibility. *J. Comput. Chem.* 30, 2785–2791. doi:10.1002/jcc.21256
- Morrow, J.K., Zhang, S., 2012. Computational Prediction of Hot Spot Residues. *Curr. Pharm. Des.* 18, 1255–1265. doi:10.2174/138161212799436412
- Moscufo, N., Simons, J., Chow, M., 1991. Myristoylation Is Important at Multiple Stages in Poliovirus Assembly. *J. Virol.* 65, 2372–2380.
- Muckelbauer, J., Kremer, M., Minor, I., Diana, G., Dutko, F., Groarke, J., Pevear, D., Rossmann, M., 1995. The structure of coxsackievirus B3 at 3.5 Å resolution. *Structure* 3, 653–667.
- Muehlenbachs, A., Bhatnagar, J., Zaki, S.R., 2015. Tissue tropism, pathology and pathogenesis of enterovirus infection. *J. Pathol.* 235, 217–228. doi:10.1002/path.4438
- Mullapudi, E., Nováček, J., Pálková, L., Kulich, P., Lindberg, A.M., van Kuppeveld, F.J.M., Plevka, P., 2016. Structure and Genome Release Mechanism of the Human Cardiovirus Saffold Virus 3. *J. Virol.* 90, 7628–7639. doi:10.1128/JVI.00746-16
- Murray, L., Luke, G.A., Ryan, M.D., Wileman, T., Knox, C., 2009. Amino acid substitutions within the 2C coding sequence of Theiler's Murine Encephalomyelitis virus alter virus growth and affect protein distribution. *Virus Res.* 144, 74–82. doi:10.1016/j.virusres.2009.04.001
- Muto, S., Miyoshi, H., Nishikawa, H., Nakashima, H., 2006. Novel recognition sequence of coxsackievirus 2A proteinase. *Biochem. Biophys. Res. Commun.* 348, 1436–1442. doi:10.1016/j.bbrc.2006.08.012
- Mutsvunguma, L.Z., Moetlhoa, B., Edkins, A.L., Luke, G.A., Blatch, G.L., Knox, C., 2011. Theiler's murine encephalomyelitis virus infection induces a redistribution of heat shock proteins 70 and 90 in BHK-21 cells, and is inhibited by novobiocin and geldanamycin. *Cell Stress Chaperones* 16, 505–515. doi:10.1007/s12192-011-0262-x

- Nedellec, P., Vicart, P., Laurent-Winter, C., Martinat, C., Prevost, M.C., Brahic, M., 1998. Interaction of Theiler's virus with intermediate filaments of infected cells. *J. Virol.* 72, 9553–9560.
- Neubauer, C., Frasel, L., Kuechler, E., Blaas, D., 1987. Mechanism of Entry of Human Rhinovirus 2 into HeLa Cells. *Virology* 158, 255–258. doi:10.1016/0042-6822(87)90264-9
- Newman, J., Asfor, A.S., Berryman, S., Jackson, T., Curry, S., Tuthill, T.J., 2017. The Cellular Chaperone Heat Shock Protein 90 Is Required for Foot-and-Mouth Disease Virus Capsid Precursor Processing and Assembly of Capsid Pentamers. *J. Virol.* 92, e01415-17. doi:10.1128/JVI.01415-17
- Nguyen, Y., Jesudhasan, P., Aguilera, E.R., Pfeiffer, J., 2019. Identification and Characterization of a Poliovirus Capsid Mutant with Enhanced Thermal Stability. *J. Virol.* 93, e01510-18. doi:10.1128/JVI.01510-18
- Nitayaphan, S., Toth, M.M., Roos, R.P., 1985. Neutralizing Monoclonal Antibodies to Theiler's Murine Encephalomyelitis Viruses. *J. Virol.* 53, 651–657.
- Nugent, C.I., Kirkegaard, K., 1995. RNA Binding Properties of Poliovirus Subviral Particles. *J. Virol.* 69, 13–22.
- Oberste, M.S., Maher, K., Kilpatrick, D.R., Pallansch, M.A., 1999. Molecular evolution of the human enteroviruses: correlation of serotype with VP1 sequence and application to picornavirus classification. *J. Virol.* 73, 1941–8.
- Ohara, Y., Senkowski, A., Fu, J., Klamann, L., Goodall, J., Toth, M., Roos, R.P., 1988. Trypsin-Sensitive Neutralization Site on VP1 of Theiler's Murine Encephalomyelitis virus. *J. Virol.* 62, 3527–3529.
- Oleszak, E.L., Chang, J.R., Friedman, H., Katsetos, C.D., Platsoucas, C.D., 2004. Theiler's Virus Infection: a Model for Multiple Sclerosis. *Society* 17, 174–207. doi:10.1128/CMR.17.1.174
- Olijve, L., Jennings, L., Walls, T., 2018. Human Parechovirus: an Increasingly Recognized Cause of Sepsis-Like Illness in Young Infants. *Clin. Microbiol. Rev.* 31, 1–17. doi:10.1128/CMR.00047-17
- Olson, N.H., Kolatkar, P.R., Oliveira, M.A., Cheng, R.H., Greve, J.M., McClelland, A., Baker, T.S., Rossmann, M.G., 1993. Structure of a human rhinovirus complexed with its receptor molecule. *Proc. Natl. Acad. Sci.* 90, 507–511. doi:10.1073/pnas.90.2.507
- Palmenberg, A.C., 1990. Proteolytic Processing of Picornaviral Polyprotein. *Annu. Rev. Microbiol.* 44, 603–623. doi:10.1146/annurev.mi.44.100190.003131
- Palmenberg, A.C., Parks, G.D., Hall, D.J., Ingraham, R.H., Seng, T.W., Pallai, P. V., 1992. Proteolytic processing of the cardioviral P2 region: primary 2A/2B cleavage in clone-derived precursors. *Virology* 190, 754–762. doi:10.1016/0042-6822(92)90913-a
- Panjwani, A., Strauss, M., Gold, S., Wenham, H., Jackson, T., Chou, J.J., Rowlands, D.J., Stonehouse, N.J., Hogle, J.M., Tuthill, T.J., 2014. Capsid Protein VP4 of Human Rhinovirus Induces Membrane Permeability by the Formation of a Size-Selective Multimeric Pore. *PLoS Pathog.* 10, 1–12. doi:10.1371/journal.ppat.1004294
- Papi, A., Contoli, M., 2011. Rhinovirus vaccination: The case against. *Eur. Respir. J.* 37, 5–7.

doi:10.1183/09031936.00145710

- Paton, D.J., Gubbins, S., King, D.P., 2018. Understanding the transmission of foot-and-mouth disease virus at different scales. *Curr. Opin. Virol.* 28, 85–91. doi:10.1016/j.coviro.2017.11.013
- Pavelko, K.D., Girtman, M.A., Mitsunaga, Y., Mendez-Fernandez, Y. V., Bell, M.P., Hansen, M.J., Allen, K.S., Rodriguez, M., Pease, L.R., 2011. Theiler's Murine Encephalomyelitis Virus as a Vaccine Candidate for Immunotherapy. *PLoS One* 6, 1–11. doi:10.1371/journal.pone.0020217
- Perilla, J.R., Hadden, J.A., Goh, B.C., Mayne, C.G., Schulten, K., 2016. All-Atom Molecular Dynamics of Virus Capsids as Drug Targets. *J. Phys. Chem. Lett.* 7, 1836–1844. doi:10.1021/acs.jpcclett.6b00517
- Pettigrew, D.M., Williams, D.T., Kerrigan, D., Evans, D.J., Lea, S.M., Bhella, D., 2006. Structural and Functional Insights into the Interaction of Echoviruses and Decay-accelerating Factor. *J. Biol. Chem.* 281, 5169–5177. doi:10.1074/jbc.M510362200
- Pevear, D.C., Tull, T.M., Seipel, M.E., Groarke, J.M., 1999. Activity of pleconaril against enteroviruses. *Antimicrob. Agents Chemother.* 43, 2109–2115.
- Pfeiffer, J.K., Kirkegaard, K., 2005. Increased Fidelity Reduces Poliovirus Fitness and Virulence under Selective Pressure in Mice. *PLoS Pathog.* 1, 0102–0110. doi:10.1371/journal.ppat.0010011
- Pfister, T., Egger, D., Bienz, K., 1995. Poliovirus subviral particles associated with progeny RNA in the replication complex. *J. Gen. Virol.* 76, 63–71. doi:10.1099/0022-1317-76-1-63
- Pfister, T., Pasamontes, L., Troxler, M., Egger, D., Bienz, K., 1992. Immunocytochemical Localization of Capsid-Related Particles in Subcellular Fractions of Poliovirus-Infected Cells. *Virology* 188, 676–684. doi:10.1016/0042-6822(92)90522-q
- Piccone, M.E., Zellner, M., Kumosinski, T.F., Mason, P.W., Grubman, M.J., 1995. Identification of the Active-Site Residues of the L Proteinase of Foot-and-Mouth Disease Virus. *J. Virol.* 69, 4950–4956.
- Pickl-Herk, A., Luque, D., Vives-Adrian, L., Querol-Audi, J., Garriga, D., Trus, B.L., Verdaguer, N., Blaas, D., Caston, J.R., 2013. Uncoating of common cold virus is preceded by RNA switching as determined by X-ray and cryo-EM analyses of the subviral A-particle. *Proc. Natl. Acad. Sci.* 110, 20063–20068. doi:10.1073/pnas.1312128110
- Plevka, P., Hafenstein, S., Harris, K.G., Cifuentes, J.O., Zhang, Y., Bowman, V.D., Chipman, P.R., Bator, C.M., Lin, F., Medof, M.E., Rossmann, M.G., 2010. Interaction of Decay-Accelerating Factor with Echovirus 7. *J. Virol.* 84, 12665–12674. doi:10.1128/jvi.00837-10
- Plevka, P., Lim, P.-Y., Perera, R., Cardoso, J., Suksatu, A., Kuhn, R.J., Rossmann, M.G., 2014. Neutralizing antibodies can initiate genome release from human enterovirus 71. *Proc. Natl. Acad. Sci.* 111, 2134–2139. doi:10.1073/pnas.1320624111
- Plevka, P., Perera, R., Yap, M.L., Cardoso, J., Kuhn, R.J., Rossmann, M.G., 2013. Structure of human enterovirus 71 in complex with a capsid-binding inhibitor. *Proc. Natl. Acad. Sci.* 110, 5463–5467. doi:10.1073/pnas.1222379110

- Pons-Salort, M., Parker, E.P.K., Grassly, N.C., 2015. The epidemiology of non-polio enteroviruses: recent advances and outstanding questions. *Curr. Opin. Infect. Dis.* 28, 479–487. doi:10.1097/QCO.0000000000000187
- Porta, C., Kotecha, A., Burman, A., Jackson, T., Ren, J., Loureiro, S., Jones, I.M., Fry, E.E., Stuart, D.I., Charleston, B., 2013. Rational Engineering of Recombinant Picornavirus Capsids to Produce Safe, Protective Vaccine Antigen. *PLoS Pathog.* 9, e1003255. doi:10.1371/journal.ppat.1003255
- Prchla, E., Kuechler, E., Blaas, D., Fuchs, R., 1994. Uncoating of human rhinovirus serotype 2 from late endosomes. *J. Virol.* 68, 3713–3723.
- Pritchard, A.E., Calenoff, M.A., Simpson, S., Jensen, K., Lipton, H.L., 1992. A single base deletion in the 5' noncoding region of Theiler's virus attenuates neurovirulence. *J. Virol.* 66, 1951–1958.
- Probst, C., Jecht, M., Gauss-Müller, V., 1999. Intrinsic Signals for the Assembly of Hepatitis A Virus Particles. *J. Biol. Chem.* 274, 4527–4531. doi:10.1074/jbc.274.8.4527
- Probst, C., Jecht, M., Gauss-Müller, V., 1998. Processing of Proteinase Precursors and Their Effect on Hepatitis A Virus Particle Formation. *J. Virol.* 72, 8013–8020.
- Putnak, J.R., Phillips, B. a, 1981. Differences between poliovirus empty capsids formed in vivo and those formed in vitro: a role for the morphopoietic factor. *J. Virol.* 40, 173–183.
- Qiao, Y., Xiong, Y., Gao, H., Zhu, X., Cheng, P., 2018. Protein-protein interface hot spots prediction based on a hybrid feature selection strategy. *BMC Bioinformatics* 19, 1–16. doi:10.1186/s12859-018-2009-5
- Quintero-Gil, C., Parra-Suescún, J., Lopez-Herrera, A., Orduz, S., 2017. In-silico design and molecular docking evaluation of peptides derivatives from bacteriocins and porcine beta defensin-2 as inhibitors of Hepatitis E virus capsid protein. *Virus Dis.* 28, 281–288. doi:10.1007/s13337-017-0383-7
- Radom, F., Pluckthun, A., Paci, E., 2018. Assessment of ab initio models of protein complexes by molecular dynamics. *PLoS Comput. Biol.* 14, 1–13. doi:10.1371/journal.pcbi.1006182
- Rajamani, D., Thiel, S., Vajda, S., Camacho, C.J., 2004. Anchor residues in protein-protein interactions. *Proc. Natl. Acad. Sci.* 101, 11287–11292. doi:10.1073/pnas.0401942101
- Rakers, C., Bermudez, M., Keller, B.G., Mortier, J., Wolber, G., 2015. Computational close up on protein–protein interactions: how to unravel the invisible using molecular dynamics simulations? *Wiley Interdiscip. Rev. Comput. Mol. Sci.* 5, 345–359. doi:10.1002/wcms.1222
- Reddi, H. V, Kumar, A.S.M., Kung, A.Y., Kallio, P.D., Schlitt, B.P., Lipton, H.L., 2004. Heparan Sulfate-Independent Infection Attenuates High-Neurovirulence GDVII Virus-Induced Encephalitis. *J. Virol.* 78, 8909–8916. doi:10.1128/JVI.78.16.8909-8916.2004
- Reddi, H. V, Lipton, H.L., 2002. Heparan Sulfate Mediates Infection of High-Neurovirulence Theiler's Viruses. *J. Virol.* 76, 8400–8407. doi:10.1128/JVI.76.16.8400–8407.2002
- Reddy, V.S., Giesing, H.A., Morton, R.T., Kumar, A., Post, C.B., Brooks, C.L., Johnson, J.E., 1998. Energetics of quasiequivalence: Computational analysis of protein- protein interactions in icosahedral viruses. *Biophys. J.* 74, 546–558. doi:10.1016/S0006-3495(98)77813-0

- Reeve, R., Borley, D.W., Maree, F.F., Upadhyaya, S., Lukhwareni, A., Esterhuysen, J.J., Harvey, W.T., Blignaut, B., Fry, E.E., Parida, S., Paton, D.J., Mahapatra, M., 2016. Tracking the Antigenic Evolution of Foot-and-Mouth Disease Virus. *PLoS One* 11, 1–17. doi:10.1371/journal.pone.0159360
- Reguera, J., Carreira, A., Rioloobos, L., Almendral, J.M., Mateu, M.G., 2004. Role of interfacial amino acid residues in assembly, stability, and conformation of a spherical virus capsid. *Proc. Natl. Acad. Sci.* 101, 2724–2729. doi:10.1073/pnas.0307748101
- Reguera, J., Grueso, E., Carreira, A., Sánchez-Martínez, C., Almendral, J.M., Mateu, M.G., 2005. Functional relevance of amino acid residues involved in interactions with ordered nucleic acid in a spherical virus. *J. Biol. Chem.* 280, 17969–17977. doi:10.1074/jbc.M500867200
- Ren, J., Wang, X., Hu, Z., Gao, Q., Sun, Y., Li, X., Porta, C., Walter, T.S., Gilbert, R.J., Zhao, Y., Axford, D., Williams, M., McAuley, K., Rowlands, D.J., Yin, W., Wang, J., Stuart, D.I., Rao, Z., Fry, E.E., 2013. Picornavirus uncoating intermediate captured in atomic detail. *Nat. Commun.* 4, 1–7. doi:10.1038/ncomms2889
- Ren, J., Wang, X., Zhu, L., Hu, Z., Gao, Q., Yang, P., Li, X., Wang, J., Shen, X., Fry, E.E., Rao, Z., Stuart, D.I., 2015. Structures of Coxsackievirus A16 Capsids with Native Antigenicity: Implications for Particle Expansion, Receptor Binding, and Immunogenicity. *J. Virol.* 89, 10500–10511. doi:10.1128/JVI.01102-15
- Reuter, G., Boros, A., Pankovics, P., 2011. Kobuviruses – a comprehensive review. *Rev. Med. Virol.* 21, 32–41. doi:10.1002/rmv.677
- Richardson, S.J., Morgan, N.G., 2018. Enteroviral infections in the pathogenesis of type 1 diabetes: new insights for therapeutic intervention. *Curr. Opin. Pharmacol.* 43, 11–19. doi:10.1016/j.coph.2018.07.006
- Rincón, V., Rodríguez-Huete, A., López-Argüello, S., Ibarra-Molero, B., Sanchez-Ruiz, J.M., Harmsen, M.M., Mateu, M.G., 2014. Identification of the Structural Basis of Thermal Lability of a Virus Provides a Rationale for Improved Vaccines. *Structure* 22, 1560–1570. doi:10.1016/j.str.2014.08.019
- Rincón, V., Rodríguez-Huete, A., Mateu, M.G., 2015. Different functional sensitivity to mutation at intersubunit interfaces involved in consecutive stages of foot-and-mouth disease virus assembly. *J. Gen. Virol.* 96, 2595–2606. doi:10.1099/vir.0.000187
- Robert, X., Gouet, P., 2014. Deciphering key features in protein structures with the new ENDscript server. *Nucleic Acids Res.* 42, 320–324. doi:10.1093/nar/gku316
- Roos, R.P., 2010. Pathogenesis of Theiler's murine encephalomyelitis virus-induced disease. *Clin. Exp. Neuroimmunol.* 1, 70–78. doi:10.1111/j.1759-1961.2010.00008.x
- Roos, R.P., Stein, S., Ohara, Y., Fu, J., Semler, B., 1989. Infectious cDNA Clones of the DA Strain of Theiler's Murine Encephalomyelitis Virus. *J. Virol.* 63, 5492–5496.
- Ross, C., Knox, C., Bishop Tastan, O., 2017. Interacting motif networks located in hotspots associated with RNA release are conserved in Enterovirus capsids. *FEBS Lett.* 591, 1687–1701. doi:10.1002/1873-3468.12663
- Ross, C., Upfold, N., Luke, G.A., Tastan, Ö., Knox, C., 2016. Subcellular localisation of Theiler's murine encephalomyelitis virus (TMEV) capsid subunit VP1 vis-à-vis host protein Hsp90. *Virus Res.* 222, 53–63. doi:10.1016/j.virusres.2016.06.003

- Ross, C.J., 2015. Prediction of interacting motifs within the protein subunits of picornavirus capsids. Rhodes University.
- Ross, C.J., Atilgan, A.R., Tastan Bishop, O., Atilgan, C., 2018. Unraveling the Motions behind Enterovirus 71 Uncoating. *Biophys. J.* 114, 822–838. doi:10.1016/j.bpj.2017.12.021
- Rossmann, M., Arnold, E., Erickson, J., Frankenberger, E., Griffith, J., Hecht, H., Johnson, J., Kamer, G., Luo, M., Mosser, A., Rueckert, R., Sherry, B., Vriend, G., 1985. Structure of a human common cold virus and functional relationship to other picornaviruses. *Nature* 317, 145–153. doi:10.1038/317145a0
- Rossmann, M.G., 1989. The canyon hypothesis. Hiding the host cell receptor attachment site on a viral surface from immune surveillance. *J. Biol. Chem.* 264, 14587–14590.
- Rossmann, M.G., Bella, J., Kolatkar, P.R., He, Y., Wimmer, E., Kuhn, R.J., Baker, T.S., 2000. Cell Recognition and Entry by Rhino- and Enteroviruses. *Virology* 269, 239–247. doi:10.1006/viro.2000.0258
- Rossmann, M.G., He, Y., Kuhn, R.J., 2002. Picornavirus-receptor interactions. *Trends Microbiol.* 10, 324–331. doi:S0966-842X(02)02383-1
- Rowlands, D.J., Sangar, D. V, Brown, F., 1975. A comparative chemical and serological study of the full and empty particles of foot-and-mouth disease virus. *J. Gen. Virol.* 26, 227–238. doi:10.1099/0022-1317-26-3-227
- Salisbury, A.M., Begon, M., Dove, W., Niklasson, B., Stewart, J.P., 2014. Ljungan virus is endemic in rodents in the UK. *Arch. Virol.* 159, 547–551. doi:10.1007/s00705-013-1731-6
- Sasaki, J., Taniguchi, K., 2003. The 5'-End Sequence of the Genome of Aichi Virus, a Picornavirus, Contains an Element Critical for Viral RNA Encapsidation. *J. Virol.* 77, 3542–3548. doi:10.1128/jvi.77.6.3542-3548.2003
- Sato, S., Zhang, L., Kim, J., Jakob, J., Grant, R.A., Wollmann, R., Roos, R.P., 1996. A Neutralization Site of DA Strain of Theiler's Murine Encephalomyelitis Virus Important for Disease Phenotype. *Virology* 226, 327–337. doi:10.1006/viro.1996.0660
- Schneider-Schaulies, J., 2000. Cellular receptors for viruses: Links to tropism and pathogenesis. *J. Gen. Virol.* 81, 1413–1429. doi:10.1099/0022-1317-81-6-1413
- Schrodinger, L., 2010. The PyMOL Molecular Graphics System, Version 1.7.2.1.
- Scott, K.A., Kotecha, A., Seago, J., Ren, J., Fry, E.E., Stuart, D.I., Charleston, B., Maree, F.F., 2017. SAT2 Foot-and-Mouth Disease Virus Structurally Modified for Increased Thermostability. *J. Virol.* 91, e02312-16. doi:10.1128/JVI.02312-16
- Scott, K.A., Maake, L., Botha, E., Theron, J., Maree, F.F., 2019. Inherent biophysical stability of foot-and-mouth disease SAT1, SAT2 and SAT3 viruses. *Virus Res.* 264, 45–55. doi:10.1016/j.virusres.2019.02.012
- Shafren, D.R., Dorahy, D.J., Ingham, R.A., Burns, G.F., Barry, R.D., 1997. Coxsackievirus A21 Binds to Decay-Accelerating Factor but Requires Intercellular Adhesion Molecule 1 for Cell Entry. *J. Virol.* 71, 4736–43.
- Shah, A.H., Lipton, H.L., 2002. Low-Neurovirulence Theiler's Viruses Use Sialic Acid Moieties on N-linked Oligosaccharide Structures for Attachment. *Virology* 304, 443–450.

doi:10.1006/viro.2002.1735

- Shakeel, S., Dykeman, E.C., White, S.J., Ora, A., Cockburn, J.J.B., Butcher, S.J., Stockley, P.G., Twarock, R., 2017. Genomic RNA folding mediates assembly of human parechovirus. *Nat. Commun.* 8, 1–11. doi:10.1038/s41467-016-0011-z
- Shakeel, S., Seitsonen, J.J.T., Kajander, T., Laurinmaki, P., Hyypia, T., Susi, P., Butcher, S.J., 2013. Structural and Functional Analysis of Coxsackievirus A9 Integrin $\alpha\beta 6$ Binding and Uncoating. *J. Virol.* 87, 3943–3951. doi:10.1128/jvi.02989-12
- Shakeel, S., Westerhuis, B.M., Domanska, A., Koning, R.I., Matadeen, R., Koster, A.J., Bakker, A.Q., Beaumont, T., Wolthers, K.C., Butcher, S.J., 2016. Multiple capsid-stabilizing interactions revealed in a high-resolution structure of an emerging picornavirus causing neonatal sepsis. *Nat. Commun.* 7, 1–8. doi:10.1038/ncomms11387
- Sherry, B., Mosser, A.G., Colonno, R.J., Rueckert, R.R., 1986. Use of Monoclonal Antibodies to Identify Four Neutralization Immunogens on a Common Cold Picornavirus, Human Rhinovirus 14. *J. Virol.* 57, 246–57.
- Shi, J., Huang, X., Liu, Q., Huang, Z., 2013. Identification of conserved neutralizing linear epitopes within the VP1 protein of coxsackievirus A16. *Vaccine* 31, 2130–2136. doi:10.1016/j.vaccine.2013.02.051
- Shingler, K.L., Cifuentes, J.O., Ashley, R.E., Makhov, A.M., Conway, J.F., Hafenstein, S., 2015. The Enterovirus 71 Procapsid Binds Neutralizing Antibodies and Rescues Virus Infection *In Vitro*. *J. Virol.* 89, 1900–1908. doi:10.1128/JVI.03098-14
- Sierra, N., Folio, C., Robert, X., Long, M., Guillon, C., Álvarez, G., 2018. Looking for Novel Capsid Protein Multimerization Inhibitors of Feline Immunodeficiency Virus. *Pharmaceuticals* 11, 1–14. doi:10.3390/ph11030067
- Smith, T.J., Kremer, M.J., Luo, M., Vriend, G., Arnold, E., Kamer, G., Rossmann, M.G., McKinlay, M.A., Diana, G.D., Otto, M.J., 1986. The site of attachment in human rhinovirus 14 for antiviral agents that inhibit uncoating. *Science* (80-.). 19, 1286–1293. doi:10.1126/science.3018924
- Smyth, M.S., Martin, J.H., 2002. Picornavirus uncoating. *J. Clin. Pathol. - Mol. Pathol.* 55, 214–219. doi:10.1136/mp.55.4.214
- Sommergruber, W., Zorn, M., Blaas, D., Fessl, F., Volkmann, P., Maurer-Fogy, I., Pallai, P., Merluzzi, V., Matteo, M., Skern, T., Kuechler, E., 1989. Polypeptide 2A of human rhinovirus type 2: Identification as a protease and characterization by mutational analysis. *Virology* 169, 68–77. doi:10.1016/0042-6822(89)90042-1
- Son, K.-N., Liang, Z., Lipton, H.L., 2015. Double-Stranded RNA Is Detected by Immunofluorescence Analysis in RNA and DNA Virus Infections, Including Those by Negative-Stranded RNA Viruses. *J. Virol.* 89, 9383–9392. doi:10.1128/jvi.01299-15
- Speir, R.W., 1962. pH and thermal stability of Mengo virus. *Virology* 17, 588–592. doi:10.1016/0042-6822(62)90160-5
- Stanway, G., 1990. Structure, function and evolution of picornaviruses. *J. Gen. Virol.* 71, 2483–2501. doi:10.1099/0022-1317-71-11-2483
- Stavrou, S., Feng, Z., Lemon, S.M., Roos, R.P., 2010. Different Strains of Theiler's Murine Encephalomyelitis Virus Antagonize Different Sites in the Type I Interferon Pathway. *J.*

- Virol. 84, 9181–9189. doi:10.1128/JVI.00603-10
- Steinbrecher, T., Zhu, C., Wang, L., Abel, R., Negron, C., Pearlman, D., Feyfant, E., Duan, J., Sherman, W., 2017. Predicting the Effect of Amino Acid Single-Point Mutations on Protein Stability - Large-Scale Validation of MD-Based Relative Free Energy Calculations. *J. Mol. Biol.* 429, 948–963. doi:10.1016/j.jmb.2016.12.007
- Stenfeldt, C., Diaz-San Segundo, F., de Los Santos, T., Rodriguez, L.L., Arzt, J., 2016. The Pathogenesis of Foot-and-Mouth Disease in Pigs. *Front. Vet. Sci.* 3, 1–12. doi:10.3389/fvets.2016.00041
- Sturbaut, S., Vrijssen, R., 2003. The morphogenesis of Theiler's murine encephalomyelitis virus is strain specific. *Arch. Virol.* 148, 1135–1153. doi:10.1007/s00705-003-0003-2
- Stobart, C.C., Nosek, J.M., Moore, M.L., 2017. Rhinovirus Biology, Antigenic Diversity, and Advancements in the Design of a Human Rhinovirus Vaccine. *Front. Microbiol.* 8, 1–8. doi:10.3389/fmicb.2017.02412
- Strauss, M., Schotte, L., Thys, B., Filman, D.J., Hogle, J.M., 2016. Five of Five VHHs Neutralizing Poliovirus Bind the Receptor-Binding Site. *J. Virol.* 90, 3496–3505. doi:10.1128/jvi.03017-15
- Su, R.T., Taylor, M.W., 1976. Morphogenesis of Picornaviruses: Characterization and Assembly of Bovine Enterovirus Subviral Particles. *J. Gen. Virol.* 30, 317–328. doi:10.1099/0022-1317-30-3-317
- Sukhwai, A., Sowdhamini, R., 2015. PPCheck: A Webserver for the Quantitative Analysis of Protein–Protein Interfaces and Prediction of Residue Hotspots. *Bioinform. Biol. Insights* 9, 141–151. doi:10.4137/BBLIS25928
- Sun, D., Chen, S., Cheng, A., Wang, M., 2016. Roles of the Picornaviral 3C Proteinase in the Viral Life Cycle and Host Cells. *Viruses* 8, 1–22. doi:10.3390/v8030082
- Suomalainen, M., Greber, U.F., 2013. Uncoating of non-enveloped viruses. *Curr. Opin. Virol.* 3, 27–33. doi:10.1016/j.coviro.2012.12.004
- Tan, C.W., Lai, J.K.F., Sam, I.C., Chan, Y.F., 2014. Recent developments in antiviral agents against enterovirus 71 infection. *J. Biomed. Sci.* 21, 1–11. doi:10.1186/1423-0127-21-14
- Tang, C., Loeliger, E., Kinde, I., Kyere, S., Mayo, K., Barklis, E., Sun, Y., Huang, M., Summers, M.F., 2003. Antiviral Inhibition of the HIV-1 capsid protein. *J. Mol. Biol.* 327, 1013–1020. doi:10.1016/S0022-2836(03)00289-4
- Ternois, F., Sticht, J., Duquerroy, S., Kräusslich, H.G., Rey, F.A., 2005. The HIV-1 capsid protein C-terminal domain in complex with a virus assembly inhibitor. *Nat. Struct. Mol. Biol.* 12, 678–682. doi:10.1038/nsmb967
- Thibaut, H.J., Lacroix, C., De Palma, A.M., Franco, D., Decramer, M., Neyts, J., 2016. Toward antiviral therapy/prophylaxis for rhinovirus-induced exacerbations of chronic obstructive pulmonary disease: challenges, opportunities, and strategies. *Rev. Med. Virol.* 26, 21–33. doi:10.1002/rmv.1856
- Thibaut, H.J., van der Linden, L., Jiang, P., Thys, B., Canela, M.D., Aguado, L., Rombaut, B., Wimmer, E., Paul, A., Pérez-Pérez, M.J., van Kuppeveld, F.J.M., Neyts, J., 2014. Binding of Glutathione to Enterovirus Capsids Is Essential for Virion Morphogenesis. *PLoS Pathog.* 10, 1–16. doi:10.1371/journal.ppat.1004039

- Tina, K.G., Bhadra, R., Srinivasan, N., 2007. PIC: Protein Interactions Calculator. *Nucleic Acids Res.* 35, W473–W476. doi:10.1093/nar/gkm423
- Toyoda, H., Nicklin, M.J.H., Murray, M.G., Anderson, C.W., Dunn, J.J., Studier, F.W., Wimmer, E., 1986. A second virus-encoded proteinase involved in proteolytic processing of poliovirus polyprotein. *Cell* 45, 761–770. doi:10.1016/0092-8674(86)90790-7
- Triantafilou, K., Triantafilou, M., Takada, Y., Fernandez, N., 2000. Human Parechovirus 1 Utilizes Integrins $\alpha\beta 3$ and $\alpha\beta 1$ as Receptors. *J. Virol.* 74, 5856–5862. doi:10.1128/jvi.74.13.5856-5862.2000
- Tsao, K.C., Chan, E.C., Chang, L.Y., Chang, P.Y., Huang, C.G., Chen, Y.P., Chang, S.C., Lin, T.Y., Sun, C.F., Shih, S.R., 2002. Responses of IgM for enterovirus 71 infection. *J. Med. Virol.* 68, 574–580. doi:10.1002/jmv.10233
- Tsunoda, I., Libbey, J.E., Fujinami, R.S., 2009. Theiler's murine encephalomyelitis virus attachment to the gastrointestinal tract is associated with sialic acid binding. *J. Neurovirol.* 15, 81–89. doi:10.1080/13550280802380563
- Tulloch, F., Luke, G.A., Denis Ryan, M., 2018. Problems in FMD Eradication: A Way Forward? *J. Vet. Med. Res.* 5, 1140.
- Tuncbag, N., Gursoy, A., Keskin, O., 2009a. Identification of computational hot spots in protein interfaces: combining solvent accessibility and inter-residue potentials improves the accuracy. *Bioinformatics* 25, 1513–1520. doi:10.1093/bioinformatics/btp240
- Tuncbag, N., Kar, G., Keskin, O., Gursoy, A., Nussinov, R., 2009b. A survey of available tools and web servers for analysis of protein-protein interactions and interfaces. *Brief. Bioinform.* 10, 217–232. doi:10.1093/bib/bbp001
- Tuncbag, N., Keskin, O., Gursoy, A., 2010. HotPoint: Hot spot prediction server for protein interfaces. *Nucleic Acids Res.* 38, W402–W406. doi:10.1093/nar/gkq323
- Tuthill, T.J., Groppe, E., Hogle, J.M., Rowlands, D.J., 2010. Picornaviruses. *Curr. Top. Microbiol. Immunol.* 343, 43–89. doi:10.1007/82_2010_37
- Tuthill, T.J., Harlos, K., Walter, T.S., Knowles, N.J., Groppe, E., David, J., Stuart, D.I., Fry, E.E., 2009. Equine Rhinitis A Virus and Its Low pH Empty Particle: Clues Towards an Aphthovirus Entry Mechanism? *PLoS Pathog.* 5, 1–11. doi:10.1371/journal.ppat.1000620
- Tuthill, T.J., Rowlands, D.J., Killington, R.A., 2007. Picornavirus entry. *Future Virol.* 2, 343–351. doi:10.2217/17460794.2.4.343
- Upfold, N., Ross, C., Bishop, Ö.T., Luke, G.A., Knox, C., 2018. The generation and characterisation of neutralising antibodies against the Theiler's murine encephalomyelitis virus (TMEV) GDVII capsid reveals the potential binding site of the host cell co-receptor, heparan sulfate. *Virus Res.* 244. doi:10.1016/j.virusres.2017.11.017
- van Dreumel, A.K., Michalski, W.P., McNabb, L.M., Shiell, B.J., Singanallur, N.B., Peck, G.R., 2015. Pan-Serotype Diagnostic for Foot-and-Mouth Disease Using the Consensus Antigen of Nonstructural Protein 3B. *J. Clin. Microbiol.* 53, 1797–1805. doi:10.1128/jcm.03491-14
- van Vlijmen, H.W.T., Curry, S., Schaefer, M., Karplus, M., 1998. Titration Calculations of Foot-and-mouth Disease Virus Capsids and their Stabilities as a Function of pH. *J. Mol. Biol.* 275, 295–308. doi:10.1006/jmbi.1997.1418

- Varrasso, A., Drummer, H.E., Huang, J.A., Stevenson, R.A., Ficorilli, N., Studdert, M.J., Hartley, C.A., 2001. Sequence Conservation and Antigenic Variation of the Structural Proteins of Equine Rhinitis A Virus. *J. Virol.* 75, 10550–10556. doi:10.1128/jvi.75.21.10550-10556.2001
- Veerasami, M., Singanallur, N.B., Thirumeni, N., Rana, S.K., Shanmugham, R., Ponselaran, S., Muthukrishnan, M., Villuppanoor, S.A., 2008. Serotyping of foot-and-mouth disease virus by antigen capture-ELISA using monoclonal antibodies and chicken IgY. *New Microbiol.* 31, 549–554.
- Veesler, D., Johnson, J.E., 2012. Virus Maturation. *Annu. Rev. Biophys.* 41, 473–496. doi:10.1146/annurev-biophys-042910-155407
- Venkataraman, S., Reddy, S.P., Loo, J., Idamakanti, N., Hallenbeck, P.L., Reddy, V.S., 2008. Structure of Seneca Valley Virus-001: An Oncolytic Picornavirus Representing a New Genus. *Structure* 16, 1555–1561. doi:10.1016/j.str.2008.07.013
- Verlinden, Y., Cuconati, A., Wimmer, E., Rombaut, B., 2000. Cell-free synthesis of poliovirus: 14S subunits are the key intermediates in the encapsidation of poliovirus RNA. *J. Gen. Virol.* 81, 2751–2754. doi:10.1099/0022-1317-81-11-2751
- Vlasak, M., Roivainen, M., Reithmayer, M., Goesler, I., Laine, P., Snyers, L., Hovi, T., Blaas, D., 2005. The Minor Receptor Group of Human Rhinovirus (HRV) Includes HRV23 and HRV25, but the Presence of a Lysine in the VP1 HI Loop Is Not Sufficient for Receptor Binding. *J. Virol.* 79, 7389–7395. doi:10.1128/jvi.79.12.7389-7395.2005
- Walter, T.S., Ren, J., Tuthill, T.J., Rowlands, D.J., Stuart, D.I., Fry, E.E., 2012. A plate-based high-throughput assay for virus stability and vaccine formulation. *J. Virol. Methods* 185, 166–170. doi:10.1016/j.jviromet.2012.06.014
- Waman, V.P., Kolekar, P.S., Kale, M.M., Kulkarni-Kale, U., 2014. Population Structure and Evolution of Rhinoviruses. *PLoS One* 9, e88981. doi:10.1371/journal.pone.0088981
- Wang, C., Jiang, P., Sand, C., Paul, A. V., Wimmer, E., 2012. Alanine Scanning of Poliovirus 2C ATPase Reveals New Genetic Evidence that Capsid Protein/2C ATPase Interactions Are Essential for Morphogenesis. *J. Virol.* 86, 9964–9975. doi:10.1128/jvi.00914-12
- Wang, G., Cao, R., Chen, R., Mo, L., Han, J., Wang, X., Xu, X., Jiang, T., Deng, Y.-Q., Lyu, K., Zhu, S.-Y., Qin, E.-D., Tang, R., Qin, C., 2013. Rational design of thermostable vaccines by engineered peptide-induced virus self-biomineralization under physiological conditions. *Proc. Natl. Acad. Sci.* 110, 7619–7624. doi:10.1073/pnas.1300233110
- Wang, H., Liu, C., Deng, L., 2018. Enhanced Prediction of Hot Spots at Protein-Protein Interfaces Using Extreme Gradient Boosting. *Sci. Rep.* 8, 1–13. doi:10.1038/s41598-018-32511-1
- Wang, L., Smith, D.L., 2005. Capsid structure and dynamics of a human rhinovirus probed by hydrogen exchange mass spectrometry. *Protein Sci.* 14, 1661–1672. doi:10.1110/ps.051390405
- Wang, T., Yu, B., Lin, L., Zhai, X., Han, Y., Qin, Y., Guo, Z., Wu, S., Zhong, X., Wang, Y., Tong, L., Zhang, F., Si, X., Zhao, W., Zhong, Z., 2012. A functional nuclear localization sequence in the VP1 capsid protein of coxsackievirus B3. *Virology* 433, 513–521. doi:10.1016/j.virol.2012.08.040
- Wang, X., Peng, W., Ren, J., Hu, Z., Xu, J., Lou, Z., Li, X., Yin, W., Shen, X., Porta, C.,

- Walter, T.S., Evans, G., Axford, D., Owen, R., Rowlands, D.J., Wang, J., Stuart, D.I., Fry, E.E., Rao, Z., 2012. A sensor-adaptor mechanism for enterovirus uncoating from structures of EV71. *Nat. Struct. Mol. Biol.* 19, 424–429. doi:10.1038/nsmb.2255
- Wang, X., Ren, J., Gao, Q., Hu, Z., Sun, Y., Li, X., Rowlands, D.J., Yin, W., Wang, J., Stuart, D.I., Rao, Z., Fry, E.E., 2015. Hepatitis A virus and the origins of picornaviruses. *Nature* 517, 85–88. doi:10.1038/nature13806
- Wang, X., Zhu, L., Dang, M., Hu, Z., Gao, Q., Yuan, S., Sun, Y., Zhang, B., Ren, J., Kotecha, A., Walter, T.S., Wang, J., Fry, E.E., Stuart, D.I., Rao, Z., 2017. Potent neutralization of hepatitis A virus reveals a receptor mimic mechanism and the receptor recognition site. *Proc. Natl. Acad. Sci.* 114, 770–775. doi:10.1073/pnas.1616502114
- Warwicker, J., 1992. Model for the differential stabilities of rhinovirus and poliovirus to mild acidic pH, based on electrostatics calculations. *J. Mol. Biol.* 223, 247–257. doi:10.1016/0022-2836(92)90729-4
- Warwicker, J., 1989. A theoretical study of the acidification of the rhinovirus capsid. *FEBS Lett.* 257, 403–407. doi:10.1016/0014-5793(89)81582-0
- Weber, F., Wagner, V., Rasmussen, S.B., Hartmann, R., Paludan, S.R., 2006. Double-Stranded RNA Is Produced by Positive-Strand RNA Viruses and DNA Viruses but Not in Detectable Amounts by Negative-Strand RNA Viruses. *J. Virol.* 80, 5059–5064. doi:10.1128/JVI.80.10.5059–5064.2006
- Wei, W., Guo, H., Chang, J., Yu, Y., Liu, G., Zhang, N., Willard, S.H., Zheng, S., Yu, X.F., 2016. ICAM-5/Telencephalin Is a Functional Entry Receptor for Enterovirus D68. *Cell Host Microbe* 20, 631–641. doi:10.1016/j.chom.2016.09.013
- Wen, A.M., Rambhia, P.H., French, R.H., Steinmetz, N.F., 2013. Design rules for nanomedical engineering: from physical virology to the applications of virus-based materials in medicine. *J. Biol. Phys.* 39, 301–325. doi:10.1007/s10867-013-9314-z
- Westerhuis, B.M., Benschop, K.S.M., Koen, G., Claassen, Y.B., Wagner, K., Bakker, A.Q., Wolthers, K.C., Beaumont, T., 2015. Human Memory B Cells Producing Potent Cross-Neutralizing Antibodies against Human Parechovirus: Implications for Prevalence, Treatment, and Diagnosis. *J. Virol.* 89, 7457–7464. doi:10.1128/JVI.01079-15
- Wu, C.N., Lin, Y.C., Fann, C., Liao, N.S., Shih, S.R., Ho, M.S., 2002. Protection against lethal enterovirus 71 infection in newborn mice by passive immunization with subunit VP1 vaccines and inactivated virus. *Vaccine* 20, 895–904. doi:10.1016/S0264-410X(01)00385-1
- Wychowski, C., van der Werf, S., Girard, M., 1985. Nuclear localization of poliovirus capsid polypeptide VP1 expressed as a fusion protein with SV40-VP1. *Gene* 37, 63–71. doi:10.1016/0378-1119(85)90258-6
- Xia, J., Zhao, X., Song, J., Huang, D., 2010. APIS: accurate prediction of hot spots in protein interfaces by combining protrusion index with solvent accessibility. *BMC Bioinformatics* 11, 1–14. doi:10.1186/1471-2105-11-174
- Xia, Y., Chu, W., Qi, Q., Xun, L., 2015. New insights into the QuikChange™ process guide the use of Phusion DNA polymerase for site-directed mutagenesis. *Nucleic Acids Res.* 43, e12. doi:10.1093/nar/gku1189
- Xia, Y., Xun, L., 2017. Revised Mechanism and Improved Efficiency of the QuikChange Site-

- Directed Mutagenesis Method. *Methods Mol. Biol.* 1498, 367–374. doi:10.1007/978-1-4939-6472-7_25
- Xue, L.C., Dobbs, D., Bonvin, A.M.J.J., Honavar, V., 2015. Computational prediction of protein interfaces: A review of data driven methods. *FEBS Lett.* 589, 3516–3526. doi:10.1016/j.febslet.2015.10.003
- Yafal, A.G., Palma, E.L., 1979. Morphogenesis of foot-and-mouth disease virus. I. Role of procapsids as virion Precursors. *J. Virol.* 30, 643–649.
- Yamayoshi, S., Ohka, S., Fujii, K., Koike, S., 2013. Functional Comparison of SCARB2 and PSGL1 as Receptors for Enterovirus 71. *J. Virol.* 87, 3335–3347. doi:10.1128/jvi.02070-12
- Yang, C., Deng, C., Wan, J., Zhu, L., Leng, Q., 2011. Neutralizing antibody response in the patients with hand, foot and mouth disease to enterovirus 71 and its clinical implications. *Virol. J.* 8, 306. doi:10.1186/1743-422X-8-306
- Yang, M., Goolia, M., Xu, W., Bittner, H., Clavijo, A., 2013. Development of a quick and simple detection methodology for foot-and-mouth disease virus serotypes O, A and Asia 1 using a generic RapidAssay Device. *Virol. J.* 10, 1–13. doi:10.1186/1743-422X-10-125
- Yang, X., Cheng, A., Wang, M., Jia, R., Sun, K., Pan, K., Yang, Q., Wu, Y., Zhu, D., Chen, S., Liu, M., Zhao, X.X., Chen, X., 2017. Structures and corresponding functions of five types of picornaviral 2A proteins. *Front. Microbiol.* 8, 1–14. doi:10.3389/fmicb.2017.01373
- Ye, X., Fan, C., Ku, Z., Zuo, T., Kong, L., Zhang, C., Shi, J., Liu, Q., Chen, T., Zhang, Y., Jiang, W., Zhang, L., Huang, Z., Cong, Y., 2016. Structural Basis for Recognition of Human Enterovirus 71 by a Bivalent Broadly Neutralizing Monoclonal Antibody. *PLoS Pathog.* 12, 1–21. doi:10.1371/journal.ppat.1005454
- Yi, E.J., Shin, Y.J., Kim, J.H., Kim, T.G., Chang, S.Y., 2017. Enterovirus 71 infection and vaccines. *Clin. Exp. Vaccine Res.* 6, 4–14. doi:10.7774/cevr.2017.6.1.4
- Yogurtcu, O.N., Erdemli, S.B., Nussinov, R., Turkay, M., Keskin, O., 2008. Restricted Mobility of Conserved Residues in Protein-Protein Interfaces in Molecular Simulations. *Biophys. J.* 94, 3475–3485. doi:10.1529/biophysj.107.114835
- Yuan, H., Li, P., Ma, X., Lu, Z., Sun, P., Bai, X., Zhang, Jing, Bao, H., Cao, Y., Li, D., Fu, Y., Chen, Y., Bai, Q., Zhang, Jie, Liu, Z., 2017. The pH stability of foot-and-mouth disease virus. *Virol. J.* 14, 1–10. doi:10.1186/s12985-017-0897-z
- Yuan, S., Li, G., Wang, Ying, Gao, Q., Wang, Yizhuo, Cui, R., Altmeyer, R., Zou, G., 2016. Identification of Positively Charged Residues in Enterovirus 71 Capsid Protein VP1 Essential for Production of Infectious Particles. *J. Virol.* 90, 741–752. doi:10.1128/jvi.02482-15
- Zell, R., 2018. Picornaviridae - the ever-growing virus family. *Arch. Virol.* 163, 299–317. doi:10.1007/s00705-017-3614-8
- Zell, R., Delwart, E., Gorbalenya, A.E., Hovi, T., King, A.M.Q., Knowles, N.J., Lindberg, A.M., Pallansch, M.A., Palmenberg, A.C., Reuter, G., Simmonds, P., Skern, T., Stanway, G., Yamashita, T., 2017. ICTV Virus Taxonomy Profile: Picornaviridae. *J. Gen. Virol.* 98, 2421–2422. doi:10.1099/jgv.0.000911

- Zhang, X., Zhu, Z., Yang, F., Cao, W., Tian, H., Zhang, K., Zheng, H., Liu, X., 2018. Review of Seneca Valley Virus: A Call for Increased Surveillance and Research. *Front. Microbiol.* 9, 1–8. doi:10.3389/fmicb.2018.00940
- Zhang, Y.X., Huang, Y.M., Li, Q.J., Li, X.Y., Zhou, Y.D., Guo, F., Zhou, J.M., Cen, S., 2017. A highly conserved amino acid in VP1 regulates maturation of enterovirus 71. *PLoS Pathog.* 13, 1–23. doi:10.1371/journal.ppat.1006625
- Zhao, X., Zhang, G., Liu, S., Chen, X., Peng, R., Dai, L., Qu, X., Li, S., Song, H., Gao, Z., Yuan, P., Liu, Z., Li, C., Shang, Z., Li, Y., Zhang, M., Qi, J., Wang, H., Du, N., Wu, Y., Bi, Y., Gao, S., Shi, Y., Yan, J., Zhang, Y., Xie, Z., Wei, W., Gao, G.F., 2019. Human Neonatal Fc Receptor Is the Cellular Uncoating Receptor for Enterovirus B. *Cell* 177, 1553–1565. doi:10.1016/j.cell.2019.04.035
- Zheng, H., Wang, J., Li, B., Guo, L., Li, Heng, Song, J., Yang, Z., Li, Hongzhe, Fan, H., Huang, X., Long, H., Cheng, C., Chu, M., He, Z., Yu, W., Li, J., Gao, Y., Ning, R., Li, N., Yang, J., Wu, Q., Shi, H., Sun, M., Liu, L., 2018. A Novel Neutralizing Antibody Specific to the DE Loop of VP1 Can Inhibit EV-D68 Infection in Mice. *J. Immunol.* 201, 2557–2569. doi:10.4049/jimmunol.1800655
- Zheng, Q., Zhu, R., Xu, L., He, M., Yan, X., Liu, D., Yin, Z., Wu, Y., Li, Y., Yang, L., Hou, W., Li, Shuxuan, Li, Zizhen, Chen, Z., Li, Zhihai, Yu, H., Gu, Y., Zhang, J., Baker, T.S., Zhou, Z.H., Graham, B.S., Cheng, T., Li, Shaowei, Xia, N., 2019. Atomic structures of enterovirus D68 in complex with two monoclonal antibodies define distinct mechanisms of viral neutralization. *Nat. Microbiol.* 4, 124–133. doi:10.1038/s41564-018-0275-7
- Zhou, D., Zhao, Y., Kotecha, A., Fry, E.E., Kelly, J.T., Wang, X., Rao, Z., Rowlands, D.J., Ren, J., Stuart, D.I., 2019. Unexpected mode of engagement between enterovirus 71 and its receptor SCARB2. *Nat. Microbiol. Lett.* 4, 414–419. doi:10.1038/s41564-018-0319-z
- Zhou, L., Luo, Y., Wu, Y., Tsao, J., Luo, M., 2000. Sialylation of the host receptor may modulate entry of demyelinating persistent Theiler's virus. *J Virol* 74, 1477–1485. doi:10.1128/JVI.74.3.1477-1485.2000
- Zhu, L., Wang, X., Ren, J., Porta, C., Wenham, H., Ekström, J.O., Panjwani, A., Knowles, N.J., Kotecha, A., Siebert, C.A., Lindberg, A.M., Fry, E.E., Rao, Z., Tuthill, T.J., Stuart, D.I., 2015. Structure of Ljungan virus provides insight into genome packaging of this picornavirus. *Nat. Commun.* 6, 1–9. doi:10.1038/ncomms9316
- Zhu, L., Xu, K., Wang, N., Cao, L., Wu, J., Gao, Q., Fry, E.E., Stuart, D.I., Rao, Z., Wang, J., Wang, X., 2018. Neutralization Mechanisms of Two Highly Potent Antibodies against Human Enterovirus 71. *MBio* 9, e01013-18. doi:10.1128/mBio.01013-18.
- Zhu, L., Zhang, X., 2015. Hepatitis A virus exhibits a structure unique among picornaviruses. *Protein Cell* 6, 79–80. doi:10.1007/s13238-014-0103-7
- Zhu, S., Ge, X.N., Gong, X.W., Guo, X., Chen, Y.H., Yang, H.C., 2011. Alteration of encephalomyocarditis virus pathogenicity due to a mutation at position 100 of VP1. *Sci. China Life Sci.* 54, 535–543. doi:10.1007/s11427-011-4172-z
- Zhu, X., Mitchell, J.C., 2011. KFC2: A knowledge-based hot spot prediction method based on interface solvation, atomic density, and plasticity features. *Proteins* 79, 2671–2683. doi:10.1002/prot.23094
- Zurbriggen, A., Fujinami, R.S., 1989. A neutralization-resistant Theiler's virus variant

produces an altered disease pattern in the mouse central nervous system. *J. Virol.* 63, 1505–1513.

Zurbriggen, A., Hogle, J.M., Fujinami, R.S., 1989. Alteration of Amino Acid 101 Within Capsid Protein VP-1 Changes the Pathogenicity of Theiler's Murine Encephalomyelitis Virus. *J. Exp. Med.* 170, 2037–2049. doi:10.1084/jem.170.6.2037

Supplementary Data

Table S1. Identification of hot spot residues within intraprotomer interfaces of the TMEV capsid.

Protein	Residue	KFC2	ROBETTA	Hot Region	PredHS	PPCheck
<i>VP1-VP2 Interface</i>						
VP1	E6					
	R94					
	W95					
	V96					
	Y124					
	W202					
	F203					
	N204					
	W206					
	F215					
	R249					
	L252					
	F253					
	T260					
VP2	E133					
	F134					
	Y135					
	T136					
	E146					
	R168					
	Y169					
	F175					
	F176					
	M178					
	Q185					
	Y189					
V211						
<i>VP1-VP3 Interface</i>						
VP1	T31					
	V33					
	F36					
	Y114					
	C118					
	F119					
	F122					
	F187					
	V189					
	R239					
	V245					
	F246					
	F254					
	W256					
	I272					
VP3	I25					
	F41					

L44					
L47					
V98					
R100					
F102					
R106					
L112					
V114					
F159					
N160					
F161					
D217					
W229					
Q232					
<i>VP1-VP4 Interface</i>					
VP1	K9				
	D128				
	K241				
<i>VP2-VP3 Interface</i>					
VP2	W184				
	Q185				
	R197				
	L230				
	S231				
VP3	F53				
	F115				
	T116				
	L209				
<i>VP2-VP4 Interface</i>					
VP2	R32				
	L33				
	Y36				
<i>VP3-VP4 Interface</i>					
No residues predicted to be important for stability of interface					

Table S1. Footnotes:

The TMEV protomer was submitted to five hotspot prediction tools for analysis. Grey blocks indicate where a program has predicted a residue to be a hotspot. Only hotspots that were detected by two or more programs are shown, as a residue was only considered to be a hotspot if it was identified by more than one prediction model.

Table S2. Identification of hot spot residues within interprotomer interfaces of the TMEV capsid.

Protein	Residue	KFC2	ROBETTA	Hot Region	PredHS	PPCheck
<i>VP1-VP1</i>						
VP1	L160					
	I161					
	Y163					
	W176					
	V178					
	M45					
	L108					
<i>VP1-VP2</i>						
VP1	V24					
<i>VP1-VP3</i>						
VP1	Q30					
	F35					
	P153					
	R171					
	P194					
	VP3	Q11				
C13						
S16						
N103						
Q104						
Q173						
I181						
M222						
<i>VP1-VP4</i>						
VP4	Y29					
	L35					
<i>VP2-VP3</i>						
VP2	S47					
	C48					
	Y104					
	L105					
VP3	P131					
	F165					
	I166					
	P168					
<i>VP3-VP3</i>						
No residues predicted to be important for stability of interface						
<i>VP3-VP4</i>						
VP4	Y25					
	Y29					
<i>VP4-VP4</i>						
VP4	G18					
	S26					

Table S2. Footnotes:

A complex of two TMEV protomers was submitted to five hot spot prediction tools for analysis. Grey blocks indicate where a program has predicted a residue to be a hot spot. Only hot spots that were detected by two or more programs are shown, as a residue was only considered to be a hot spot if it was identified by more than one prediction model.

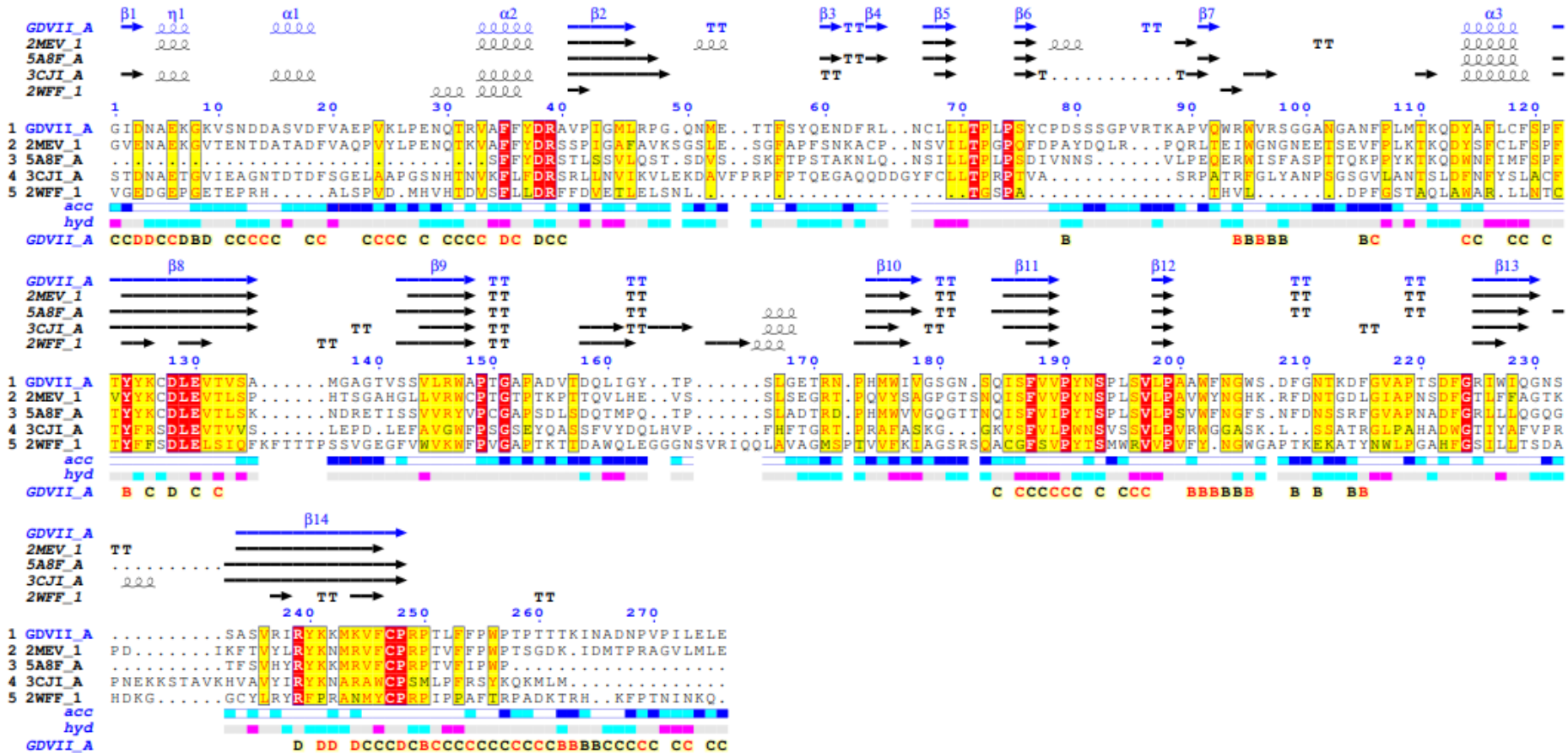


Figure S1. Sequence and structure-based alignment of TMEV VP1 and cardiovascular, senecavirus and aphthovirus representatives. The TMEV protomer structure was submitted to ENDscript 2 and chain A corresponding to VP1 was selected for analysis. A subset of structures for comparison were selected from the list generated by ENDscript. These structures include: cardiovasculars MEV and SAFV (PDB: 2MEV, 5A8F); senecavirus SVV-1 (PDB: 3CJI) and the aphthovirus ERAV (PDB: 2WFF). Enterovirus structures were not selected by ENDscript and so a sequence alignment was performed using the ESript webserver linked to ENDscript in the supplementary figure below.

```

                                     1      10      20
GDVII_A                               .....GIDNAEKGVSNDDASVDFVAEPVKLPEN
2MEV_1|PDBID|CHAIN|SEQUENCE         .....GVENAEEKGVTTENTDATADFVAQPVYLPEN
5A8F_A|PDBID|CHAIN|SEQUENCE         .....
3CJI_A|PDBID|CHAIN|SEQUENCE         .....STDNAETGVIEAGNTDDFSSELAAPGSN
1FMD_1|PDBID|CHAIN|SEQUENCE         .....TT...TTGESADPVTTTVENYGGGETQVQRRH
5ACA_1|PDBID|CHAIN|SEQUENCE         .....TT...SSGEGADVTTDPSTHGGAVTEKKRV
2XBO_1|PDBID|CHAIN|SEQUENCE         .....VTNVGEDGEPGETEPRHALSPVDMHV
3VBF_A|PDBID|CHAIN|SEQUENCE         GDRVADVIESSIGDSVSR.....ALTH..ALPAPTGQNTQVSSHRLDTGKVPALQAAEIGASSNASDESMIETRCVLSHSTA
1R08_1|PDBID|CHAIN|SEQUENCE         .....GLGDELEEVIVEKTKQTVASISSGPKHTQKVPILTANETGATMPVLPDSIETRTTYMHFNCS
1FPN_1|PDBID|CHAIN|SEQUENCE         .....NPVENYIDEVLNEVLVVPNINSSNPSTTSNSAPALDAAETGHTSSVQPEDVIETRYVQTSQTRD
1RHI_1|PDBID|CHAIN|SEQUENCE         .....GLSDELEEVIVEKTKQTLASVSSGPKHTQSVPALANETGATLPTRPSPDNVETRTTYMHFNCS
2PLV_1|PDBID|CHAIN|SEQUENCE         .....GLGQMLSESMIDNTVSSTVGAATSRDALPNTASGPTHSKEIPALTAVETGATNPLVPSDVTQTRHVVQHRSR
1D4M_1|PDBID|CHAIN|SEQUENCE         .....GD.....VEEA..IERAVVHVADTMRSGPNSASVPALTAVETGHTSQVTPSDTMTQTRHVKNYHSR
4WM7_A|PDBID|CHAIN|SEQUENCE         .....V..ESIIKTATDTVKSEINAELGVVPSLNAVETGATSNTPEPEAIQTRTVINQHGVS
consensus>70                           .....e.....e

```

```

                                     30      40      50      60      70      80      90      100
GDVII_A                               QTRVAFYDRAVPYIGMLRPGQNMET.T.TFSYQE.NDFRLNCLLTLPLPSYCPDSSSGPVRTKAPVQWRWVRSGL..ANGANFPLM
2MEV_1|PDBID|CHAIN|SEQUENCE         QTKVAFYDRSSPIGAFAVKSGSL...ESGFAPFS..NKACPNVILTPGPQFD...PAYDQLRPQRRLTEIWGNNGNEETSEVFPPLK
5A8F_A|PDBID|CHAIN|SEQUENCE         ...SFYDRSTLSSVLQSTSDVS...S.KFTPST.AKNLQNSILTLPLPSDIVN...NSVLPEQERWISFAS.PTTQKPPYK
3CJI_A|PDBID|CHAIN|SEQUENCE         HTNVKFLFDKRLNVIKVKLEKDAVFPFRF.PTQEGA..QQDDGYFCLTLPRPTVAS...RPATRFGLYA.NPSGSGVLAN
1FMD_1|PDBID|CHAIN|SEQUENCE         HTDVAFVLDKRFVKTVS...DNQHTLDVMQA...
5ACA_1|PDBID|CHAIN|SEQUENCE         HTDVAFVMDKRFTHV.LTN...RTAFALDMDT...
2XBO_1|PDBID|CHAIN|SEQUENCE         HTDVSFLLDRFFDVEITLNSN...LTGSPATHVLDPFGS...
3VBF_A|PDBID|CHAIN|SEQUENCE         ETLDSKFSRAGLVGEIDLPL...KGTI.NPNGYANWDIDIT...
1R08_1|PDBID|CHAIN|SEQUENCE         ETDVECFLGRAACVHVEIQNKDA...T.GIDNHR..EAKLFNDWKINLS...
1FPN_1|PDBID|CHAIN|SEQUENCE         EMSLESFLGRSGCIHESKLEVTL...ANY..NKENFTVWAINLQ...
1RHI_1|PDBID|CHAIN|SEQUENCE         ETDVESFLGRAACVHVEIKNKNA...A.GLDNHR..KEGLFNDWKINLS...
2PLV_1|PDBID|CHAIN|SEQUENCE         ESSIESFARGACVTIMTVDNPAS...T..TN..KDKLFAVWKITYK...
1D4M_1|PDBID|CHAIN|SEQUENCE         ESTVENFLGRSACVMEYKTTD...ND..VNKKFVAWPIINTK...
4WM7_A|PDBID|CHAIN|SEQUENCE         ETLVENFLGRAALVSKSFEYKNH...A.S..SSAGTHKNFFKWTINTK...
consensus>70                           .t.v.f.R.v

```

```

                                     110     120     130     140     150     160     170
GDVII_A                               TKQDYAFCLFSPFTYYKCDLEVTVSAMGA.....GTVS..SVLRWAPT GAPADVTDQLI.....GYTPSLGETRNPHMWI
2MEV_1|PDBID|CHAIN|SEQUENCE         TKQDYSFCLFSPFTYYKCDLEVTLSPHTS.....GAHG..LLVRWCPGTGPTKPTTQVL.....HEVSSLSEGRTPQVYS
5A8F_A|PDBID|CHAIN|SEQUENCE         TKQDWNFIMFSPFTYYKCDLEVTLSKNDR.....ETIS..FVVRVPC GAPSDLSQTM.....PQTPSLADTRDPHMWV
3CJI_A|PDBID|CHAIN|SEQUENCE         TSLDFNFYSLACFTYFRSDLEVTVVSLEP.....DLE..FVAVGFPSGSEYQASSFVY.....DQLHVPFHFTGRTPRAFA
1FMD_1|PDBID|CHAIN|SEQUENCE         HKDNIYGALLRAATYFYFCDLEIAVHTH.....GKLTWVPNGAPVSA.....LNNTTNPTAYH
5ACA_1|PDBID|CHAIN|SEQUENCE         NEKTLYGALLRAATYFYFCDLEIACLGE.....HERVW..WQPN GAPRTT.....TLRDNPMVFS
2XBO_1|PDBID|CHAIN|SEQUENCE         TAQLAWARLNTCTYFFSDELSIQFKFTTTP....SSVGEFGF..VWVKWFPV GAPTKTTDAWQLEGGGNSVRIQQLAVAGMSPTVVF
3VBF_A|PDBID|CHAIN|SEQUENCE         .GYAQRKRKVELFTYMRFOAEFTVACTP.....TGEVVPQL..LQYMFVPP GAPKPSDR.....ESLAWQATNPSVVF
1R08_1|PDBID|CHAIN|SEQUENCE         .SLVQRKRKLELFTYVRFDSYTYILATASQP..DS..ANYSSNLV..VQAMVYPP GAPNPKEW.....DDYTQWSSASNPSVVF
1FPN_1|PDBID|CHAIN|SEQUENCE         .EMAQIRRKLELFTYVRFDSYTYILATASQP..EA..SSYSSNLT..VQAMVYPP GAPNPKEW.....DDYTQWSSASNPSVVF
1RHI_1|PDBID|CHAIN|SEQUENCE         .SLVQRKRKLELFTYVRFDSYTYILATASQP..EA..SSYSSNLT..VQAMVYPP GAPNPKEW.....DDYTQWSSASNPSVVF
2PLV_1|PDBID|CHAIN|SEQUENCE         .DTVQRKRKLELFTYVRFDSYTYILATASQP..E..TNNGHALNQV..YQIMVYPP GAPVPEKW.....DDYTQWSSASNPSIFV
1D4M_1|PDBID|CHAIN|SEQUENCE         .QMVQRKRKLELFTYVRFDSYTYILATASQP..PGTTLAQDMPVLT..HQIMVYPP GAPVPEKW.....DDYTQWSSASNPSIFV
4WM7_A|PDBID|CHAIN|SEQUENCE         .SFVQRKRKLELFTYVRFDSYTYILATASQP..LQAMVYPP GAPVPEKW.....DDYTQWSSASNPSIFV
consensus>70                           .....ftY...D.E.t.....P.Gap.....np.vf.)

```



```

180          190          200          210          220          230
GDVII_A      VGSGLNSQISFVVPYNSPLSVLPAAWFNGWSDF.....GNTKDF.....GVAPTSDFGRIWIQG....
2MEV_1|PDBID|CHAIN|SEQUENCE  AGPGT.SNQISFVVPYNSPLSVLPAVWYNGHKRF.....DNTGDL.....GIAPNSDFGTLFFAGTK...
5A8F_A|PDBID|CHAIN|SEQUENCE  VGQGT.TNQISFVVPYTSPLSVLPSVWFNGFSNF.....DNSSRF.....GVAPNADFGRLLLQG...
3CJI_A|PDBID|CHAIN|SEQUENCE  SK...GGKVSFVLPWNSVSVLPPVR.WGGASKL.....S.SATR.....GIPAHADWGTIYAFVVRPNE
1FMD_1|PDBID|CHAIN|SEQUENCE  ....KGPVTRLALPYTAPHRVLATA.YTGT.....TTYTASARGDLAHLTTTHAA...HLPTSFNFGAVKAE....
5ACA_1|PDBID|CHAIN|SEQUENCE  ....HNNVTRFALPYTAPHRLLSTR.YNGE.....CKYTQQSTAIRGDRAVLAAKYANTKHLKLPSTFNF...YVT....
2XB0_1|PDBID|CHAIN|SEQUENCE  KIAGSRSQACGFSVPYTSMWRVVPVF.YNGWGAP.....TKEKATY.....NWLPGAHFGSILLTSDA...
3VBF_A|PDBID|CHAIN|SEQUENCE  KLS...DPPAQVSVPEMSPA.SAYQWF.YDGYPTFG...EHKQEKDLEY.....GAMPNNMGTFSVRTVGT...
1R08_1|PDBID|CHAIN|SEQUENCE  KVG...DTSRFSVPYVGLA.SAYNCF.YDGYSHD.....DAETQY.....GITVLNMGSMFRIVNEHD
1FPN_1|PDBID|CHAIN|SEQUENCE  QHG...QAYPRFSLPFLSVA.SAYYMF.YDGYDE.....QDQNY.....GTANTNMGSLCSRIVTEKH
1RHI_1|PDBID|CHAIN|SEQUENCE  KVG...ETSRFSVPYVGLA.SAYNCF.YDGYSHD.....DPDTPY.....GITVLNMGSMFRIVNEHD
2PLV_1|PDBID|CHAIN|SEQUENCE  TYG...TAPARISVPYVGLA.SAYSHF.YDGFYSKVPLKDQSAALGDSL.Y.....GAASLNDFGILAVRVVNDHN
1D4M_1|PDBID|CHAIN|SEQUENCE  TEG...NAPARMSLPYFISIG.NAYSNF.YDGSNF.....DQRGSY.....GYNTLNLGHIYVRHVSQSS
4WM7_A|PDBID|CHAIN|SEQUENCE  KIS...DPPARMTLPEMCMIN.SAYSVF.YDGFAGF.....EKNGLY.....GINPADTIGNLKYVRIVNEHQ
consensus>70  ....vPy.....ydg.....g.....G.....

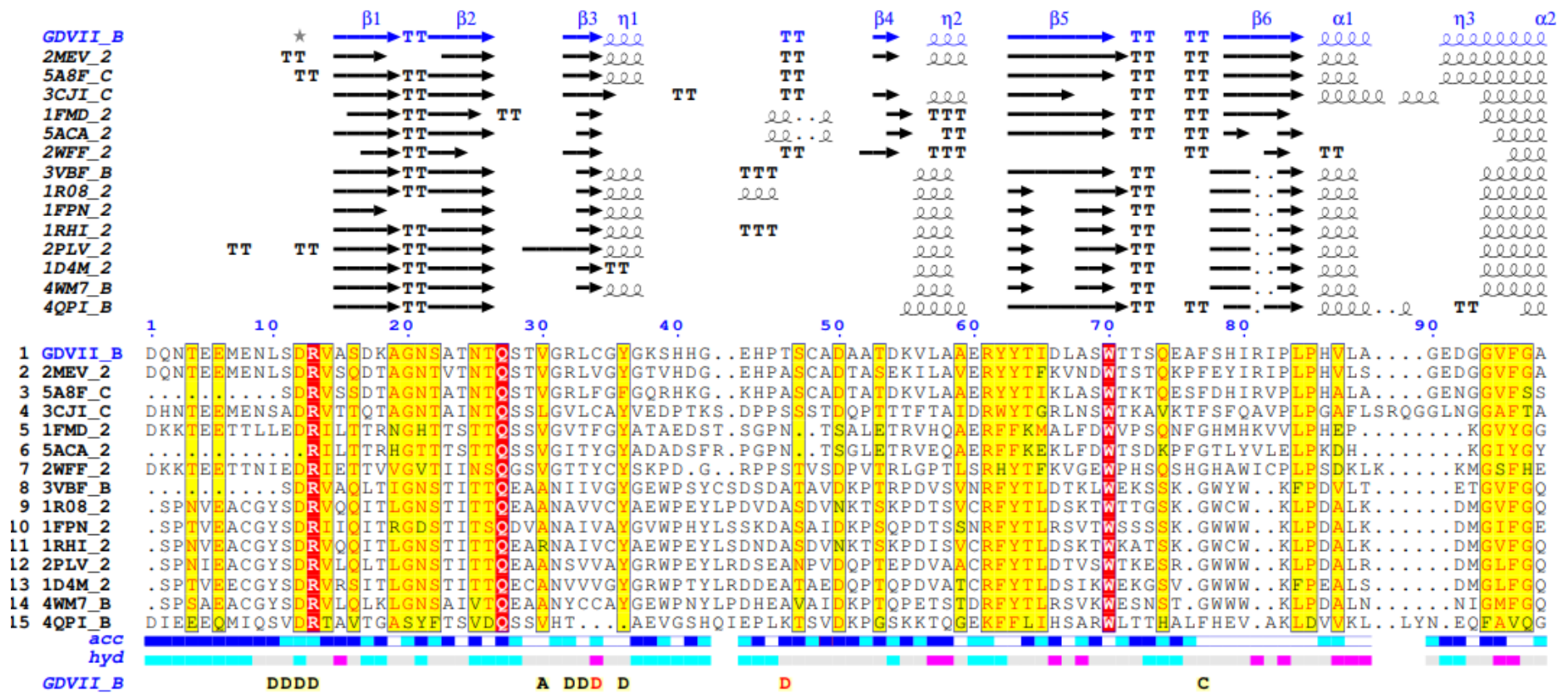
```

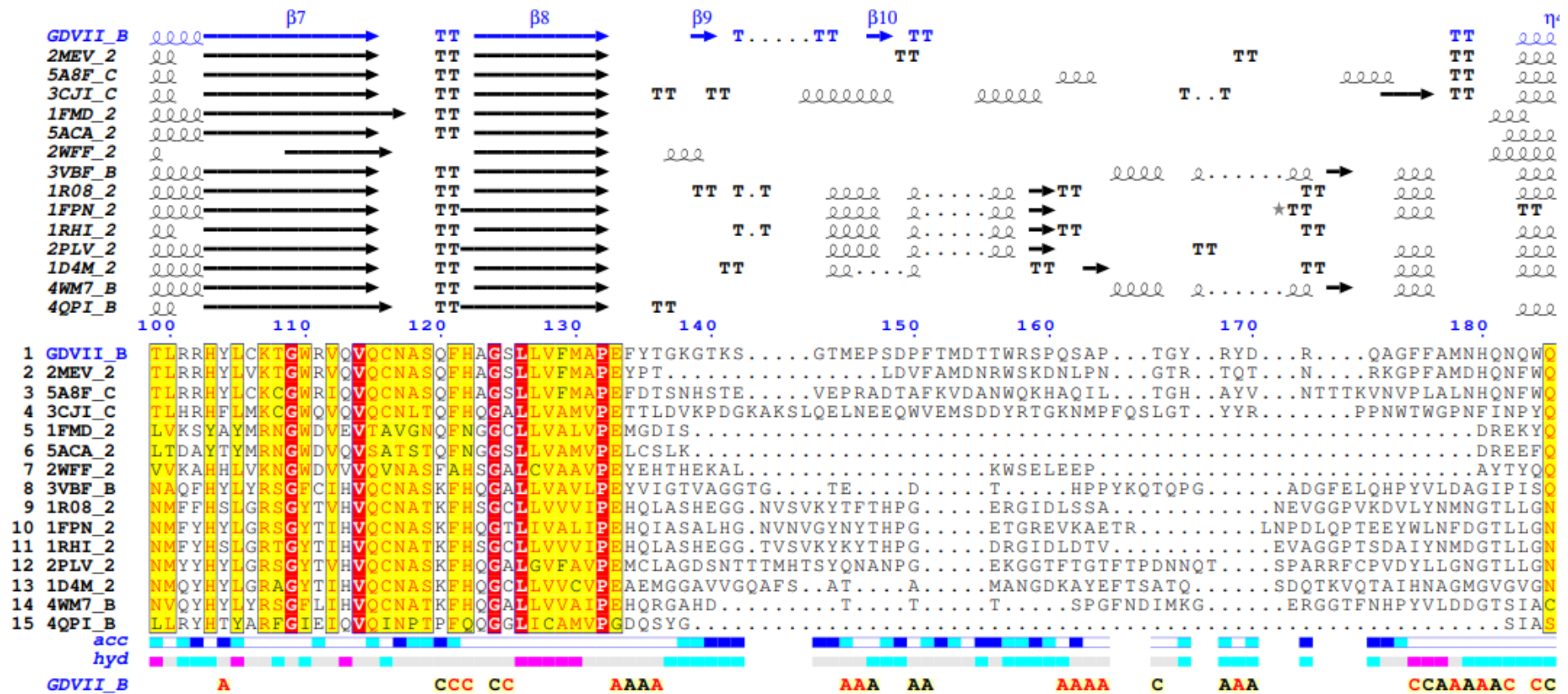
```

          240          250          260          270
GDVII_A      ....NSS..ASVRIYKMKVFCPRPTLFFPWPTPTTTKINAD.NPVPILELE.....
2MEV_1|PDBID|CHAIN|SEQUENCE  ....PDIK..FTVYLRYNMRFVCPPTVFFPWPTSGDKIDMTP.RAGVLMLE.....
5A8F_A|PDBID|CHAIN|SEQUENCE  ....QGT..FSVHYRYKMRVFCPRPTVVFIPWP.....
3CJI_A|PDBID|CHAIN|SEQUENCE  KKSTAVKH..VAVYIRYKNARAWCSMLPFRSYKQKMLM.....
1FMD_1|PDBID|CHAIN|SEQUENCE  ....TI..TELLVRMKRAELYCPRPILPIQPTGDRHKQPLVA.PAKQL.....
5ACA_1|PDBID|CHAIN|SEQUENCE  ....ADKVDVYVYRMKRAELYCPRPLLPGYDHADRDRFDSPIGVEKQ.....
2XB0_1|PDBID|CHAIN|SEQUENCE  ...HDKGG..CYLRYRFRANMYCPRPIPFAFTRPADKTRHKFP.TNINKQCT.....
3VBF_A|PDBID|CHAIN|SEQUENCE  K.SKYPLV.VRIYMRMKHVRAWIPRPMRNQNYLFKANPNYAGN.SIKPTGASRTAI...TTL.....
1R08_1|PDBID|CHAIN|SEQUENCE  E.HKTLVK..IRVYHRAKHVEAWIPRAPRALPYTSIGRTNYPKN.TEPVIKKRKGDI...KSY.....
1FPN_1|PDBID|CHAIN|SEQUENCE  I.HKVHIM..TRIYHKAKHVKAWCPRPPRALEYTRAHRTNFKIE.DRSIQTAIVTRP...IITTAGPSDMY.....
1RHI_1|PDBID|CHAIN|SEQUENCE  V.HTTIVK..IRVYHRAKHVEAWIPRAPRALPYVSIGRTNYPKD.SKTIVKKRTNIK...TY.....
2PLV_1|PDBID|CHAIN|SEQUENCE  P.TKVTSK..IRVYLRKPKHIRVWCPRPPRAVAYYGGVVDYKDGTL.TPLSTKDLTT...Y.....
1D4M_1|PDBID|CHAIN|SEQUENCE  P.HPITST..IRVYFKPKHTRAWVPRPRLCQYKKAFSVDFTPT.PITDTRKDINTV...TTVAQSRRRGDMSTLNTH
4WM7_A|PDBID|CHAIN|SEQUENCE  P.VGFTVT..VRVYMKPKHIKAWAPRPPRTMPYMSIANANYKGR.DTAPNTLNAIIGNRASVTTMPHNIVTT.....
consensus>70  ....vy.r.k.....Prp.....

```

Figure S2. Sequence-based alignment of TMEV VP1 with cardiovirus, senecavirus, aphthovirus and enterovirus representatives. VP1 protein sequences were obtained from the PDB database and included: cardioviruses MEV and SAFV (PDB: 2MEV, 5A8F); senecavirus SVV-1 (PDB: 3CJI); aphthoviruses FMDV type C and SAT 2, ERAV (PDB: 1FMD, 5ACA, 2XB0); and enteroviruses EV-71, HRV-B14, HRV-2, HRV-3, PV-1, CV-A9, EV-D68 (PDB: 3VBF, 1R08, 1FPN, 1RHI, 2PLV, 1D4M, 4WM7). These sequences were submitted to ESript, built into ENDscript, to generate a multiple sequence alignment.





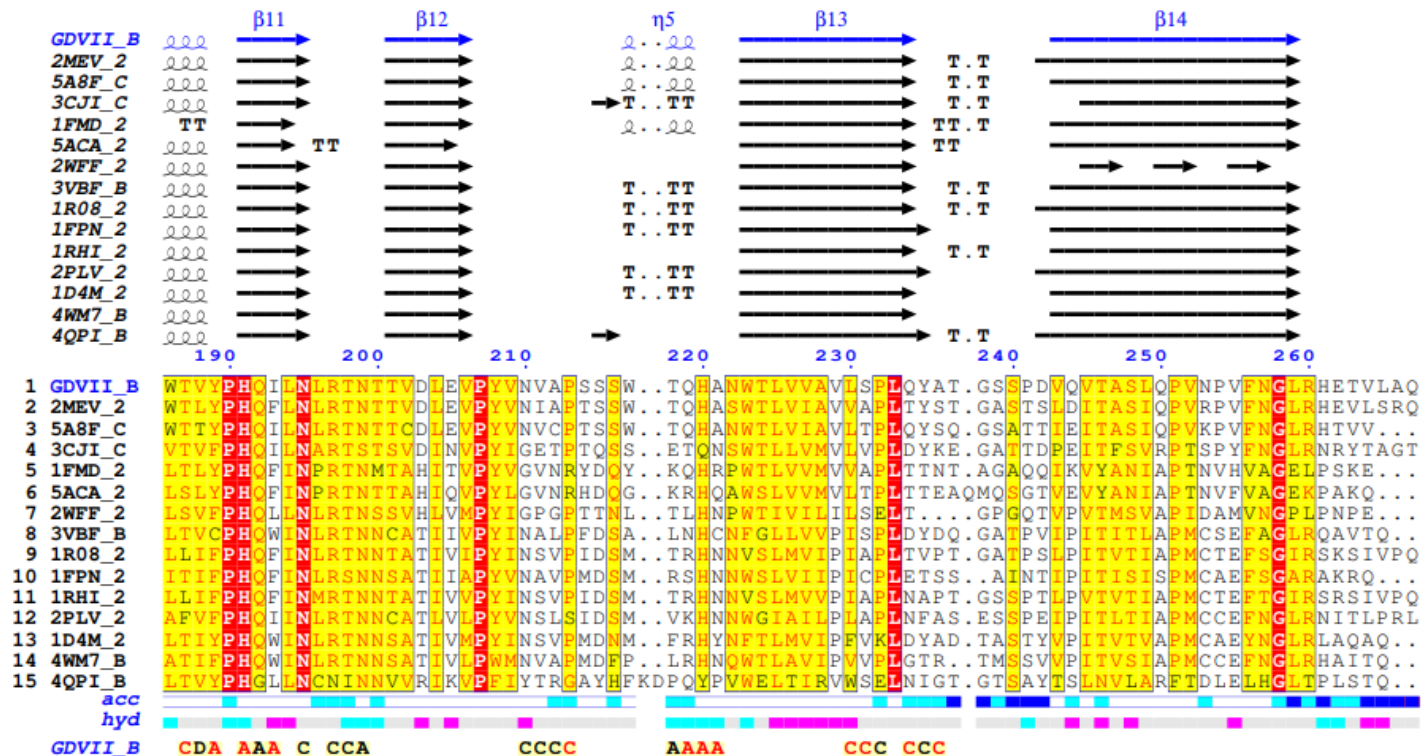
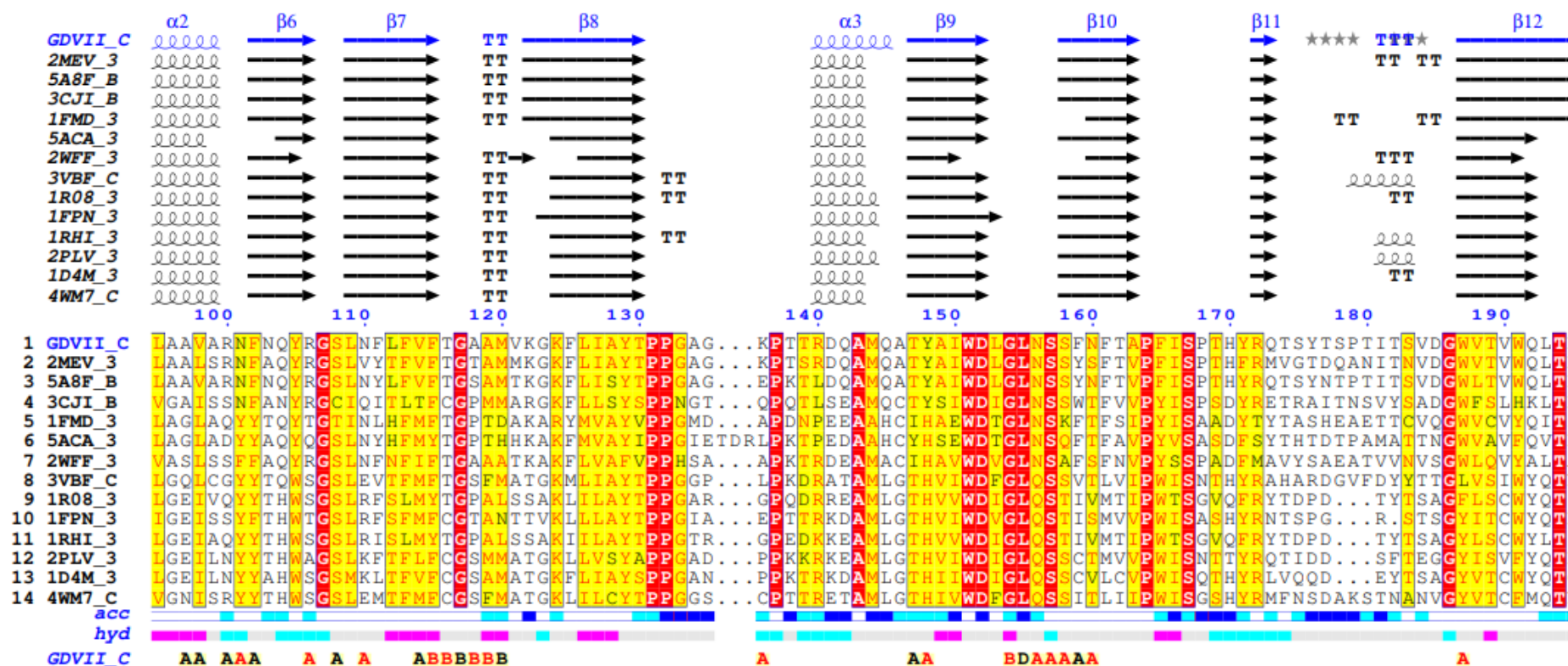


Figure S3. Sequence and structure-based alignment of TMEV VP2 with cardiovirus, senecavirus, aphthovirus and enterovirus representatives. The TMEV protomer structure was submitted to ENDscript 2 and chain B corresponding to VP2 was selected for analysis. A subset of structures for comparison were selected from the list generated by ENDscript. These structures include: cardioviruses MEV and SAFV (PDB: 2MEV, 5A8F); senecavirus SVV-1 (PDB: 3CJI); aphthoviruses FMDV type C and SAT 2, ERAV (PDB: 1FMD, 5ACA, 2WFF); and enteroviruses EV-71, HRV-B14, HRV-2, HRV-3, PV-1, CV-A9, EV-D68 (PDB: 3VBF, 1R08, 1FPN, 1RHI, 2PLV, 1D4M, 4WM7).



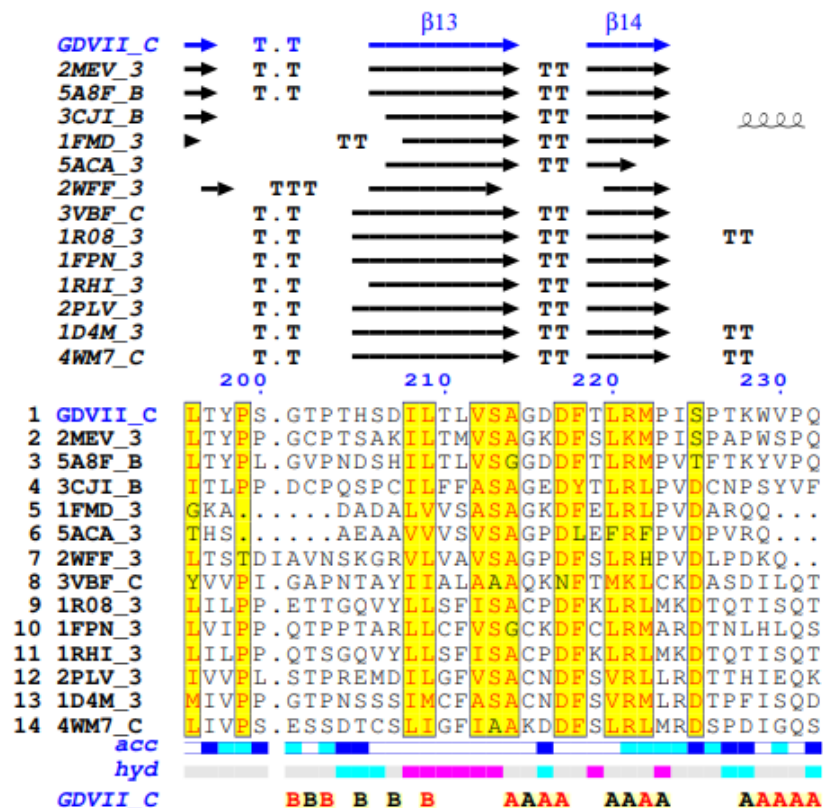


Figure S4. Sequence and structure-based alignment of TMEV VP3 with cardiovascular, senecavirus, aphthovirus and enterovirus representatives. The TMEV protomer structure was submitted to ENDscript 2 and chain C corresponding to VP3 was selected for analysis. A subset of structures for comparison were selected from the list generated by ENDscript. These structures include: cardiovasculars MEV and SAFV (PDB: 2MEV, 5A8F); senecavirus SVV-1 (PDB: 3CJI); aphthoviruses FMDV type C and SAT 2, ERAV (PDB: 1FMD, 5ACA, 2WFF); and enteroviruses EV-71, HRV-B14, HRV-2, HRV-3, PV-1, CV-A9, EV-D68 (PDB: 3VBF, 1R08, 1FPN, 1RHI, 2PLV, 1D4M, 4WM7).

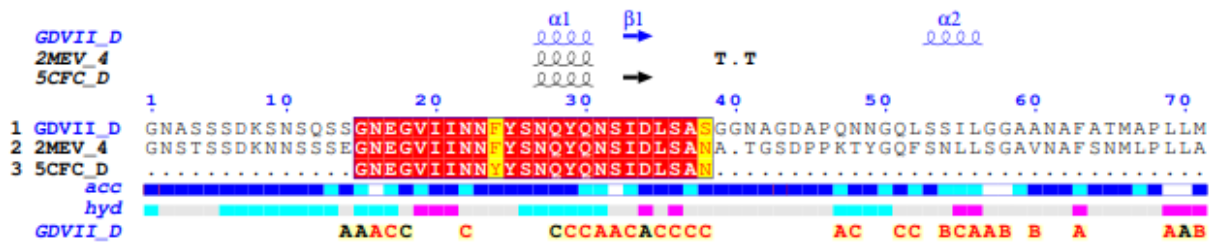


Figure S5. Sequence and structure-based alignment of TMEV, MEV and SAFV VP4 proteins. The TMEV protomer structure was submitted to ENDscript 2 and chain D corresponding to VP4 was selected for analysis. A subset of structures for comparison were selected from the list generated by ENDscript. These structures include: cardioviruses MEV and SAFV (PDB: 2MEV, 5CFC).

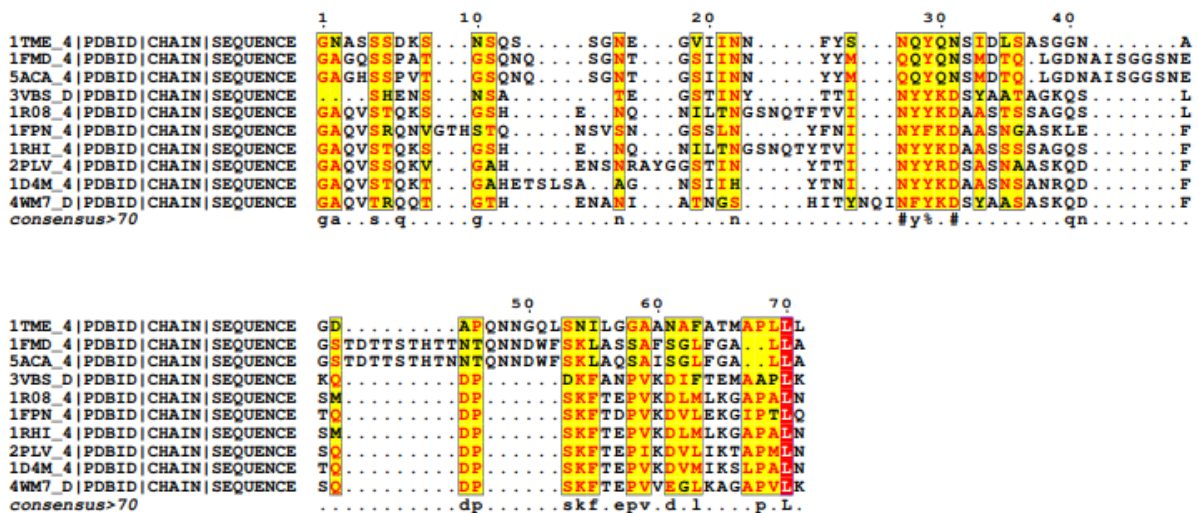


Figure S6. Sequence-based alignment of TMEV, aphthovirus and cardiovirus VP4 proteins. VP4 protein sequences were obtained from the PDB database and included: TMEV (PDB: 1TME); aphthoviruses FMDV type C and SAT 2, ERAV (PDB: 1FMD, 5ACA, 2WFF); and enteroviruses EV-71, HRV-B14, HRV-2, HRV-3, PV-1, CV-A9, EV-D68 (PDB: 3VBS, 1R08, 1FPN, 1RHI, 2PLV, 1D4M, 4WM7). These sequences were submitted to ESript, built into ENDscript, to generate a multiple sequence alignment.

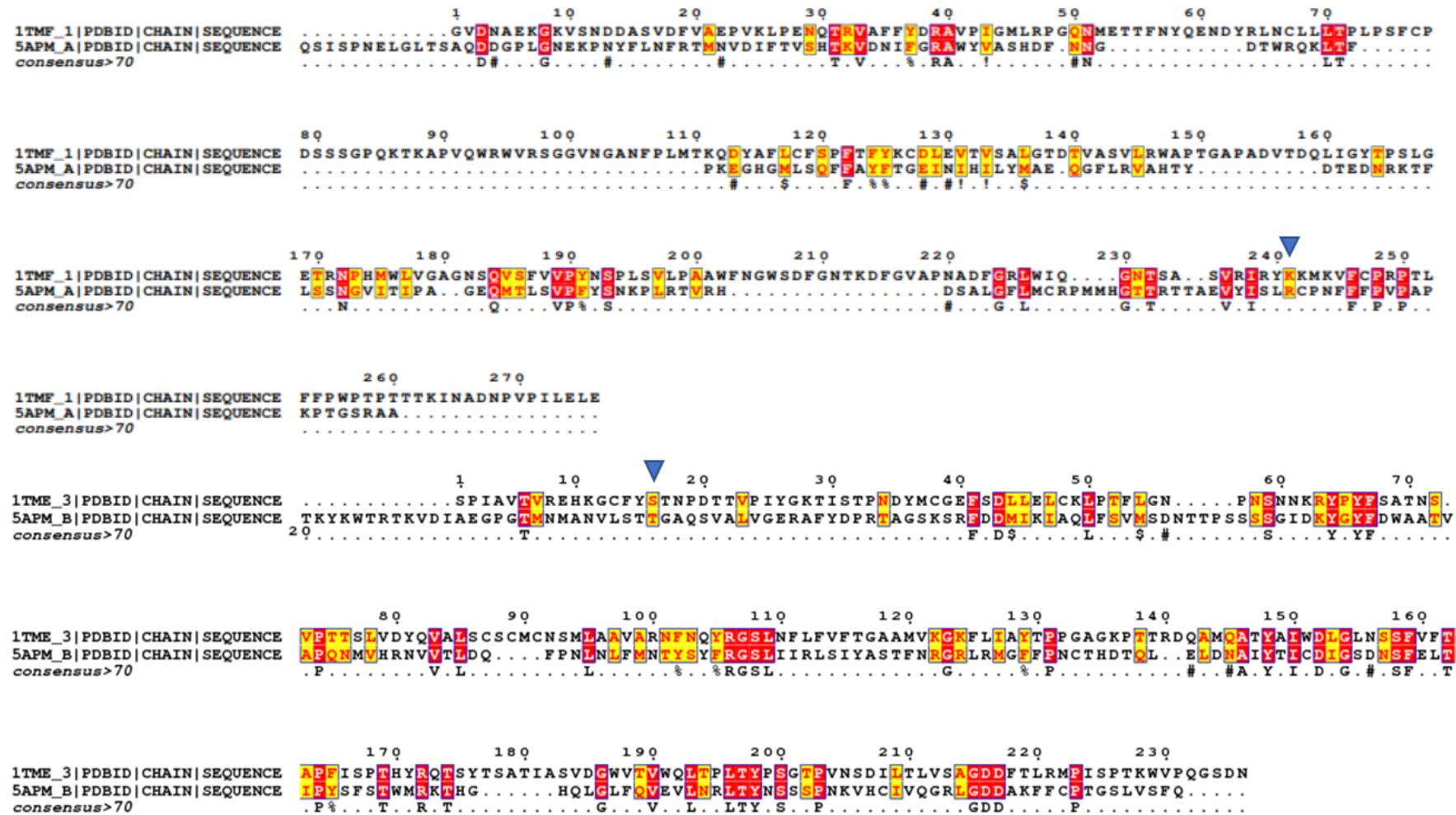


Figure S7. Sequence-based alignments of TMEV and HPV-3 VP1 and VP3 proteins. VP1 and VP3 protein sequences were obtained from the PDB database and included: TMEV (PDB: 1TME) and HPV-3 (PDB: 5APM). Alignments were generated using ESript which is linked to ENDscript. Blue arrow heads indicate conserved residues K241 (VP1) in TMEV corresponding R202 in HPV-3, and S16 (VP3) in TMEV corresponding to T47 in HPV-3.

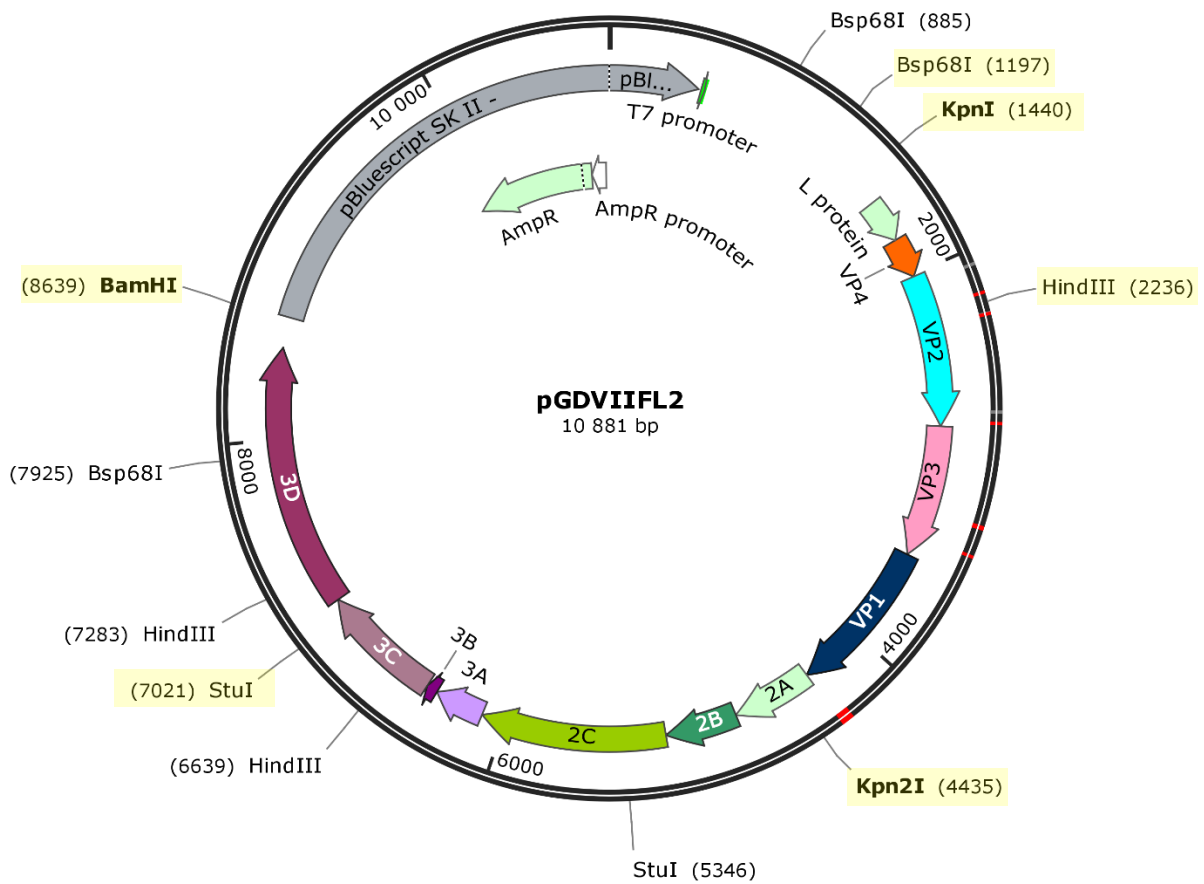
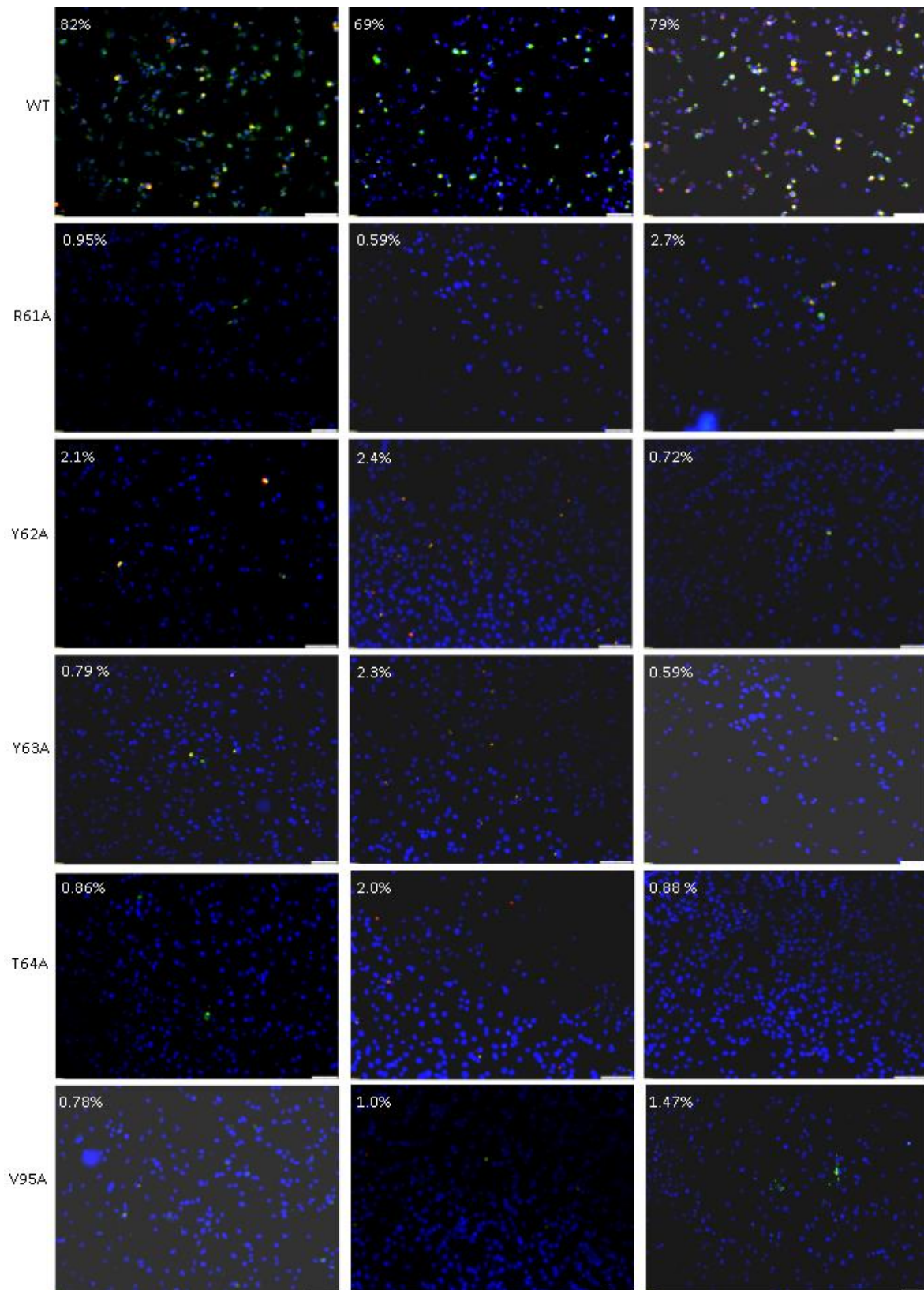
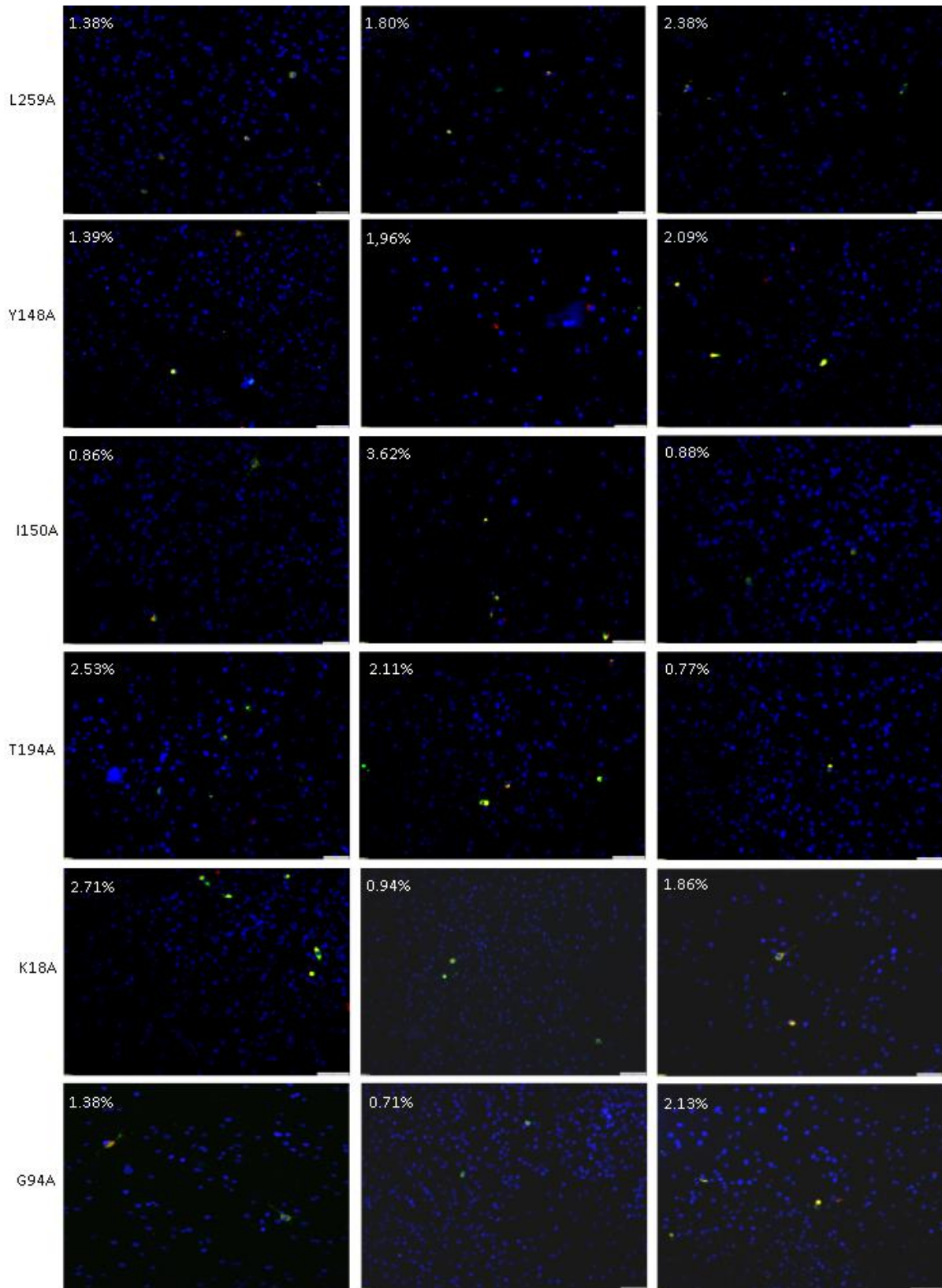


Figure S8. The plasmid map of pGDVIIFL2. pGDVIIFL2 contains the cDNA of TMEV GDVII in the pBlueScript® II Phagemid Vector (Fu et al., 1990). Restriction enzymes used to generate or assess the recombinant pGDVIIFL2-*HindIII*-1 mutants are highlighted. Red and grey lines indicated the sites of individual mutations within the genome that were individually engineered into the pGDVII/*HindIII*-1 mutants. All plasmid maps were generated using SnapGene® version 4.2.4.

Table S4. Identification of hot spot residues within interpentamer interfaces of the TMEV capsid.

Mutation	Nucleotide Sequence	Amino Acid change	Protein	Primer	Sequence 5'→3'
Control Mt- <i>HindIII</i>	AAGCTT→AAGC GT	None	VP2	Mt2Ctrl-Hin F Mt2Ctrl-Hin R	AGGATTCTCTCCCTCACGTCCTT GATGTGAGAGAA CG CTTCTTGGGAAGT
K18A	AAA→ GCA	18 LYS→ALA	VP2	Mt2-K18A-F Mt2-K18A-R	TTCTGAC GC AGCAGGGAATTCCG GCTACTCTGTCAGAGAGGTTTTCCA
R61A	CGT→ GCT	61 ARG→ALA	VP2	Mt2-R61A-F Mt2-R61A-R	ATCTGGCTAGTTGGACCACTTCCC CGATAGTGTAGTAA GC TTCCAGCCGCG
Y62A	TAC→ GCC	62 TYR→ALA	VP2	Mt2-Y62A-F Mt2-Y62A-R	GGCTAGTTGGACCACTTCCCAAG GATCGATAGTGTAG GC ACGTTCCAGCC
Y63A	TAC→ GCC	63 TYR→ALA	VP2	Mt2-Y63A-F Mt2-Y63A-R	GCTAGTTGGACCACTTCCCAAGAAGC CAGATCGATAGTG GC GTAACGTTCCAG
T64A	ACT→ GCT	64 THR→ALA	VP2	Mt2-T64A-F Mt2-T64A-R	CTAGTTGGACCACTTCCCAAGAAGCTT CCAGATCGATAG CG TAGTAACGTTCCAGC
G94A	GGG→ GCG	94 GLY→ALA	VP2	Mt2-G94A/V95A-F Mt2-G94A-R	CTCTGCAAGACTGGATGGCGCGTACAAGT GTAGTGTCTCCTTAAGGTAGCTCCAAAAACC GCTCC
V95A	GTT→ GCT	95 VAL→ALA	VP2	Mt2- G94A/V95A-F Mt2-V95A-R	CTCTGCAAGACTGGATGGCGCGTACAAGT GTAGTGTCTCCTTAAGGTAGCTCCAAAA GCCCCT
D242A	GAC→ GCC	242 ASP→ALA	VP2	Mt2-D242-F Mt2-D242-R	CTTCACCGG CG TTCAAGTCACAGCC AACCGGTGGCGTACTGAAGAGGGCTG
L259A	TTG→ GCG	259 LEU→ALA	VP2	Mt2-L259A-F Mt2-L259A-R	ACTGTGCTTGCACAAAGTCCTATTC TTCGTGTCTC GC ACCATTAACAC
Y148A	TAC→ GCT	148 TYR→ALA	VP3	Mt3-Y148A-F Mt3-Y148A-R	TGGGACTTGGGCTTGAATTCC AATGGC AGC GGTAGCCTGCATAG
I150A	ATT→ GCT	150 ILE→ALA	VP3	Mt3-I150A-F Mt3-I150A-R	CTACCTACGCC GCT TGGGACTTG CCTGCATAGCTTGGTCCCGG
T194A	ACC→ GCC	194 THR→ALA	VP3	Mt3-T194A-F Mt3-T194A-R	TCACTGTTTGGCAGCTG GCCCCC CCCAACCGTCAACAGATGTGATGGTGG





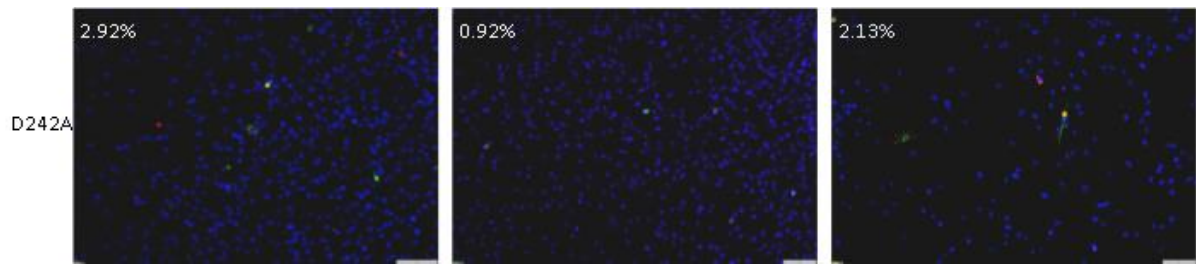
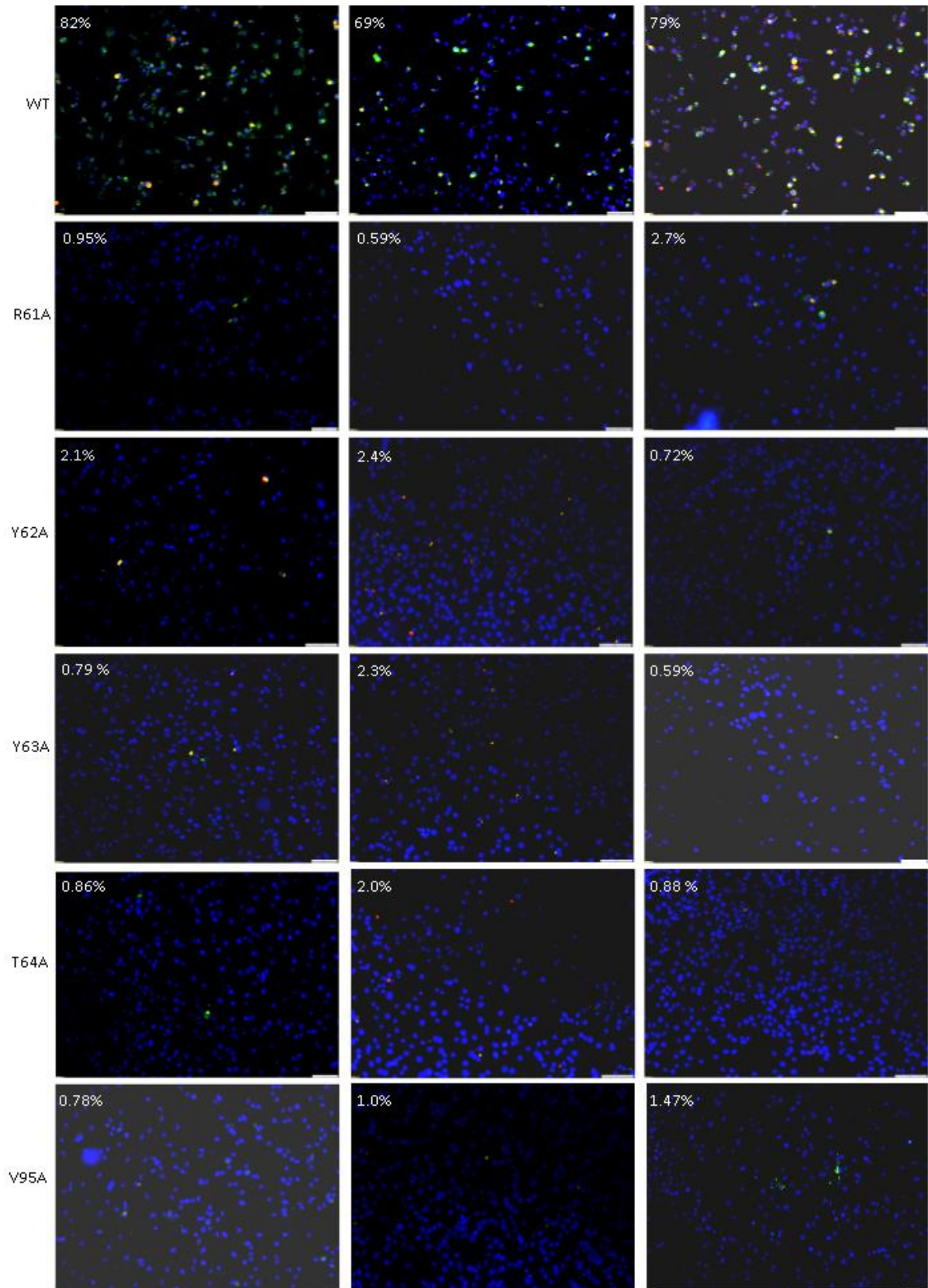
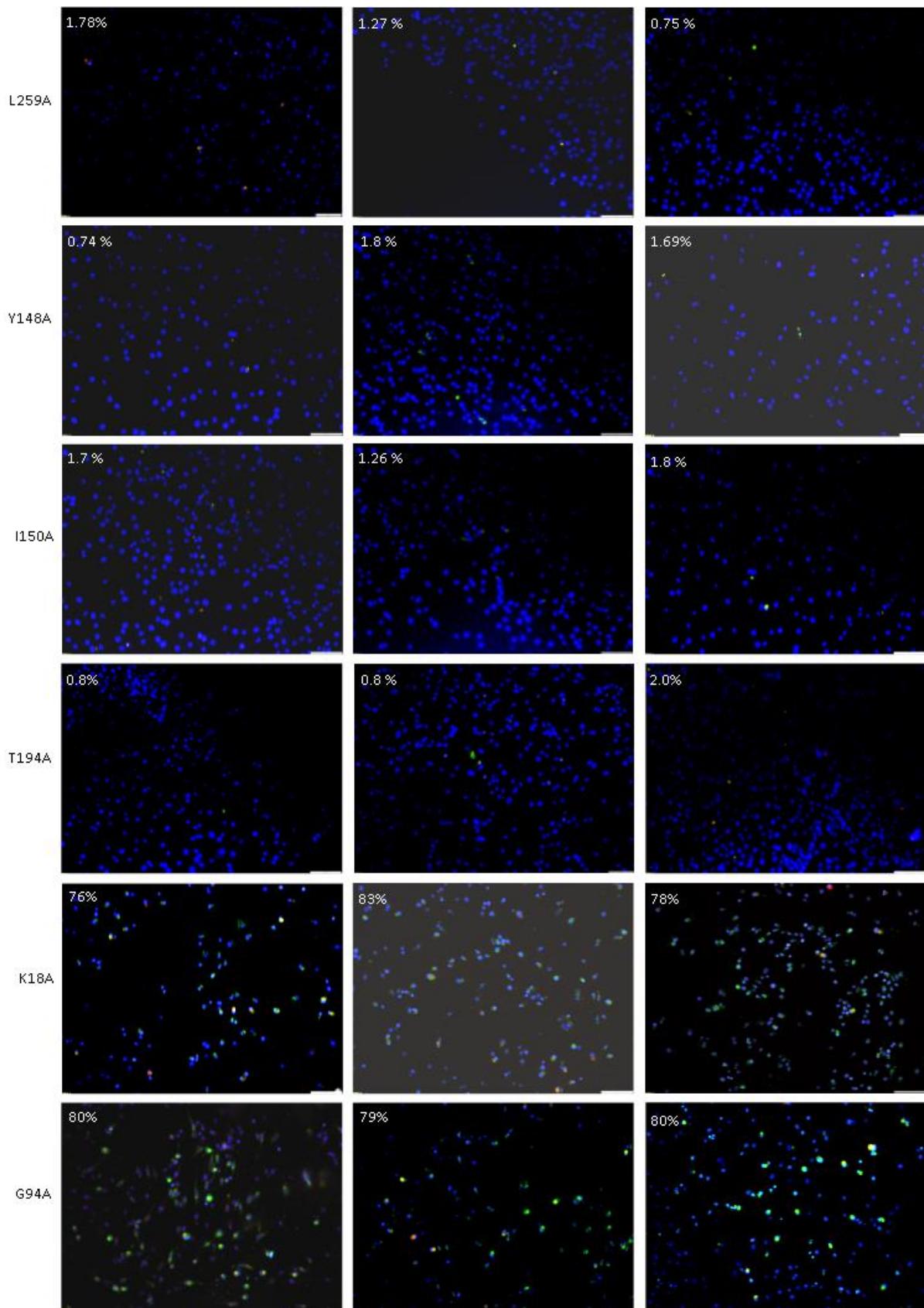


Figure S9. Immunofluorescence analysis of cells at 14 h following transfection with mutant and wild type TMEV RNAs. The number of infected cells is indicated as a percentage in the top left corner of each image. Three images taken each from three replicate transfections of each viral RNA were used to calculate the average number of infected cells following transfection in figure 4.7 B.





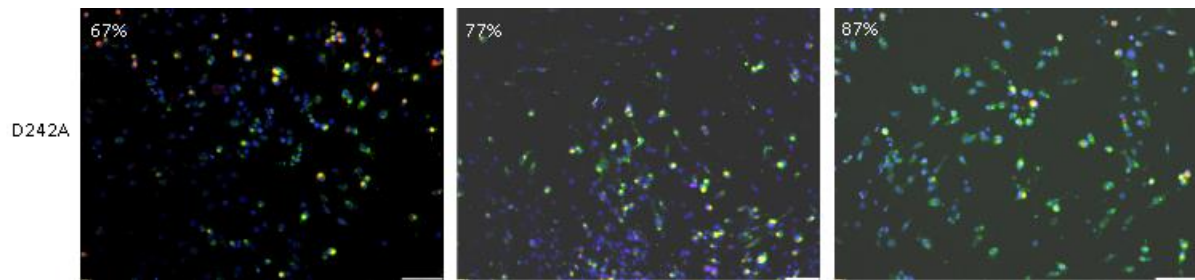


Figure S10. Immunofluorescence analysis of cells at 24 h following transfection with mutant and wild type TMEV RNAs. The number of infected cells is indicated as a percentage in the top left corner of each image. Three images taken each from three replicate transfections of each viral RNA were used to calculate the average number of infected cells following transfection in figure 4.7 B.

Table S5. Tukey's HSD matrix of pairwise comparison possibilities between the number of cells positive for TMEV at 14 and 24 hpt following transfection of mutant and WT RNAs. A Two-Way ANOVA followed by a Tukey post hoc analysis was used to determine the level of significant difference between the number of transfected cells at 14 hpt and 24 hpt. Numerical values indicate the adjusted P values as determined by the Tukey analysis in RStudio. P values ≤ 0.05 are considered significant.

	R61A	Y62A	Y63A	T64A	V95A	L259A	Y148A	I150A	T194A	K18A	G94A	D242A	WT	Adjusted p values between mutant and WT TMEV at 14 hpt	
R61A		1.000	1.000	1.000	1.000	1.000	1.000	1.000	1.000	1.000	1.000	1.000	1.000		
Y62A	1.000		1.000	1.000	1.000	1.000	1.000	1.000	1.000	1.000	1.000	1.000	1.000		
Y63A	1.000	1.000		1.000	1.000	1.000	1.000	1.000	1.000	1.000	1.000	1.000	1.000		
T64A	1.000	1.000	1.000		1.000	1.000	1.000	1.000	1.000	1.000	1.000	1.000	1.000		
V95A	1.000	1.000	1.000	1.000		1.000	1.000	1.000	1.000	1.000	1.000	1.000	1.000		
L259A	1.000	1.000	1.000	1.000	1.000		1.000	1.000	1.000	1.000	1.000	1.000	1.000		
Y148A	1.000	1.000	1.000	1.000	1.000	1.000		1.000	1.000	1.000	1.000	1.000	1.000		
I150A	1.000	1.000	1.000	1.000	1.000	1.000	1.000		1.000	1.000	1.000	1.000	1.000		
T194A	1.000	1.000	1.000	1.000	1.000	1.000	1.000	1.000		1.000	1.000	1.000	1.000		
K18A	0.000	0.000	0.000	0.000	0.000	0.000	0.000	0.000	0.000		1.000	1.000	1.000		
G94A	0.000	0.000	0.000	0.000	0.000	0.000	0.000	0.000	0.000	0.976		1.000	1.000		
D242A	0.000	0.000	0.000	0.000	0.000	0.000	0.000	0.000	0.000	0.999	0.810		1.000		
WT	0.000	0.000	0.000	0.000	0.000	0.000	0.000	0.000	0.000	0.999	0.999	0.996			
Adjusted p values between mutant and WT TMEV at 24 hpt															

